

**RETROFITTING OF VULNERABLE REINFORCED
CONCRETE FRAMES WITH SHOTCRETE WALLS**

**Ph.D. Thesis by
Pınar TEYMÜR**

Department : Civil Engineering

Programme: Structural Engineering

JUNE 2009

**RETROFITTING OF VULNERABLE REINFORCED
CONCRETE FRAMES WITH SHOTCRETE WALLS**

**Ph.D. Thesis by
Pınar TEYMÜR, M.Sc.
(501992332)**

**Date of submission: 10 March 2009
Date of defence examination: 8 June 2009**

**Co-Supervisor (Chairman): Prof. Dr. Sumru PALA
Co-Supervisor : Assist. Prof. Dr. Ercan YÜKSEL
Members of the Examining Committee Prof. Dr. H. Faruk KARADOĞAN (ITU)
Prof. Dr. Feridun ÇILI (ITU)
Prof. Dr. Tuncer ÇELİK (Beykent U.)
Prof. Dr. Erdal İRTEM (Balıkesir U.)
Assoc. Prof. Dr. Cem YALÇIN (BU)**

JUNE 2009

İSTANBUL TEKNİK ÜNİVERSİTESİ ★ FEN BİLİMLERİ ENSTİTÜSÜ

**PÜSKÜRTME BETON PANELLER İLE DEPREM DAYANIMI DÜŞÜK
BETONARME ÇERÇEVELERİN GÜÇLENDİRİLMESİ**

**DOKTORA TEZİ
Pınar TEYMÜR
(501992332)**

Tezin Enstitüye Verildiği Tarih : 10 Mart 2009

Tezin Savunulduğu Tarih : 08 Haziran 2009

**Tez Danışmanı : Prof. Dr. Sumru PALA
Yrd. Doç. Dr. Ercan YÜKSEL
Diğer Jüri Üyeleri : Prof. Dr. H. Faruk KARADOĞAN (İTÜ)
Prof. Dr. Feridun ÇILI (İTÜ)
Prof. Dr. Tuncer ÇELİK (Beykent Ü.)
Prof. Dr. Erdal İRTEM (Balıkesir Ü.)
Doç. Dr. Cem YALÇIN (BÜ)**

HAZİRAN 2009

FOREWORD

I wish to express my gratitude to my co-supervisors Prof.Dr. Sumru Pala and Assist.Prof.Dr.Ercan Yuksel for their ideas, enthusiasm and encouragement. I am grateful for their guidance, support and assistance they have given me during my PhD. I would also like to thank Prof. Dr. Faruk Karadođan and Prof. Dr. Feridun ılı for his valuable inputs, suggestions and his support throughout the preparation of this thesis.

I would like to thank the technicians at the Structural and Earthquake Engineering Laboratory for their invaluable technical assistance without them the experimental work would not have happened. I would like to express my thanks to Mahmut Őamlı and Hakan Saruhan, C.E., MSc for all the help with my experiments. I would like to thank Research Assist. Kıvan TaŐkın for his help during the tests.

Special thanks must go to Dr. Cüneyt Vatansever who has helped me during the experiments and his friendship is appreciated. I would like to thank Assist.Prof. Dr. Rui Pinho especially for his contributions on the usage of SeismoStruct program and his guidance. I am indebted to him for providing me with the opportunity to conduct research in ROSE School, Italy.

I would also like to thank the technicians of Structural Materials Laboratory and Assist.Prof.Dr. Hasan Yıldırım for all their help. I would like to thank Assoc.Prof.Dr. Hüseyin Yıldırım and Alternatif Zemin firm as without their help last two specimens could not be prepared.

I would like to acknowledge the financial supports of TUBİTAK and ITU BAP division are appreciated.

Finally I would like to thank my twin sister Assit.Prof.Dr. Berrak Teymur, my father Prof.Dr.Mevlut Teymur and my mother Duygu Teymur, Chemical Engineer, MSc, for their encouragement, faith, morale support and assistance during my difficult times.

March 2009

Pınar TEYMUR

TABLE OF CONTENTS

	<u>Page</u>
FOREWORD	v
TABLE OF CONTENTS	vii
ABBREVIATIONS	ix
LIST OF TABLES	xi
LIST OF FIGURES	xiii
LIST OF SYMBOLS	xix
ÖZET	xxi
SUMMARY	xxiii
1. INTRODUCTION	1
1.1. General	1
1.2. Objectives and Scope	2
1.3. Organization of the Thesis	3
2. SEISMIC RETROFIT FOR REINFORCED CONCRETE BUILDING STRUCTURES	5
2.1. System Strengthening and Stiffening	5
2.1.1 Shear walls	6
2.1.2 Carbon fiber reinforced polymer (CFRP) applied on the infill wall	6
2.1.3 Braced frames	7
2.1.4 Moment resisting frames	8
2.1.5 Diaphragm strengthening	8
2.2. Enhancing Deformation Capacity	8
2.2.1 Column strengthening	9
2.2.2 Local stress reductions	10
2.2.3 Supplemental support	10
2.3. Reducing Earthquake Demands	10
2.3.1 Base isolation	10
2.3.2 Energy dissipation systems	11
2.3.3 Mass reduction	11
2.4. Rehabilitation Methods for Unreinforced Masonry Walls	11
2.4.1 Surface treatment	11
2.4.2 Injection grouting	13
2.4.3 Jacketing	14
2.4.4 Reinforcing bars	14
2.4.5 Mechanical anchors	15
2.5. What is Shotcrete	16
2.5.1 Types of shotcrete according to the application process	17
2.5.2 Usage of shotcrete	18
2.5.3 Types of shotcrete	18
3. TEST PROGRAM AND MATERIAL CHARACTERIZATION	21
3.1. Test Specimens	21
3.2. Test Setup, Instrumentation and Data Acquisition	31

3.2.1. Test setup and loading system	31
3.2.2. Instrumentation and data acquisition	32
3.3. Load Pattern	35
3.4. Material Tests	36
3.4.1. Concrete tests	37
3.4.2. Steel reinforcement tests	38
4. EXPERIMENTAL RESULTS	39
4.1. Test Results of Specimen 1	39
4.2. Test Results of Specimen 2	42
4.3. Test Results of Specimen 2S	45
4.4. Test Results of Specimen 3	52
4.5. Test Results of Specimen 4	58
4.6. Test Results of Specimen 4S	60
4.7. Test Results of Specimen 5	68
4.8. Test Results of Specimen 6	74
4.9. Test Results of Specimen 7	81
4.10. Test Results of Specimen 8	89
4.11. Evaluation of the Test Results	95
4.11.1. Failure modes	95
4.11.2. Lateral load carrying capacity	97
4.11.3. Initial stiffness	102
4.11.4. Cumulative energy dissipation	103
4.11.5. Equivalent damping characteristics	107
4.11.6. Lateral stiffness	109
4.11.7. Rotation of the panels	112
5. ANALYTICAL STUDIES USING THE FINITE ELEMENT METHOD ...	115
5.1. Nonlinear Static Analysis using SeismoStruct	116
5.2. Description of Element Types Used	117
5.3. Material Models	117
5.3.1. Material model used for steel reinforcement	118
5.3.2. Material model used for concrete	119
5.4. Inelastic Infill Panel Element	121
5.5. Comparison of the Results of Analysis with Experimental Results	130
5.5.1. Specimen 1	133
5.5.2. Specimen 3	136
5.5.3. Specimen 5	140
5.5.4. Specimen 6	145
5.5.5. Specimen 7	149
6. PARAMETRIC STUDIES	155
6.1. The Effect Panel Thickness	155
6.2. The Effect of the Distance between the Panel and the Frame	163
6.3. Panel Concrete Compressive Strengths	167
6.4. Application of the Retrofitting Technique to a Representative Frame	170
7. CONCLUSIONS	189
REFERENCES	193
VITA	201

ABBREVIATIONS

AC	: Alternative Current
CFRP	: Carbon Fiber Reinforced Polymer
DC	: Direct Current
ED	: Energy Dissipation
EDU	: Energy Dissipation Units
FEMA	: Federal E M Agency
FRP	: Fiber Reinforced Polymer
FRS	: Fiber-Reinforced Shotcrete
LRB	: Lead Rubber Bearings
LVDT	: Linear Variable Displacement Transducers
MTS	: Material Test System
RC	: Reinforced Concrete
SFRS	: Steel Fiber-Reinforced Shotcrete
STEEL	: Structural and Earthquake Engineering Laboratory
SWAT	: Soil and Water Assessment Tool
TEC	: Turkish Earthquake Code
URM	: Unreinforced Masonry Wall

LIST OF TABLES

	<u>Page No</u>
Table 3.1: Test specimens	23
Table 3.2: LVDTs used for bare frame	33
Table 3.3: LVDTs used for fully infilled frame	33
Table 3.4: LVDTs used for partially infilled frame	35
Table 3.5: Steps of the loading protocol	36
Table 3.6: Concrete mix proportions for frame concrete	37
Table 3.7: Concrete mix proportions for shotcrete panel concrete	37
Table 3.8: The average concrete compressive strengths for frames	37
Table 3.9: The average concrete compressive strengths for panels	38
Table 3.10: Mechanical properties of steel bars	38
Table 4.1: Width of cracks in mm at specific story drifts	42
Table 4.2: Width of cracks in mm at specific story drifts	45
Table 4.3: Width of cracks in mm at specific story drifts	49
Table 4.4: Effect of strengthening in general	49
Table 4.5: Maximum base shears recorded during the tests	50
Table 4.6: Initial stiffness of the specimens	50
Table 4.7: Width of cracks in mm at specific story drifts	56
Table 4.8: Effect of strengthening in general	57
Table 4.9: Maximum base shears observed during the tests	57
Table 4.10: Initial stiffness of the specimens	57
Table 4.11: Width of cracks in mm at specific story drifts	65
Table 4.12: Effect of strengthening in general	65
Table 4.13: Maximum base shears observed during the tests	66
Table 4.14: Initial stiffness of the specimens	66
Table 4.15: Width of cracks in mm at specific story drifts	71
Table 4.16: Effect of strengthening in general	72
Table 4.17: Maximum base shears occurred during the tests	72
Table 4.18: Initial stiffness of the specimens	72
Table 4.19: Width of cracks in mm at specific story drifts	78
Table 4.20: Effect of strengthening in general	79
Table 4.21: Maximum base shears observed during the tests	79
Table 4.22: Initial stiffness of the specimens	79
Table 4.23: Width of cracks in mm at specific story drifts	86
Table 4.24: Effect of strengthening in general	87
Table 4.25: Maximum base shears occurred during the tests	87
Table 4.26: Initial stiffness of the specimens	87
Table 4.27: Width of cracks in mm at specific story drifts	92
Table 4.28: Effect of strengthening in general	93

Table 4.29: Maximum base shears observed during the tests	93
Table 4.30: Initial stiffness of the specimens	93
Table 4.31: Effect of retrofiting on general quantities	96
Table 4.32: Maximum base shears observed during the tests	97
Table 4.33: Initial stiffness of the specimens	103
Table 5.1: Input parameters for steel reinforcement	118
Table 5.2: Input parameters for concrete	120
Table 5.3: Input parameters for the infill model	123
Table 5.4: Suggested and limit values for empiric parameters	126
Table 5.5: Input parameters of the shear spring	127
Table 5.6: Limit strain values to define damage states in structural members according to TEC 2007	132
Table 5.7: Damage levels for Specimen 1	135
Table 5.8: Damage levels for Specimen 3	139
Table 5.9: Damage levels for Specimen 5	143
Table 5.10: Damage levels for Specimen 6	147
Table 5.11: Damage levels for Specimen 7	151
Table 6.1: The change in the thickness of the panel	155
Table 6.2: The change in the distance between the column and the panel	163
Table 6.3: The dimensions and reinforcement of the columns	172
Table 6.4: The reinforcement of the beams	172
Table 6.5: Concentrated mass values at each floor levels	173
Table 6.6: Forces applied during pushover analysis	174
Table 6.7: Earthquake records	175

LIST OF FIGURES

	<u>Page No</u>
Figure 2.1: Global modification of the structural system Thermou and Elnashai (2006)	5
Figure 2.2: Local modification of structural components, Thermou and Elnashai (2006)	9
Figure 3.1: General view of the fully infilled frame	21
Figure 3.2: General view of the partially infilled frame	22
Figure 3.3: Geometry of the specimens	25
Figure 3.4: Reinforcement details of the frame	26
Figure 3.5: Reinforcement details of the panel	26
Figure 3.6: Repairing process of the damaged bare frames	28
Figure 3.7: Construction of the shotcrete panels	29
Figure 3.8: Specimen 6 and 7 having pre-reverse deflection on beam	30
Figure 3.9: Construction of Specimen 8	30
Figure 3.10: Test setup	31
Figure 3.11: Locations of LVDTs on bare frames	34
Figure 3.12: Locations of LVDTs on fully infilled frames	34
Figure 3.13: Locations of LVDTs on partially infilled frames	34
Figure 3.14: Loading protocol	36
Figure 4.1: Lateral load-top displacement curve of Specimen 1	40
Figure 4.2: Envelope curve of Specimen 1	40
Figure 4.3: Calculation of rotation at the ends of the columns	41
Figure 4.4: Rotation at the bottom end of the right and left column	41
Figure 4.5: Rotation at the top end of the right and left column	41
Figure 4.6: Crack pattern of Specimen 1 at the end of test	42
Figure 4.7: Lateral load-top displacement curve of Specimen 2	43
Figure 4.8: Envelope curve of Specimen 2	43
Figure 4.9: Rotation at the bottom end of the right and left column	44
Figure 4.10: Rotation at the top end of the right and left column	44
Figure 4.11: Crack pattern of Specimen 2 at the end of test	44
Figure 4.12: Lateral load-top displacement curve of Specimen 2S	45
Figure 4.13: Envelope curve of Specimen 2S	46
Figure 4.14: Rotation at the bottom end of the right and left column	46
Figure 4.15: Rotation at the top end of the right and leftcolumn	46
Figure 4.16: Panel displacement	47
Figure 4.17: Specimen 2S at the end of test	48
Figure 4.18: Crack pattern of Specimen 2S at the end of test	48
Figure 4.19: Comparison of envelope curves of Specimen 2S and Specimen 1	49

Figure 4.20: The comparison of cumulative energy dissipation capacities of Specimens 1 and 2S	50
Figure 4.21: Cumulative energy dissipation capacities of Specimens 1 and 2S at various story drifts	51
Figure 4.22: Lateral load-top displacement curves of Specimen 3	52
Figure 4.23: Envelope curve of Specimen 3	53
Figure 4.24: Rotation at the bottom end of the right and left column	53
Figure 4.25: Rotation at the top end of the right and left column	53
Figure 4.26: Panel displacement	54
Figure 4.27: Specimen 3 at the end of test	55
Figure 4.28: Crack pattern of Specimen 3 at the end of test	55
Figure 4.29: Comparison of envelope curves of Specimens 3 and 1 with analytical bare 3	56
Figure 4.30: The comparison of cumulative energy dissipation capacities of Specimens 1 and 3	57
Figure 4.31: Cumulative energy dissipation capacities of Specimens 1 and 3 at various story drifts	58
Figure 4.32: Lateral load-top displacement curve of Specimen 4	59
Figure 4.33: Rotation at the bottom end of the right and left column	59
Figure 4.34: Rotation at the top end of the right and left column	59
Figure 4.35: Crack pattern of Specimen 4 at the end of test	60
Figure 4.36: Lateral load-top displacement curve of Specimen 4S	61
Figure 4.37: Envelope curve of Specimen 4S	61
Figure 4.38: Rotation at the bottom end of the right and left column	62
Figure 4.39: Rotation at the top end of the right and left column	62
Figure 4.40: Panel horizontal displacement at top	62
Figure 4.41: Panel horizontal displacement at middle	63
Figure 4.42: Panel horizontal displacement at bottom	63
Figure 4.43: Specimen 4S at the end of test	64
Figure 4.44: Crack pattern of Specimen 4S at the end of test	64
Figure 4.45: Comparison of envelope curves of Specimens 4S and 1 with analytical bare 4S	65
Figure 4.46: The comparison of cumulative energy dissipation capacities of Specimens 1 and 4S	66
Figure 4.47: Cumulative energy dissipation capacities of Specimens 1 and 4S at various story drifts	67
Figure 4.48: Lateral load-top displacement curve of Specimen 5	68
Figure 4.49: The envelope curve of Specimen 5	69
Figure 4.50: Rotation at the bottom end of the right and left column	69
Figure 4.51: Rotation at the top end of the right and left column	69
Figure 4.52: Specimen 5 at the end of test	70
Figure 4.53: Crack pattern of Specimen 5 at the end of test	71
Figure 4.54: Comparison of envelope curves of Specimens 5 and 1 with analytical bare 5	72
Figure 4.55: The comparison of cumulative energy dissipation capacities of Specimens 1 and 4S	73
Figure 4.56: Cumulative energy dissipation capacities of Specimens 1 and 5 at various story drifts	73
Figure 4.57: Lateral load-top displacement curve of Specimen 6	75
Figure 4.58: The envelope curve of Specimen 6	75

Figure 4.59: Rotation at the bottom end of the right and left column	76
Figure 4.60: Rotation at the top end of the right and left column	76
Figure 4.61: Panel displacement	76
Figure 4.62: Specimen 6 at the end of test	77
Figure 4.63: Crack pattern of Specimen 6 at the end of test	78
Figure 4.64: Comparison of envelope curves of Specimens 6 and 1 with analytical bare 6	79
Figure 4.65: The comparison of cumulative energy dissipation capacities of Specimens 1 and 6	80
Figure 4.66: Cumulative energy dissipation capacities of Specimens 1 and 6 at various story drifts	80
Figure 4.67: Lateral load-top displacement curve of Specimen 7	82
Figure 4.68: The envelope curve of Specimen 7	82
Figure 4.69: Rotation at the bottom end of the right and left column	83
Figure 4.70: Rotation at the top end of the right and left column	83
Figure 4.71: Panel horizontal displacement at top	83
Figure 4.72: Panel horizontal displacement at middle	84
Figure 4.73: Panel horizontal displacement at bottom	84
Figure 4.74: Specimen 7 at the end of test	85
Figure 4.75: Crack pattern of Specimen 7 at the end of test	85
Figure 4.76: Comparison of envelope curves of Specimens 7 and 1 with analytical bare 7	86
Figure 4.77: The comparison of cumulative energy dissipation capacities of Specimens 1 and 7	87
Figure 4.78: Cumulative energy dissipation capacities of Specimens 1 and 7 at various story drifts	88
Figure 4.79: Lateral load-top displacement curve of Specimen 8	89
Figure 4.80: The envelope curve of Specimen 8	90
Figure 4.81: Rotation at the bottom end of the right and left column	90
Figure 4.82: Rotation at the top end of the right and left column	90
Figure 4.83: Panel displacement	91
Figure 4.84: Specimen 8 at the end of test	92
Figure 4.85: Crack pattern of Specimen 8 at the end of test	92
Figure 4.86: Comparison of envelope curves of Specimens 8 and 1 with analytical bare 8	93
Figure 4.87: The comparison of cumulative energy dissipation capacities of Specimens 1 and 8	94
Figure 4.88: Cumulative energy dissipation capacities of Specimens 1 and 8 at various story drifts	94
Figure 4.89: The comparison of envelope curves of Specimens 1, 2S and 3	98
Figure 4.90: The comparison of envelope curves of Specimens 2S and 3 with analytical 3_2S	98
Figure 4.91: The comparison of envelope curves of Specimens 1, 4S and 5	99
Figure 4.92: The comparison of envelope curves of Specimens 1, 3 and 6	100
Figure 4.93: The comparison of envelope curves of Specimens 3 and 6 with analytical 3_6	100
Figure 4.94: The comparison of envelope curves of Specimens 1, 5 and 7	101
Figure 4.95: The comparison of envelope curves of Specimens 1, 6 and 7	101
Figure 4.96: The comparison of envelope curves of Specimens 1, 3, 5 and 8	102
Figure 4.97: The comparison of envelope curves of Specimens 1, 3, 5 and 8	

with analytical 3_8 and analytical 1_8	102
Figure 4.98: Initial stiffnesses of the specimens	103
Figure 4.99: Cumulative energy dissipation capacities at various story drifts ..	104
Figure 4.100: The comparison of cumulative energy dissipation capacities of Specimens 1, 2S and 3	104
Figure 4.101: The comparison of cumulative energy dissipation capacities of Specimens 1, 4S and 5	105
Figure 4.102: The comparison of cumulative energy dissipation capacities of Specimens 1, 3 and 6	105
Figure 4.103: The comparison of cumulative energy dissipation capacities of Specimens 1, 5 and 7	106
Figure 4.104: The comparison of cumulative energy dissipation capacities of Specimens 1, 6 and 7	106
Figure 4.105: The comparison of cumulative energy dissipation capacities of Specimens 1, 3, 5 and 8	107
Figure 4.106: Dissipated and strain energy	108
Figure 4.107: Equivalent damping for various tests	108
Figure 4.108: The comparison of lateral stiffnesses of Specimen 1, 2S and 3 ..	109
Figure 4.109: The comparison of lateral stiffnesses of Specimen 1, 4S and 5 ..	109
Figure 4.110: The comparison of lateral stiffnesses of Specimen 1, 3 and 6 ...	110
Figure 4.111: The comparison of lateral stiffnesses of Specimen 1, 5 and 7 ...	110
Figure 4.112: The comparison of lateral stiffnesses of Specimen 1, 6 and 7 ...	111
Figure 4.113: The comparison of lateral stiffnesses of Specimen 1, 3, 5 and 8	111
Figure 4.114: Calculation of rotation of the shotcrete panel	112
Figure 4.115: The rotation of the panel for Specimen 3	113
Figure 4.116: The rotation of the panel for Specimen 5	113
Figure 4.117: The rotation of the panel for Specimen 8	114
Figure 5.1: Fibre analysis approach	116
Figure 5.2: Gauss Integration points in beam column elements	117
Figure 5.3: Strut model used	122
Figure 5.4: General characteristics of the proposed model for cyclic axial behaviour of masonry, Crisafulli, 1997	122
Figure 5.5: Analytical response for cyclic shear response of mortar joints	127
Figure 5.6: Change in the strut area	129
Figure 5.7: Frame model used in SeismoStruct	131
Figure 5.8: Infilled frame models used in SeismoStruct	131
Figure 5.9: Definition of frame element names and the loadings in the mathematical model used in SeismoStruct	132
Figure 5.10: The displacement pattern applied to Specimen 1	133
Figure 5.11: Comparison of the hysteretic curves of the experimental and analytical results of Specimen 1	133
Figure 5.12: Comparison of the envelope curves of the experimental and analytical results of Specimen 1	134
Figure 5.13: Damage states obtained at drift levels at certain drift levels at Specimen 1	136
Figure 5.14: Damages occurred at the end of the analysis at Specimen 1	136
Figure 5.15: The displacement pattern applied to Specimen 3	137
Figure 5.16: Comparison of the hysteretic curves of the experimental and analytical results of Specimen 3	137
Figure 5.17: Comparison of the envelope curves of the experimental and	

analytical results of Specimen 3	138
Figure 5.18: Damage states obtained at drift levels at certain drift levels at Specimen 3	140
Figure 5.19: Damage occurred at the end of the analysis at Specimen 3	140
Figure 5.20: The displacement pattern applied to Specimen 5	141
Figure 5.21: Comparison of the hysteretic curves of the experimental and analytical results of Specimen 5	141
Figure 5.22: Comparison of the envelope curves of the experimental and analytical results of Specimen 5	142
Figure 5.23: Damage states obtained at drift levels at certain drift levels at Specimen 5	144
Figure 5.24: Damage occurred at the end of the analysis at Specimen 5	145
Figure 5.25: The displacement pattern applied to Specimen 6	145
Figure 5.26: Comparison of the hysteretic curves of the experimental and analytical results of Specimen 6	146
Figure 5.27: Comparison of the envelope curves of the experimental and analytical results of Specimen 6	146
Figure 5.28: Damage states obtained at drift levels at certain drift levels at Specimen 6	148
Figure 5.29: Damage occurred at the end of the analysis at Specimen 6	149
Figure 5.30: The displacement pattern applied to Specimen 7	149
Figure 5.31: Comparison of the hysteretic curves of the experimental and analytical results of Specimen 7	150
Figure 5.32: Comparison of the envelope curves of the experimental and analytical results of Specimen 7	150
Figure 5.33: Damage states obtained at drift levels at certain drift levels at Specimen 7	152
Figure 5.34: Damage occurred at the end of the analysis at Specimen 7	153
Figure 6.1: Lateral load-top displacement curves for the infill panel thickness changes in Specimen 3	156
Figure 6.2: Envelope curves for the thickness changes in Specimen 3	156
Figure 6.3: Initial stiffness of Specimen 3 for the change in panel thickness	157
Figure 6.4: The comparison of cumulative energy dissipation capacities of Specimen 3 for the change in panel thickness	158
Figure 6.5: Base shear-top displacement curves for the infill panel thickness changes in Specimen 3	159
Figure 6.6: Envelope curves for the thickness changes in Specimen 3	159
Figure 6.7: Lateral load-top displacement curves for the infill panel thickness changes in Specimen 5	160
Figure 6.8: Envelope curves for the thickness changes in Specimen 5	160
Figure 6.9: Initial stiffness of Specimen 5 for the change in panel thickness	161
Figure 6.10: The comparison of cumulative energy dissipation capacities of Specimen 5 for the change in panel thickness	162
Figure 6.11: The gap, a , and the distance between the inside face of the columns, L , in the model used	163
Figure 6.12: Lateral load-top displacement curves for the gap size changes in Specimen 5	164
Figure 6.13: Envelope curves for the gap size changes in Specimen 5	165
Figure 6.14: The comparison of cumulative energy dissipation capacities of Specimen 5 for the gap size changes	166

Figure 6.15: Base shear-top displacement curves for the infill panel concrete compressive changes in Specimen 3	168
Figure 6.16: Envelope curves for the infill panel concrete compressive changes in Specimen 3	168
Figure 6.17: Initial stiffness of Specimen 3 for the infill panel concrete compressive changes	169
Figure 6.18: The comparison of cumulative energy dissipation capacities of Specimen 3 for the infill panel concrete compressive changes	170
Figure 6.19: The representative frame	171
Figure 6.20: Retrofitting of the frame by shotcreted walls	171
Figure 6.21: Cross section of the column	172
Figure 6.22: Cross section of the typical beam	172
Figure 6.23: Constitutive models used in analytical study	173
Figure 6.24: First mode shapes of bare and retrofitted frame	174
Figure 6.25: Base shear-top displacement and base shear/total weight-top displacement/total height diagram	175
Figure 6.26: The acceleration record of Erzincan Earthquake	176
Figure 6.27: The acceleration record of İzmit Earthquake	176
Figure 6.28: The acceleration record of Düzce Earthquake	176
Figure 6.29: “Service” type acceleration records	177
Figure 6.30: “Design” type acceleration records	177
Figure 6.31: Design spectrum defined in TEC, 2007	173
Figure 6.32: Time versus top displacement graphs for bare and retrofitted frame under service earthquakes	179
Figure 6.33: Time versus base shear force graphs for bare and retrofitted frame under service earthquakes	180
Figure 6.34: Time versus top displacement graphs for bare and retrofitted frame under design earthquakes	181
Figure 6.35: Time versus base shear force graphs for bare and retrofitted frame under design earthquakes	182
Figure 6.36: Comparison of the maximum story displacements of the frame with and without shotcrete panel for service and design earthquakes	183
Figure 6.37: Comparison of the maximum interstorey drift of the frame with and without shotcrete panel for service and design earthquakes	183
Figure 6.38: Comparison of the maximum interstorey shear force of the frame with and without shotcrete panel for service and design earthquakes	184
Figure 6.39: Performance of the bare and retrofitted systems under design earthquakes	185
Figure 6.40: Comprasion of the reinforcement strains of some critical sections with and without shotcrete panel for design Düzce earthquake	186
Figure 6.41: Comprasion of the reinforcement strains of some critical sections with and without shotcrete panel for design Erzincan earthquake	187

LIST OF SYMBOLS

a_1	: Transition Curve Shape Calibrating Coefficients
a_2	: Transition Curve Shape Calibrating Coefficients
A_1	: Strut Area 1
A_2	: Strut Area 2
b_w	: Equivalent width of the strut
D	: Longitudinal Bar Diameter
d_m	: Diagonal of the infill panel
D_r	: Lateral Displacement for Retrofitted Specimen
D_{ur}	: Lateral Displacement for Unretrofitted Specimen
$E_c I_c$: Bending stiffness of the columns
E_m	: Initial Young modulus of wall
E_s	: Modulus of Elasticity of Reinforcement
E_{sp}	: Post-yield Stiffness
e_{x1}	: Plastic unloading stiffness factor
e_{x2}	: Repeated cycle strain factor
f_c	: Compressive Strength of Concrete
f_{max}	: Maximum Stress of Reinforcement
f_{m0}	: Compressive strength of wall
F_r	: Lateral Resistance for Retrofitted Specimen
f_t	: Tensile Strength of Concrete
f_t	: Tensile strength of wall
F_u	: Lateral Resistance for Unretrofitted Specimen
f_{ult}	: Ultimate Stress Capacity
f_y	: Yield Stress of Reinforcement
H	: Specimen Height
h_w	: Height of the infill panel
h_z	: Equivalent contact length
K_A	: Strut stiffness
K_S	: Shear stiffness
k_c	: Confinement factor
L	: Transverse Reinforcement Spacing
$l_i(t)$: Load Factor
P	: Kinematic/isotropic Weighing Coefficient
P_i	: The applied load in a nodal position i
P_i^0	: Nominal Load
P_{max}	: Maximum Load
$P_{ultimate}$: Ultimate Load
r	: Spurious Unloading Corrective Parameter
R_0	: Transition Curve Initial Shape Parameter
t	: Infill Panel Thickness
x	: Column Width
X_{oi}	: Horizontal offsets

Y_{oi}	: Vertical offsets
Z	: Actual contact length
α_{ch}	: Strain inflection factor
α_{re}	: Strain reloading factor
α_s	: Reduction shear factor
β_a	: Complete unloading strain factor
β_{ch}	: Stress inflection factor
δ	: Displacement
Δ_{max}	: Maximum Displacement
$\Delta_{ultimate}$: Ultimate Displacement
ϵ_1	: Strut area reduction strain of wall
ϵ_2	: Residual strut area strain of wall
ϵ_c	: Strain at peak stress
ϵ_{cl}	: Closing strain of wall
ϵ_m	: Strain at maximum stress of wall
ϵ_{su}	: Ultimate Strain of Reinforcement
ϵ_{ult}	: Ultimate Strain Capacity
γ	: Specific weight
γ_{plr}	: Reloading stiffness factor
γ_{plu}	: Zero stress stiffness factor
γ_{un}	: Starting unloading stiffness factor
γ_s	: Proportion of stiffness assigned to shear
Λ	: Dimensionless relative stiffness parameter
μ	: Friction coefficient
μ	: Strain Hardening Parameter
τ_{max}	: Maximum shear strength
τ_0	: Shear bond strength
θ	: Angle of the diagonal strut with respect to the beams

DEPREM GÜVENLİĞİ YETERSİZ BETONARME ÇERÇEVELERİN PÜSKÜRTME BETON PANELLER İLE GÜÇLENDİRİLMESİ

ÖZET

Deprem güvenliği yetersiz olan yığma ve betonarme binaların güçlendirilmesinde kullanılmakta olan yöntemlerden biri, sistemde var olan dolgu duvarlara püskürtme beton uygulamasıdır. Bu uygulamadan yola çıkarak, püskürtme beton ve hasır donatı ile oluşturulan panellerin, betonarme çerçevelerin güçlendirilmesinde kullanılması konusu bu tez çalışmasında ele alınmıştır. Çalışma, deneysel ve analitik olmak üzere iki bölümden meydana gelmektedir.

Püskürtme beton ile oluşturulan panelin çerçeve davranışına katkısı, deneysel çalışma ile araştırılmıştır. Ülkemizdeki binaların çoğunluğunu temsil edebilmek amacıyla, deprem güvenliği yetersiz, güçlü kiriş/zayıf kolonlardan oluşan bir betonarme çerçeve ele alınmış ve bu çerçeve yaklaşık $\frac{1}{2}$ geometrik ölçekle küçültülerek deney numunesinin boyutları ve kesit özellikleri belirlenmiştir. Bu betonarme çerçeveler, içerisine klasik tuğla duvar yerine hasır donatı ve ıslak karışumlu püskürtme beton ile oluşturulmuş paneller yerleştirilerek güçlendirilmiştir. Toplam sekiz adet numune üretilmiştir. Numunelerden biri panelsiz bırakılan yalın çerçeve, bir diğeri ise içerisine geleneksel betonarme perde yerleştirilen perdeli çerçevedir. Bu şekilde üretilen yalın çerçeve ve perdeli çerçeve referans çerçevesi olarak kullanılmıştır. Numunelerden dört tanesi hasarsız betonarme çerçevenin, püskürtme beton ve hasır donatı ile oluşturulan paneller ile güçlendirilmesi ile elde edilen standart deney numuneleridir. Son iki numune ise, önceden hasar verilmiş ve tamir edilmiş betonarme çerçevenin püskürtme beton ve hasır donatı ile oluşturulan paneller ile güçlendirilmesi ile elde edilen deney numuneleridir. Numuneler, panelin çerçeveye bağlantısı bakımından iki gruba ayrılmaktadır. Birinci grup numunelerde, panel tüm çevresi boyunca çerçeveye bağlanmıştır. İkinci grup numunelerde ise panel sadece alt ve üstten kirişlere bağlanmış, kolonlara mesafeli olarak yerleştirilmiştir. Tek katlı, tek açıklıklı olarak üretilen numuneler, kolonlar üzerine etkiyen sabit eksenel yükler ile kiriş hizasından etkiyen tersinir tekrarlı yatay yükler etkisinde denenmiştir.

Çalışmanın kuramsal bölümünde; yapı sistemlerinin doğrusal olmayan analizini yapan *SeismoStruct* programı kullanılarak, deneysel olarak incelenen numunelerin kuramsal modelleri oluşturulmuştur. Bu kuramsal modellerde elde edilen kesit ve sistem davranışlarına ait büyüklükler, deneysel sonuçlar ile karşılaştırılmış ve yorumlanmıştır.

Deneysel ve kuramsal çalışmalar sonucunda; önerilen güçlendirme yönteminin betonarme çerçevenin yatay yük taşıma kapasitesi, yatay rijitlik ve enerji sönümleme özelliklerini önemli ölçüde arttırdığı görülmüştür. Önerilen yöntemin, binaların

depreme karşı güçlendirmesinde hızlı, kolay ve ucuz bir teknik olarak kullanılabilceđi düşünölmektedir.

RETROFITTING OF VULNERABLE REINFORCED CONCRETE FRAMES WITH SHOTCRETE PANELS

SUMMARY

Application of shotcrete concrete on the walls within the existing vulnerable reinforced concrete and masonry buildings is a known retrofitting technique. As an alternative to this application, construction of shotcrete infill panels in bare reinforced concrete frames is aimed in this thesis. The suggested method can be beneficial against conventional shear wall, when formwork and workmanship is expensive and accessing to the work area is difficult. The study consists of experimental and analytical parts.

In the experimental part, to evaluate the effectiveness of this retrofitting technique, an experimental research program was accomplished. Infill panels made from wet-mixed shotcrete in lieu of a traditional masonry are used in vulnerable reinforced concrete frames. The frames were chosen to represent weak column/strong beam type structures that were very common in Turkey especially for the buildings constructed before the two latest earthquake codes. The experimental work is composed of strengthening of four undamaged and two damaged frames with shotcrete panels and a bare frame and a conventional shear wall specimens as a reference. Nearly ½ scale, one bay- one story specimens were tested under constant vertical loads acting on the columns and lateral reversed cycling loads. The infill panels are connected to the surrounding reinforced concrete frame in two different ways. In the first case, full integration along four edges of the infill panel is achieved. In the second case, the infill panel is connected only to the beams of the frame having a distance between the columns and edges of the infill panel. To evaluate effectiveness of the proposed technique, response parameters of the retrofitted frame experiments were compared with those of the bare frame's and the conventional shear wall's.

In the analytical part of the thesis, SeismoStruct, a nonlinear finite element computer analysis program, has been used to generate the theoretical models of the tested specimens. The sectional and overall behaviors of the frames obtained from experimental and analytical works are compared with each other.

The experimental and analytical studies show that the proposed retrofitting technique for vulnerable reinforced concrete frames increases the lateral load carrying capacity, the lateral rigidity and the energy dissipation capacity of the system. It is considered that the suggested technique can be used as an efficient, easy and cost effective method in retrofitting the existing vulnerable reinforced concrete buildings.

1. INTRODUCTION

1.1 General

The existence of many vulnerable reinforced concrete buildings in earthquake prone areas built before the current Turkish earthquake code, presents one of the most serious problems facing Turkey, especially in Istanbul today. During 1999 Kocaeli Earthquake, buildings had greater damage than expected at that magnitude of an earthquake in the city. Since then researchers have been trying to find out cheap and easily applicable strengthening solutions for the vulnerable reinforced concrete (RC) and masonry buildings.

The experiments carried on, show that infill walls increase the lateral load carrying capacity and the lateral stiffness of the structures, (Klingner and Bertero, 1978, Govindan et al. 1986, Al-Chaar et al. 1996, Lee and Woo 2002). It can be stated that when the necessary precautions are taken, the infill walls can be used to strengthen the building against lateral loads, (Sugano and Fujimura, 1980, Zarnic and Tomazevic, 1984, Altin et al. 1992).

Strengthening a damaged RC frame with forming a thin concrete wall on the existing masonry walls (Zarnic and Tomazevic 1988, Yuksel et al. 1998a and 1998b) or using shotcrete on special wall-like structures in lieu of masonry walls (Mourtaja et al. 1998) showed that, these kinds of easily applicable retrofitting techniques increases lateral load carrying capacity and lateral rigidity of the structure.

Strengthening of infill walls using shotcrete is typically used in strengthening of damaged and/or undamaged masonry buildings in Turkey as stated in the studies of Wasti et al. (1997), Celep (1998), Aydođan and Öztürk (2002). In this thesis, using shotcrete panels in lieu of traditional masonry walls in reinforced concrete buildings is proposed and the overall responses of these frames responding in-plane lateral loading are investigated.

1.2 Objectives and Scope

In this study wet-mixed sprayed concrete is used to form an infill wall within a vulnerable RC frame. Nearly ½ scale, one story, one bay specimens were tested under constant vertical loads acting on the columns and lateral reversed cycling loads. The experimental work is composed of testing one bare frame for reference, six vulnerable RC frames by forming an infill wall using wet-mixed sprayed concrete and one conventional shear wall. In four of them, the walls are connected to the frames through shear studs used at four edges of them to create strong bond between walls and the members of the frames. In three of them; the walls are connected only to the beams through shear studs used at two edges of the infill wall, while the other two edges are distanced to the columns. One of the specimens from each group is slightly damaged and repairing of cracks has taken place before strengthening with shotcrete panels. Pre-reverse deflection is applied to the beam during construction of the shotcrete panel for the other two.

The main objectives of this research are:

- 1) To find out fast, cheap and adequate retrofitting techniques for vulnerable RC structures,
- 2) To set up and conduct a test program to investigate the behaviour of RC frames infilled with wet-mixed shotcrete panels, and to characterize the strength and stiffness behaviour of these frames responding to in-plane lateral loading.

In order to fulfill the objectives stated above, the following summarizes the work done in this study as undertaken in chronological order:

- 1) State the need for retrofitting the vulnerable RC frames and the advantages of using wet-mixed shotcrete (this will be stated in the upcoming literature review)
- 2) Select a reasonable testing scale considering the capacities of the testing facilities in Structural and Earthquake Engineering Laboratory of Istanbul Technical University (STEEL).
- 3) Conduct the standard material tests for the four different materials used, namely: frame concrete, shotcrete concrete, frame steel and panel steel.

- 4) Perform the main experimental program to investigate the effect of the shotcrete panel addition to the system.
- 5) A finite element program, named as SeismoStruct is used to develop an analytical model which is used for modelling the response of RC frames retrofitted with shotcrete panels. The experimental results were verified using the analytical models in the program.
- 6) Investigate the effects of the proposed retrofitting technique on a representative frame by using the analytical model developed for the response of the shotcrete wall,

1.3 Organization of the Thesis

This thesis is composed of seven chapters. Following this chapter, Chapter 2 explores the other retrofitting techniques as well as the types of shotcrete and tries to state the advantages of using wet-mixed shotcrete that is used in this study.

The experimental program is given in Chapter 3. The geometry and reinforcement details of the specimens, the data acquisition and loading system, and the results of material tests are also presented. The experimental results which discuss the effect of retrofitting the RC frames with wet-mixed shotcrete panels are given briefly in Chapter 4.

The analytical model used is explained in Chapter 5 and also the proposed model is verified using the experimental results. By using the analytical models developed, a parametric study is performed in Chapter 6. The panel thickness, the concrete compressive strength of the panel, the distance between the frame and the panel are the parameters that are examined in this study. The effect of the proposed retrofitting technique on a 2D frame of building representing the typical reinforced concrete frame type structures in Turkey is also discussed in this chapter. Finally, conclusions are presented in Chapter 7.

2. SEISMIC RETROFIT FOR REINFORCED CONCRETE BUILDING STRUCTURES

The ways to enhance the seismic capacity of existing structures are usually considered in two main ideas. First one is based on increasing the strength and stiffness of the structural system which can be done by major modifications to it. These modifications include the addition of structural walls, steel braces. The second way is based on deformation capacity of the components of the system. Here the ductility of components with inadequate capacities is increased and their specific limit states are satisfied. Retrofitting of each component of the system involves methods like the addition of concrete, steel or fiber reinforced polymer (FRP) jackets to columns for confinement.

2.1 System Strengthening and Stiffening

Strengthening the system increases the total lateral force capacity of the system. When the seismic capacity of the existing structures is improved, the performance of the building is moved to a better level by the stiffening of the system.

The retrofitting methods of existing structures are described below briefly. The influences of these methods on the overall behaviour of the structure are summarized in Figure 2.1.

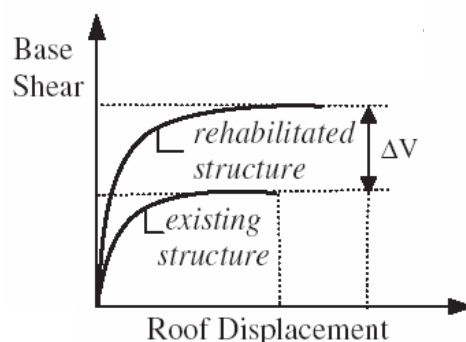


Figure 2.1: Global modification of the structural system, Thermou and Elnashai (2006)

The methods listed below are some of the repair and strengthening methods used for existing concrete structures.

2.1.1 Shear walls

Placing of reinforced concrete shear walls into an existing building is one of the most common methods used as repair and strengthening of structures. Although it increases the strength and stiffness of vulnerable buildings it is necessary to evacuate the habitants of the building during the construction.

Shear walls are efficient in controlling the overall lateral drifts and thereby reducing damage in frame members. Application of shear walls involves partial or total infilling of some of the bays of the frame. Existing infill walls can also be turned into shear walls and shotcrete can be used instead of regular concrete to increase the adherence between the existing and new material. To reduce time and cost, precast panels can be used as well.

Many research on structural walls and results of detailed applications have been reported, (Sugano and Fujimura 1980, Yuzugullu 1980, Higashi et al. 1980, Altin et al. 1992, Pincheira and Jirsa 1995, Frosh et al. 1996, Lombard et al. 2000, Inukai and Kaminosono 2000). The results show that the response of panels with the structure depends mainly on the application details. Proper anchorage of re-bars to beams and closely spaced mesh increases the deformation abilities and the strength is increased by full continuity between levels. If there is poor detailing and lack of load transfer between old and new members, this may lead to brittle failure of infill panels or reduction of ductility of the system.

One down side of the method is the need to strengthen the foundations. The strengthening is necessary, so that the foundations can resist the increased weight of the structure and the overturning moment. The application of this technique is usually costly, disruptive and unsuitable for building with an insufficient foundation system.

2.1.2 Carbon fiber reinforced polymer (CFRP) applied on the infill wall

Another method used in the rehabilitation of reinforced concrete structures is strengthening infill walls with fiber reinforced polymers (FRP). This technique improves the seismic performance of structures in terms of strength, stiffness and energy

dissipation capacity. When it is compared with other techniques, it is very simple and fast to apply and it is an efficient method because evacuation of the building is not required during the process, however it is expensive.

Marshall and Sweeney (2004) tested the effect of FRP strengthening. They observed that the failure mode of wall sections has also been changed by the different FRP configurations. As can be seen by these tests, FRP composites can be applied to increase the strength and change the failure mode of masonry walls in shear.

Erol et al. (2004, 2005, 2006 and 2008) performed a series of tests for examining the differences between the structural behaviour of infilled RC frames strengthened by CFRP fabric with different connection details. They observed that, the existence of CFRP keeps the brittle wall to fall apart and hence contributes to the overall in-plane and out- of-plane stability of structure during the load reversals.

2.1.3 Braced frames

Bracing frames with steel is one of the other methods to strengthen. However it does not provide as much strength and stiffness as the shear walls method. Mass of braced frames is less than the shear walls' and they do not increase the building mass significantly. Therefore seismic forces induced by the lateral load do not increase. Steel bracings are usually installed between existing members and an improvement for the foundation system might not be necessary.

It is difficult to connect bracing steel members to the existing concrete structure and the connections are vulnerable during earthquakes. The addition of steel bracing is effective for the strengthening and stiffening of existing buildings. In the selected bays of an RC frame, to increase the lateral resistance of the structure, concentric or eccentric bracings can be used.

Successful results of usage of steel bracing to upgrade RC structures have been reported by several researches; (Sugano and Fujimura 1980, Higashi et al. 1984, Badoux and Jirsa 1990, Miranda and Bertero 1990, Bush et al. 1991, Teran-Gilmore et al. 1995, Pincheira and Jirsa 1995, Goel and Masri 1996). After the 1985 Michoacan Earthquake a series of RC buildings retrofitted with steel bracing have been reported with no structural damage (Del Valle 1980, Foutch et al. 1988).

Taşkın et al. (2007) have examined effects of different types of bracings with different geometrical characteristics on the behavior of the system. In this study, instead of using conventional bracing system, a new concept has been tested and compared with the other systems. This approach is called as "Disposable Knee Bracing" and parametric analytical studies done giving successful results. As expected bracing has increased the horizontal load carrying capacity and energy absorption capacity, and most importantly, reduced the amount of damage on the main structure. After obtaining these promising results Yorgun et al. (2008) have done the experiments of these analytical models and come up with close results.

To increase damping; shear links and passive energy dissipation devices may also be used with bracings (Okada et al., 1992, Martinez-Romero, 1993). The addition of post-tensioned rods, which will yield at smaller deformations to the system, will allow energy dissipation at early stage of a large event. The initial brace prestressing induces additional forces in the structure and the internal force distribution is modified. These need to be considered for serviceability limit states.

2.1.4 Moment resisting frames

Moment resisting frames placed in buildings improve strength of the structure. Its advantage is that they occupy minimum floor space. However they have large lateral drift capacity when compared to the building they are placed in and this limits their use and cause the main problem for the system.

2.1.5 Diaphragm strengthening

Diaphragm strengthening uses methods such as topping slabs, metal plates laminated onto the top of the slab surface, bracing diaphragms below the concrete slabs and increasing the existing nailing in the covering. The covering can be replaced with stronger material or for buildings with timber diaphragms they could be replaced with plywood.

2.2 Enhancing Deformation Capacity

To enhance deformation capacity; column jacketing, strengthening and providing additional supports at places subjected to deformation are used. Below these will be explained in detail.

The methods to increase the deformation capacity of existing structures are described below briefly. How these methods affect the behaviour of the structure is summarized in Figure 2.2.

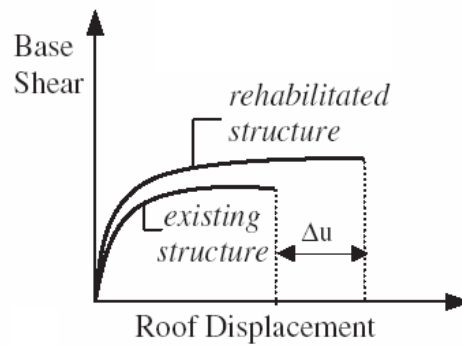


Figure 2.2: Local modification of structural components, Thermou and Elnashai (2006).

2.2.1 Column strengthening

For building with strong beam-weak column configurations, column strengthening is necessary as it will permit larger drifts and story mechanisms to be formed. In the seismic performance of a structure, column retrofitting is often critical as columns should not be the weakest components in the building structure. To increase the shear and flexural strength of columns, column jacketing may be used so that columns will not be damaged. The welding of the links between the new and existing reinforcement bars only need specialist knowledge. Rodriguez and Park (1991), Al-Chaar et al. (1996), Bousias et al. (2005), observed good results in their research.

Confining of columns with continuous steel plates and with fiber reinforced plastic fibers are the two techniques that jacketing can be made. Recent research has also shown the applications of composites especially fiber reinforced polymer (FRP) materials used as jackets when retrofitting columns. As these jackets confine the columns, column failure due to forming of a plastic hinge zone is prevented. The uncertainty of the bond between the jacket and the original member is the main disadvantage of this method.

Jacketing up of the slab has to be done before the construction of the jacketing of the column. If it is not done, then the load sharing does not take place until some large

seismic displacement has occurred. Until then this can cause considerable cracking, even under small frequent earthquakes.

2.2.2 Local stress reductions

Local stress reductions are applied to the elements which do not effect the performance of the building primarily. These can be done by demolition of local members that are not stiff and introducing joints between face of the column and adjacent architectural elements.

2.2.3 Supplemental support

Supplemental bearing supports are used on the gravity load bearing structural elements which are not effective in resisting lateral force induced by an earthquake.

2.3 Reducing Earthquake Demands

Reducing earthquake demands involve new and expensive special protective systems which modify the demand spectrum of the building while other methods improve the capacity of the building. The special protective systems are appropriate to use for important buildings such as historical buildings or for buildings which accommodate valuable equipments and machinery.

Base isolation, energy dissipation systems and mass reduction are the methods used in reducing earthquake demands will be explained briefly below.

2.3.1 Base isolation

In the upgrading of historical monuments, seismic isolation is accepted because it causes minimal disturbances. It is also applied in the upgrading of RC structures which are critical and need to be operational after seismic events. The aim of base isolation is to isolate the structure from the ground motion during earthquakes. This is achieved by installing bearings between the superstructure and its foundation. As most bearings have good energy dissipation characteristics, this method is effective for relatively stiff buildings with low rises and heavy loads.

Kawamura et al. (2000), applied seismic isolation technique to two middle-rise reinforced concrete buildings in Japan. One is a 16 story building, which was upgraded by lead rubber bearings (LRB's) were installed in their mid-height in 22 columns on the 8th story. Due to the reduction of seismic force by isolation, strengthening of the

structure is not necessary. The other building has 7 stories and is supported on piles, where base isolation method was adopted. After cutting off the head of piles, rubber and sliding isolators were installed in parallel. Therefore strengthening of the super structure has come to be unnecessary.

Base or seismic isolation methods are efficient in reducing response acceleration and interstorey drift which minimize structural and nonstructural damage.

2.3.2 Energy dissipation systems

Another method is using energy dissipation units (EDUs). These systems are used to reduce the displacement demands on the structure by the energy dissipation and are most effective when used in structures with great lateral deformation capacity. Frame structures are appropriate for these systems. These systems can also be used to protect critical systems and contents in a building.

Energy dissipation equipments are added to a structure via installing frictional, hysteretic or visco-elastic dampers as parts of braced frames. Many researchers have studied these energy dissipation methods, (Gates et al. 1990, Pekcan et al. 1995, Fu 1996, Tena-Colunga et al. 1997, Munshi 1998, Kunisue et al. 2000 and Kawamura et al. 2000). However, these methods are expensive and the application of them to all structures is costly.

2.3.3 Mass reduction

Mass reduction which decreases the natural period of the building is one of the methods used to lessen the demand on buildings. It can be done by removing some of the stories in the building.

2.4 Rehabilitation Methods for Unreinforced Masonry Walls

Various rehabilitation methods for unreinforced masonry walls (URM) exist and they can be listed as surface treatment, injection grouting, jacketing, internal reinforcement and mechanical fasteners. They will be explained in detail below.

2.4.1 Surface treatment

Surface treatment can be done by various materials and procedures. The most common types of surface treatment involve using reinforced plaster, shotcrete and ferrocement which are applied on top of a metal grid that is anchored to the existing wall. Hutchinson

et al. (1984) conducted experiments on various surface coatings to determine their effectiveness in restoring and improving the in-plane strength of a damaged masonry wall. They have concluded that they are usually effective.

Ferrocement is ideal for low cost housing since it is cheap and can be done with unskilled workers. It consists of closely spaced multiple layers of mesh of fine rods placed in a high strength (15-30 MPa) cement mortar layer of 10-50 mm thick. The reinforcement ratio used is 3-8%. Usage of ferrocement improves both in-plane and out-of-plane behavior of the wall. In-plane inelastic deformation capacity is improved as the mesh helps confining the masonry units after cracking. Abrams and Lynch (2001) used this retrofitting technique in a static cyclic test and observed that the in-plane lateral resistance is increased by a factor of 1.5. Out-of-plane stability is improved as ferrocement increases the ratio of the wall height-to-thickness.

Sheppard and Terceli (1980) used a thin layer of cement plaster which is applied over high strength steel reinforcement for retrofitting. The steel reinforcement is usually arranged as diagonal bars or vertical and horizontal meshes. This technique improves the in-plane resistance in diagonal tension and static cyclic tests by a factor of 1.25 to 3. In this method, the degree of masonry damage, strength of the cement mortar, thickness of layer, the reinforcement quantity and how it is bonded with the retrofitted wall effect how much improvement is achieved in strength.

Onto the masonry wall surface, shotcrete is sprayed over a mesh of reinforcement. When shotcrete is compared with other cast in-situ jackets, it is more convenient and cost less. Shotcrete thickness changes according to seismic conditions and it is at least 6 cm (Kahn 1984, Hutchison et al. 1984, Karantoni and Fardis 1992, Tomazevic 2000, Abrams and Lynch 2001). Shear dowels which are 6 to 13 mm in diameter and 25 to 120 mm in length are fixed into holes in the masonry wall using epoxy or cement grout. These are used to transfer the shear stresses between shotcrete and masonry.

Some researchers think that epoxy is required to be used on the brick as to develop the bond between shotcrete and the wall. Kahn (1984) has shown that dowels did not improve the response of composite panels or the bond between brick and shotcrete. He

has also observed that wetting the surface of the wall before the application of shotcrete did not affect the cracking or ultimate load. It slightly effects the inelastic deformations.

Using shotcrete on the retrofitted walls increases its ultimate load considerably. Kahn (1984) used a 90 mm thick shotcrete on one side of the wall in a diagonal tension test and found the ultimate load of URM panels to increase by a factor of 6.25. In a static cyclic test conducted by Abrams and Lynch (2001), the ultimate load of the retrofitted specimen increased by a factor of 3. They have observed contrary to Kahn (1984) that the increase in the cracking load was irrelevant in a diagonal tension test after shotcrete application.

Along with the advantages given above, there are some disadvantages in the application of the shotcrete such as the need for special equipment, skill and the significant waste in material due to rebound.

Application of shotcrete on the wall is assumed to resist lateral force applied to a retrofitted wall and the brick masonry is ignored (Hutchison et al. 1984, Abrams and Lynch 2001). This is reasonable as the flexural and shear strength of the reinforced shotcrete can be more than that of the URM wall, but cracking in the masonry can occur as the strains in the reinforcement in the shotcrete exceed yield. This can compromise the performance objective for the immediate occupancy or operations to be continued after a seismic event.

2.4.2 Injection grouting

Injection grouting is another method used as rehabilitation of unreinforced masonry walls. It is usually applied to repair small cracks or to fill ungrouted cores. The main purpose of injections is to restore the original integrity of the retrofitted wall and to fill the voids and cracks, which are present in the masonry due to physical and chemical deterioration and/or mechanical actions.

Epoxy is used for small cracks or small holes (less than 2 mm wide) and sand cement mixed grout is used for larger holes (Calvi and Magenes 1994, Schuller et al. 1994). The results of four clay brick walls which were repaired using injection grouting tested show that the original strength of the wall prior to its damage was restored (Manzouri et al. 1996).

Holes and cracks are present in the masonry walls as it weakens due mechanical actions or physical and chemical deterioration. Injection grouting is used to fill these and to re-establish the integrity of the wall. Whether the grout mix can be injected which depends on its mechanical and chemical properties or the method used affect the success of the retrofit of the wall.

Schuller et al. (1994) found that a cement based grout injection can restore about 80% of the compressive strength of the unretrofitted masonry. Other researchers reported that 80 to 110% of in-plane stiffness and 80 to 140% of in-plane lateral resistance of the unretrofitted wall can be restored with that kind of injection (Sheppard and Terceli 1980, Calvi and Magenes 1994, Manzouri et al. 1996). Also, the interface shear bond of multiwythe stonewalls can be amplified by a factor of 25-40 (Hamid et al. 1999). If epoxy is used as an injection material, the retrofitted wall is usually stiffer than the unretrofitted one, then the increase in stiffness which is 10-20% is much less than the increase in strength. Lateral resistance of the retrofitted wall increases by a factor of 2-4.

2.4.3 Jacketing

Jacketing forms a frame around the damaged wall with cast in-place concrete or external steel elements. For the existing URM buildings, steel plates or tubes can be used as external reinforcement which can be attached directly to the existing diaphragm and wall. Cracking in the masonry structure will occur in a seismic event and when this reaches sufficient amount, the jacketed steel system will have comparable stiffness and be effective (Hamid et al. 1994, Rai and Goel 1996).

Taghdi (2000a, 2000b) showed that the lateral in-plane resistance of the retrofitted wall increases by a factor of 4.5 with the usage of vertical and diagonal bracing. This increase is limited as the masonry is crushed and the vertical strips are buckled. The external steel system presents an effective energy dissipation mechanism (Rai and Goel 1996, Taghdi 2000a, 2000b).

2.4.4 Reinforcing bars

Reinforcing bars are usually used in hollow walls where cores will be opened and a steel bar will be placed inside and grouted. Prestressed tendons can also be used to improve the performance of the wall (Lissel et al. 1998). The holes opened are vertical which

extent from the top of the wall to the basement wall. When it is grouted with the reinforcing bar inside it, it provides a "homogeneous" structural element (Plecnik et al. 1986). This vertical column provides strength to the wall with a capacity to resist both in-plane and out-of-plane loading and it is anchored to the roof and floors with lateral ties.

The grout consists of a binder material like cement, polyester or epoxy and a filler material like sand. Plecnik et al. (1986) have performed shear tests on cement grout specimens which were 30% weaker than the ones with sand/epoxy or sand/polyester grouts. When the cost is considered, it is better to use polyester keeping the volume ratio of sand to polyester 1:1 and 2:1. Shear resistance depends on the volume ratios of the components for cement-based grout. The best type of grout has a volume ratio of cement to lime to sand of 1:0.125:1.

Abrams and Lynch (2001) used the reinforcing bars method to double the resistance of URM wall in a static cyclic test. They have observed that even though the lateral displacement achieved was high, the energy dissipated was limited. One advantage of using this system as a retrofit method is that, it will not alter the appearance of wall surface or the function of the building as it is done externally. The main disadvantage of this method is that, it creates zones with widely varying stiffness and strength.

2.4.5 Mechanical anchors

Mechanical anchors or ties can be used between the wall and the surrounding structure to provide better transfer of forces and continuity. Main disadvantage of this method is that, steel bars corrode. Lissel and Shrive (2003) overcome this problem by introducing fiber reinforced plastic.

Post-tensioning can be used to retrofit structures like historical monuments. This method involves a compressive force applied to masonry wall which counteracts the tensile stresses resulting from lateral loads. In the last ten years, there have been many researches on post-tensioning globally (Karantoni and Fardis 1992, Ingham et al. 1998, Lissel et al. 1999, Foti and Monac 2000, Laursen et al. 2002, Lissel and Shrive 2003, Rosenboom and Kowalsky 2004, Schultz et al. 2003).

In and out of plane ultimate behaviors of wall, cracking load and distribution improve when vertical post-tensioning is applied. Some basic calculations of principle stresses show that the horizontal post tensioning improves the resistance. However the experimental test performed by Page and Huizer (1994) did not prove these calculations. Karantoni and Fardis (1992) show that horizontal post-tensioning of spandrels did not significantly improve the building behavior by a linear finite element model they have done. They also show that when horizontal and vertical post-tensioning is combined together, the resulting positive effect is higher than the sum of the individual effects of the two directions post-tensioning.

The methods discussed in this section need rigorous work and in some cases involve the use of expert workmanship. They could be disruptive to the normal operation of a building and some methods can add up to 15 cm thickness to the wall which could require foundations to be improved. These may increase the inertial forces generated by an earthquake.

2.5 What is Shotcrete

Spraying of concrete is applied first in the United States as early as 1907 and has been known since. The product used was named “gunite” which was sprayed with easily operated compressed air pumps. In some cases, instead of conventional concrete shotcrete is used for its convenience, cost or time saving. It can be used when formwork is expensive or not practical and access to the work area is difficult, thin layers or variable thicknesses are required or normal casting techniques cannot be employed. Shotcrete requires a small, portable plant for manufacture and placement and can be applied in areas where limited access is available to make repairs in structures.

When shotcrete is accurately applied, it will show good bonding characteristics to existing concrete, rock, steel and be a structurally sound and durable construction material. If physical properties of shotcrete are compared with concrete or mortar with the same composition, it is similar and sometimes better than them. It has low absorption, good resistance to weathering and some chemical attacks, and high strength.

2.5.1 Types of shotcrete according to the application process

Types of shotcrete depend on which technique is used during its application. These are dry and wet mix processes that will be explained in detail below.

a) Dry-mix process:

The dry-mix process is a method where the cement and aggregate are mixed either at a site-based plant or pre-mixed and filled dried into silos or bags. This mixed material is placed into a dry-mix sprayed concrete pump and by the help of compressed air, it is brought to the nozzle. At the nozzle, the water necessary for hydration is added depending on the judgment of the operator.

Dry-mix system is simple and it has been used in the past as there could be few mechanical and mix design issues which can go wrong. The disadvantages of this method are the dust generated from the system which has an impact on the environment, the cost of wear of components of the machine used and the rebound of the material. The rebound from the surface can be between 15% to 40%, and it can be reduced with the usage of additives and admixtures. The capacity of machines effect the performance and the properties of the sprayed concrete vary. The reason is the materials may not be mixed properly, the cement-water ratios are unknown and changes and the mix might be hydrated before it is brought to the pump.

b) Wet-mix process

As in the case of conventional concrete, a ready-mixed concrete is used. Therefore it is possible to control the ratio of cement and water mixed, and the quality. The concrete from the ready mix plant is placed into the pump, pushed through with pressure and at the nozzle air is added at a rate between 7 to 15 m³/min, and the pressure used is 7 bars. To achieve good compaction and adherence to the surface, the air is added to increase the speed of the concrete.

The advantages of this method are 5 to 10% of aggregate rebound occurs, as low dust is produced the working environment is better, and as admixtures are used, thick layers are produced. Ratio of water to cement is controlled and can be as low as 0.37, and the concrete can be considered as a permanent element of the structure. As the materials are mixed before, change in quality is minimized and the effect of the operator is reduced.

Capacity of the output varies from 4 to 25 m³/hr, it is possible to add steel/synthetic fibres and additives. The listed advantages make this method economical.

The disadvantages of the wet-mix are that the cleaning costs, limited conveying distance which is maximum 300 m and the need for mix design. Also if it is not mixed on site, the mixing plant has to be given the volumes of the mixtures and it has to be controlled thoroughly.

2.5.2 Usage of shotcrete

Shotcrete can be used in other applications like repair of buildings, bridges, in underground excavations, slope and surface protection, and in new structures.

Shotcrete is commonly used for repair of fire and earthquake damage and deterioration and encasing structural steel for fireproofing. The repair of structural members such as beams, columns, strengthening walls and connections is common for structures damaged by an earthquake. It can also be used to repair the damaged surface of steel, wood or concrete structures if the surfaces can be reached.

Shotcrete can be used to save time when thin sections and large areas are present in the construction of new structures. These structures are pools, tanks, floors, walls and domes. Zynda (2007) published a report about constructing a four-story parking garage using shotcrete and precast beams, columns, and architectural walls. The project was completed in record time with shotcrete application. Shotcrete was used throughout the project, starting with the original shoring needed, the structural shear walls, and the 9.1 m-high retaining walls. Shotcrete is also used in forming and construction of structural shotcrete walls and foundation walls, (Robbins 2004 and Von der Hofen 2008).

2.5.3 Types of shotcrete

There are different types of shotcrete like fiber-reinforced, silica-fume, polymer-modified and accelerated. These will be explained briefly below.

a) Fiber-reinforced shotcrete

When shotcrete is subjected to tensile stresses or strains, it will crack like the concrete if it is not reinforced. Therefore fibers are added to the shotcrete mixtures to increase capacity of energy absorption, impact resistance and ductility of the material. This

composite material will have an increased ultimate strength. Steel, glass or synthetic fibers can be used in shotcrete.

- Steel fibers have been used since the late 1950s. Uniform distribution of fibers in a mixture was caused by problems in mixing and handling them earlier. These have been minimized by keeping the ratio of length to diameter low of the fibers produced, surface deformations and improved shape.
- Glass-fibers and a resin binder are used together to obtain glass fiber reinforced shotcrete. The application of this type of concrete requires a special gun and equipment. This process is used extensively in the construction of lightweight panels for building cladding and special architectural features and is usually applied in a plant production situation.
- Nylon, polypropylene, polyethylene, polyester and rayon make synthetic fibers. Decreasing the width of shrinkage cracks in the material is the primary benefit of adding synthetic fibers to shotcrete.

b) Silica-fume shotcrete

Silica-fume which is a fine non-crystalline pozzolanic material that is mostly made up of silica is used in shotcrete to increase strength. It also decreases permeability and enhance cohesion and adhesion. Advantages of using silica-fume shotcrete are to improve the bond strength between shotcrete and applied surfaces and cohesion. Thicker layers of shotcrete can be applied in a single pass to surfaces whether vertical or overhead.

When silica-fume shotcrete is used, the rebound is significantly reduced and the action of flowing water is reduced. Also this type of shotcrete can have more resistance to aggressive chemicals.

Silica-fume shotcrete can be used in polymer modified and accelerated shotcrete applications. It can be used in many applications instead of ordinary shotcrete due to its high performance in bonding and strength.

Silica-fume shotcrete is used in construction of tunnels with fibers to control shrinkage cracking.

c) Polymer-modified shotcrete

There are two methods to introduce polymers into shotcrete which are to use polymer material as a binder and to form a continuous polymer matrix with replacing mixing water with a polymer. In the first method, the shotcrete becomes a polymer shotcrete and in the second one which is more common is to add a polymer emulsion to the hydraulic-cement mixture and it is named as polymer-portland-cement shotcrete.

The polymers used in shotcrete improve tensile and flexural strengths, improve bonding and reduce absorption.

d) Accelerated shotcrete

Accelerating admixtures are used in shotcrete to rapidly set shotcrete. These are powdered materials added to dry-mix shotcrete which are called super-accelerators. They can be powdered or liquid admixtures used in dry and wet-mix shotcrete. In the wet-mix shotcrete usually the accelerator are added at the nozzle.

Accelerated shotcrete are used in tunnel support and linings, seawalls, dams, roof construction, slope protection and water-retaining structures such as canals, thick concrete sections, rapid repairs and sealing leaks.

3. TEST PROGRAM AND MATERIAL CHARACTERIZATION

This chapter describes the experimental test program that was carried out at STEEL to evaluate the performance of a structural system consisting of shotcrete panel in existing vulnerable RC frames. All test specimens are single story, single bay frames. One bare frame and a conventional shear wall, three fully and three partially infilled RC frames with shotcrete panels were tested. Description of the test specimens, test-setup, data acquisition, instrumentation and material properties are presented here.

3.1 Test Specimens

In this study, panels made from wet-mixed shotcrete in lieu of a traditional masonry are used to form an infill wall within existing vulnerable RC frame as shown in Figure 3.1 and Figure 3.2. The RC frames were chosen to represent the weak column/strong beam type structures that were very common in Turkey especially for the buildings constructed before 1998 Turkish Earthquake Code. The specimens had non-seismic details such as large spacing of hoops, no hoop in beam-column connection region and no use of 135° seismic hooks.

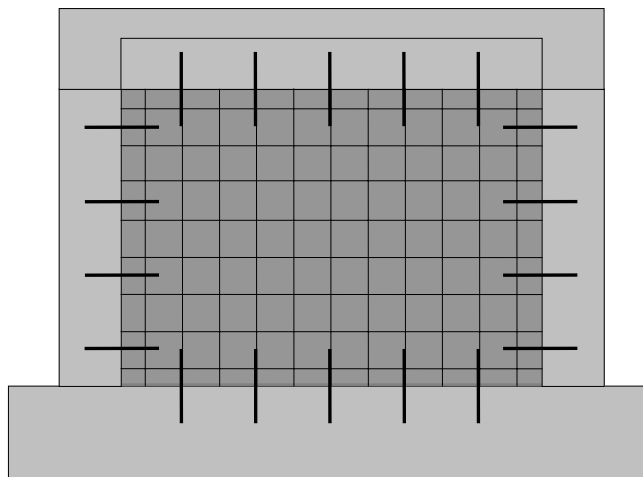


Figure 3.1: General view of the fully infilled frame

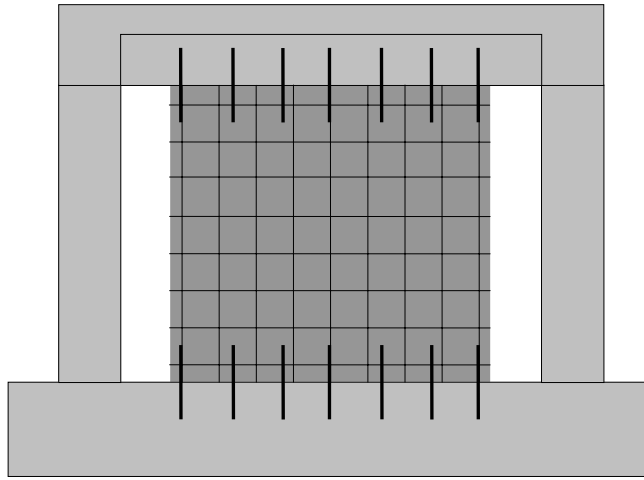


Figure 3.2: General view of the partially infilled frame

Tested specimens are summarised in Table 3.1.

Foundations of the specimens are fixed to the adapter foundation through 28 $\phi 50$ mm holes with $\phi 39$ mm anchorage bolts as shown in Figure 3.3. Depending on the experiences obtained from other infilled frame experiments, the rocking and global sliding of the frame does not occur during the experiments. Therefore the number of $\phi 39$ mm anchorage bolts is enough to assume that the connection of foundation of the specimens is similar to fixed supports.

One story, one bay nearly half-scale RC frames with a portion of slab on top and a foundation at the bottom has been constructed in the laboratory. The cross sectional dimensions of columns and beam of the frames are 20 cm by 25 cm and 20 cm by 32.5 cm, respectively. The height and the width of the frames are 152.5 cm and 220 cm, respectively. The height of the shotcrete panel is 170 cm and the width is 170 cm and 130 cm. The dimensions and the reinforcement detail of the frames are given in Figures 3.3 and 3.4. The details of panels are given in Figure 3.5. Longitudinal reinforcement of the frames consist of 16 mm steel bars which have average yield stress of 270 N/mm^2 , and the wire mesh used in the panels has a diameter of 4.5 mm and yield stress of 320 N/mm^2 . The reinforcement ratio of the column and the panel are %1.6 and %0.2 respectively.

Table 3.1: Test specimens

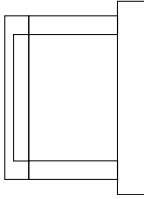
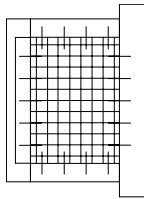
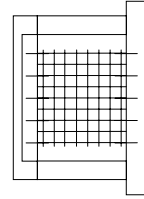
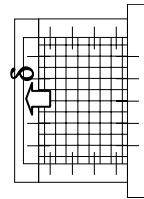
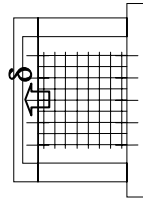
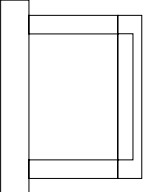
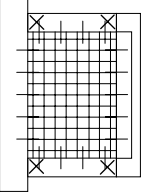
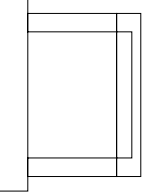
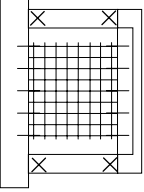
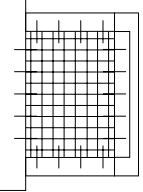
Specimen	Type	Frame condition		Gap space between panel and columns	Pre-reverse deflection	28 day concrete compressive strength (MPa)	
		Undamaged	Damaged & repaired			Frame	Panel
Specimen 1		YES	NO	NO	NO	16	-
Specimen 3		YES	NO	NO	NO	10	22
Specimen 5		YES	NO	YES	NO	12	35
Specimen 6		YES	NO	NO	YES	14	25
Specimen 7		YES	NO	YES	YES	12	25

Table 3.1: Test specimens (contd.)

Specimen	Type	Frame condition		Gap space between panel and columns	Pre-reverse deflection	28 day concrete compressive strength (MPa)	
		Undamaged	Damaged & repaired			Frame	Panel
Specimen 2		YES	NO	NO	NO	16	-
Specimen 2S		NO	YES	NO	NO	16	35
Specimen 4		YES	NO	NO	NO	12	
Specimen 4S		NO	YES	YES	NO	12	35
Specimen 8		YES	NO	NO	NO	12	40

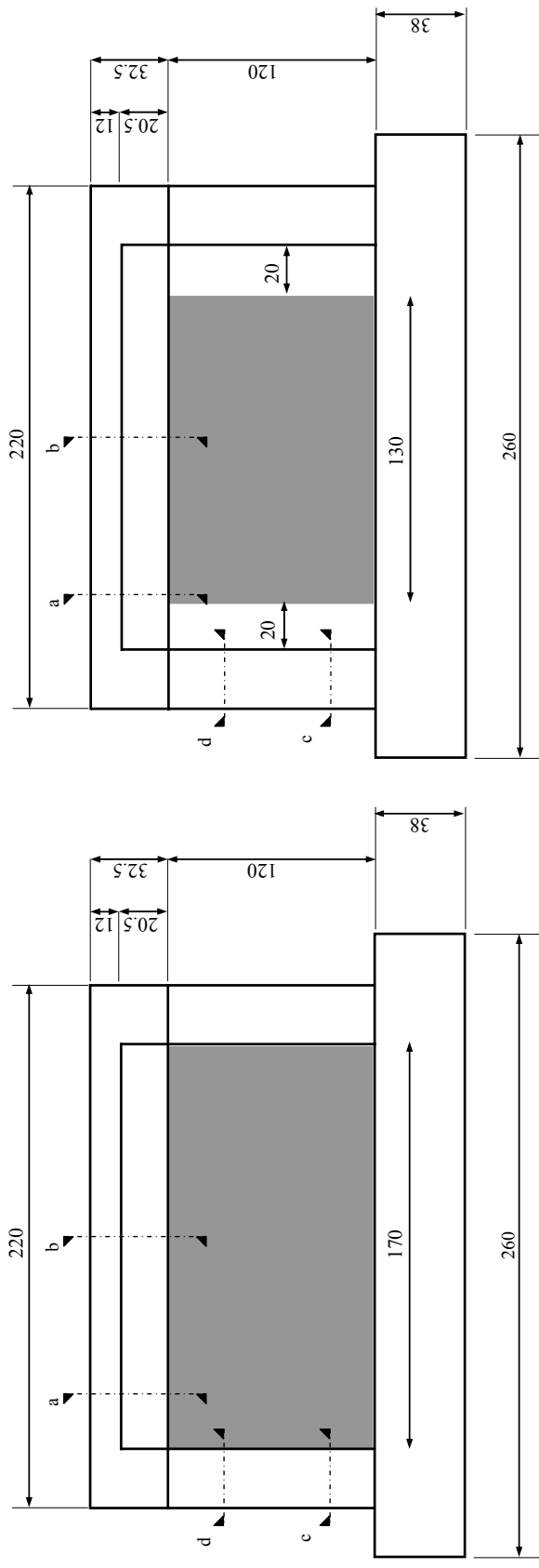
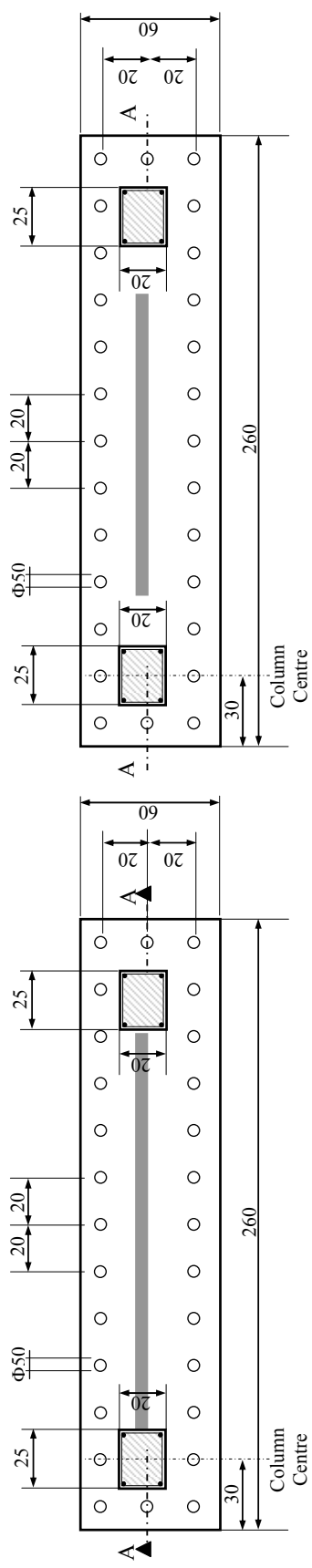


Figure 3.3: Geometry of the specimens

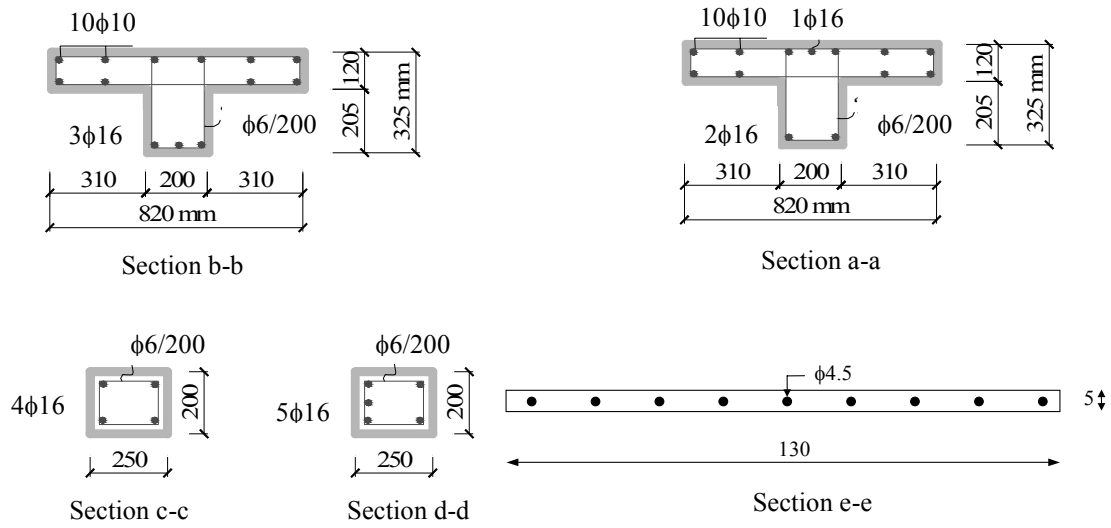


Figure 3.4: Reinforcement details of the frame

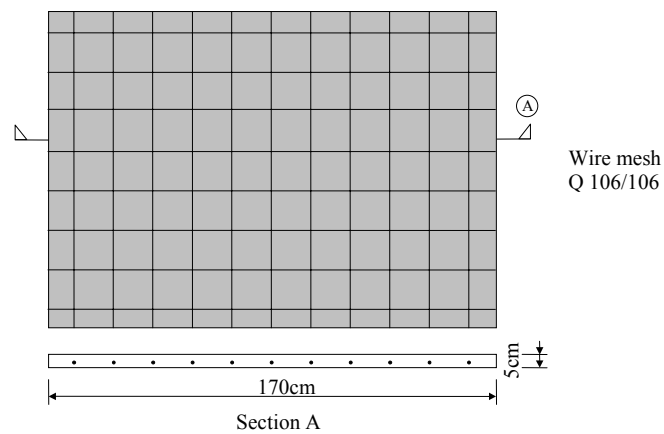


Figure 3.5: Reinforcement details of the panel

Longitudinal reinforcement of the columns continues to the bottom of the foundations of the specimens which are 38 cm thick. There is no lap-splice at the level of foundation.

Specimen 1 is the bare frame which is tested as a reference specimen.

Specimens 2 and 4 are the bare frames which are tested up to a certain damage level, before constructing the shotcrete panel in Specimens 2S and 4S. These bare frames are tested till 10.5 cm-displacement which is the displacement level at which the main reinforcement yield. These damaged bare frames are repaired by injection of epoxy into the cracks which were formed at different locations of the columns following the subsequent steps below;

- 10 cm deep holes are drilled at the edge of the cracks,
- the steel dowels are fixed into these holes by using epoxy resin as can be seen in Figures 3.6b and 3.6c,
- at least 8 hours later, the epoxy resin are injected into these dowels and all these cracks are filled with epoxy resin as can be seen in Figures 3.6d and 3.6e.

After that, a wire mesh (Q 106/106) consisting of $\Phi 4.5$ mm steel bars is placed at the center axis of the frame. Full contact of the panel is established by lapping the infill reinforcement to the anchorages placed in the frame members. The anchorages used are $\Phi 10$ mm steel bars which are placed in the beam of the frame 20 cm apart from each other in partially infilled frames by epoxy resin. In fully infilled frames, the anchorages are placed in the beam and the columns 30 cm apart from each other. The lengths of the anchorages are 35 cm; 25 cm of it is in the panel while 15 cm is in the beam. By using wet-mixed sprayed concrete, 5 cm thick RC panel is formed as shown in Figure 3.7. The panel formed is attached to the frame by all sides to form Specimen 2S while in Specimen 4S, the panel is attached only to the beams and the panel is placed 20 cm to the columns.

Construction of Specimens 3, 5, 6 and 7 are identical except that the RC frames were not damaged.

Specimen 5 is identical to Specimen 4S in which the shotcrete panel is only connected to the beams, not connected to the columns and is placed 20 cm away

from the columns as shown in Figure 3.7. Shotcrete panel is constructed in a non-damaged frame. While deciding the width of this panel, the region on the beam where moment is supposed to be small under lateral and vertical loads is taken into account.

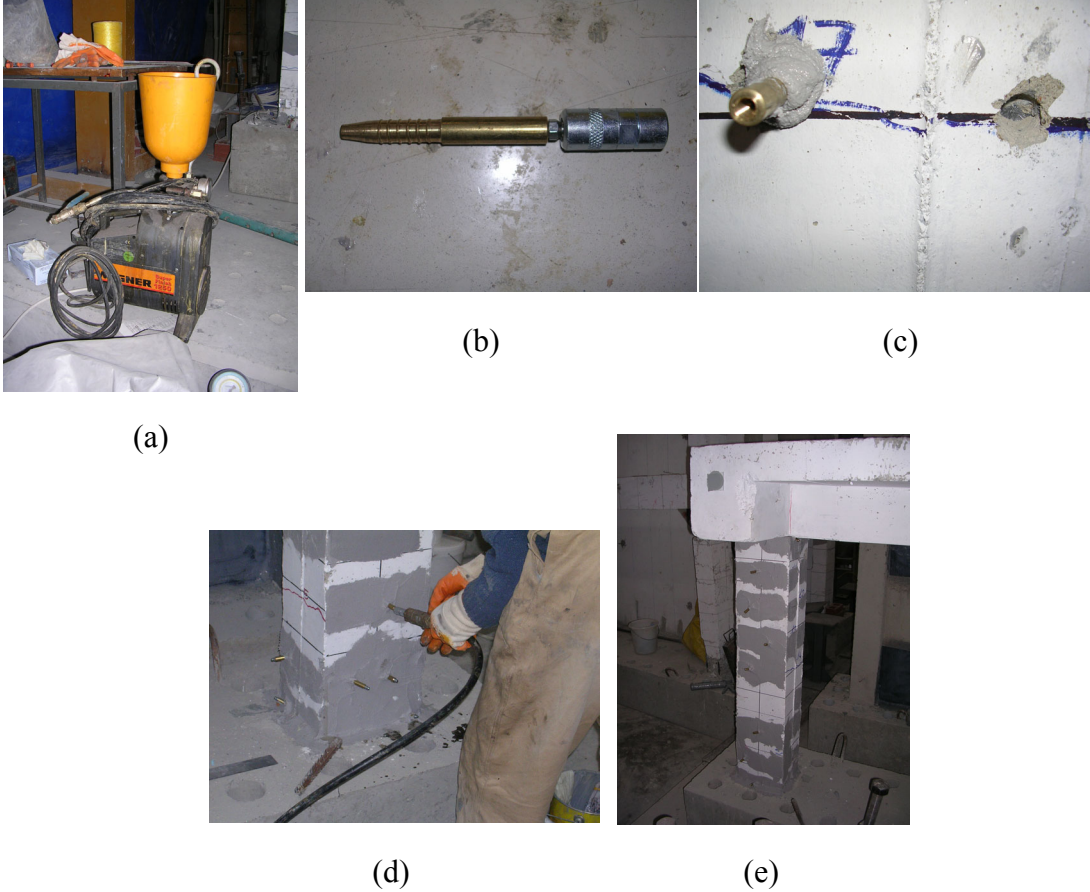


Figure 3.6: Repairing process of the damaged bare frames

Although the construction of Specimens 6 and 7 are similar to the others explained above, pre-reverse deflection is applied to the beam during construction of the shotcrete panel as can be seen in Figure 3.8. Before constructing the shotcrete panel, special screws are placed symmetrically to the right and left side of the beam in the middle between the foundation and the floor. Pre-reverse deflection applied to both specimens is 7.4 mm and it was applied with mechanical force which is produced by the screws. The idea behind the amount of the pre-reverse deflection is that after the application of the pre-reverse deflection, the cracks that will occur in beams and columns to be small in width and therefore no special repairing will be needed. Considering this fact, some calculations are done and the reasonable amount of the pre-reverse deflection is found to be 1/300-1/250 of the span. In Specimen 6, the

panel is connected to the surrounding frame by all its four sides, while in Specimen 7 the panel is connected only to the beams.

During the process, the deflection is continuously measured in the middle of the beam with a displacement transducer. As expected, shear cracks at columns and flexural cracks at the tension side of the beam occurred during pre-reverse deflection process. The amount of deflection is 7.4 mm which is almost 1/260 of the span. The maximum crack width occurred is 0.1 mm on the columns and 0.4 mm on the beam.

By applying the pre-reverse deflection to the beam; the shotcrete panel and the frame around it, are supposed to work together for a long time ensuring that the lateral loads are transferred better through the system.



Figure 3.7: Construction of the shotcrete panels

Specimen 8 is a typical shear wall having the same reinforcement as the shotcrete panels which can be seen in Figure 3.9. Two layers of formwork are used and the concrete is poured from right beside the beam. The concrete of the shear wall is prepared in Construction Materials Laboratory of ITU Civil Engineering Faculty. After removing the formwork of the shear wall, some gaps were present at the upper side of the wall where the concrete is poured from. Therefore these gaps are fixed with “repairing mortar”.



Figure 3.8: Specimens 6 and 7 having pre-reverse deflection on beam



Figure 3.9: Construction of Specimen 8

3.2 Test Setup, Instrumentation and Data Acquisition

Test setup, instrumentation and data acquisition system are described in this section. Details of the test setup including figures and experimental requirements are given in the following subsections.

3.2.1 Test setup and loading system

A typical test-setup is shown in Figure 3.10. Axial load which is kept constant throughout the test is applied on the columns and lateral cycling load imposed as displacement reversals is applied to the specimen by means of a hydraulic jack and two MTS 250 kN-capacity hydraulic actuators that are placed at the beam level, respectively.

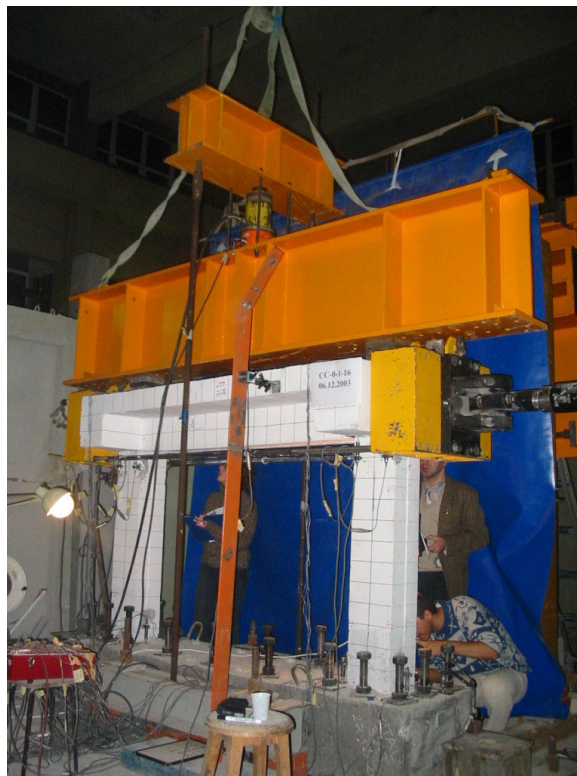


Figure 3.10: Test setup

The physical capacities of one actuator for load are ± 250 kN and for displacement is ± 300 mm. Controlling of actuators are force-based or displacement-based. The data collected during the tests are force and displacement of the actuators, and the displacements taken by the linear variable displacement transducers (LVDT) connected to various positions on the specimen. Displacement-based load protocol

was used during the tests. The high sensitive LVDT which has measured top displacement of the specimen was assigned as the control displacement.

The axial loading system works independently from the lateral loading system. The axial loads acting on two columns of the specimen are the support reactions of the rigid steel beam placed on top of the specimen. The required axial load level is controlled by a hydraulic jack and a load cell placed on steel beam. The intensity of the axial load which is kept constant throughout the test is 20 % of the axial load carrying capacity of columns.

3.2.2 Instrumentation and data acquisition

LVDTs are placed on some critical positions to measure the displacements and deformations of the specimens. The applied load and displacement of the hydraulic actuator are also measured and recorded. The LVDTs are connected to a TML ASW 50C switch-box and TDS 302 data logger, which provide AC power, signal amplification, AC-to-DC conversion and electrical balancing.

The number of LVDTs used, their types and the measurement purpose are listed in Table 3.2 and their places are shown in Figure 3.11 for bare frame; in Table 3.3 and in Figure 3.12 for fully infilled frames and in Table 3.4 and in Figure 3.13 for partially infilled frames. The rotation of the columns and the wall, the relative displacement of the whole specimen and the frame, the target displacement which is watched through two channels that is the relative top displacement of the specimen, the top displacements of the column and the wall, the out of plane behaviour of the specimen, elongation and shortening of the wall are measured. For the specimens with pre-reversed beam, six more LVDTs are placed on the specimens. The two of them are for measuring the displacement of reversely deflected beam and four of them are for measuring the axial deformation of the columns.

Table 3.2: LVDTs used for bare frame

Name	LVDT type	Measurement purpose	Attached to
T1	CDP5	Top displacement	Reference frame
T2	CDP25	Top displacement	Reference frame
T3	CDP5	Displacement of the whole system	Reference frame
T4	CDP5	Displacement of the frame	Reference frame
T5	CDP25	Column displacement	Reference frame
T6	CDP25	Out of plane displacement	Reference frame
T7	CDP10	Column lower rotation	Specimen
T8	CDP10	Column lower rotation	Specimen
T9	CDP10	Column lower rotation	Specimen
T10	CDP10	Column lower rotation	Specimen
T11	CDP10	Column upper rotation	Specimen
T12	CDP10	Column upper rotation	Specimen
T13	CDP5	Column upper rotation	Specimen
T14	CDP5	Column upper rotation	Specimen

Table 3.3: LVDTs used for fully infilled frame

Name	LVDT type	Measurement purpose	Attached to
T1	CDP25	Top displacement	Reference frame
T2	CDP100	Top displacement	Reference frame
T3	CDP5	Panel displacement	Reference frame
T4	CDP25	Column displacement	Reference frame
T5	CDP100	Panel front diagonal	Specimen
T6	CDP5	Panel back diagonal	Specimen
T7	CDP50	Displacement of the frame	Reference frame
T8	CDP25	Displacement of the whole system	Reference frame
T9	CDP25	Right column lower rotation	Specimen
T10	CDP25	Right column lower rotation	Specimen
T11	CDP25	Panel rotation	Specimen
T12	CDP25	Panel rotation	Specimen
T13	CDP25	Panel rotation	Specimen
T14	CDP25	Left column lower rotation	Specimen
T15	CDP25	Left column lower rotation	Specimen
T16	CDP10	Out of plane displacement	Reference frame
T17	CDP10	Right column upper rotation	Specimen
T18	CDP10	Right column upper rotation	Specimen
T19	CDP10	Left column upper rotation	Specimen
T20	CDP10	Left column upper rotation	Specimen

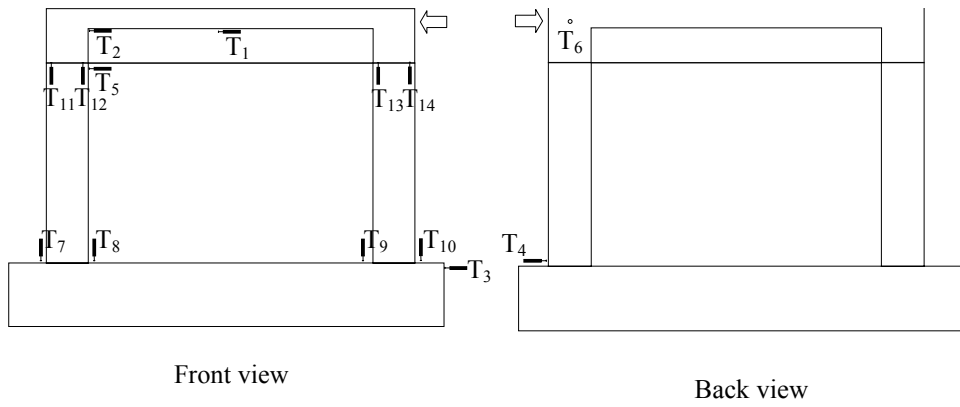


Figure 3.11: Locations of LVDTs on bare frames

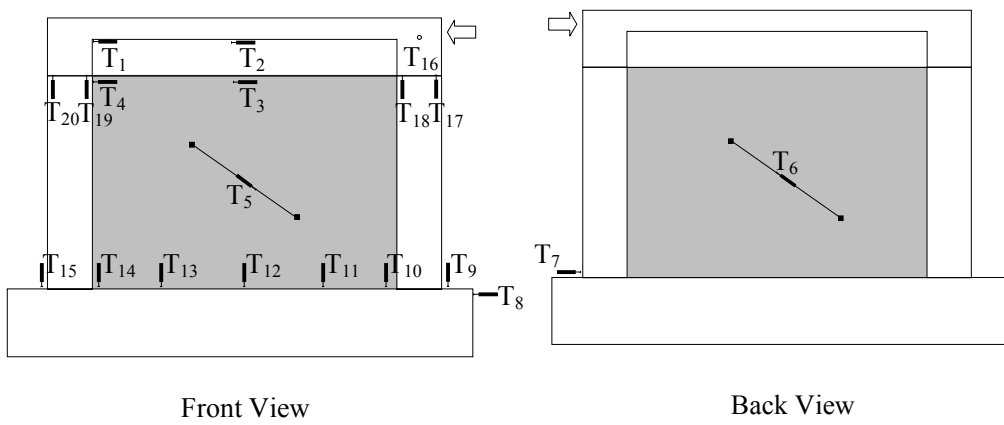


Figure 3.12: Locations of LVDTs on fully infilled frames

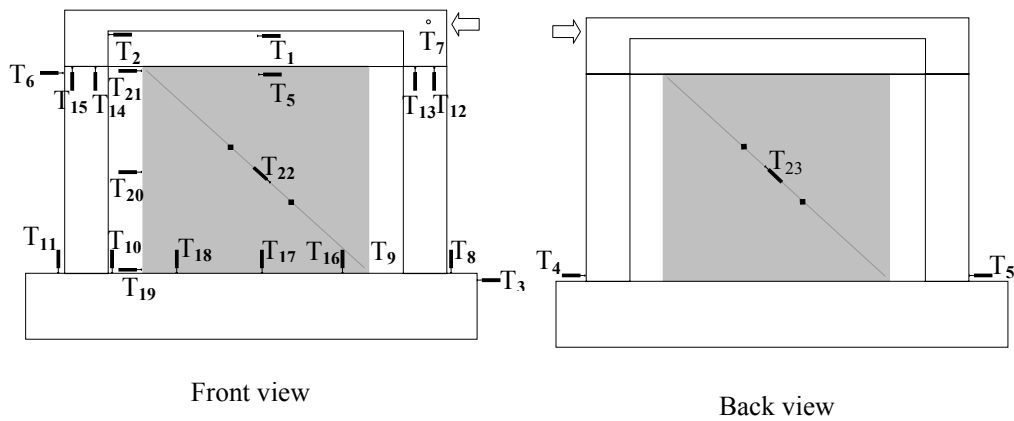


Figure 3.13: Locations of LVDTs on partially infilled frames

Table 3.4: LVDTs used for partially infilled frame

Name	LVDT type	Measurement purpose	Attached to
T1	CDP25	Top displacement	Reference frame
T2	CDP100	Top displacement	Reference frame
T3	CDP5	Displacement of the whole system	Reference frame
T4	CDP5	Displacement of the frame	Reference frame
T5	CDP5	Displacement of the frame	Reference frame
T6	CDP100	Column displacement	Reference frame
T7	CDP50	Out of plane	Reference frame
T8	CDP25	Right column lower rotation	Specimen
T9	CDP25	Right column lower rotation	Specimen
T10	CDP25	Left column lower rotation	Specimen
T11	CDP25	Left column lower rotation	Specimen
T12	CDP25	Right column upper rotation	Specimen
T13	CDP25	Right column upper rotation	Specimen
T14	CDP25	Left column upper rotation	Specimen
T15	CDP25	Left column upper rotation	Specimen
T16	CDP10	Panel rotation	Reference frame
T17	CDP10	Panel rotation	Reference frame
T18	CDP10	Panel rotation	Reference frame
T19	CDP10	Displacement of the bottom part of panel	Reference frame
T20	CDP25	Displacement of the middle part of panel	Reference frame
T21	CDP25	Displacement of the top part of panel	Reference frame
T22	CDP10	Panel front diagonal	Specimen
T23	CDP10	Panel back diagonal	Specimen

3.3 Load Pattern

Since the loading is to simulate the effect of seismic action, reversed cycling loading is applied to all specimens. Displacement reversals with increasing intensity are applied to the specimens by actuators. Up to 0.467 mm top displacement, the target values are applied once on the specimens observing the elastic behaviour of the specimens. After this step, each displacement cycle is repeated thrice for both forward and backward cycles. At the end of each displacement target, the occurred cracks are marked.

The details of the loading protocol are presented in Table 3.5 and Figure 3.14.

Table 3.5: Steps of the loading protocol

Load level	Top displacement [mm]	Relative Story Drift δ/H
1	0.035	0.000025
2	0.070	0.000050
3	0.140	0.000100
4	0.280	0.000200
5	0.350	0.000250
6	0.467	0.000300
7	0.700	0.000500
8	1.400	0.001000
9	2.800	0.002000
10	3.500	0.002500
11	4.200	0.003000
12	4.900	0.003500
13	5.600	0.004000
14	7.000	0.005000
15	10.500	0.007500
16	14.000	0.010000
17	28.000	0.020000
18	42.000	0.030000

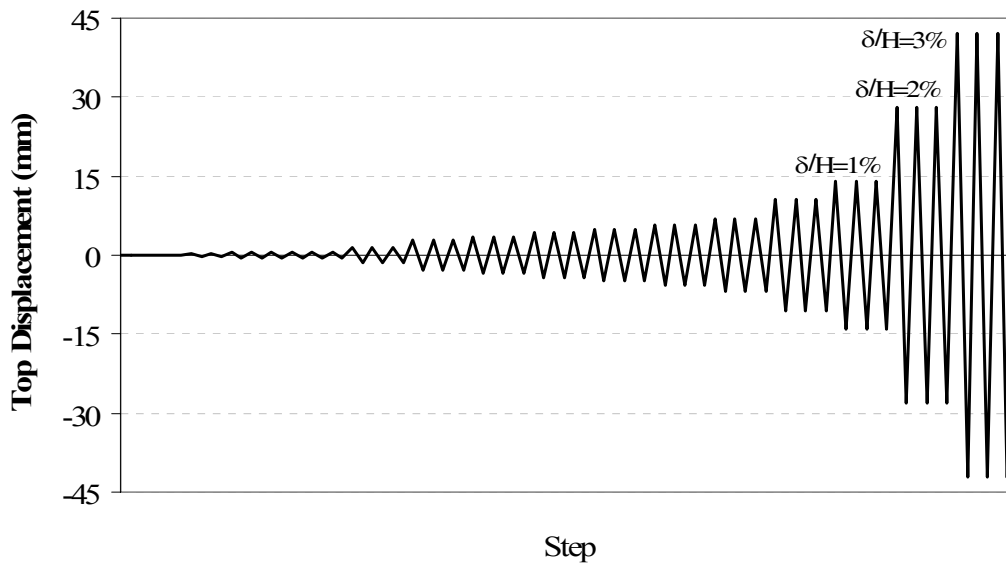


Figure 3.14: Loading protocol

3.4 Material Tests

Samples of materials used in the specimens were tested to determine their mechanical properties because success of the numerical models is highly dependent on correctly defining the material characteristics.

3.4.1 Concrete tests

Mix proportions of concrete used for constructing the frames and the shotcrete panels are given in Table 3.6 and Table 3.7, respectively. Compressive strengths of the concrete were obtained from compressive tests on standard cylinders (150 mm*300 mm) taken at various stages of the construction. Minimum of three standard cylinders were tested for each specimen. The compressive strength of the concrete used in the numerical models was the average values obtained from these tests. Results are summarised in Table 3.8 for the frame concrete and in Table 3.9 for the shotcrete panel concrete.

All cylinders were tested at the Construction Materials Laboratory of ITU Civil Engineering Faculty using a 5000 kN capacity Amsler compression press. Concrete cylinders were loaded in compression at a rate of 0.02 mm/min.

Table 3.6: Concrete mix proportions for frame concrete

Material	Weight for one cubic meter
Portland Cement	300 kg (32.5 R)
Water	140 kg
Sand	690 kg
Gravel	1070 kg (No:1)

Table 3.7: Concrete mix proportions for shotcrete panel concrete

Material	Weight for one cubic meter
Portland Cement	400 kg (42.5 R)
Water	300 kg
Sand	900 kg
Gravel	600 kg (No:2)

Table 3.8: The average concrete compressive strengths for frames

Name of specimen	Number of samples	Compressive strength [MPa]
1	3	16
2	3	16
3	4	10
4	3	12
5	3	12
6	3	14
7	3	12
8	3	12

Table 3.9: The average concrete compressive strengths for panels

Name of specimen	No. of samples	Compressive strength [MPa]
2S	3	35
3	3	22
4S	3	35
5	3	35
6	3	25
7	3	25
8	3	40

3.4.2 Steel reinforcement tests

Tensile tests were carried out to determine the mechanical characteristics of each type of reinforcing bar used in the specimens. All the samples were tested at the Material Testing Laboratory of ITU Civil Engineering Faculty using Amsler testing machine of 200 kN tension capacity. Free length between the two heads of the machine was chosen as 10ϕ . Locations of the bars tested in test specimens are given below:

- 1) $\phi 16$ bars are used as longitudinal reinforcement for the columns and the beams,
- 2) $\phi 10$ bars are used as longitudinal reinforcement for the slabs and dowel bars,
- 3) $\phi 6$ bars are used as stirrups for frames.

Three samples were taken from each type of reinforcement. Mechanical properties of these bars obtained from the tests are summarised in Table 3.10. Values given in the table are the average of the three samples tested.

Table 3.10: Mechanical properties of steel bars

Diameter [mm]	$\phi 16$	$\phi 10$	$\phi 6$
σ_y [MPa]	270	290	325
σ_{max} [MPa]	420	450	481
ϵ_{su} [mm/mm]	0.25	0.30	0.35

4. EXPERIMENTAL RESULTS

Although there are several measurement points on the specimens, the top displacements versus base shear relationships and some of the graphs drawn for the critical sections and damage modes are selected to be presented here. Through Section 4.1 to 4.9, the results are also compared with Specimen 1 (bare frame) results. Since some of the specimens don't have the same concrete compressive strength unintentionally as presented in Table 3.1; the analytical bare frame, which is explained in detail in Chapter 5, having identical concrete compressive strength as the retrofitted specimens are also introduced into the comparison of envelope curve diagrams. This will help to have a more accurate comparison and evaluation of the test results. In Section 4.10; all specimens are compared with each other according to their failure modes, lateral load carrying capacity, initial stiffness, dissipated energy, ductility and stiffness.

4.1 Test Results of Specimen 1

This specimen is the bare frame used as a reference frame and the effect of the different strengthening methods is compared and discussed with this specimen's results. The types of the LVDTs and what was measured by them on the bare frame was given in Table 3.2 and Figure 3.11.

The largest displacement applied to the specimen was 42 mm in both pulling and pushing displacement cycles. The axial load applied on each column was 165 kN which equals to 20% of the axial load carrying capacity of the column.

Base shear versus top displacement diagram is given in Figure 4.1. The maximum strengths in tension and compression are 133 kN and 123 kN, respectively, obtained at 28 mm cycles which correspond to 2% story drift. The envelope curve of the base shear-top displacement relationship is also given in Figure 4.2. The data of envelope curve are calculated as the average of the three cycles at each target displacement levels given in Table 3.5. As it is seen in Figure 4.2, the maximum story drift reached

is 3% where the lateral load carrying capacities of the frame are 104 kN and 86 kN in tension and compression, respectively.

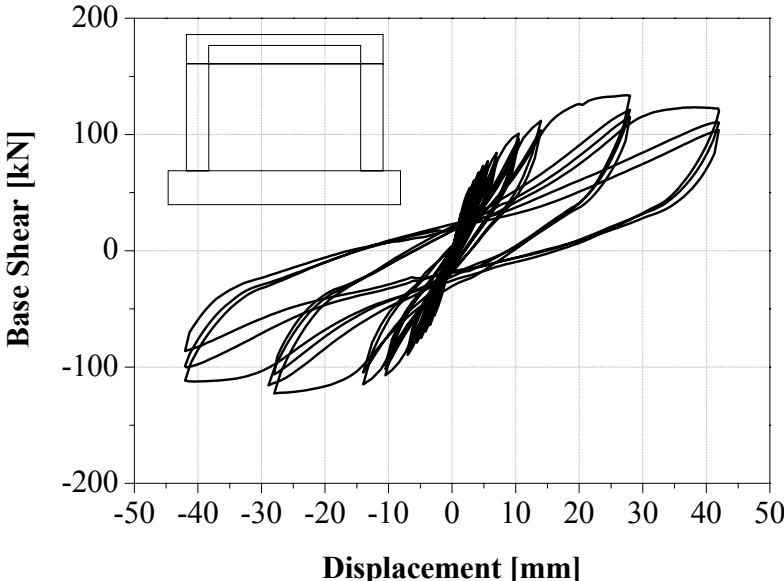


Figure 4.1: Base shear-top displacement curve of Specimen 1

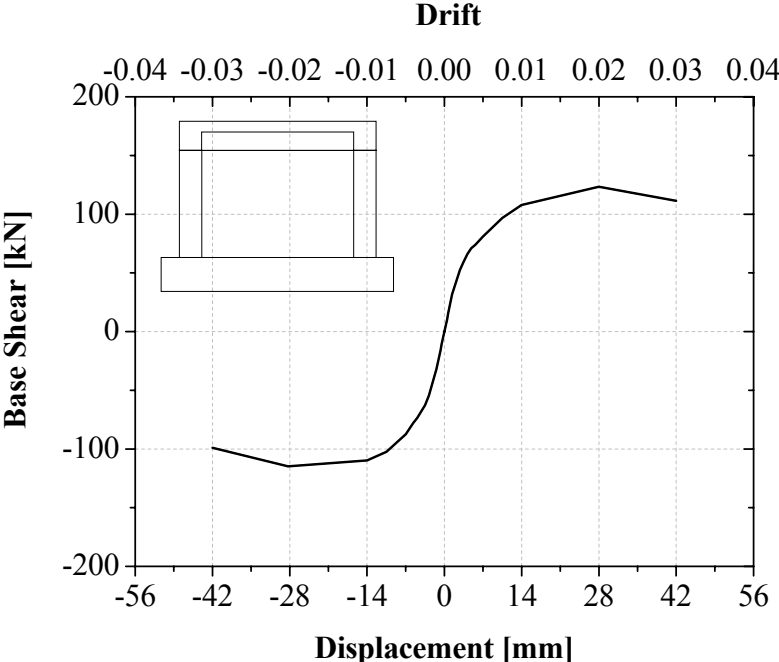


Figure 4.2: Envelope curve of Specimen 1

Rotation at the critical sections is calculated as the sum of displacement values (Δ_1 , Δ_2), measured from the two LVDTs placed at 12.5 cm from the end of the column, divided by the column width, x , as seen in Figure 4.3.

The rotation is calculated using Equation 4.1;

$$\theta = (\Delta_1 + \Delta_2) / x \tag{4.1}$$

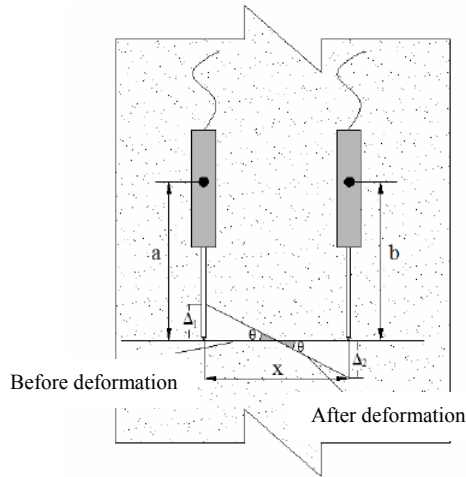


Figure 4.3 Calculation of rotation at the ends of the columns

In Figures 4.4, base shear versus bottom end rotation of right (the one that is near to the actuator) and left columns and in Figures 4.5 base shear versus top end rotation of the right and left columns are given, respectively.

The maximum rotations obtained at the column sections are about 0.02 radian. At the top end of the right column when the rotation is 0.01 radian, the corresponding load at that level is 133 kN. At the bottom end of the right column when the rotation is 0.01 radian, the corresponding load at that level is 106 kN.

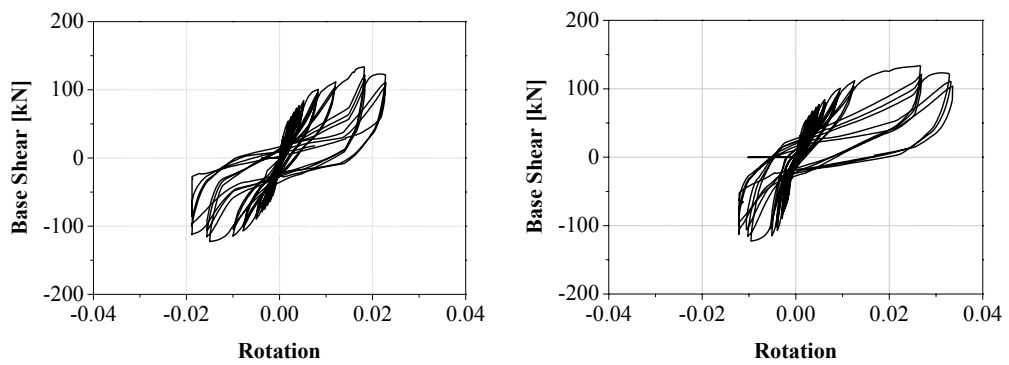


Figure 4.4: Rotation at the bottom end of the right and left column

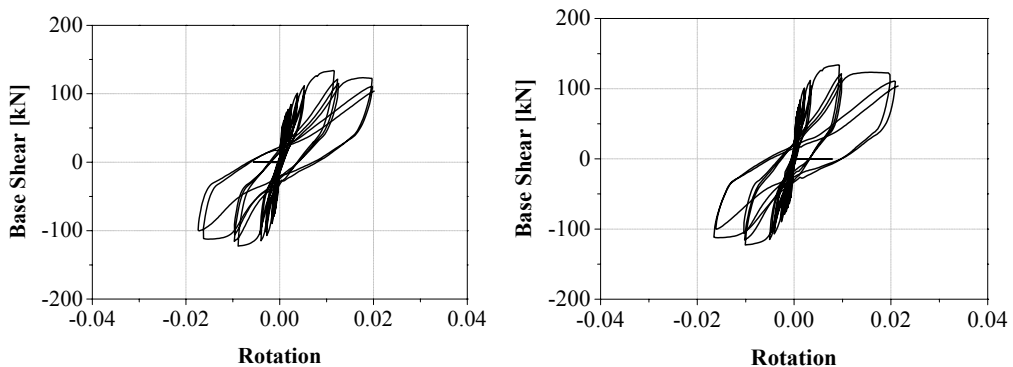


Figure 4.5: Rotation at the top end of the right and left column

Crack pattern of the specimen after test is given in Figure 4.6 and Table 4.1 shows the width of cracks at specific drift ratios.

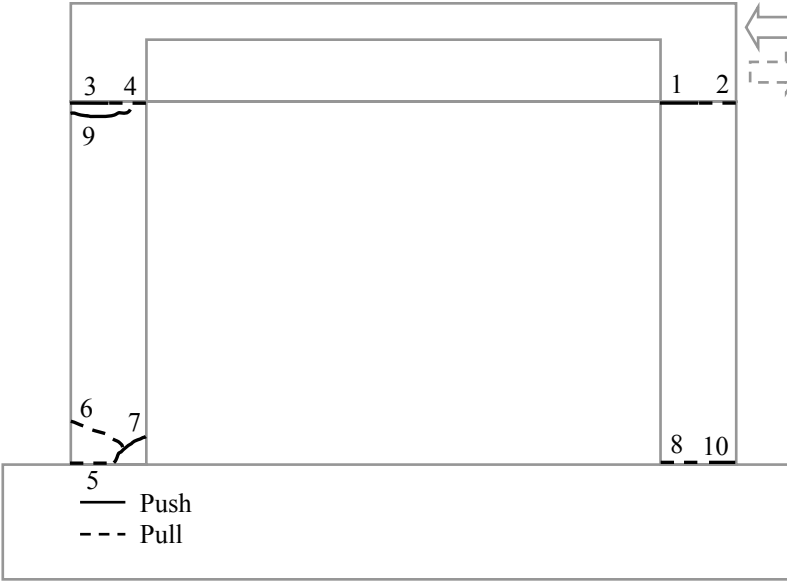


Figure 4.6: Crack pattern of Specimen 1 at the end of test

Table 4.1: Width of cracks in mm at specific story drifts

Crack no	Drift = 1%	Drift = 2%	Drift = 3%
1	1.6	3.0	-
2	0.6	1.4	>3.5
3	0.1	0.1	0.2
4	1.2	2.5	-
5	0.5	0.9	0.9
6	0.2	0.9	-
7	0.15	1.4	3.4
8	0.3	1.0	>3.5
9	0.1	1.4	3.5
10	-	0.2	0.9

4.2 Test Results of Specimen 2

This is a bare frame which is tested up to a certain damage level before strengthening with shotcrete panel to form Specimen2S. The types of the LVDTs and what was measured by them on the bare frame was given in Table 3.2 and Figure 3.11.

The specimen was tested up to 10.5 mm which is the displacement level at which the longitudinal reinforcement of the columns started to yield in previous experiments. The axial load applied on each column was 162.5 kN which equals to 20% of the axial load carrying capacity the column.

Base shear versus top displacement diagram is given in Figure 4.7. The envelope curve of the hysteretic response of the specimen is given in Figure 4.8.

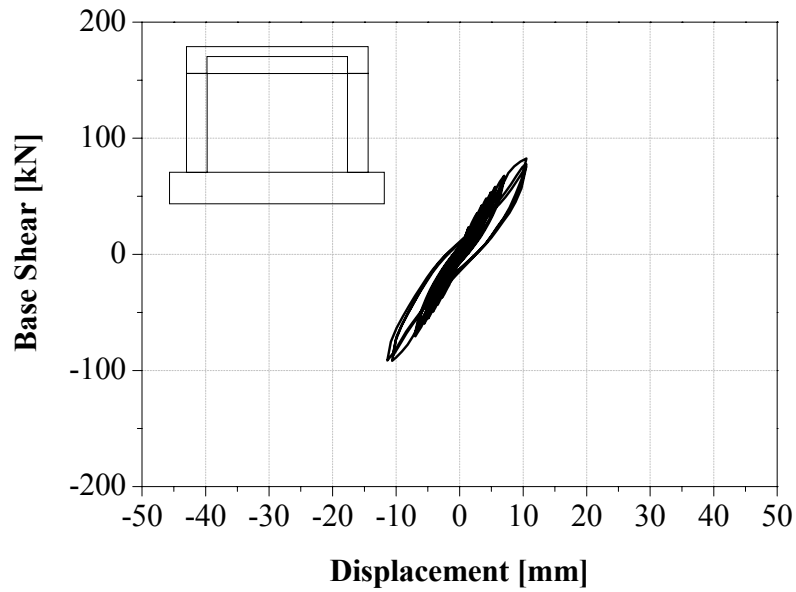


Figure 4.7: Base shear-top displacement curve of Specimen 2

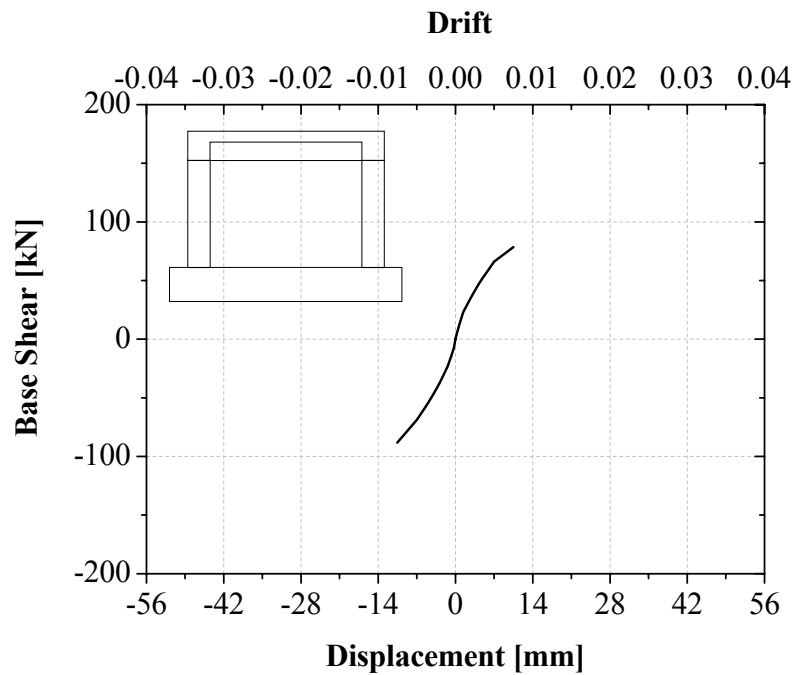


Figure 4.8: Envelope curve of Specimen 2

In Figures 4.9, bottom end rotation of right and left columns and in Figures 4.10, top end rotation of right and left columns versus base shear are given, respectively. Inelastic behaviour has started at bottom ends of the columns, while top ends stayed elastic.

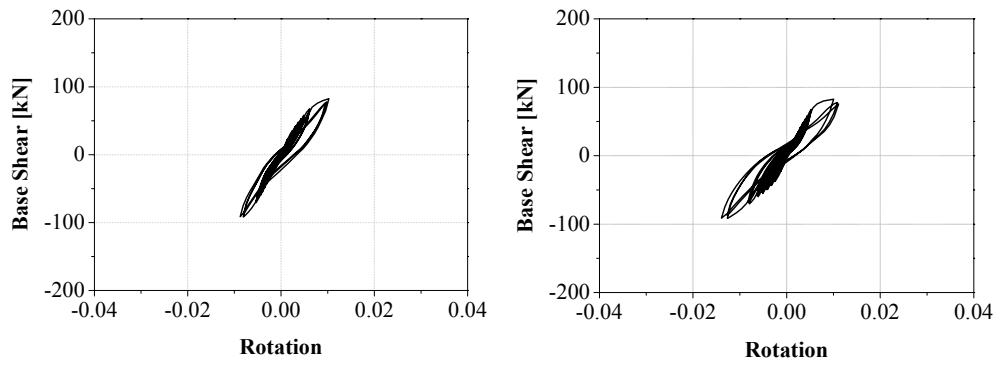


Figure 4.9: Rotation at the bottom end of the right and left column

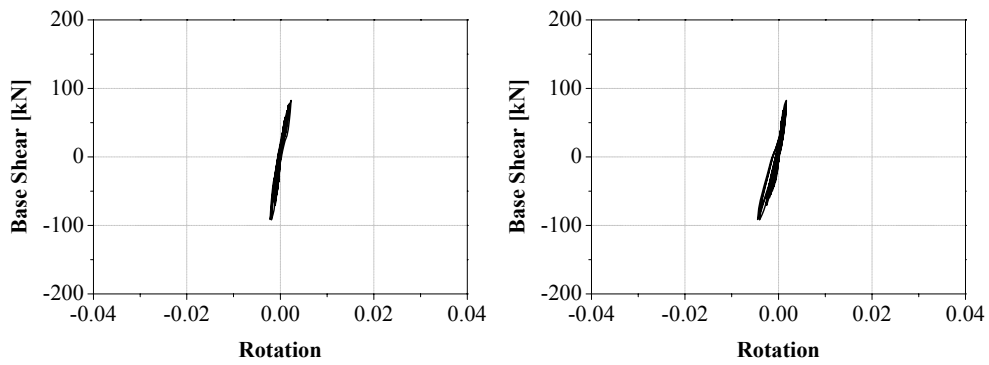


Figure 4.10: Rotation at the top end of the right and left column

Crack pattern of the specimen after test is given in Figure 4.11. Table 4.2 shows the width of cracks at specific drift ratios.

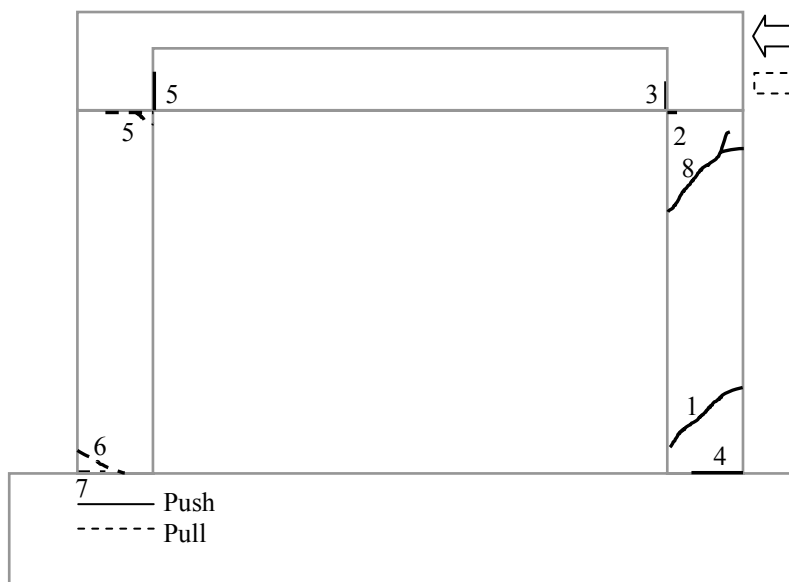


Figure 4.11: Crack pattern of Specimen 2 at the end of test

Table 4.2: Width of cracks in mm at specific story drift

Crack No:	Drift = 0.5%
1	0.6
2	0.2
3	0.8
4	0.8
5	0.9
6	0.6
7	0.9
8	0.5

4.3 Test Results of Specimen 2S

The observed cracks of Specimen 2 was repaired with epoxy resin and retrofitted with a shotcrete panel and named as Specimen 2S. The types of the LVDTs and what was measured by them for the specimen are given in Table 3.3 and Figure 3.12.

The largest displacement applied was 28 mm. The axial load applied on each column was 162.5 kN which equals to 20% of the axial load carrying capacity of the column.

Base shear versus top displacement diagram is given in Figure 4.12. The maximum strengths in tension and compression are 342 kN and 394 kN, respectively, occurred at 2% story drift which is also the maximum story drift reached. The ultimate lateral load carrying capacities corresponding to the maximum drifts of the frame are 166 kN and 249 kN in tension and compression, respectively. The envelope curve of the hysteretic response of the specimen is given in Figure 4.13.

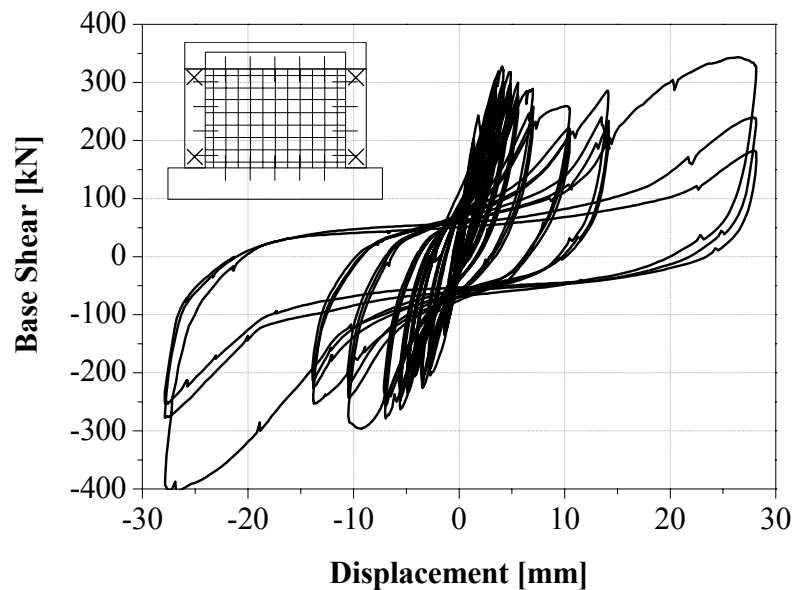


Figure 4.12: Base shear-top displacement curve of Specimen 2S

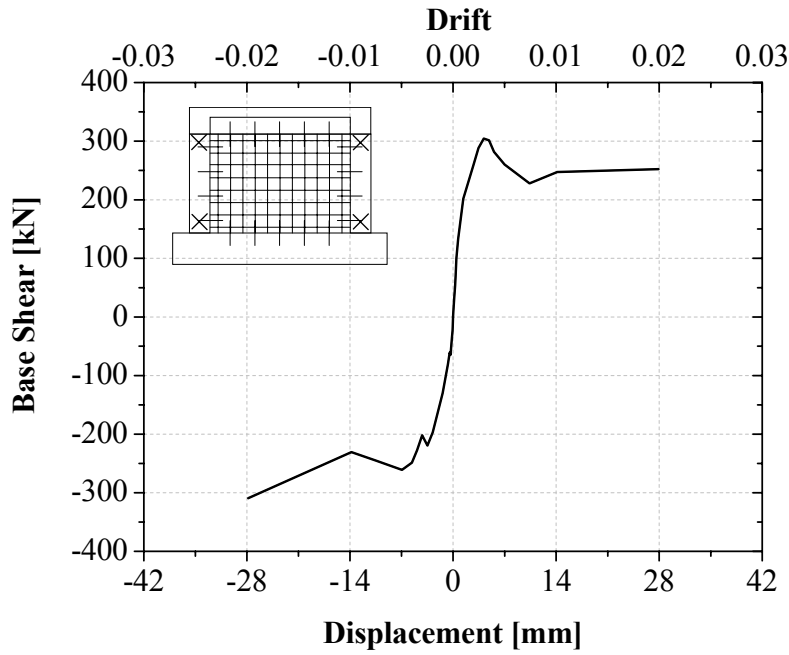


Figure 4.13: Envelope curve of Specimen 2S

In Figures 4.14, bottom end rotation of right and left column and in Figures 4.15, top end rotation of right and left columns versus base shear are given, respectively. At the top end of the right column when the rotation is 0.01 radian, the corresponding load at that level is 250 kN. At the bottom end of the right column when the rotation is 0.01 radian, the corresponding load at that level is 290 kN.

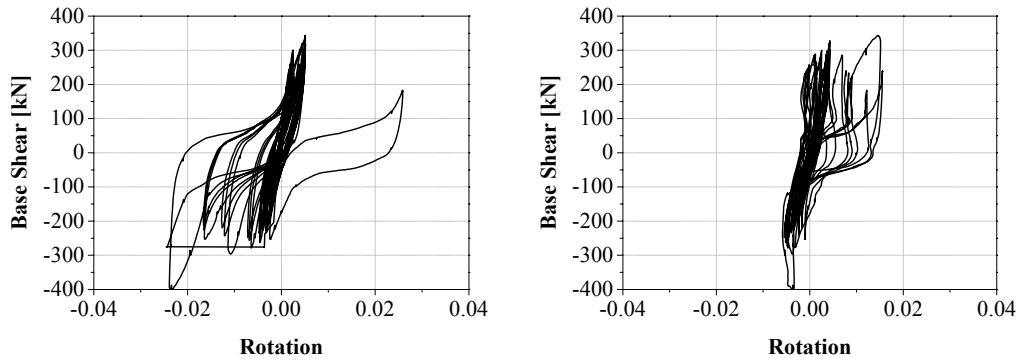


Figure 4.14: Rotation at the bottom end of the right and left column

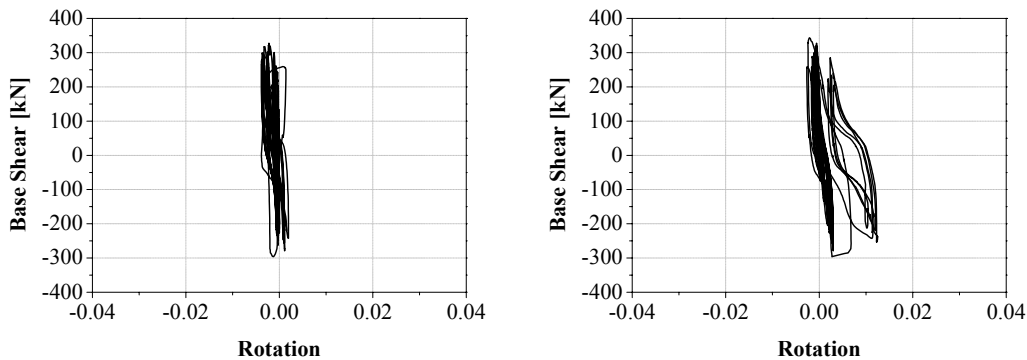


Figure 4.15: Rotation at the top end of the right and left column

The observed maximum displacement in the shotcrete panel is 5 mm in pushing and 10 mm in pulling sides as seen in Figure 4.16. Figure 4.17 shows the specimen at the end of the test and the crack patterns of all specimens at the ultimate state are given in Figure 4.18.

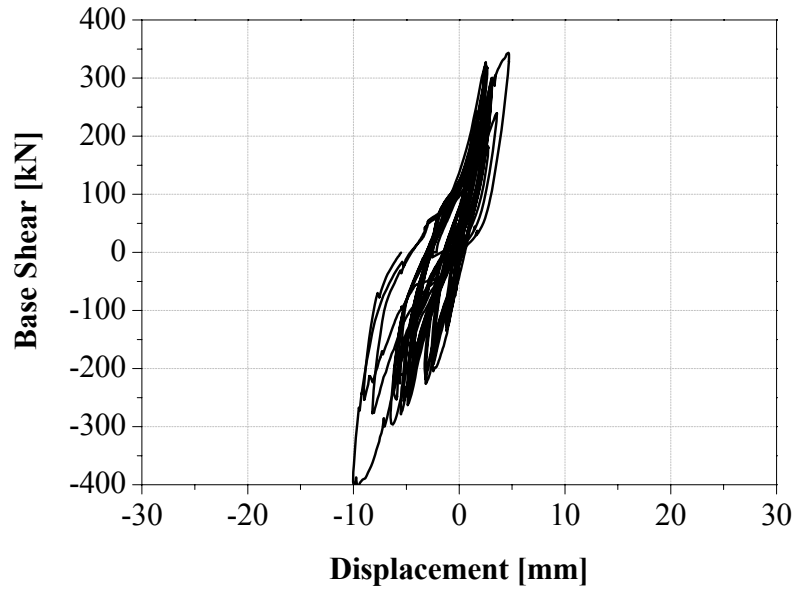


Figure 4.16: Panel displacement

Nominal shear stress of the shotcrete panel is calculated using Equation 4.2,

$$\tau = \frac{Q_s}{A_{eff}} \quad (4.2)$$

where Q_s is the specific load obtained. A_{eff} is the total area, which is the sum of cross sections of the panel and columns, which resist the shear forces.

Maximum load that has occurred at the end of the pushing displacement cycles was 342.5 kN and in the pulling displacement cycles was 393.5 kN. The nominal shear stresses corresponding to these values are 1850 kN/mm² and 2127 kN/mm². The first cracks observed in the system were the shear crack at the bottom end of the column which was closer to the actuators that have been repaired by epoxy injection, the shear crack at the top of the same column and the separation of this column from beam. These cracks were observed during the displacement cycle of +0.467 mm. The load was reported as 107 kN where the nominal shear stress is 578 kN/mm². The first separation between the panel and the frame members occurred during the displacement cycle of +0.7 mm. The load was reported as 132 kN where the nominal shear stress is 713 kN/mm² at that state. The first diagonal crack was observed on

the panel during the -0.467 mm cycles. In that cycle, the load was 55 kN. Maximum displacement of the panel recorded was 5 mm in the positive displacement cycles and 10 mm in the negative ones. The widths of the cracks observed are given in Table 4.3.

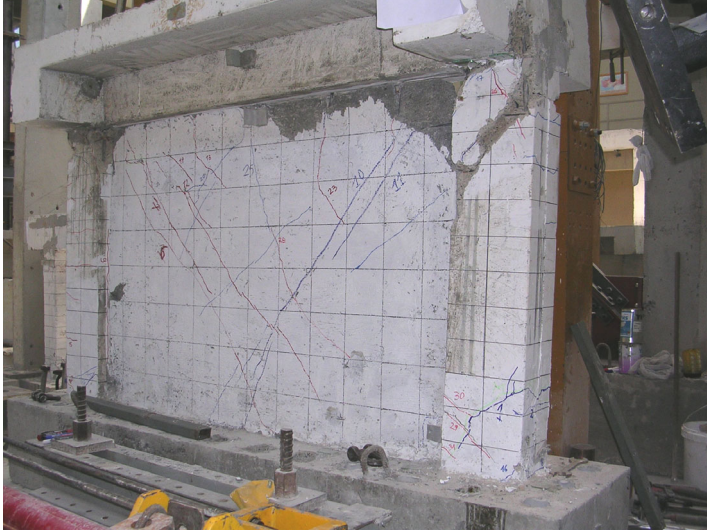


Figure 4.17: Specimen 2S at the end of test

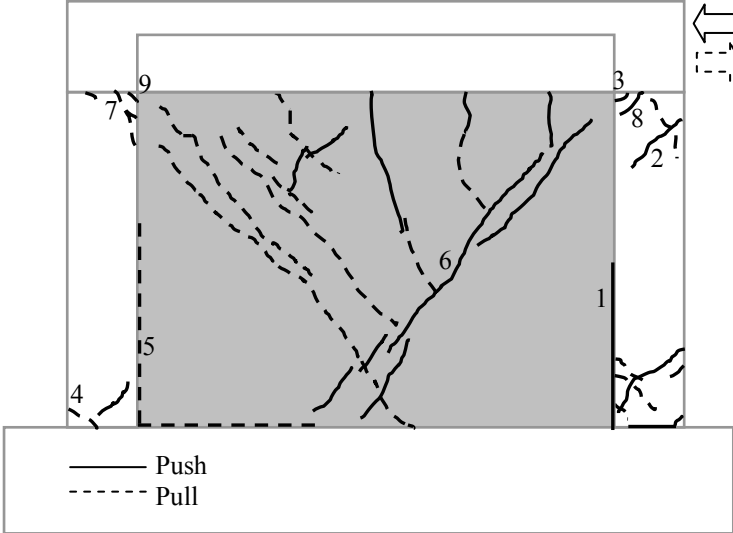


Figure 4.18: Crack pattern of Specimen 2S at the end of test

Table 4.3: Width of cracks in mm at specific story drifts

Crack No:	Drift = 1%	Drift = 2%
1	1.4	
2	0.3	>3.5
3	>3.5	>3.5
4	1.6	
5	>3.5	>3.5
6	1.6	
7	>3.5	>3.5
8	>3.5	>3.5
9	>3.5	>3.5

Comparison of the results of the retrofitted frame with shotcrete panel with the bare frames' are given below. In Figure 4.19 and Tables 4.4 and 4.5, the comparison of the load carrying capacity; in Table 4.6 the comparison of initial stiffnesses, in Figure 4.20 and 4.21 the comparison of energy dissipation capacities of both frames are summarised.

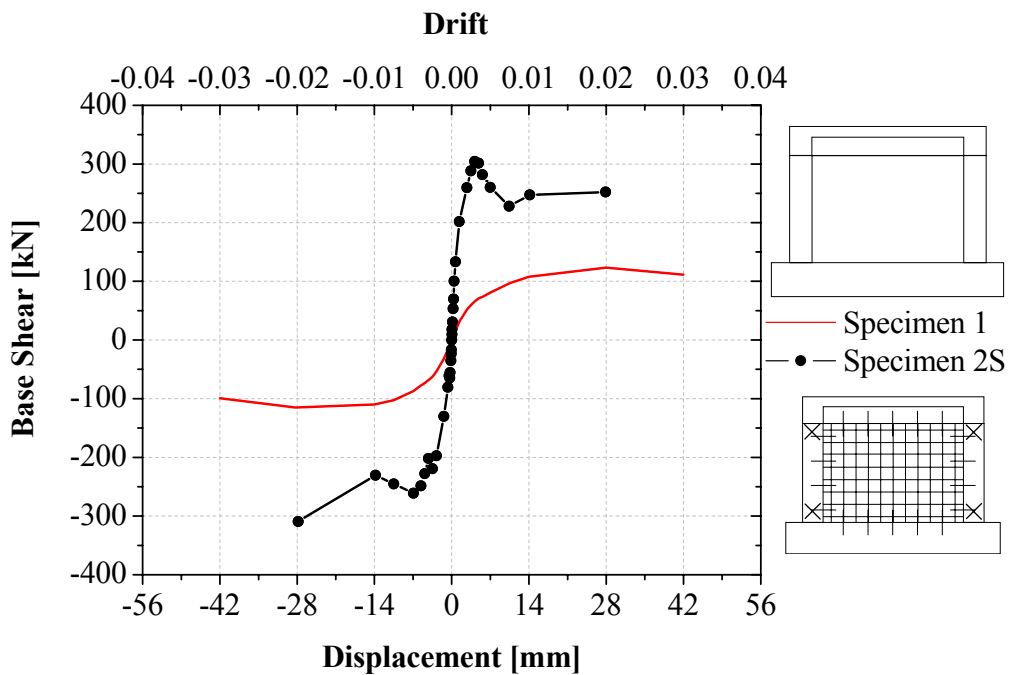


Figure 4.19: Comparison of envelope curves of Specimen 2S and Specimen 1

Table 4.4: Effect of strengthening in general

Specimen name	Failure mode	+P _{max} (kN)	+Δ _{max} (mm)	-P _{max} (kN)	-Δ _{max} (mm)	+P _{ult} (kN)	-P _{ult} (kN)	Δ _{ult} (mm)
Specimen 1	Bending + Shear failure at column ends	133	28	-123	-28	104	-86	42
Specimen 2S	Shear failure at column ends	342	28	-394	-28	166	-249	28

In Table 4.4, $+P_{max}$ and $-P_{max}$ indicates the maximum loads occurred during pushing and pulling cycles, while $+\Delta_{max}$ is the displacement corresponds to $+P_{max}$ and $-\Delta_{max}$ the displacement corresponds to $-P_{max}$ during the experiment. $+P_{ult}$ and $-P_{ult}$ are residual lateral load carrying capacity of the system at the end of the test. Δ_{ult} is the displacement level at which the experiment ends.

Table 4.5: Maximum base shears recorded during the tests

Specimen name	Maksimum load [kN]		Proportion ratio	
	Push	Pull	Push	Pull
Specimen 1	133	-123	1.0	1.0
Specimen 2S	342	-394	2.6	3.2

Table 4.6: Initial stiffness of the specimens

Specimen name	Initial stiffness [kN/mm]	Proportion ratio
Specimen 1	22.0	1.0
Specimen 2S	231.0	10.7

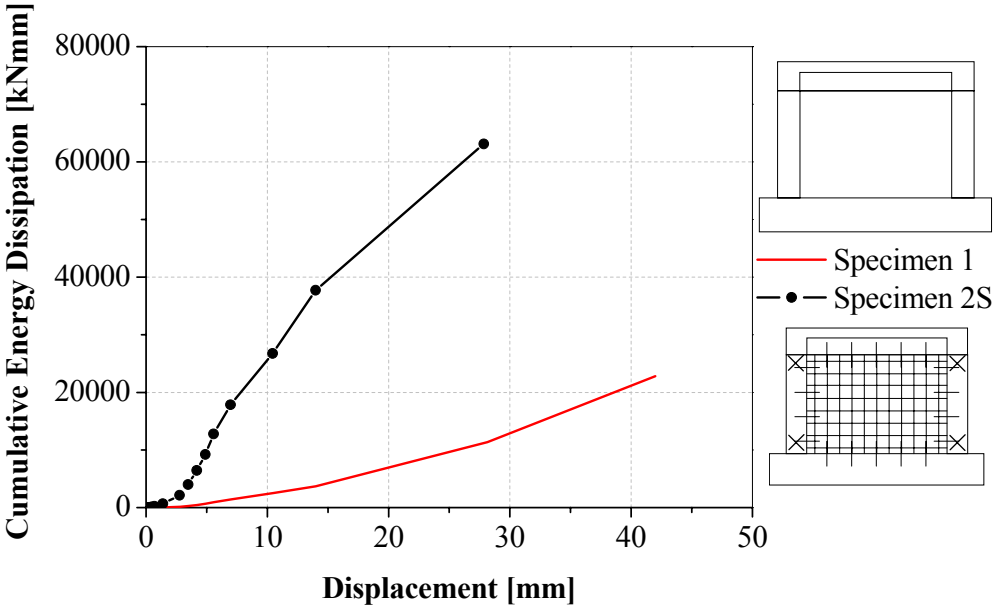


Figure 4.20: The comparison of cumulative energy dissipation capacities of Specimens 1 and 2S

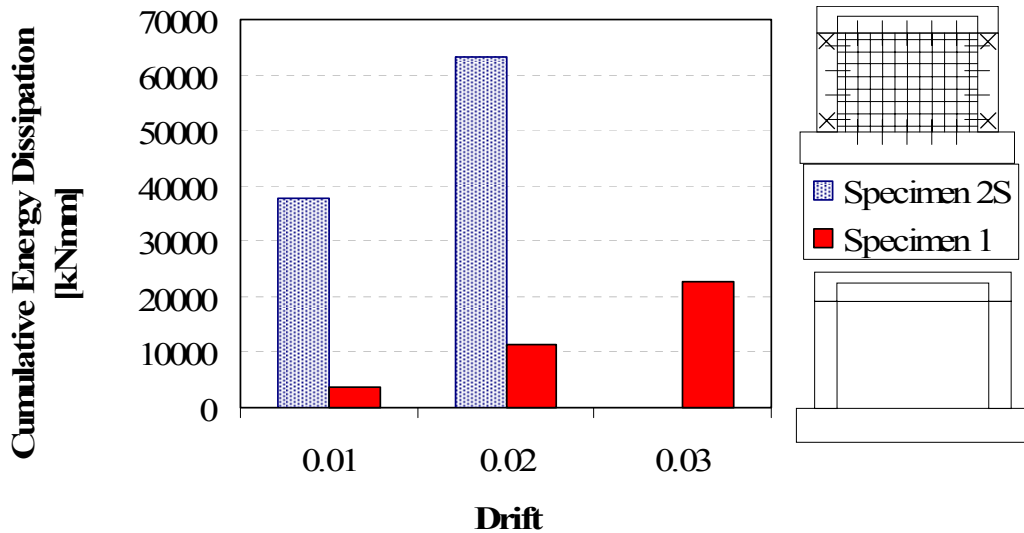


Figure 4.21: Cumulative energy dissipation capacities of Specimens 1 and 2S at various story drifts

The results are summarised below:

- The lateral stiffness of the frames, right before the first cracks occurred in the system, increased by 10.7 times for Specimen 2S compared with the bare frame's as seen in Table 4.6.
- The lateral load carrying capacity increased by between 2.6 to 3.2 times for the specimens with shotcrete panel compared with the bare frame's as seen in Figure 4.19 and Table 4.4 and 4.5.
- Comparison of Figures 4.14 and 4.15 with Figures 4.4 and 4.5,
 - At the top end of the right column when the rotation is 0.01 radian, the corresponding load at that level for Specimen 1 is 133 kN while for Specimen 2S is 250 kN which is almost 1.9 times of the bare frame's,
 - At the bottom end of the right column when the rotation is 0.01 radian, the corresponding load at that level for Specimen 1 is 106 kN while for Specimen 2S is 290 kN which is almost 2.7 times of the bare frame's,
- The cumulative energy dissipation of the Specimen 2S at 1% story drift are 10 times, at 2% story drift are 5.5 times compared to the bare frame's shown in Figure 4.20 and 4.21.

4.4 Test Results of Specimen 3

This is the RC frame retrofitted with shotcrete panel which is connected to frame at all four sides. The types of the LVDTs and what was measured by them for Specimen 3 are given in Table 3.3 and Figure 3.12.

The largest displacement applied was 14 mm. The axial load applied on each column was 112.5 kN which equals to 20% of the axial load carrying capacity the column.

Base shear versus top displacement diagram is given in Figure 4.22. The maximum strengths in tension and compression are 291 kN and 279 kN, respectively, obtained at 10.5 mm cycles which correspond to 0.75% story drift. The maximum story drift reached is 1%. The lateral load carrying capacities corresponding to maximum story drift reached are 165 kN and 136 kN in tension and compression, respectively.

The envelope curve of the hysteretic response of the specimen is given in Figure 4.23.

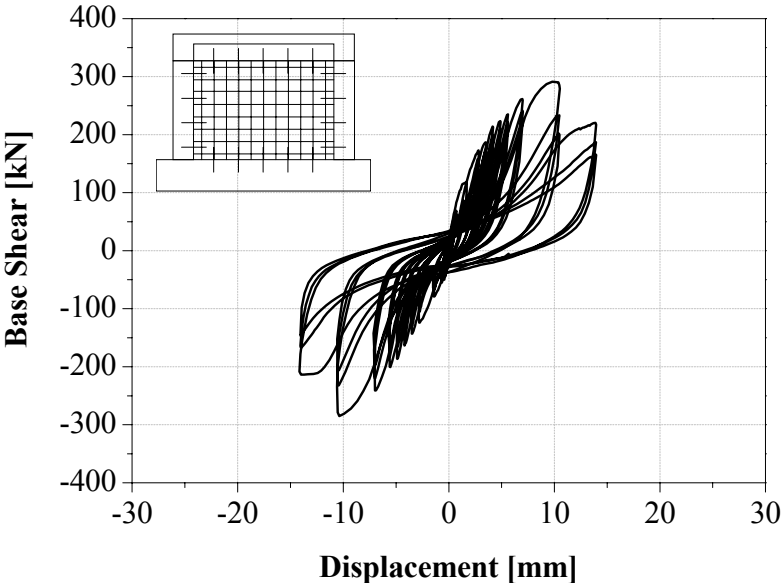


Figure 4.22: Base shear-top displacement curves of Specimen 3

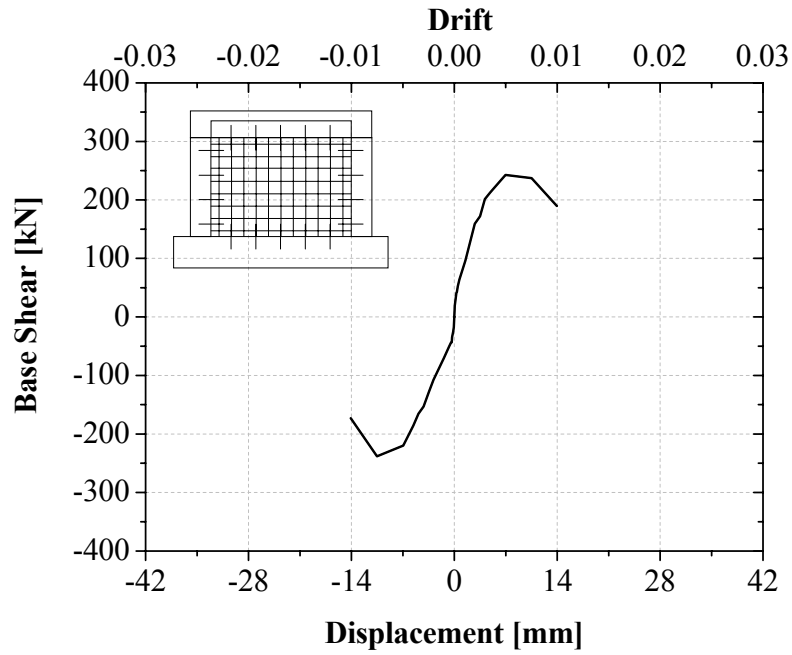


Figure 4.23: Envelope curve of Specimen 3

In Figures 4.24, bottom end rotation of right and left columns and in Figures 4.25, top end rotation of the right and left columns versus base shear are given, respectively.

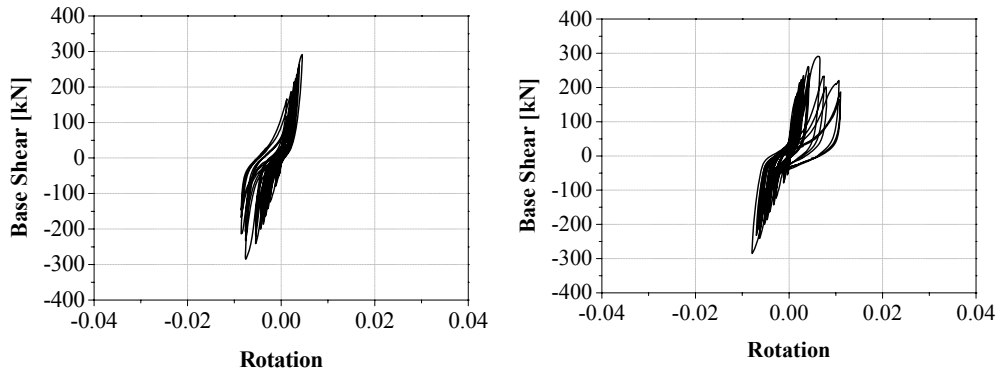


Figure 4.24: Rotation at the bottom end of the right and left column

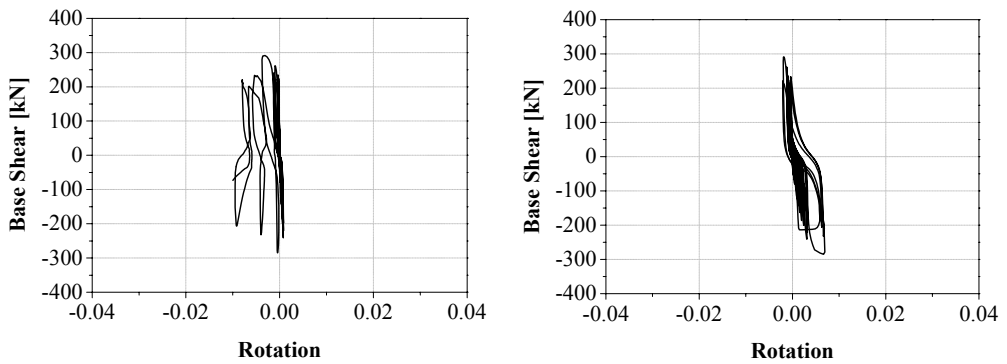


Figure 4.25: Rotation at the top end of the right and left column

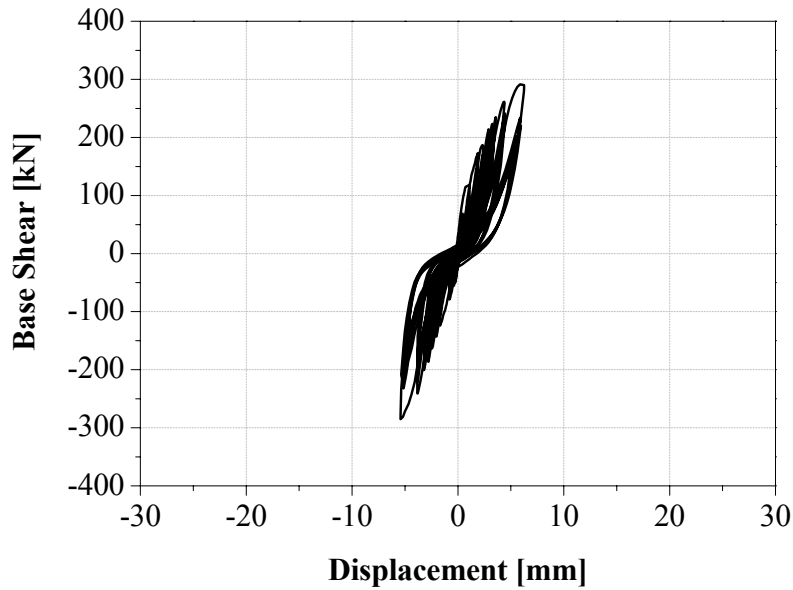


Figure 4.26: Panel displacement

Maximum load that has occurred at the end of the positive displacement cycles was 290 kN and in negative displacement cycles was 279 kN. The nominal shear stresses corresponding to these values are 1568 kN/mm² and 1508 kN/mm². The first separation between the panel and the frame members and also the first diagonal crack observed during the +1.4 mm cycles. The load was reported as 85 kN where the nominal shear stress corresponds to 460 kN/mm² at that state. In the later cycles, several cracks occurred parallel to this crack. The first shear crack occurred at the upper end of the right column during +2.8 mm cycles. The load was reported as 147 kN where the nominal shear stress corresponds to 795 kN/mm² at that state. Maximum displacement of the panel recorded was 6 mm in the positive displacement cycles and 5.5 mm in the negative ones shown in Figure 4.26.

The specimen after test can be seen in Figure 4.27. Cracks occurred in the pulling and pushing cycles are seen in Figure 4.28. Table 4.7 shows the width of cracks at specific drift ratios.



Figure 4.27: Specimen 3 at the end of test

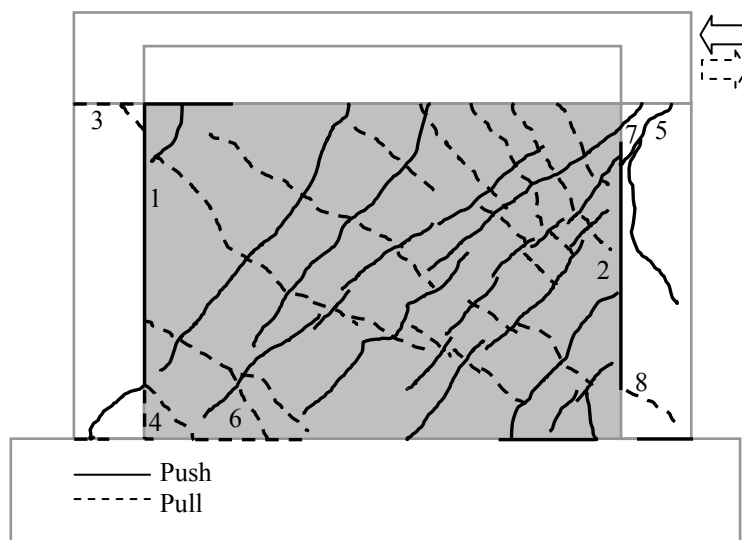


Figure 4.28: Crack pattern of Specimen 3 at the end of test

Table 4.7: Width of cracks in mm at specific story drift

Crack no:	Drift = 1%
1	>3.5
2	2.0
3	>3.5
4	0.8
5	>3.5
6	0.9
7	>3.5
8	1.0

Comparisons of the results of the retrofitted frame with shotcrete panel with the bare frames' are given below.

In Figure 4.29 and Tables 4.8 and 4.9, the comparison of the load carrying capacity; in Table 4.10 the comparison of initial stiffnesses, in Figure 4.30 and 4.31 the comparison of energy dissipation capacities of both frames are summarised. Since Specimen 1 and 3 don't have the same concrete compressive strength, an analytical calculation is done to interpret the behavior of Specimen 3 as a bare frame introduced in Figure 4.29 and named as "analytical bare 3".

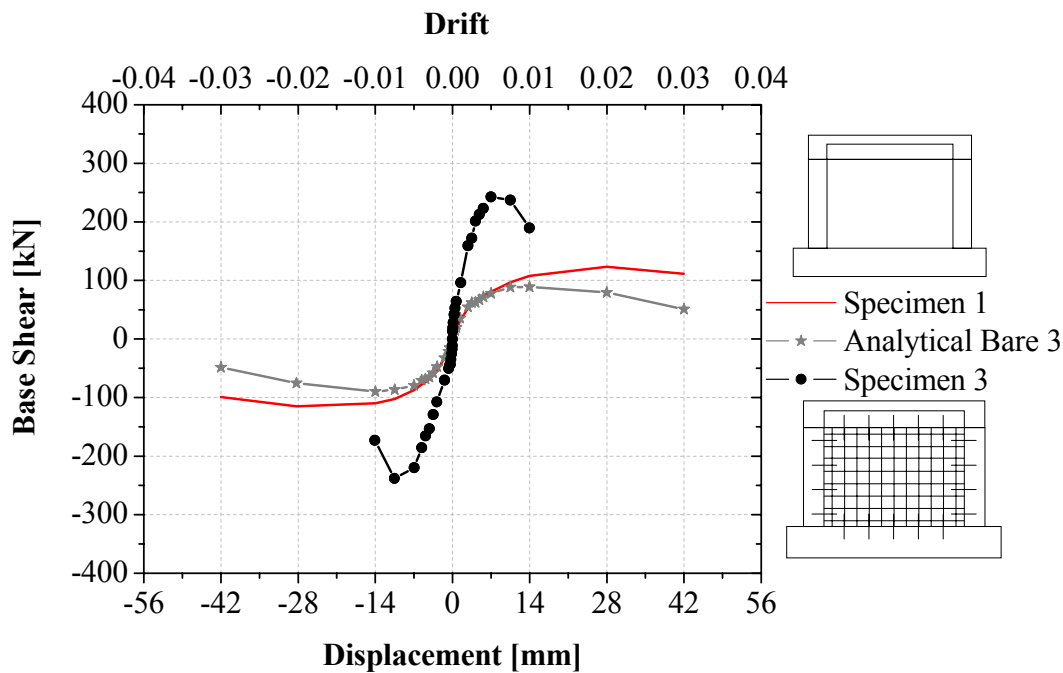


Figure 4.29: Comparison of envelope curves of Specimens 3 and 1 with analytical bare 3

Table 4.8: Effect of strengthening in general

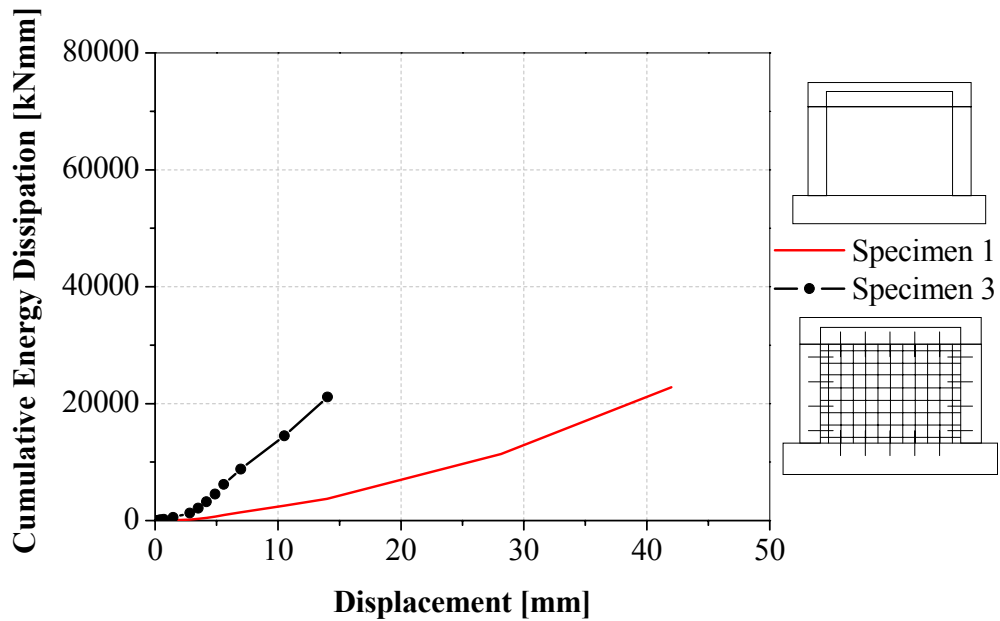
Specimen Name	Failure Mode	+P _{max} (kN)	+Δ _{max} (mm)	-P _{max} (kN)	-Δ _{max} (mm)	+P _{ult} (kN)	-P _{ult} (kN)	Δ _{ulti} (mm)
Specimen 1	Bending + Shear failure at column ends	133	28.0	-123	-28.0	104	-86	42
Specimen 3	Shear failure at column ends	291	10.5	-279	-10.5	165	-136	14

Table 4.9: Maximum base shears observed during the tests

Specimen name	Maksimum load [kN]		Proportion ratio	
	Push	Pull	Push	Pull
Specimen 1	133	-123	1.0	1.0
Specimen 3	291	-279	2.2	2.3

Table 4.10: Initial stiffness of the specimens

Specimen name	Initial stiffness [kN/mm]	Proportion ratio
Specimen 1	22.0	1.0
Specimen 3	184.0	8.5

**Figure 4.30:** The comparison of cumulative energy dissipation capacities of Specimens 1 and 3

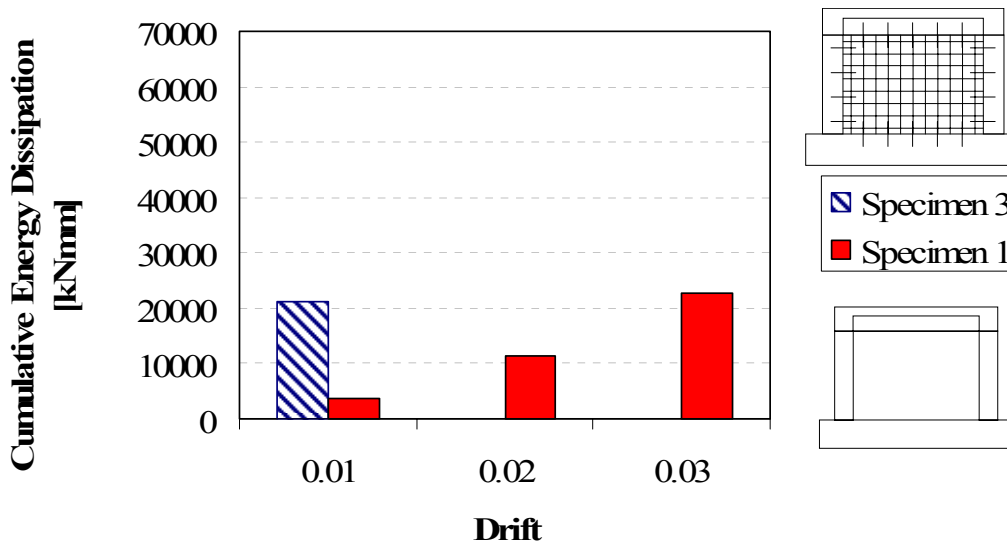


Figure 4.31: Cumulative energy dissipation capacities of Specimens 1 and 3 at various story drifts

The results are summarised below:

- The lateral stiffness of the frames, right before the first cracks occurred in the system, increased by 8.5 times for Specimen 3 compared with the bare frame's as shown in Table 4.10.
- The lateral load carrying capacity increased by between 2.2-2.3 times for the specimens with shotcrete panel compared with the bare frame's shown in Figure 4.29 and Table 4.8 and 4.9.
- Comparison of Figures 4.24 and 4.25 with Figures 4.4 and 4.5, it can be seen that at the top and bottom end of the right column the rotation did not reach 0.01 radian like the specimens.
- The energy dissipation of the Specimen 3 at 1% story drift is 10 times compared to the bare frame's shown in Figure 4.30 and 4.31.

4.5 Test Results of Specimen 4

This is a bare frame which is tested up to a certain damage level before strengthening with shotcrete panel to form Specimen 4S. The types of the LVDTs and what was measured by them for Specimen 4 are given at Table 3.2 and Figure 3.11.

The largest displacement applied was 7 mm. The axial load applied on each column was 132.5 kN which is 20% of the axial load carrying capacity of the column.

Base shear versus top displacement diagram is given in Figure 4.32.

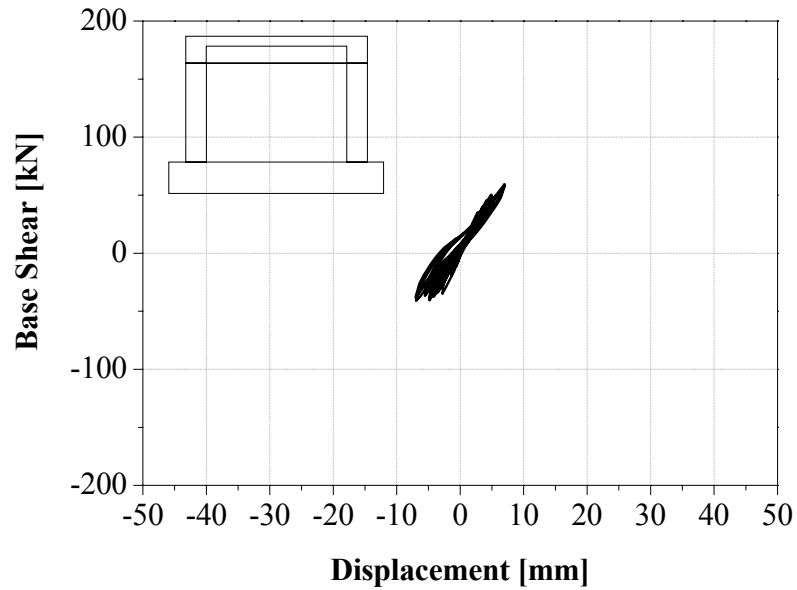


Figure 4.32: Base shear-top displacement curve of Specimen 4

In Figures 4.33 bottom end rotation of right and left columns and in Figures 4.34 top end rotation of right and left column versus base shear are given, respectively.

Cracks occurred in the pulling and pushing cycles are seen in Figure 4.35.

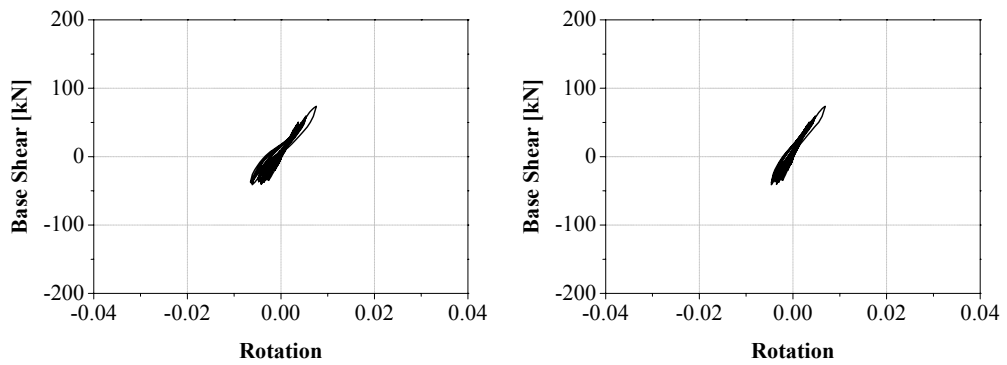


Figure 4.33: Rotation at the bottom end of the right and left column

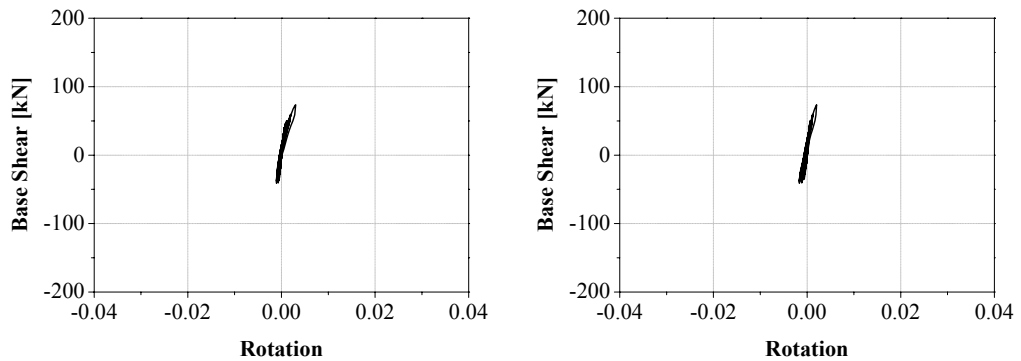


Figure 4.34: Rotation at the top end of the right and left column

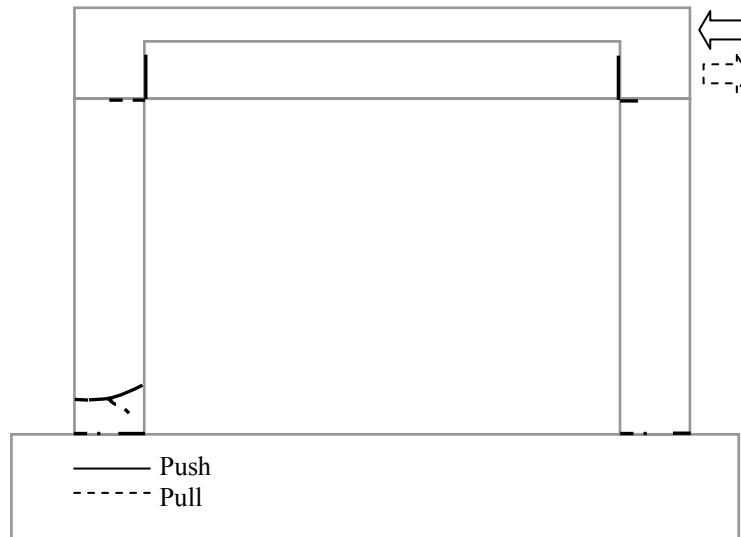


Figure 4.35: Crack pattern of Specimen 4 at the end of test

4.6 Test Results of Specimen 4S

The observed cracks of Specimen 4 are repaired with epoxy resin and retrofitted with a shotcrete panel that is not connected to the columns and named as Specimen 4S. The types of the LVDTs and what was measured by them for the specimen are given in Table 3.4 and Figure 3.13.

The largest displacement applied was 42 mm. The axial load applied on each column was 132.5 kN which equals to 20% of the axial load carrying capacity the column.

Base shear versus top displacement diagram is given in Figure 4.36. The maximum strengths in tension and compression are 236 kN and 190 kN, respectively, obtained at 28 mm cycles which correspond to 2% story drift. The maximum story drift reached is 3%. The ultimate lateral load carrying capacities of the frame are 120 kN and 118 kN in tension and compression, respectively.

The envelope curve of the hysteretic response of the specimen is given in Figure 4.37.

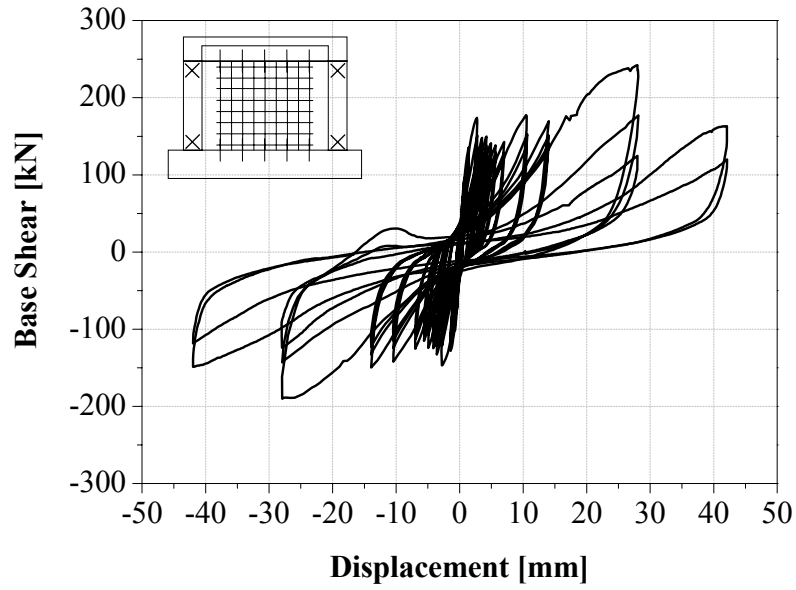


Figure 4.36: Base shear-top displacement curve of Specimen 4S

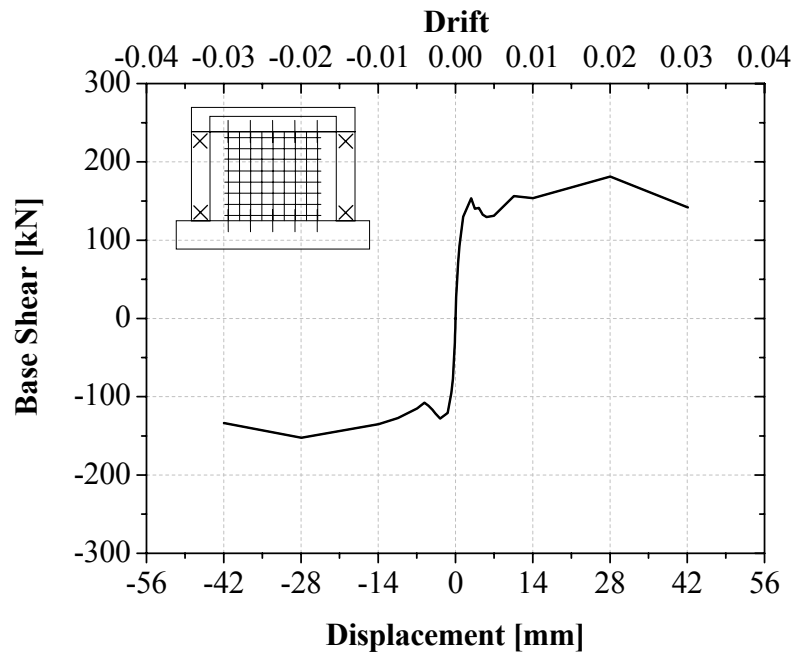


Figure 4.37: Envelope curve of Specimen 4S

In Figures 4.38, bottom end rotation of right and left columns and in Figures 4.39, top end rotation of the right and left column versus base shear are given, respectively. At the top end of the right column, the rotation did not reach 0.01 radian like the other specimens. At the bottom end of the right column when the rotation is 0.01 radian, the corresponding load at that level is 150 kN.

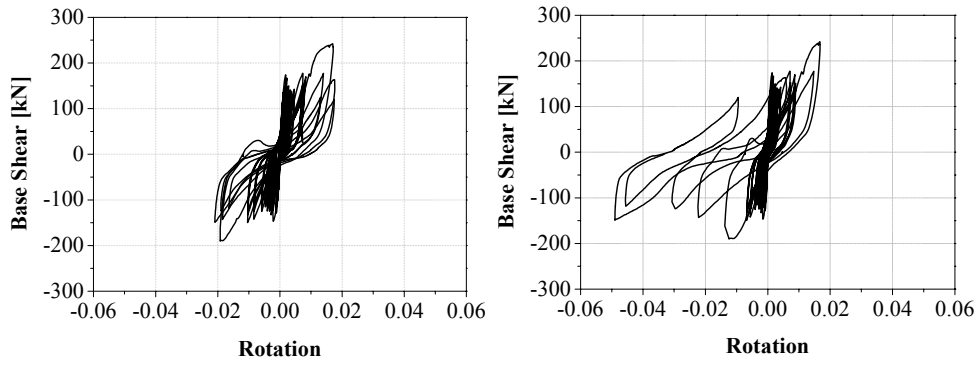


Figure 4.38: Rotation at the bottom end of the right and left column

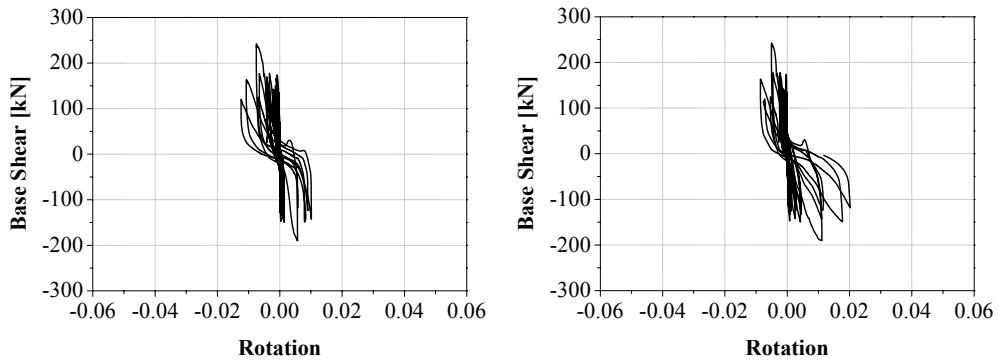


Figure 4.39: Rotation at the top end of the right and left column

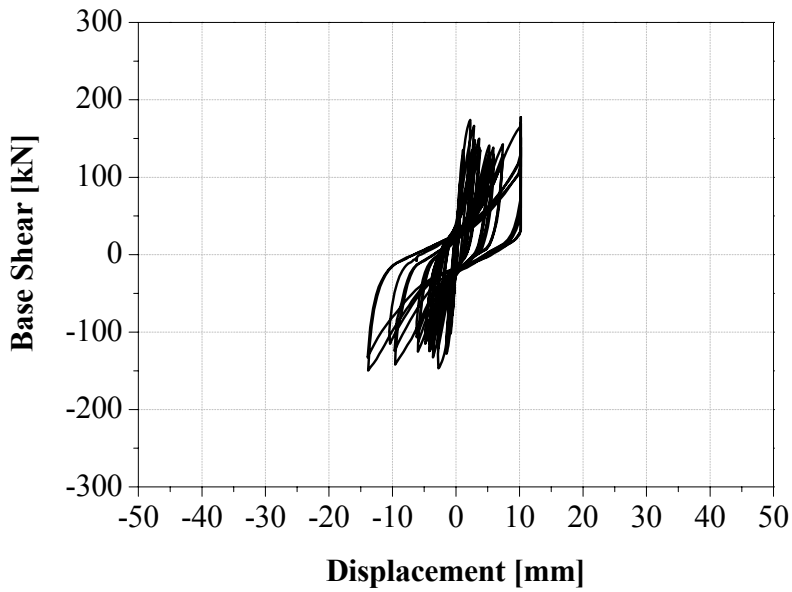


Figure 4.40: Panel horizontal displacement at top

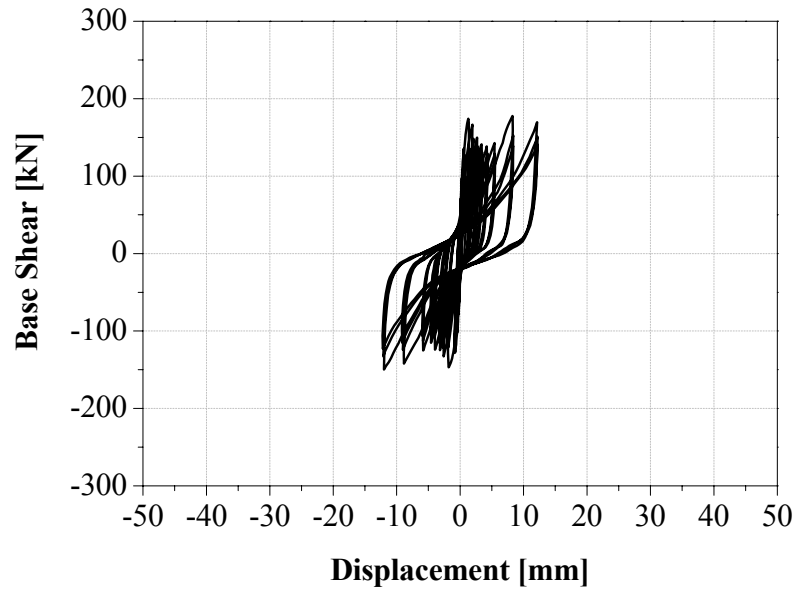


Figure 4.41: Panel horizontal displacement at middle

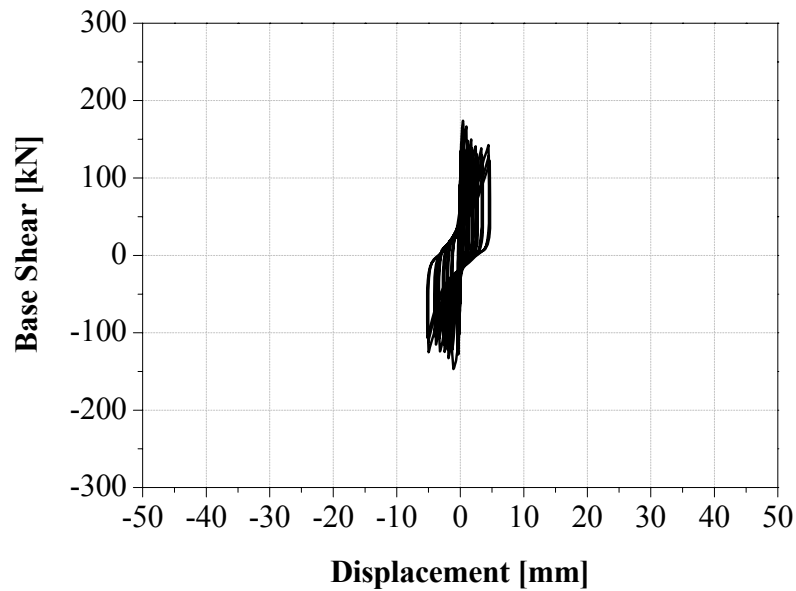


Figure 4.42: Panel horizontal displacement at bottom

Maximum load observed at the end of the positive displacement cycles was 290 kN and in negative displacement cycles was 285 kN. The nominal shear stresses corresponding to these values are 1758 kN/mm^2 and 1727 kN/mm^2 . The first shear crack occurred at lower end of the left column and the beam during -2.8 mm cycles. The load was reported as 116 kN where the nominal shear stress corresponds to 703 kN/mm^2 at that state. Bottom-right corner of the panel has crushed during $+7.0 \text{ mm}$. The load was reported as 124 kN where the nominal shear stress corresponds to 670 kN/mm^2 at that state. Diagonal cracks of the panel occurred during $+28.0 \text{ mm}$.

Maximum displacement of the panel recorded was 10.5 mm in the positive displacement cycles and 14 mm in the negative ones can be seen in Figure 4.40. In Figure 4.41 and 4.42, the displacements occurred at the middle and at the bottom of the wall can be seen. The specimen after test can be seen in Figure 4.43. The observed cracks in the pulling and pushing cycles are seen in Figure 4.44. Table 4.11 shows the width of cracks at specific drift ratios.



Figure 4.43: Specimen 4S at the end of test

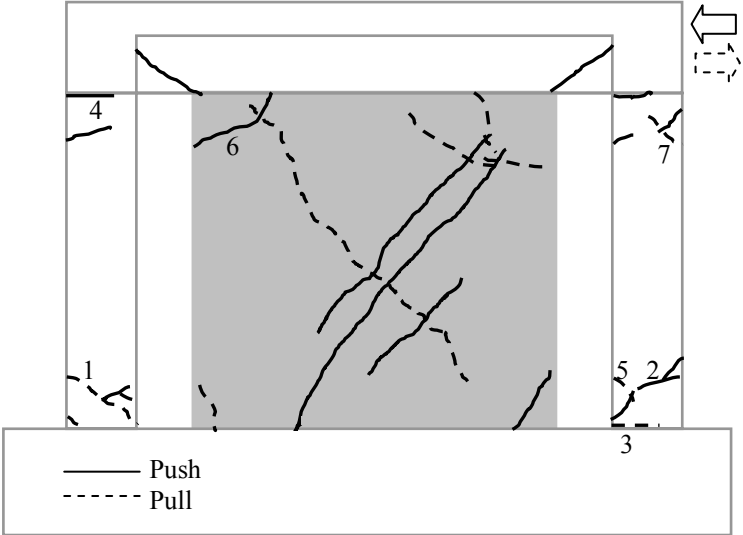


Figure 4.44: Crack pattern of Specimen 4S at the end of test

Table 4.11: Width of cracks in mm at specific story drifts

Crack no:	Drift = 1%	Drift = 2%
1	1.2	>3.5
2	0.6	0.9
3	0.4	0.9
4	1.0	1.0
5	0.3	1.2
6	0.7	1.0
7	-	1.4

Comparisons of the results of the retrofitted frame with shotcrete panel with the bare frames' are given below.

In Figure 4.45 and Tables 4.12 and 4.13, the comparison of the load carrying capacity; in Table 4.14 the comparison of initial stiffnesses, in Figure 4.46 and 4.47 the comparison of energy dissipation capacities of both frames are summarised. Since Specimen 1 and 4S don't have the same concrete compressive strength, an analytical calculation is done to interpret behavior of Specimen 4S as a bare frame introduced in Figure 4.45 and named as "analytical bare 4S".

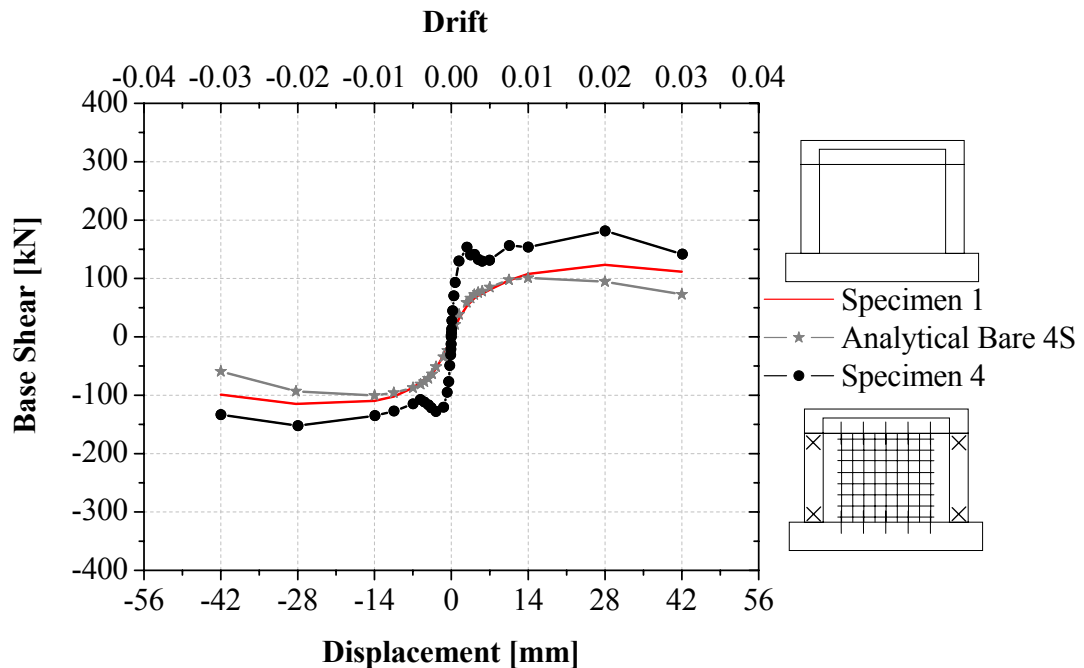


Figure 4.45: Comparison of envelope curves of Specimens 4S and 1 with analytical bare 4S

Table 4.12: Effect of strengthening in general

Specimen Name	Failure Mode	+P _{max} (kN)	+Δ _{max} (mm)	-P _{max} (kN)	-Δ _{max} (mm)	+P _{ult} (kN)	-P _{ult} (kN)	Δ _{ult} (mm)
Specimen 1	Bending + Shear failure at column ends	133	28	-123	-28	104	-86	42
Specimen 4S	Shear failure at column ends	236	28	-190	-28	120	-118	42

Table 4.13: Maximum base shears observed during the tests

Specimen name	Maksimum load [kN]		Proportion ratio	
	Push	Pull	Push	Pull
Specimen 1	133	-123	1.0	1.0
Specimen 4S	236	-190	1.8	1.5

Table 4.14: Initial stiffness of the specimens

Specimen Name	Initial stiffness [kN/mm]	Proportion Ratio
Specimen 1	22.0	1.0
Specimen 4S	223.0	10.3

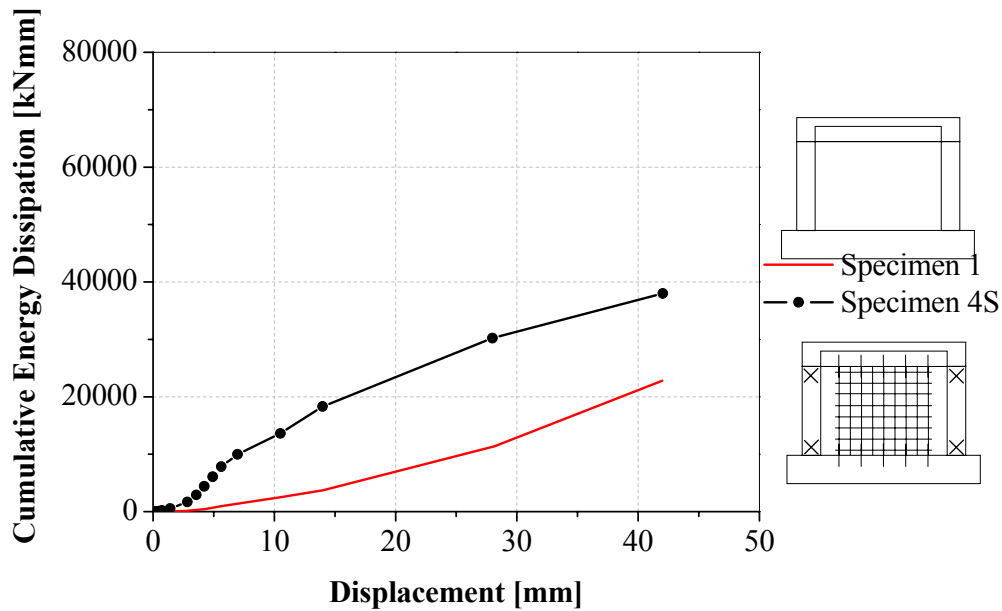


Figure 4.46: The comparison of cumulative energy dissipation capacities of Specimens 1 and 4S

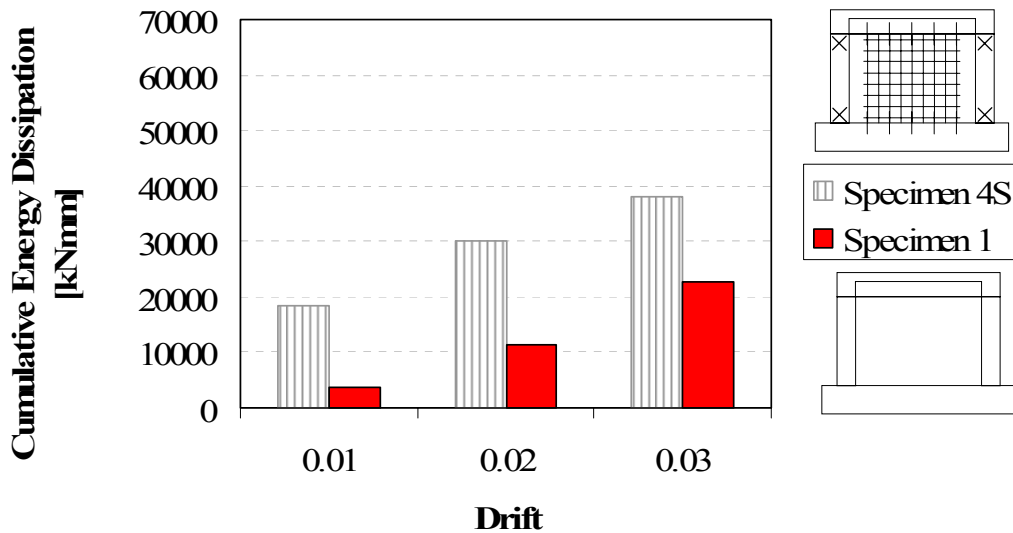


Figure 4.47: Cumulative energy dissipation capacities of Specimens 1 and 4S at various story drifts

The results are summarised below:

- The lateral stiffness of the frames, right before the first cracks occurred in the system, increased by 10 times for Specimen 4S compared with the bare frame's as shown in Table 4.12.
- The lateral load carrying capacity increased by between 1.8 to 1.5 times for the specimens with shotcrete panel compared with the bare frame's Figure 4.45 and Table 4.12 and 4.13.
- Comparison of Figures 4.38 and 4.39 with Figures 4.4 and 4.5;
 - At the top end of the right column, the rotation didnot reach 0.01 radian like the other specimens.
 - At the bottom end of the right column when the rotation is 0.01 radian, the corresponding load at that level for Specimen 1 is 106 kN while for Specimen 4S is 150 kN which is almost 1.4 times of the bare frame's,
- The energy dissipation of the Specimen 4S at 1% story drift are 4.9 times, at 2% story drift are 2.7 times, at 3% story drift are 1.7 times compared to the bare frame's shown in Figure 4.46 and 4.47.

4.7 Test Results of Specimen 5

This specimen is an undamaged RC frame retrofitted with a shotcrete panel that is connected only to the beams. The types of the LVDTs and what was measured by them for the Specimen 5 are given in Table 3.4 and Figure 3.13.

The largest displacement applied was 42 mm. The axial load applied on each column was 132.5 kN which equals to 20% of the axial load carrying capacity the column.

Base shear versus top displacement diagram is given in Figure 4.48. The maximum strengths in tension and compression are 217 kN and 207 kN, respectively, obtained at 28 mm cycles which correspond to 2% story drift. The maximum story drift reached is 3%. The ultimate lateral load carrying capacities of the frame are 77 kN and 89 kN in tension and compression, respectively. The envelope curve of the hysteretic response of the specimen is given in Figure 4.49.

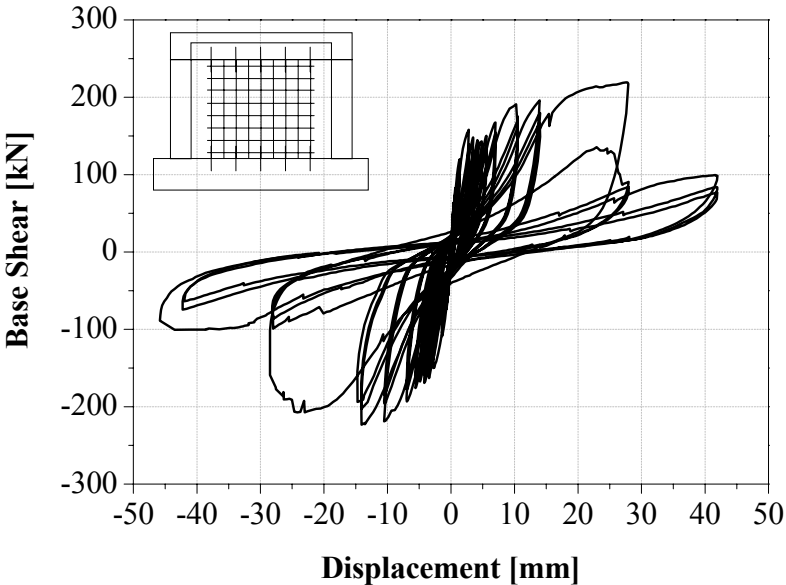


Figure 4.48: Base shear-top displacement curve of Specimen 5

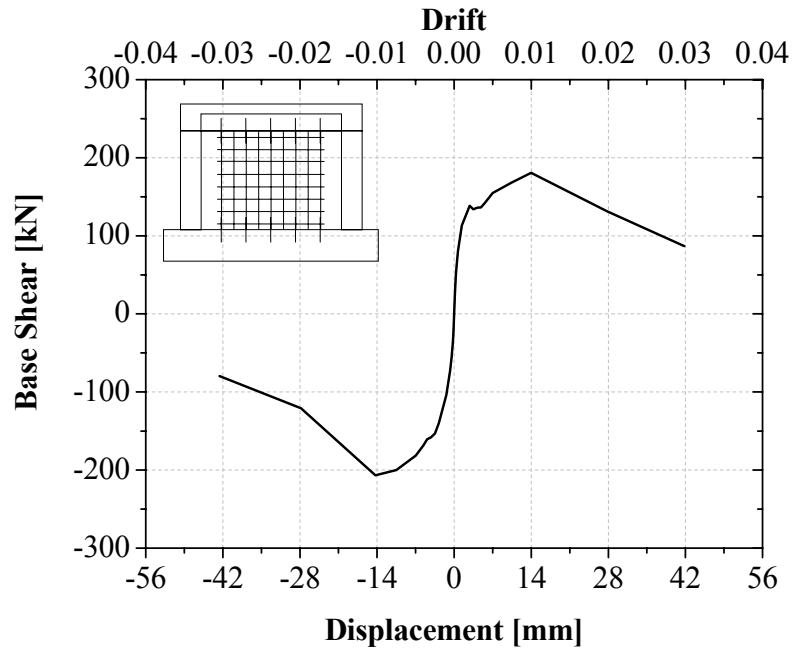


Figure 4.49: The envelope curve of Specimen 5

In Figures 4.50 bottom end rotation of right and left columns and in Figures 4.51 top end rotation of the right and left column versus base shear are given, respectively. At the top end of the right column when the rotation is 0.01 radian, the corresponding load at that level is 200 kN. At the bottom end of the right column when the rotation is 0.01 radian, the corresponding load at that level is 200 kN.

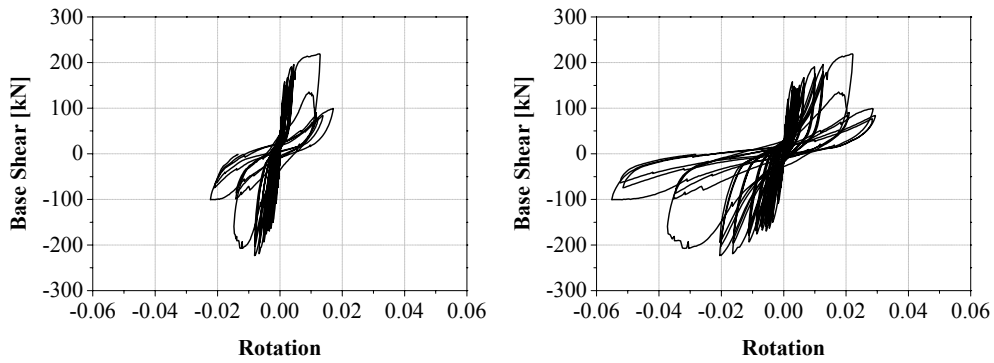


Figure 4.50: Rotation at the bottom end of the right and left column

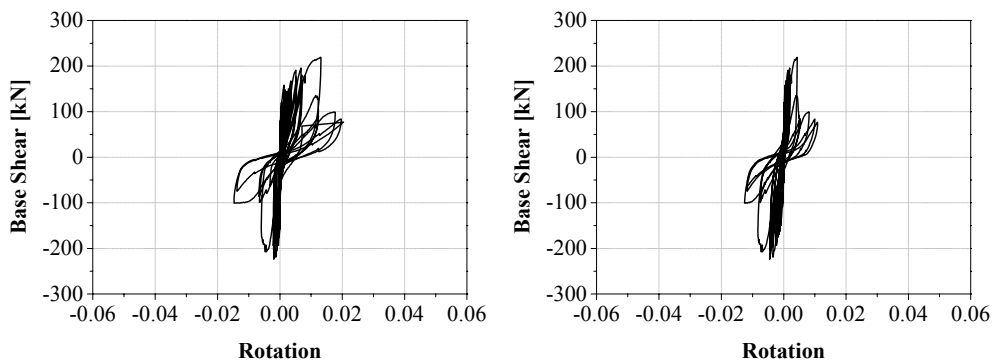


Figure 4.51: Rotation at the top end of the right and left column

The maximum force response that has occurred at the end of the positive displacement cycles was 217 kN and in negative displacement cycles was 207 kN. The nominal shear stresses corresponding to these values are 1173 kN/mm² and 1119 kN/mm². The separation at the ends of the right column and the shear crack at the right end of the beam occurred during the +2.8 mm cycles. In that cycle, the load was 118 kN where the nominal shear stress corresponds to 715 kN/mm². The first diagonal crack observed on the panel, the separation at the ends of the left column and the shear crack at the left end of the beam occurred during the -2.8 mm cycles. In that cycle, the load was 131 kN where the nominal shear stress corresponds to 794 kN/mm².

The specimen after test can be seen in Figure 4.52. Cracks occurred in the pulling and pushing cycles are seen in Figure 4.53. Table 4.15 summarises the width of cracks at specific drift ratios.



Figure 4.52: Specimen 5 at the end of test

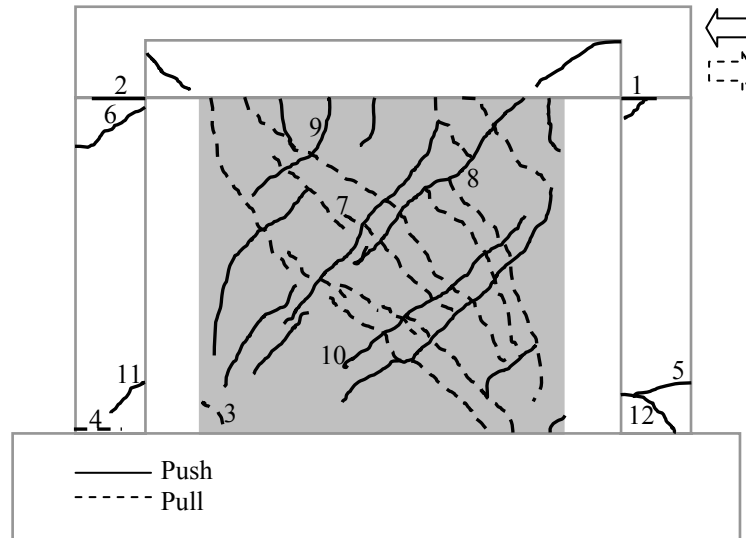


Figure 4.53: Crack pattern of Specimen 5 at the end of test

Table 4.15: Width of cracks in mm at specific story drifts

Crack No:	Drift = 1%	Drift = 2%	Drift = 3%
1	2.5	2.5	2.5
2	1.3	1.8	2.5
3	>3.5	>3.5	>3.5
4	1.7	1.8	>3.5
5	0.4	1.6	3
6	0.3	1.0	2.5
7	0.7	1.8	>3.5
8	0.7	3.0	>3.5
9	0.7	0.8	2.5
10	0.6	0.8	0.9
11	-	0.9	2.7
12	-	-	3.5

Comparisons of the results of the retrofitted frame with shotcrete panel with the bare frames' are given below. In Figure 4.54 and Tables 4.16 and 4.17, the comparison of the load carrying capacity; in Table 4.18 the comparison of initial stiffnesses, in Figure 4.55 and 4.56 the comparison of energy dissipation capacities of both frames are summarised. Since Specimen 1 and 5 don't have the same concrete compressive strength, an analytical calculation is done to interpret behavior of Specimen 5 as a bare frame introduced in Figure 4.54 and named as "analytical bare 5".

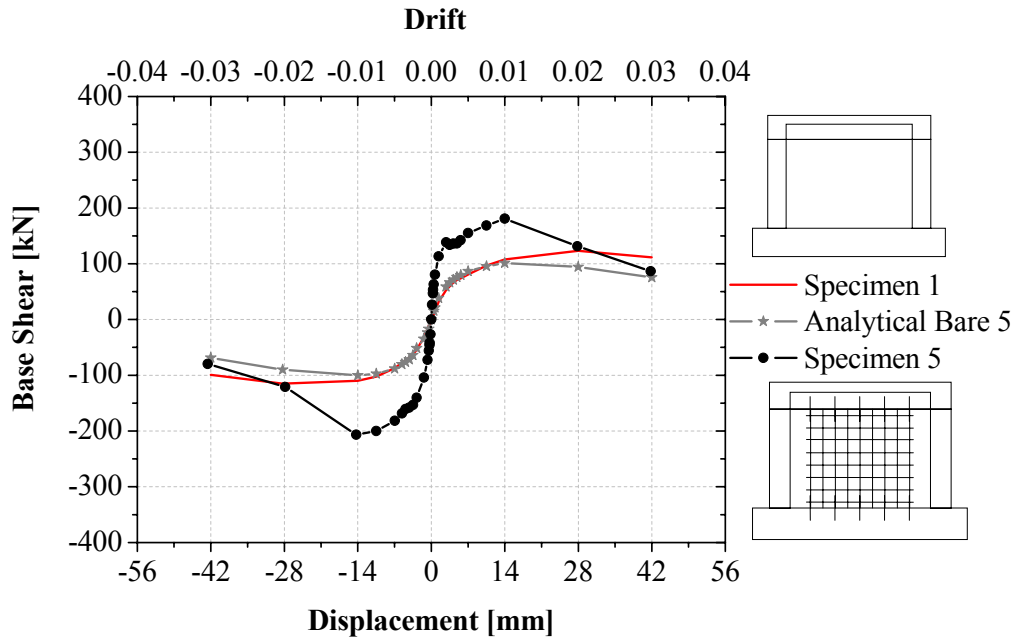


Figure 4.54: Comparison of envelope curves of Specimens 5 and 1 with analytical bare 5

Table 4.16: Effect of strengthening in general

Specimen name	Failure mode	+P _{max} (kN)	+Δ _{max} (mm)	-P _{max} (kN)	-Δ _{max} (mm)	+P _{ult} (kN)	-P _{ult} (kN)	Δ _{ult} (mm)
Specimen 1	Bending + Shear failure at column ends	133	28	-123	-28	104	-86	42
Specimen 5	Shear failure at column ends	217	28	-207	-28	77	-89	42

Table 4.17: Maximum base shears observed during the tests

Specimen Name	Maksimum Load [kN]		Proportion Ratio	
	Push	Pull	Push	Pull
Specimen 1	133	-123	1.0	1.0
Specimen 5	217	-207	1.6	1.7

Table 4.18: Initial stiffness of the specimens

Specimen name	Initial stiffness [kN/mm]	Proportion ratio
Specimen 1	21.6	1.0
Specimen 5	188.5	8.7

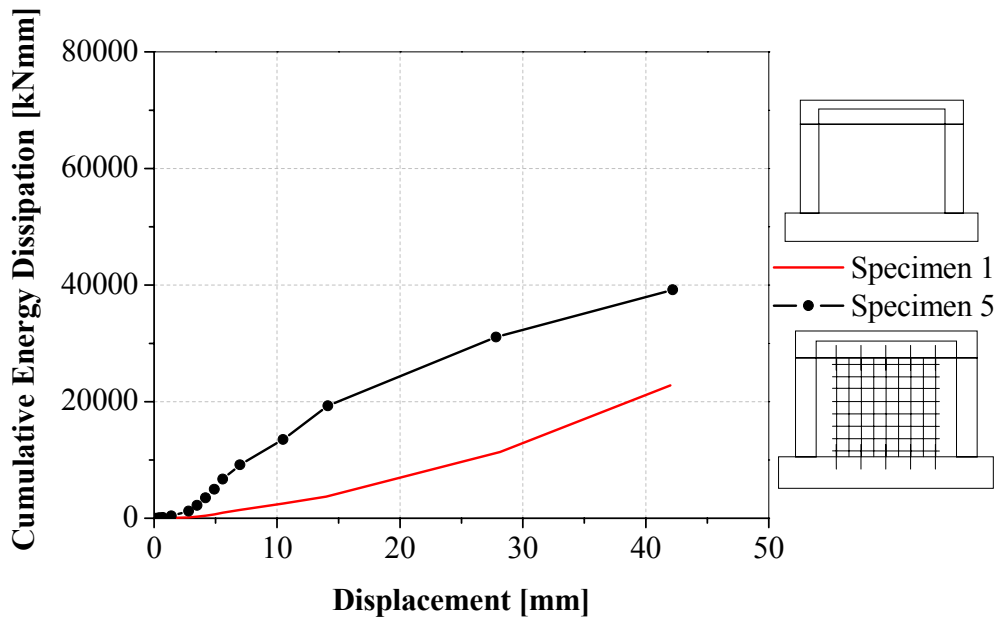


Figure 4.55: The comparison of cumulative energy dissipation capacities of Specimens 1 and 5

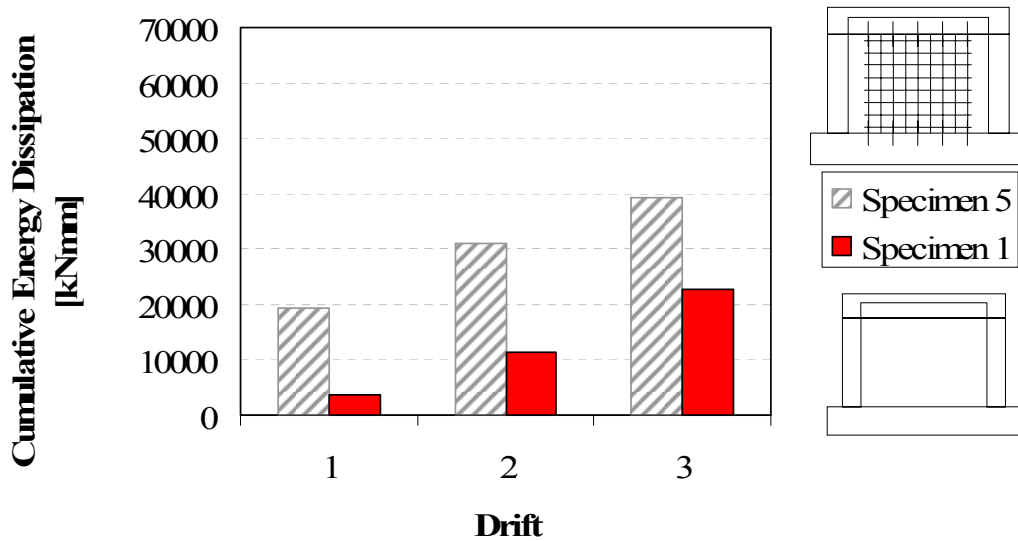


Figure 4.56: Cumulative energy dissipation capacities of Specimens 1 and 5 at various story drifts

The results are summarised below:

- The lateral stiffness of the frames, right before the first cracks occurred in the system, increased by 8.7 times for Specimen 5 compared with the bare frame's, Table 4.18.
- The lateral load carrying capacity increased by between 1.6 to 1.7 times for the specimens with shotcrete panel compared with the bare frame's, Figure 4.54 and Table 4.16 and 4.17.

- Comparison of Figures 4.50 and 4.51 with Figures 4.4 and 4.5;
 - At the top end of the right column when the rotation is 0.01 radian, the corresponding load at that level for Specimen 1 is 133 kN while for Specimen 5 is 200 kN which is almost 1.5 times of the bare frame's,
 - At the bottom end of the right column when the rotation is 0.01 radian, the corresponding load at that level for Specimen 1 is 106 kN while for Specimen 5 is 200 kN which is almost 1.9 times of the bare frame's,
- The energy dissipation of the Specimen 5 at 1% story drift are 5.2 times, at 2% story drift are 2.7 times, at 3% story drift are 1.7 times compared to the bare frame's shown in Figure 4.55 and 4.56.

4.8 Test Results of Specimen 6

This is the undamaged RC frame, retrofitted with shotcrete panel that is connected to frame at all four sides after a pre-reverse deflection applied to the beam. The types of the LVDTs and what was measured by them for the Specimen 6 are given at Table 3.3 and Figure 3.12.

The largest displacement applied was 28 mm. The axial load applied on each column was 147 kN which equals to 20% of the axial load carrying capacity the column.

Base shear versus top displacement diagram is given in Figure 4.57. The maximum strengths in tension is 374 kN obtained at 28 mm cycles which correspond to 2% story drift and in compression is 359 kN obtained at 10.5 mm cycles. The maximum story drift reached is 2%. The ultimate lateral load carrying capacities of the frame are 132 kN and 110 kN in tension and compression, respectively. The envelope curve of the hysteretic response of the specimen is given in Figure 4.58.

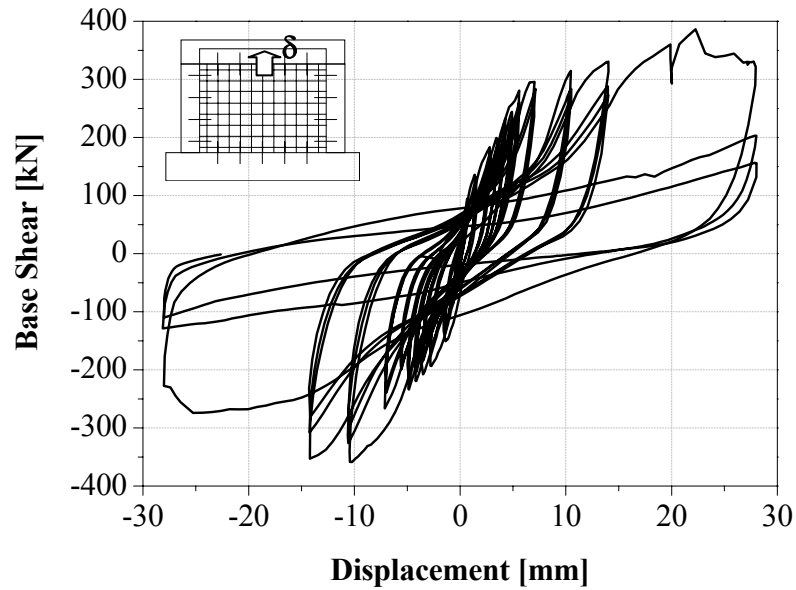


Figure 4.57: Base shear-top displacement curve of Specimen 6

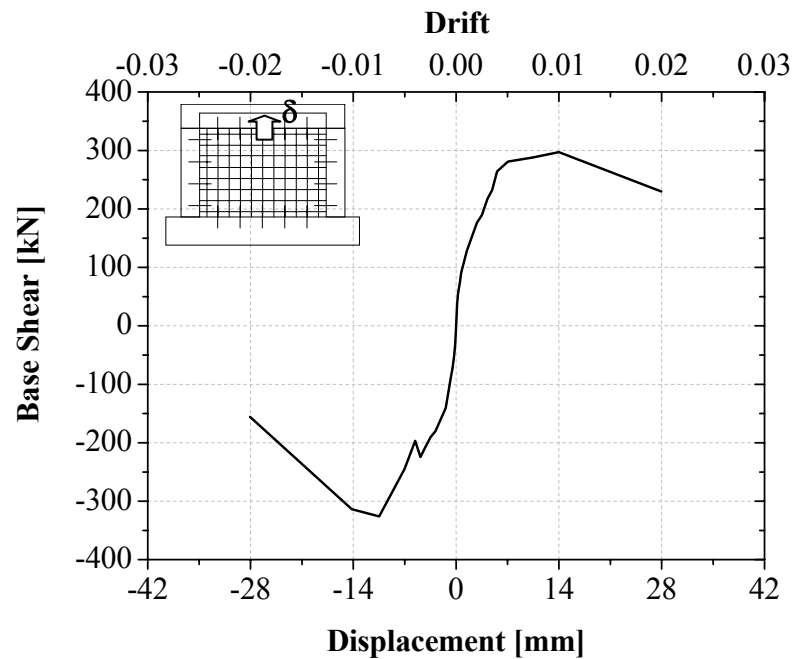


Figure 4.58: The envelope curve of Specimen 6

In Figures 4.59 bottom end rotation of right and left columns and in Figures 4.60 top end rotation of the right and left columns versus base shear are given, respectively. At the top end of the right column when the rotation is 0.01, the corresponding load at that level for Specimen 6 is 330 kN. At the bottom end of the right column when the rotation is 0.01 radian, the corresponding load at that level for Specimen 6 is 386 kN.

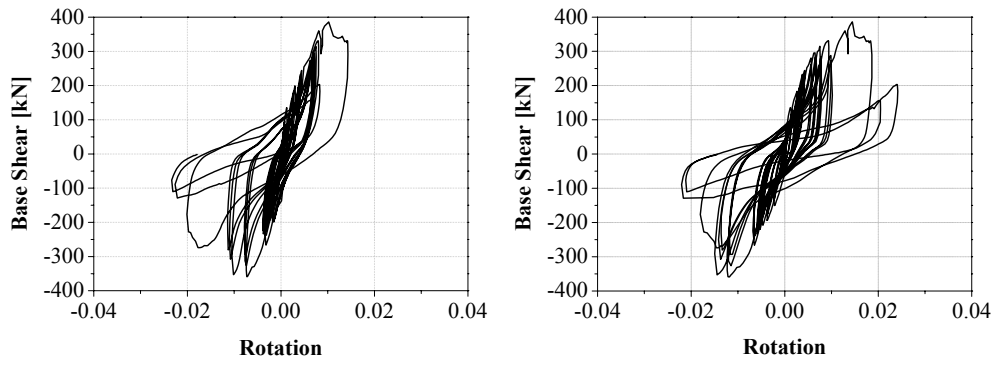


Figure 4.59: Rotation at the bottom end of the right and left column

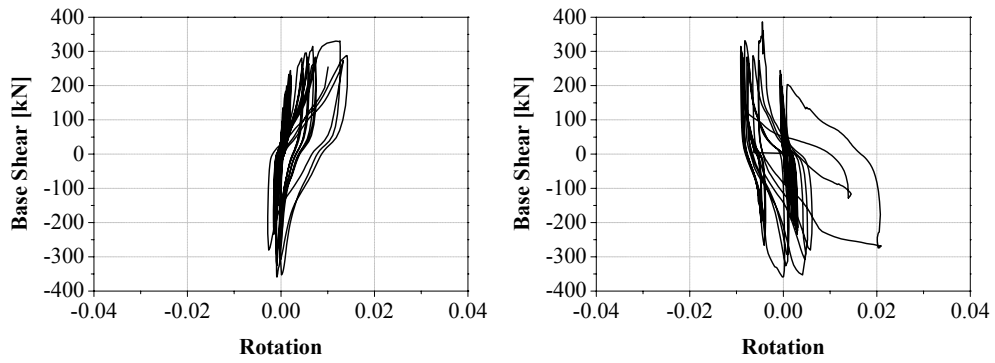


Figure 4.60: Rotation at the top end of the right and left column

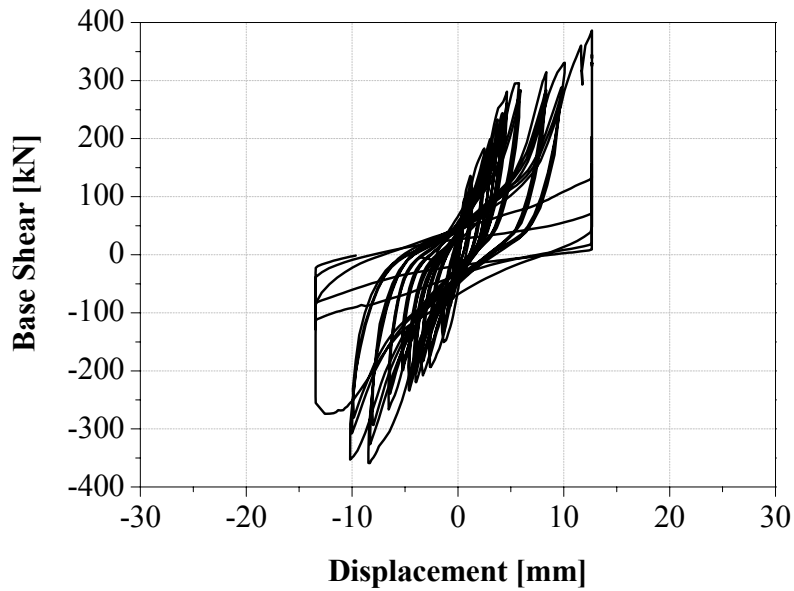


Figure 4.61: Panel displacement

Maximum load that has occurred at the end of the positive displacement cycles was 374 kN and in negative displacement cycles was 358.5 kN. The nominal shear stresses corresponding to these values are 2022 kN/mm² and 1938 kN/mm². The first

separation between the panel and the frame members and the first shear crack occurred at lower end of the right column happened during the +0.467 mm cycles. The load was reported as 71.4 kN where the nominal shear stress corresponds to 386 kN/mm² at that state. The first diagonal crack was observed on the panel during the – 0.467 mm cycles. The load was reported as 70.5 kN where the nominal shear stress corresponds to 381 kN/mm² at that state. Maximum displacement of the panel recorded was 10.5 mm in the positive and negative displacement cycles in Figure 4.61.

The specimen after test can be seen in Figure 4.62. Cracks occurred in the pulling and pushing cycles are seen in Figure 4.63. Table 4.19 summarizes the width of cracks at specific drift ratios.



Figure 4.62: Specimen 6 at the end of test

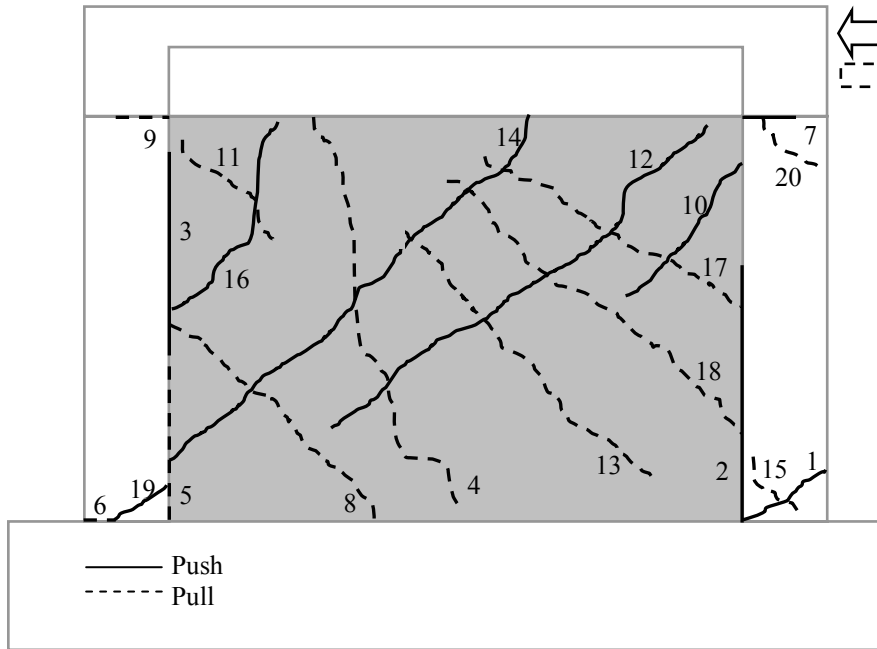


Figure 4.63: Crack pattern of Specimen 6 at the end of test

Table 4.19: Width of cracks in mm at specific story drifts

Crack no:	Drift = 1%	Drift = 2%	Crack no:	Drift = 1%	Drift = 2%
1	1.6	2.5	11	0.4	>3.5
2	1.6	1.6	12	1.2	1.8
3		<3.5	13	1.2	3.5
4	1.2	>3.5	14	0.8	>3.5
5	2.5	>3.5	15	0.3	2.0
6	1.2	1.2	16	1.0	<3.5
7	2.5	>3.5	17	0.7	2.0
8	0.7	>3.5	18	0.3	3.5
9	3.0	>3.5	19	-	2.5
10	0.3	<3.5	20	-	2.0

Comparisons of the results of the retrofitted frame with shotcrete panel with the bare frames' are given below. In Figure 4.64 and Tables 4.20 and 4.21, the comparison of the load carrying capacity; in Table 4.22 the comparison of initial stiffnesses, in Figure 4.65 and 4.66 the comparison of energy dissipation capacities of both frames are summarised. Since Specimen 1 and 6 don't have the same concrete compressive strength, an analytical calculation is done to interpret behavior of Specimen 6 as a bare frame introduced in Figure 4.63 and named as "analytical bare 6".

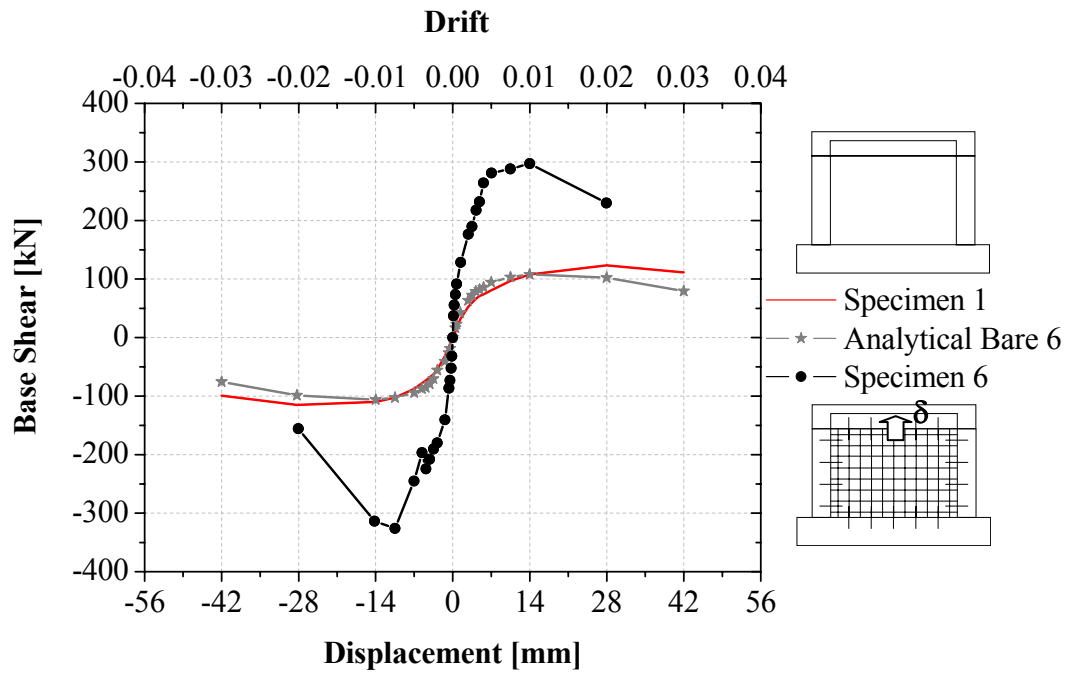


Figure 4.64: Comparison of envelope curves of Specimens 6 and 1 with analytical bare 6

Table 4.20: Effect of strengthening in general

Specimen name	Failure mode	+P _{max} (kN)	+Δ _{max} (mm)	-P _{max} (kN)	-Δ _{max} (mm)	+P _{ult} (kN)	-P _{ult} (kN)	Δ _{ult} (mm)
Specimen 1	Bending + Shear failure at column ends	133	28	-123	-28.0	104	-86	42
Specimen 6	Shear failure at column ends	374	28	-359	-10.5	132	-110	28

Table 4.21: Maximum base shears observed during the tests

Specimen name	Maksimum load [kN]		Proportion ratio	
	Push	Pull	Push	Pull
Specimen 1	133	-123	1.0	1.0
Specimen 6	374	-359	2.8	2.9

Table 4.22: Initial stiffness of the specimens

Specimen name	Initial stiffness [kN/mm]	Proportion ratio
Specimen 1	21.6	1.0
Specimen 6	249.9	11.6

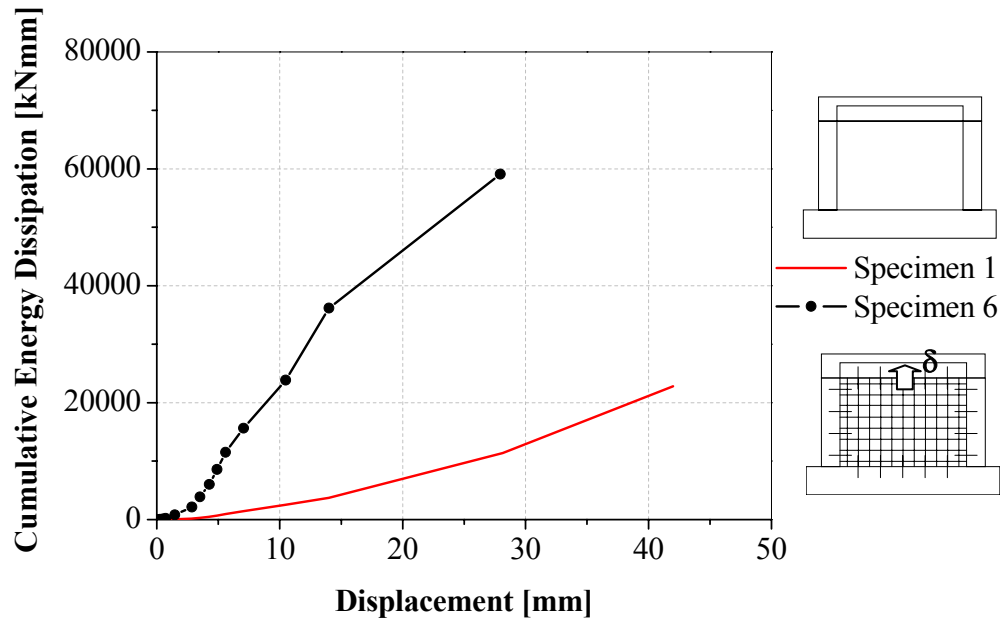


Figure 4.65: The comparison of cumulative energy dissipation capacities of Specimens 1 and 6

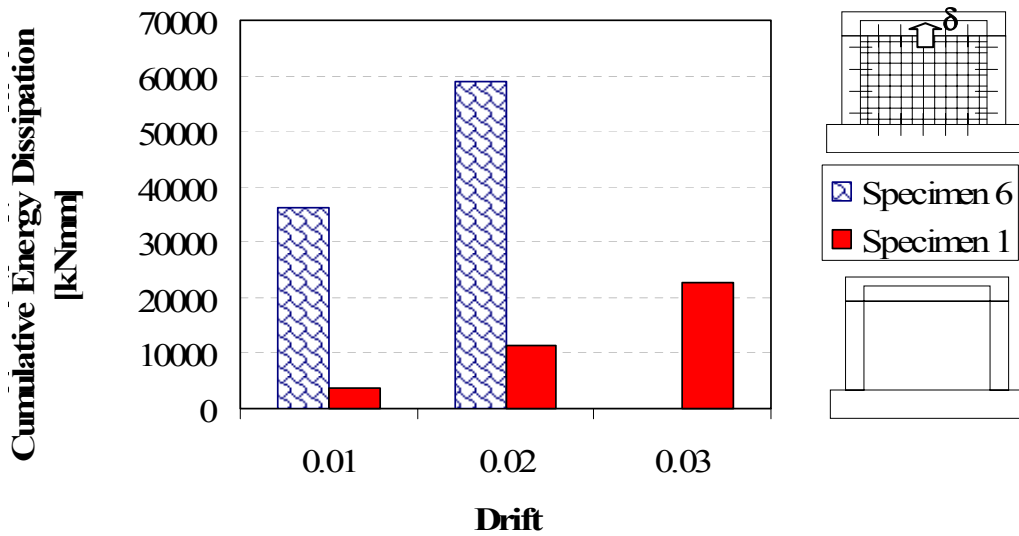


Figure 4.66: Cumulative energy dissipation capacities of Specimens 1 and 6 at various drifts

The results are summarised below:

- The lateral stiffness of the frames, right before the first cracks occurred in the system, increased by 11.6 times for Specimen 6 compared with the bare frame's, Table 4.22.
- The lateral load carrying capacity increased by between 2.8-2.9 times for the specimens with shotcrete panel compared with the bare frame's, Figure 4.64 and Table 4.20 and 4.21.

- Comparison of Figures 4.59 and 4.60 with Figures 4.4 and 4.5;
 - At the top end of the right column when the rotation is 0.01 radian, the corresponding load at that level for Specimen 1 is 133 kN while for Specimen 6 is 330 kN which is almost 2.5 times of the bare frame's,
 - At the bottom end of the right column when the rotation is 0.01 radian, the corresponding load at that level for Specimen 1 is 106 kN while for Specimen 6 is 386 kN which is almost 3.6 times of the bare frame's,
- The energy dissipation of the Specimen 6 at 1% story drift are 9.7 times, at 2% story drift are 5.2 times compared to the bare frame's shown in Figure 4.65 and 4.66.

4.9 Test Results of Specimen 7

This is the undamaged RC frame, retrofitted with shotcrete panel that is connected only to the beams after a pre-reverse deflection applied to the beam. The types of the LVDTs and what was measured by them for the Specimen 7 are given in Table 3.4 and Figure 3.13.

The largest displacement applied was 42 mm. The axial load applied on each column was 132.5 kN which equals to 20% of the axial load carrying capacity the column.

Base shear versus top displacement diagram is given in Figure 4.67. The maximum strengths in tension is 209 kN obtained at 28 mm cycles which correspond to 2% story drift and in compression is 211 kN obtained at 10.5 mm cycles. The maximum story drift reached is 3%. The ultimate lateral load carrying capacities of the frame are 45 kN and 42 kN in tension and compression, respectively. The envelope curve of the hysteretic response of the specimen is given in Figure 4.68.

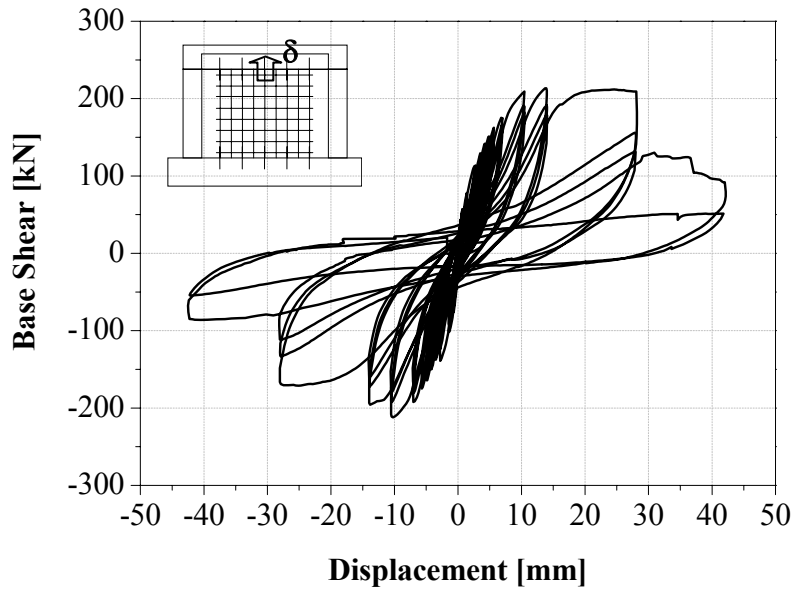


Figure 4.67: Base shear-top displacement curve of Specimen 7

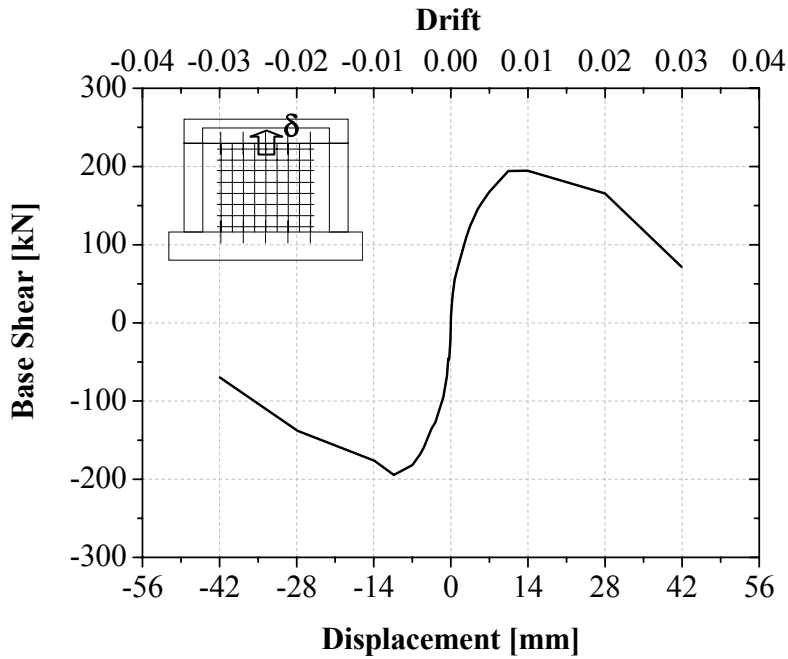


Figure 4.68: The envelope curve of Specimen 7

In Figures 4.69 bottom end rotation of right and left columns and in Figures 4.70 top end rotation of the right and left column versus base shear are given, respectively. At the top end of the right column when the rotation is 0.01 radian, the corresponding load at that level for Specimen 7 is 205 kN. At the bottom end of the right column when the rotation is 0.01 radian, the corresponding load at that level for Specimen 7 is 210 kN.

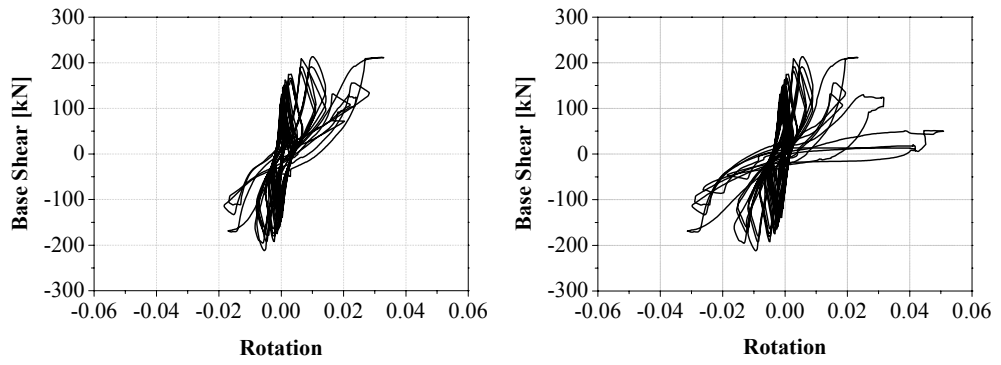


Figure 4.69: Rotation at the bottom end of the right and left column

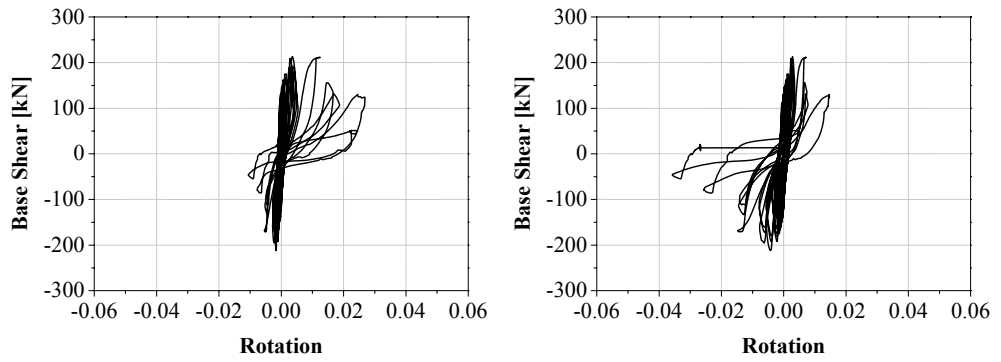


Figure 4.70: Rotation at the top end of the right and left column

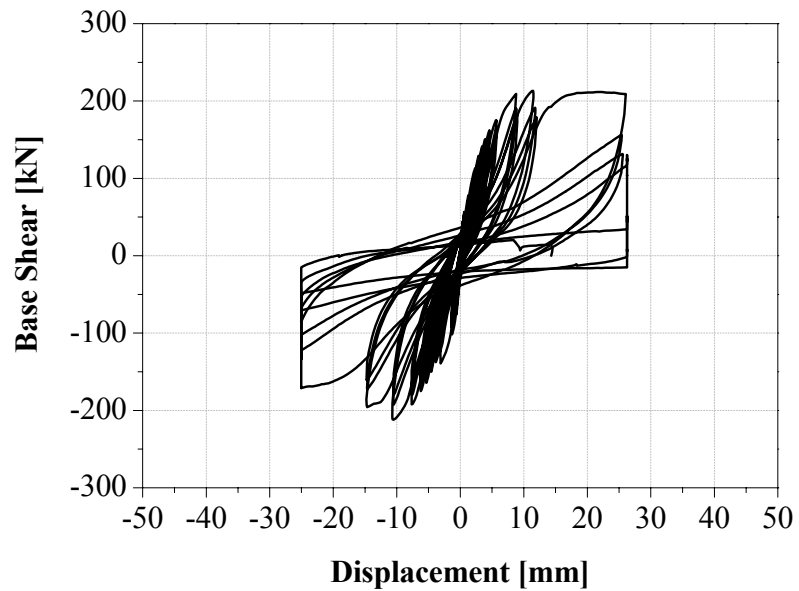


Figure 4.71: Panel horizontal displacement at top

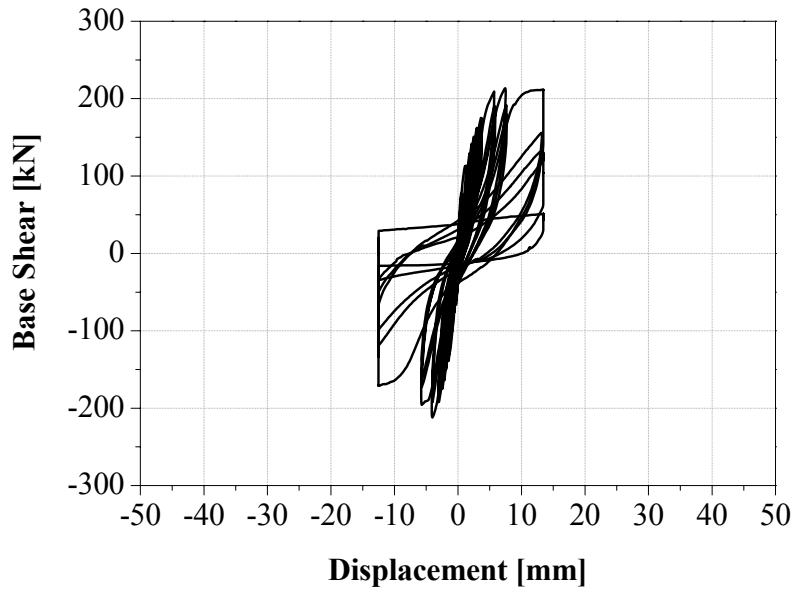


Figure 4.72: Panel horizontal displacement at middle

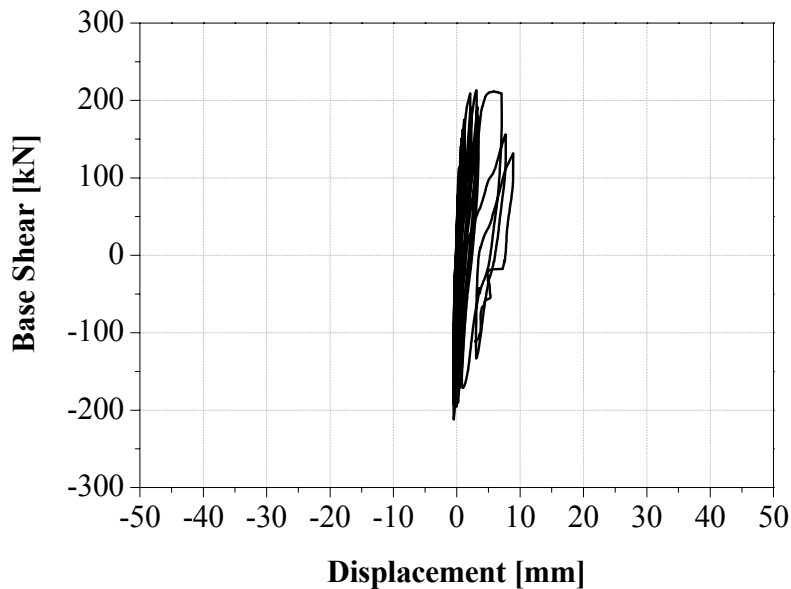


Figure 4.73: Panel horizontal displacement at bottom

The maximum force response that has occurred at the end of the positive displacement cycles was 209 kN and in negative displacement cycles was 211 kN. The nominal shear stresses corresponding to these values are 1267 kN/mm^2 and 1279 kN/mm^2 . The separation at the end of the left column occurred during the -0.7 mm cycles. In that cycle, the load was 54 kN. The shear crack at the upper end of the right column occurred during the $+4.2 \text{ mm}$ cycles. In that cycle, the load was 131 kN where the nominal shear stress correspond to 794 kN/mm^2 . The first diagonal crack observed on the panel occurred during the $+2.8 \text{ mm}$ cycles. In that cycle, the load

was 106 kN where the nominal shear stress correspond to 642 kN/mm^2 . Maximum displacement of the panel recorded was 25 mm in the positive displacement cycles and 25 mm in the negative ones can be seen in Figure 4.71. In Figure 4.72 and 4.73, the displacements occurred at the middle and at the bottom of the wall can be seen.

The specimen after test can be seen in Figure 4.74. Cracks occurred in the pulling and pushing cycles are seen in Figure 4.75. Table 4.23 summarizes the width of cracks at specific drift ratios.



Figure 4.74: Specimen 7 at the end of test

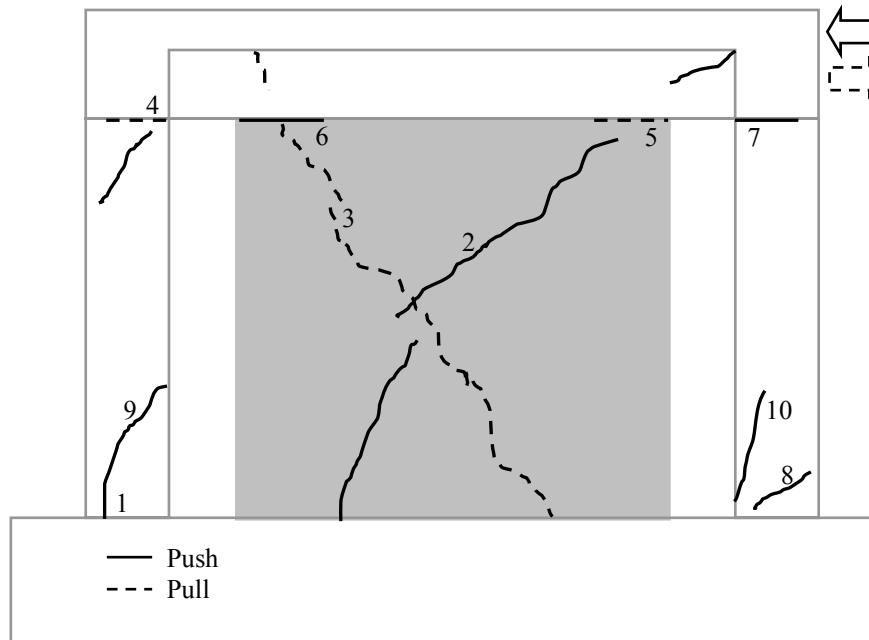


Figure 4.75: Crack pattern of Specimen 7 at the end of test

Table 4.23: Width of cracks in mm at specific story drifts

Crack no:	Drift = 1%	Drift = 2%
1	1.8	3.5
2	2.0	3.5
3	1.4	0.8
4	2.5	3.5
5	3.5	>3.5
6	3.0	>3.5
7	0.7	3.5
8	2.5	>3.5
9	0.7	>3.5
10	0.3	1.4
11	2.0	>3.5
12	-	3.5
13	-	1.8
14	-	1.8

Comparisons of the results of the retrofitted frame with shotcrete panel with the bare frames' are given below. In Figure 4.76 and Tables 4.24 and 4.25, the comparison of the load carrying capacity; in Table 4.26 the comparison of initial stiffnesses, in Figure 4.77 and 4.78 the comparison of energy dissipation capacities of both frames are summarised. Since Specimen 1 and 7 don't have the same concrete compressive strength, an analytical calculation is done to interpret behavior of Specimen 7 as a bare frame introduced in Figure 4.76 and named as "analytical bare 7".

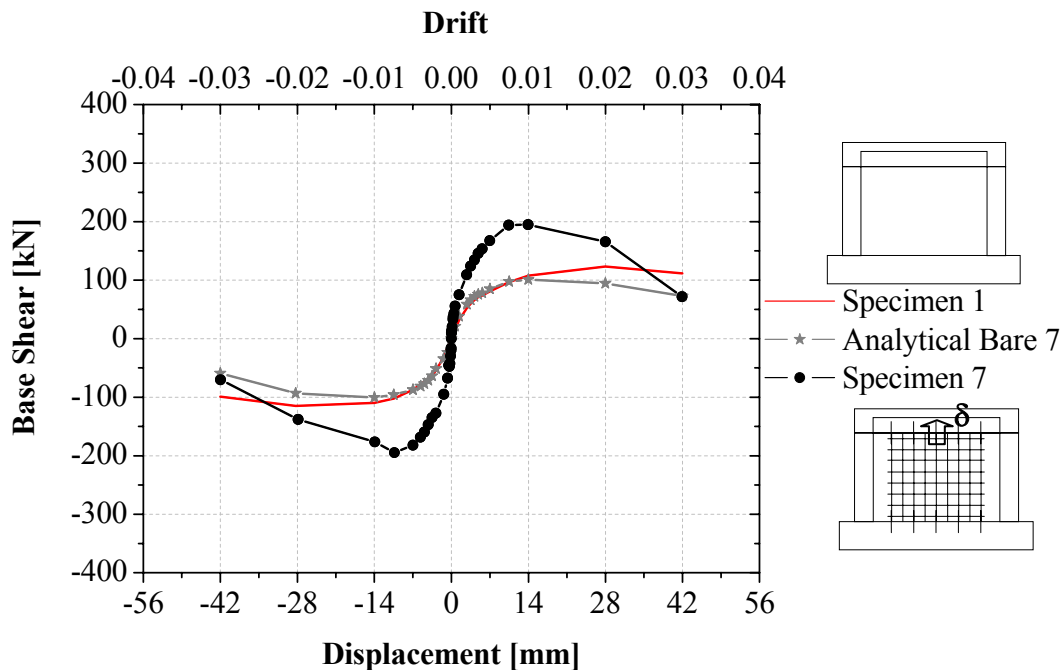


Figure 4.76: Comparison of envelope curves of Specimens 7 and 1 with analytical bare 7

Table 4.24: Effect of strengthening in general

Specimen name	Failure mode	+P _{max} (kN)	+Δ _{max} (mm)	-P _{max} (kN)	-Δ _{max} (mm)	+P _{ult} (kN)	-P _{ult} (kN)	Δ _{ulti} (mm)
Specimen 1	Bending + Shear failure at column ends	133	28	-123	-28.0	104	-86	42
Specimen 7	Shear failure at column ends	209	28	-211	-10.5	45	-52	42

Table 4.25: Maximum base shears recorded during the tests

Specimen name	Maksimum load [kN]		Proportion ratio	
	Push	Pull	Push	Pull
Specimen 1	133	-123	1.0	1.0
Specimen 7	209	-211	1.6	1.7

Table 4.26: Initial stiffness of the specimens

Specimen name	Initial stiffness [kN/mm]	Proportion ratio
Specimen 1	21.6	1.0
Specimen 7	179.3	8.3

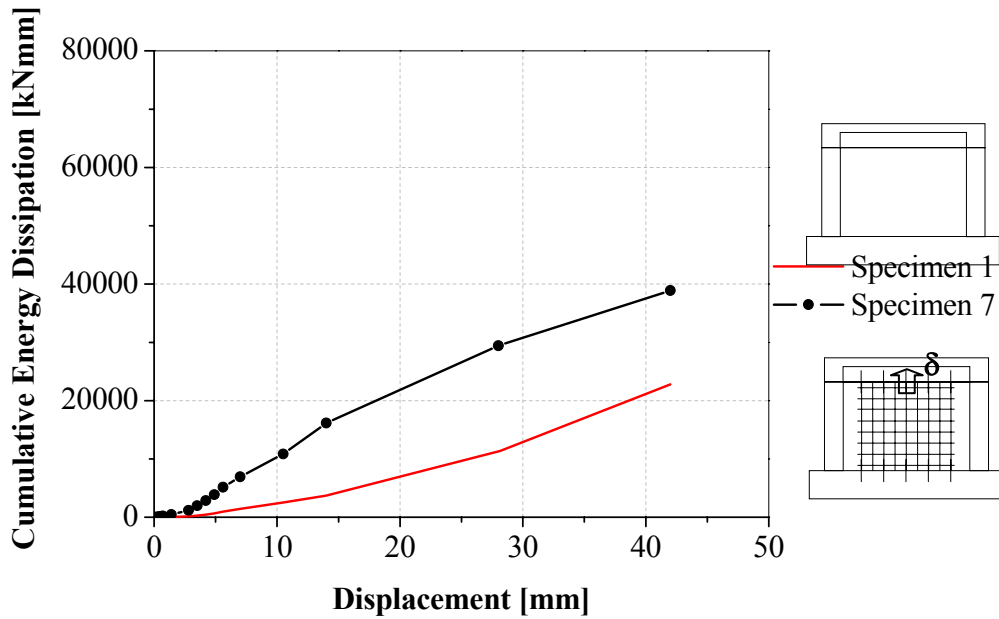


Figure 4.77: The comparison of cumulative energy dissipation capacities of Specimens 1 and 7

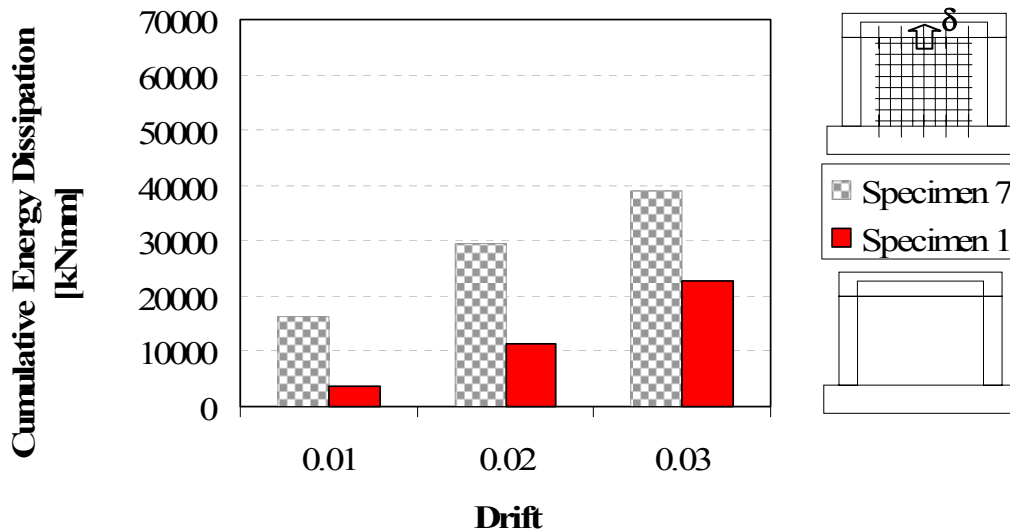


Figure 4.78: Cumulative energy dissipation capacities of Specimens 1 and 7 at various story drifts

The results are summarised below:

- The lateral stiffness of the frames, right before the first cracks occurred in the system, increased by 8.3 times for Specimen 7 compared with the bare frame's, Table 4.26.
- The lateral load carrying capacity increased by between 1.6-1.7 times for the specimens with shotcrete panel compared with the bare frame's, Figure 4.76 and Table 4.24 and 4.25.
- Comparison of Figures 4.69 and 4.70 with Figures 4.4 and 4.5;
 - At the top end of the right column when the rotation is 0.01 radian, the corresponding load at that level for Specimen 1 is 133 kN while for Specimen 7 is 205 kN which is almost 1.5 times of the bare frame's,
 - At the bottom end of the right column when the rotation is 0.01 radian, the corresponding load at that level for Specimen 1 is 106 kN while for Specimen 7 is 210 kN which is almost 2.0 times of the bare frame's,
 - The energy dissipation of the Specimen 7 at 1% story drift are 4.3 times, at 2% story drift are 2.6 times, at 3% story drift are 1.7 times compared to the bare frame's shown in Figure 4.77 and 4.78.

4.10 Test Results of Specimen 8

This specimen is a conventional shear wall used as a reference frame and the effect of the different strengthening methods is compared and discussed with this specimen's results. The types of the LVDTs and what was measured by them for Specimen 8, are given at Table 3.3 and Figure 3.12.

The largest displacement applied was 14 mm. The axial load applied on each column was 132.5 kN which equals to 20% of the axial load carrying capacity the column.

Base shear versus top displacement diagram is given in Figure 4.79. The maximum strengths in tension is 329 kN obtained at 10.5 mm cycles which correspond to 0.75% story drift and in compression is 275 kN obtained at 3.5 mm cycles. The maximum story drift reached is 1%. The ultimate lateral load carrying capacities of the frame are 261 kN and 129 kN in tension and compression, respectively. The envelope curve of the hysteretic response of the specimen is given in Figure 4.80.

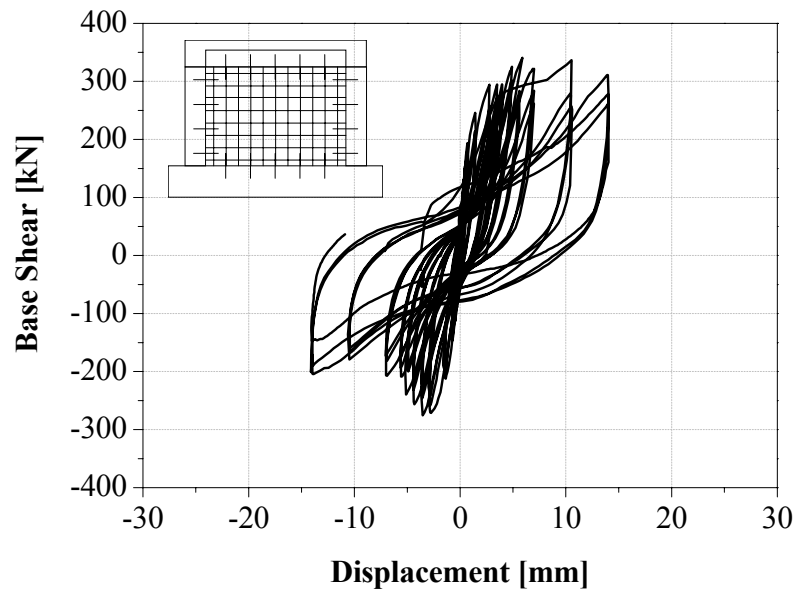


Figure 4.79: Base shear-top displacement curve of Specimen 8

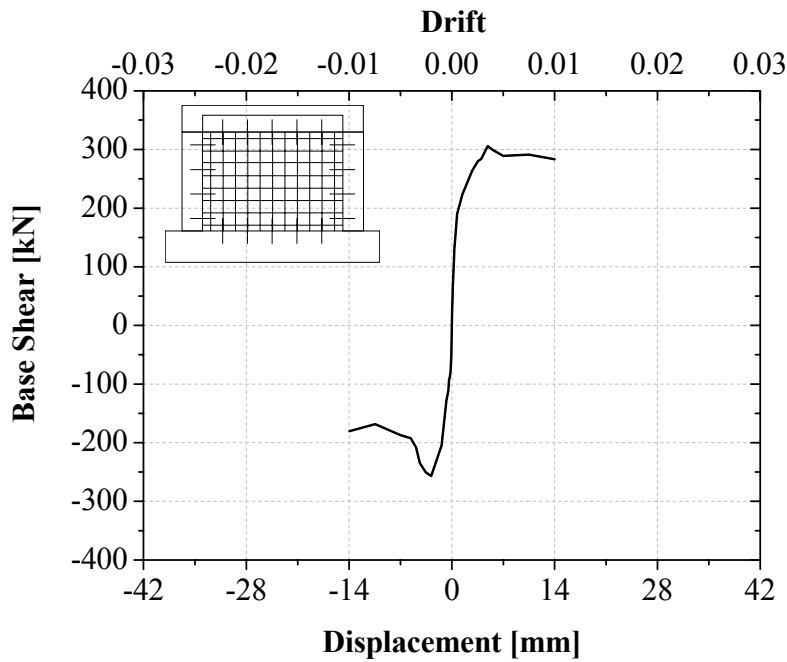


Figure 4.80: The envelope curve of Specimen 8

In Figures 4.81 bottom end rotation of right and left columns and in Figures 4.82 top end rotation of the right and left column versus base shear are given, respectively. At the top and bottom end of the right column, the rotation did not reach 0.01 radian like the other specimens.

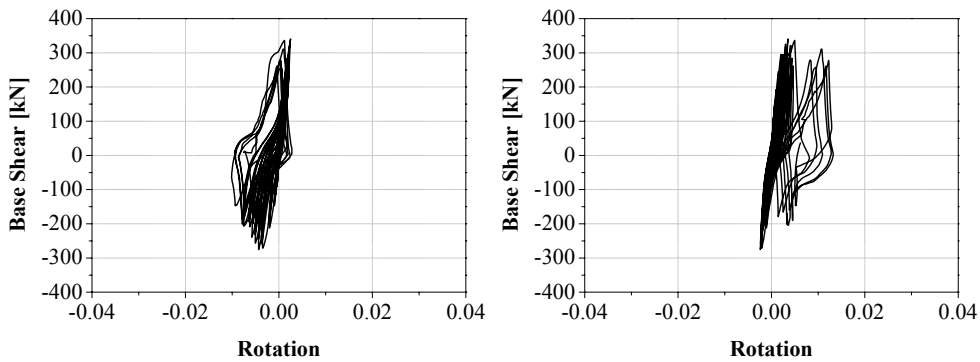


Figure 4.81: Rotation at the bottom end of the right and left column

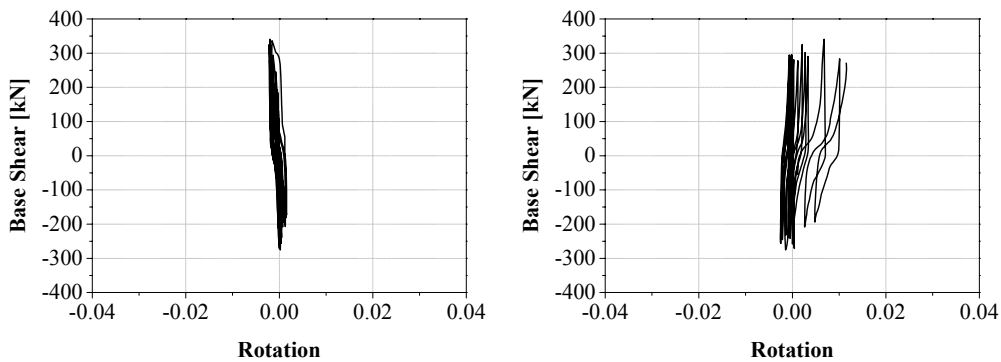


Figure 4.82: Rotation at the top end of the right and left column

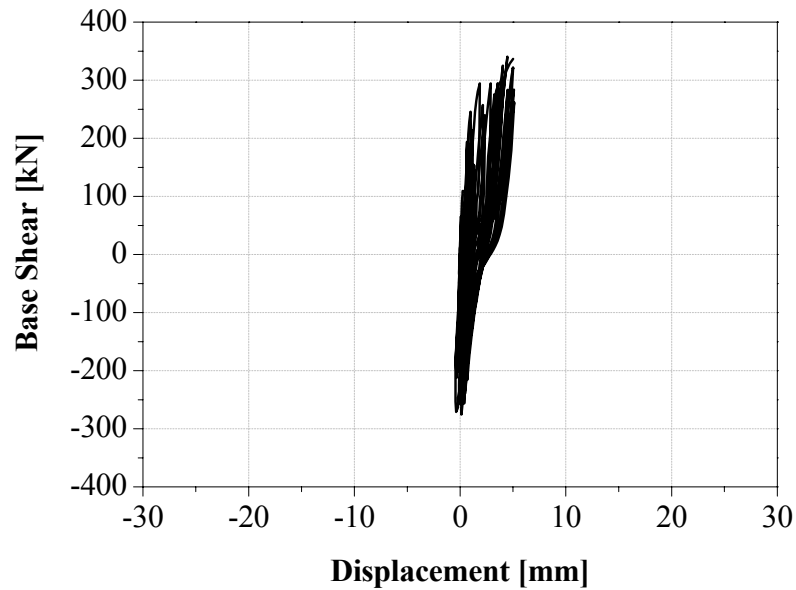


Figure 4.83: Panel displacement

Maximum load that has occurred at the end of the positive displacement cycles was 329 kN and in negative displacement cycles was 275 kN. The nominal shear stresses corresponding to these values are 1778 kN/mm² and 1486 kN/mm². The first separation between the panel and the frame members happened during the +0.7 mm cycles. The load was reported as 191 kN where the nominal shear stress corresponds to 1032 kN/mm² at that state. The first diagonal crack and the first shear crack at the upper end of the left column was observed on the panel during the -0.467 mm cycles. Maximum displacement of the panel recorded was 5 mm in the positive displacement cycles and 0.4 mm in the negative ones shown in Figure 4.83.

The specimen after test can be seen in Figure 4.84. Cracks occurred in the pulling and pushing cycles are seen in Figure 4.85. Table 4.27 shows the width of cracks at specific drift ratios.



Figure 4.84: Specimen 8 at the end of test

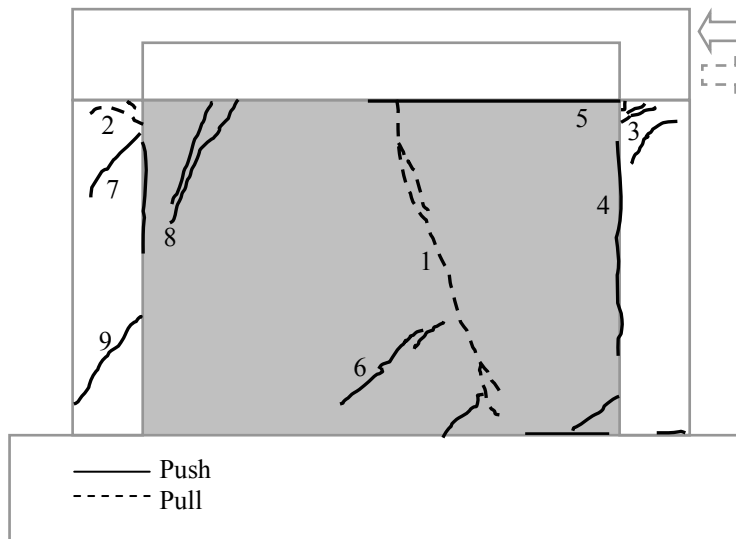


Figure 4.85: Crack pattern of Specimen 8 at the end of test

Table 4.27: Width of cracks in mm at specific story drift

Crack no:	Drift = 1%
1	>3.5
2	>3.5
3	>3.5
4	1.0
5	>3.5
6	0.9
7	>3.5
8	>3.5
9	1.2

Comparisons of the results of the retrofitted frame with shotcrete panel with the bare frames' are given below. In Figure 4.86 and Tables 4.28 and 4.29, the comparison of

the load carrying capacity; in Table 4.30 the comparison of initial stiffnesses, in Figure 4.87 and 4.88 the comparison of energy dissipation capacities of both frames are summarised. Since Specimen 1 and 8 don't have the same concrete compressive strength, an analytical calculation is done to interpret behavior of Specimen 8 as a bare frame introduced in Figure 4.86 and named as "analytical bare 8".

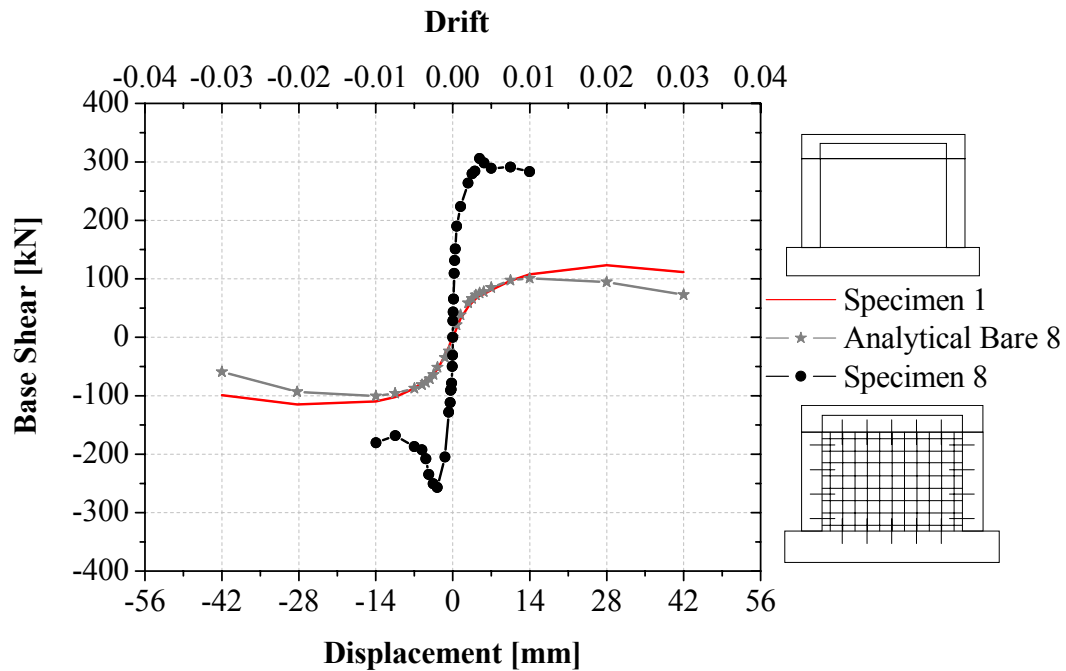


Figure 4.86: Comparison of envelope curves of Specimens 8 and 1 with analytical bare 8

Table 4.28: Effect of strengthening in general

Specimen name	Failure mode	+P _{max} (kN)	+Δ _{max} (mm)	-P _{max} (kN)	-Δ _{max} (mm)	+P _{ult} (kN)	-P _{ult} (kN)	Δ _{ult} (mm)
Specimen 1	Bending + Shear failure at column ends	133	28	-123	-28	104	-86	42
Specimen 8	Shear failure at column ends	329	10.5	-275	-3.5	261	-129	14

Table 4.29: Maximum base shears observed during the tests

Specimen name	Maksimum load [kN]		Proportion ratio	
	Push	Pull	Push	Pull
Specimen 1	133	-123	1.0	1.0
Specimen 8	329	-275	2.5	2.2

Table 4.30: Initial stiffness of the specimens

Specimen name	Initial stiffness [kN/mm]	Proportion ratio
Specimen 1	21.6	1.0
Specimen 8	444.0	20.5

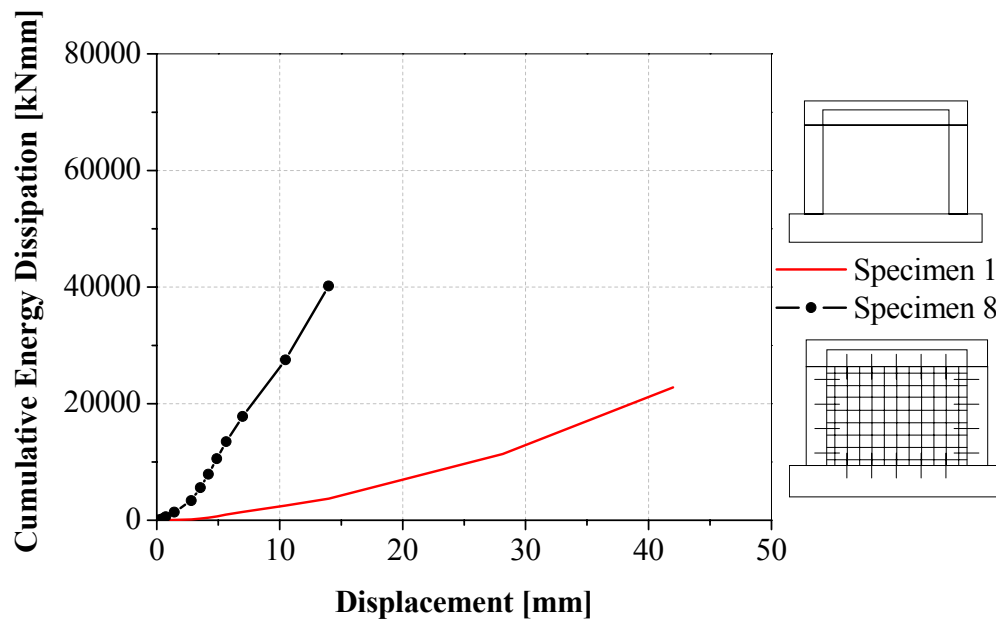


Figure 4.87: The comparison of cumulative energy dissipation capacities of Specimens 1 and 8

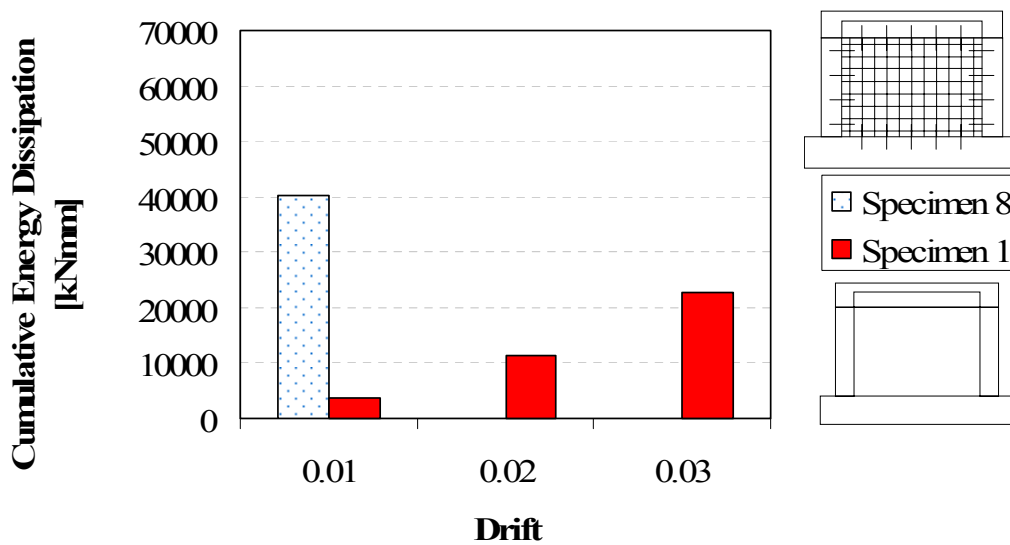


Figure 4.88: Cumulative energy dissipation capacities of Specimens 1 and 8 at various story drifts

The results are summarised below:

- The lateral stiffness of the frames, right before the first cracks occurred in the system, increased by 20.5 times for Specimen 8 compared with the bare frame's, Table 4.30.

- The lateral load carrying capacity increased by between 2.5-2.2 times for the specimens with shotcrete panel compared with the bare frame's, Figure 4.86 and Table 4.28 and 4.29.
- Comparison of Figures 4.81 and 4.82 with Figures 4.4 and 4.5; at the top and bottom end of the right column, the rotation did not reach 0.01 radian like the other specimens.
- The energy dissipation of the Specimen 8 at 1% story drift is 10.8 times compared to the bare frame's shown in Figure 4.87 and 4.88.

4.11 Evaluation of the Test Results

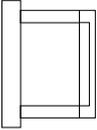
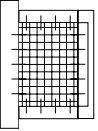
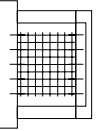
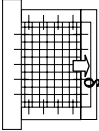
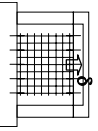
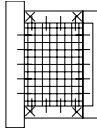
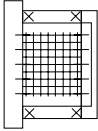
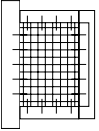
The comparison of results of the six test specimens with shotcrete panel and one shear wall specimen to the bare frame (Specimen 1) and within each other are explained briefly below. Each specimen is evaluated according to the parameters stated in Table 3.1. Failure modes, load carrying capacities, initial stiffnesses, energy dissipation capacities and lateral stiffnesses are discussed here.

4.11.1 Failure modes

Table 4.31 summarizes the maximum loads, the ultimate loads frames carried in pull and push cycles and the failure modes occurred. These data are taken from the experimental study. As can be seen in the table; bending and shear failure at column ends occurred in the bare frame, while generally shear failure at column ends observed in the retrofitted frames. This is because the specimens have low shear strength properties to represent the building stock of Turkey. No matter how strong wet-mixed sprayed concrete panels were, the ultimate failure mode of the systems were controlled by the existing shear capacity of the outer frames. All of the strengthened frame experiments were ended due to severe shear cracks occurring at the end of the columns.

On the web of short beams which exist on the right and left side of the panel in the case of partially infilled specimen, some 0.2 mm-width shear cracks are observed. The cracks are seen first at 0.2% story drift. At the end of the tests, the width of these cracks increased to 0.5 mm. However these kinds of cracks are not observed at the same region of the fully infilled specimens.

Table 4.31: Effect of retrofitting on general quantities

Specimen	Type	Failure mode	$+P_{max}$ (kN)	$+\Delta_{max}$ (mm)	$-P_{max}$ (kN)	$-\Delta_{max}$ (mm)	$+P_{ult}$ (kN)	$-P_{ult}$ (kN)	Δ_{ult} (mm)
1		Bending + Shear failure at column ends	133.0	28.0	-123.0	-28.0	104.0	-86.0	42.0
3		Shear failure at column ends	291.0	10.5	-279.0	-10.5	165.0	-136.0	14.0
5		Shear failure at column ends	217.0	28.0	-207.0	-28.0	77.0	-89.0	42.0
6		Shear failure at column ends	374.0	28.0	-359.0	-10.5	132.0	-110.0	28.0
7		Shear failure at column ends	209.0	28.0	-211.0	-10.5	45.0	-52.0	42.0
2S		Shear failure at column ends	342.0	28.0	-394.0	-28.0	166.0	-249.0	28.0
4S		Shear failure at column ends	236.0	28.0	-190.0	-28.0	120.0	-118.0	42.0
8		Shear failure at column ends	329.0	10.5	-275.0	-3.5	261.0	-129.0	14.0

4.11.2 Lateral load carrying capacity

Table 4.32 summarizes the maximum loads carried by the retrofitted RC frames in push and pull cycles. The lateral load carrying capacity increases are also calculated and presented in proportion ratios compared with that of the bare frame's.

Table 4.32: Maximum base shears observed during the tests

Specimen	Maximum load [kN]		Ratio to Specimen 1	
	Push	Pull	Push	Pull
1	133	-123	1.0	1.0
3	291	-279	2.2	2.3
5	217	-207	1.6	1.7
6	374	-359	2.8	2.9
7	209	-211	1.6	1.7
2S	342	-394	2.6	3.2
4S	236	-190	1.8	1.5
8	329	-275	2.5	2.2

The lateral load carrying capacity increased between 2.2 to 3.2 times for the specimens with shotcrete panel that were fully connected to the frame, and between 1.6 to 1.8 times for the specimens with shotcrete panel with a gap between the panel and the columns compared with the bare frame's. Because the frames were pre-damaged, the capacity differences between push and pull cycles both for Specimen 2S and 4S has occurred. The specimen with the shear wall shows the same amount of increase with the fully connected shotcrete panel ones. Pre-reverse deflection seems to make a 30% increase in the lateral load carrying capacity of the specimen for the specimens with shotcrete panel fully connected to the frame and no significant effect on the specimens which have shotcrete panels that are connected only to the beams.

The comparison of the envelope curves of the hysteretic responses of the two fully connected shotcrete panel specimens to the bare frame's are given in Figure 4.89.

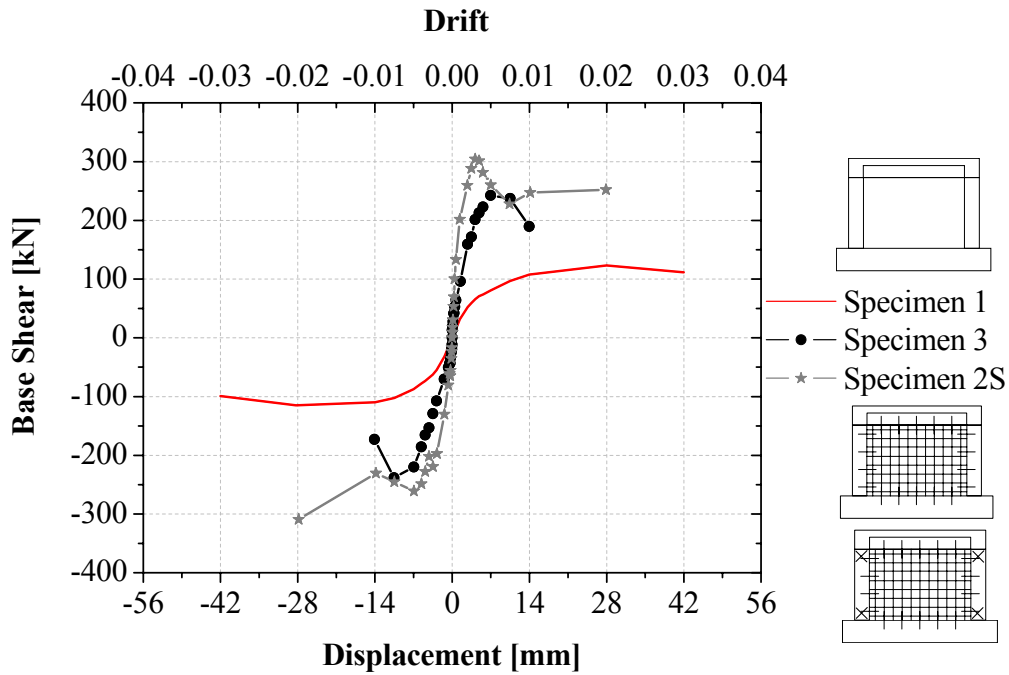


Figure 4.89: The comparison of envelope curves of Specimens 1, 2S and 3

Although Specimen 2S was a representative of a damaged frame, its performance was higher than Specimen 3. It is attributed to the higher compressive strength of outer frame and wet-mixed sprayed concrete panel. For this reason in Figure 4.90, the analytical solution of Specimen 3 with using the frame and the shotcrete panel concrete compressive strength of Specimen 2S, named as “analytical 3_2S”, are sketched with Specimen 2S and 3.

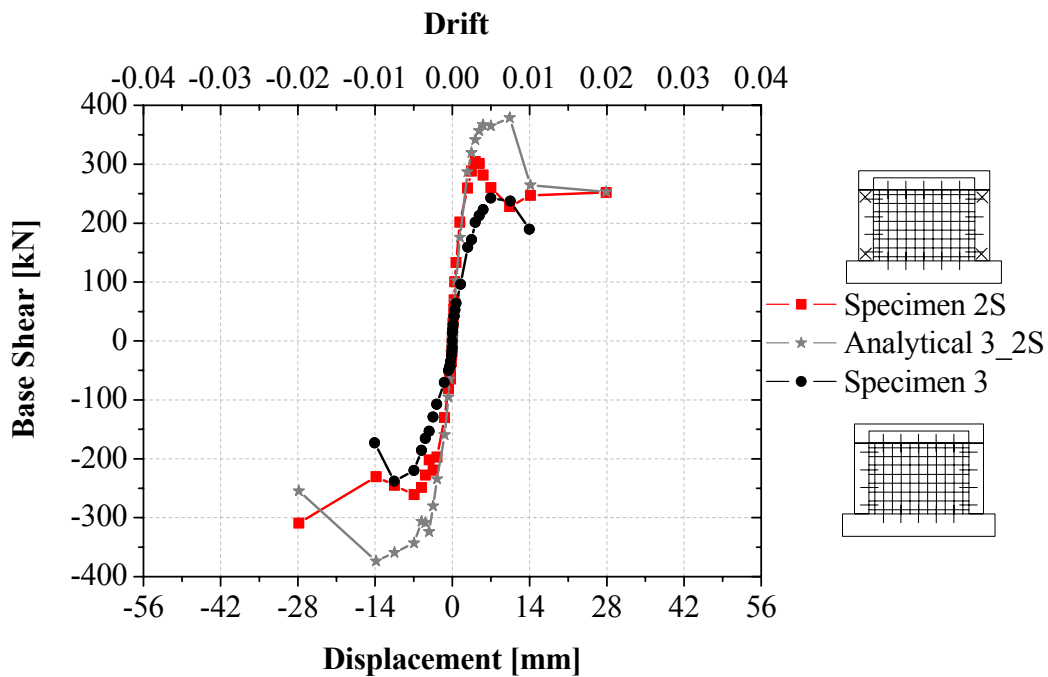


Figure 4.90: The comparison of envelope curves of Specimens 2S and 3 with analytical 3_2S

The two shotcrete specimens, which are connected only to the beams, are given in Figure 4.91.

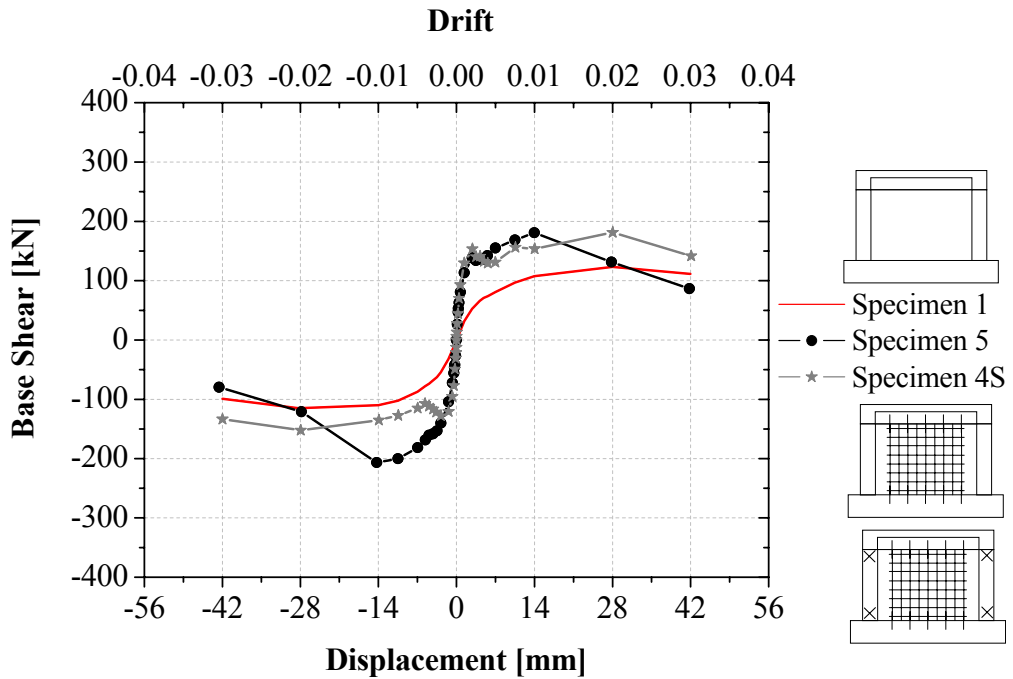


Figure 4.91: The comparison of envelope curves of Specimens 1, 4S and 5

The pre-reverse effect on the load carrying capacities can be seen in Figure 4.92 for fully connected shotcrete panel specimens. Since the concrete compressive strengths of Specimen 3 and 6 are not the same, Specimen 3's behaviour is predicted analytically using Specimen 6's concrete strengths, named as "analytical 3_6", and introduced as an envelope curve in Figure 4.93. In Figure 4.94 for shotcrete specimens, which are connected only to the beams are presented. In Figure 4.95 only the pre-reversed beam specimens are compared within each other.

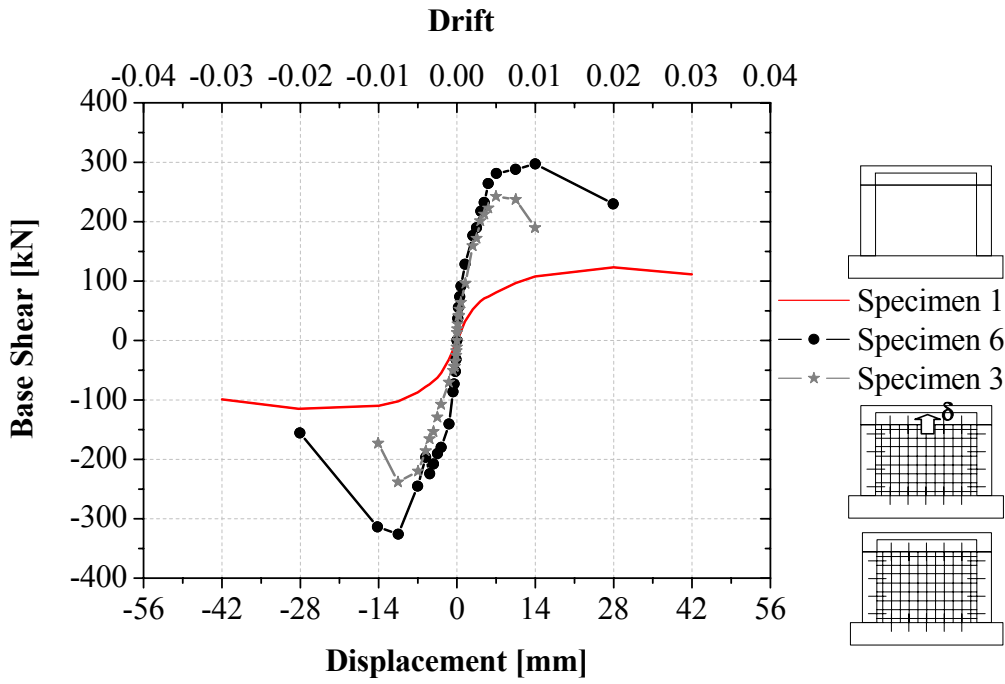


Figure 4.92: The comparison of envelope curves of Specimens 1, 3 and 6

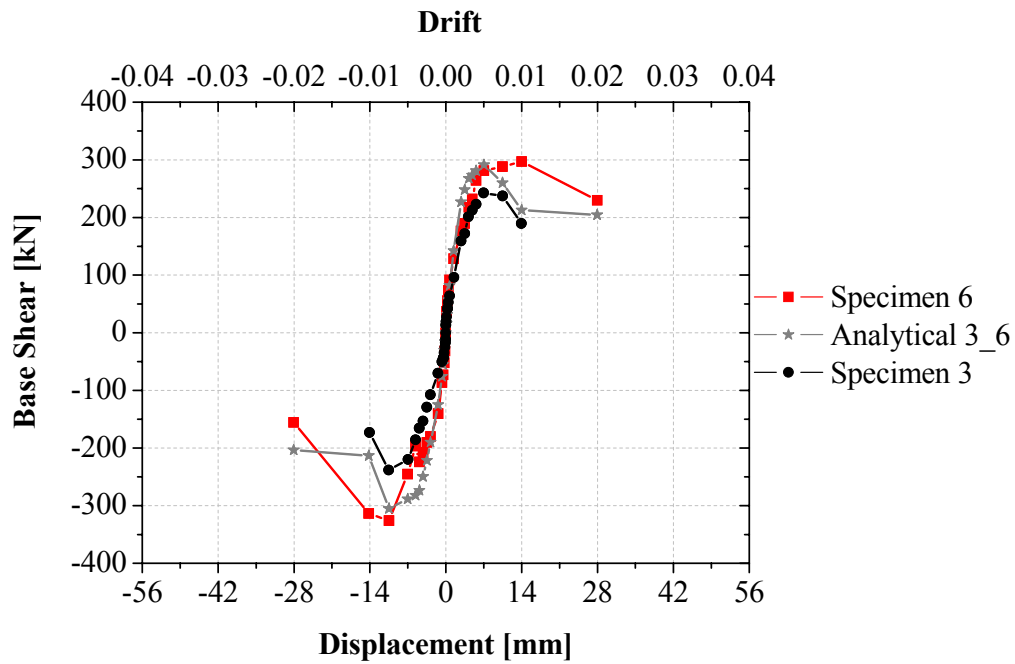


Figure 4.93: The comparison of envelope curves of Specimens 3 and 6 with analytical 3_6

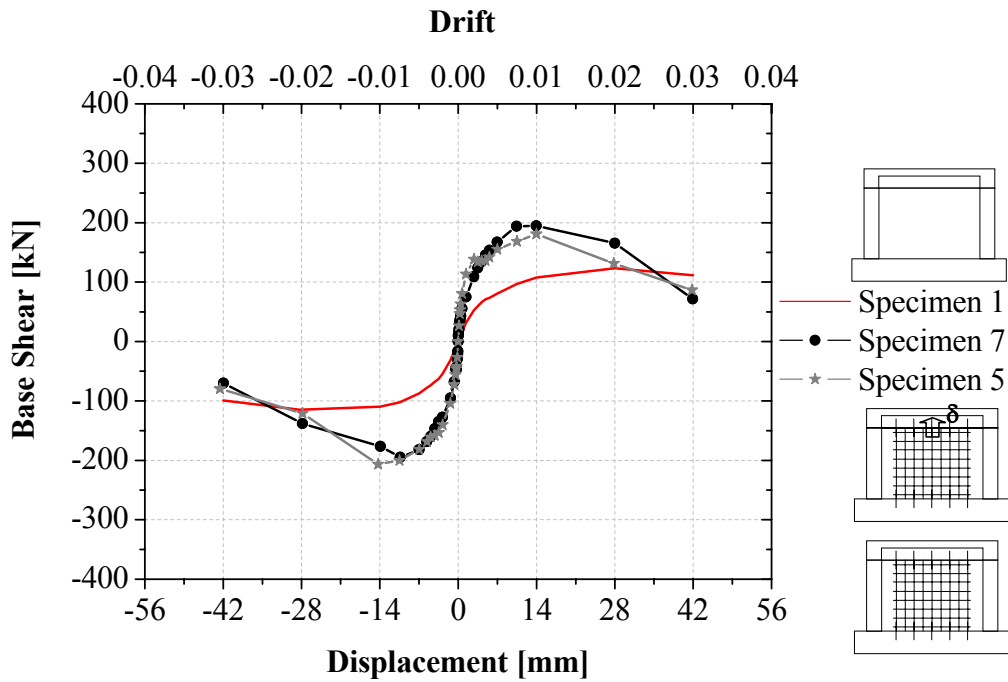


Figure 4.94: The comparison of envelope curves of Specimens 1, 5 and 7

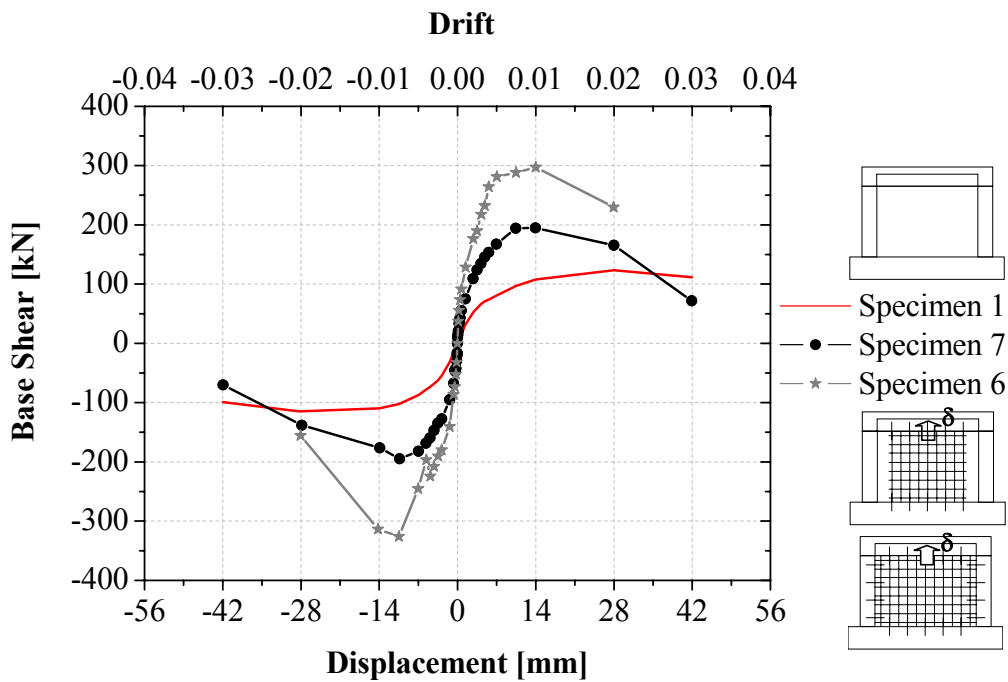


Figure 4.95: The comparison of envelope curves of Specimens 1, 6 and 7

The comparison of shotcrete walls with the shear wall (Specimen 8) is given in Figure 4.96. Since the concrete compressive strengths of Specimen 1, 3 and 8 are not the same, Specimen 1 and 3's behaviours are predicted analytically using Specimen 8's concrete strengths and introduced as envelope curves in Figure 4.97.

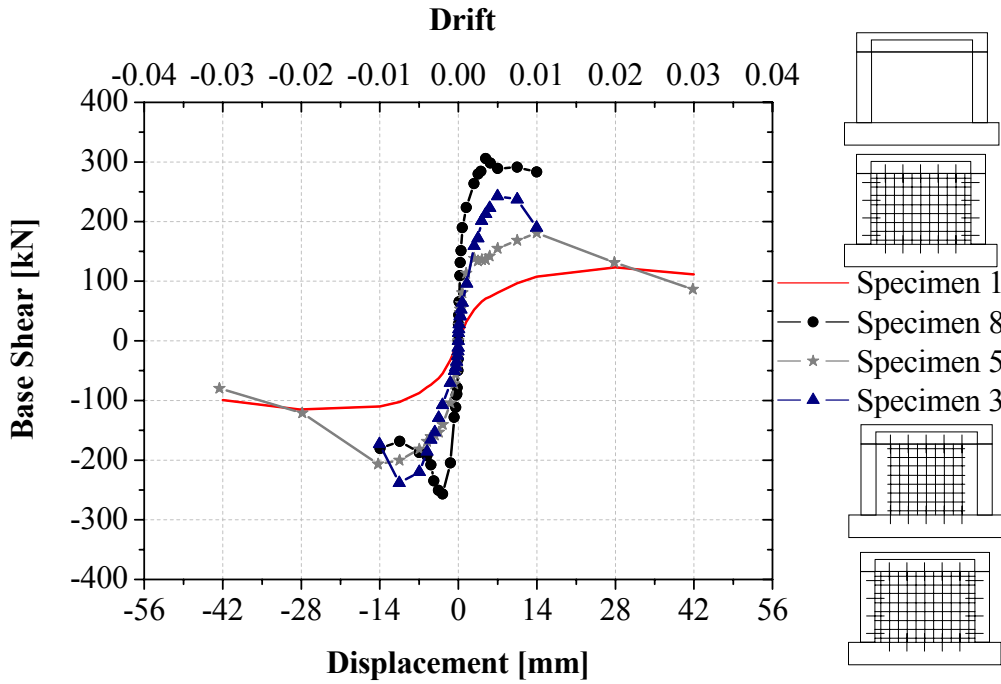


Figure 4.96: The comparison of envelope curves of Specimens 1, 3, 5 and 8

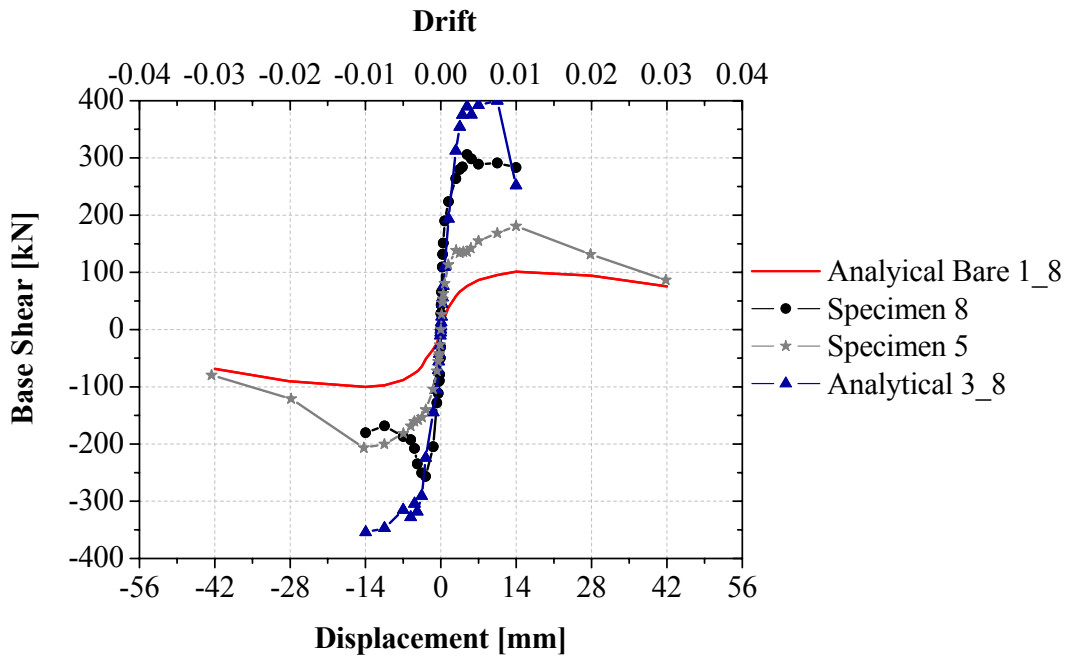


Figure 4.97: The comparison of envelope curves of Specimens 1, 3, 5 and 8 with analytical 3_8 and analytical 1_8

4.11.3 Initial stiffness

Table 4.33 compares the initial stiffness of the eight specimens in this study and the increases given as proportion ratios to that of the bare frame's are also presented. The initial stiffness values are calculated as the slope of the line joining the points of the maximum loads in push and pull cycle occurred during initial stages.

Table 4.33: Initial stiffness of the specimens

Specimen	Initial stiffness [kN/mm]	Ratio to Specimen 1
1	21.6	1.0
3	183.9	8.5
5	188.5	8.7
6	249.9	11.6
7	179.3	8.3
2S	230.9	10.7
4S	223.3	10.3
8	444.0	20.5

The damaged and undamaged frames strengthened in this study yield the following results: The lateral stiffness of the frames right before the first cracks occurred in the system increased by 10 times for the damaged frames Specimen 2S and 4S, and 8.5 times for undamaged frames Specimen 3 and 5 compared with the bare frame's. The pre-reversed shotcrete panel specimens also showed almost the same amount of increase in stiffness while the shear wall has increased the stiffness of the frame 20 times.

In Figure 4.98 initial stiffness of the specimens are compared in graphic format.

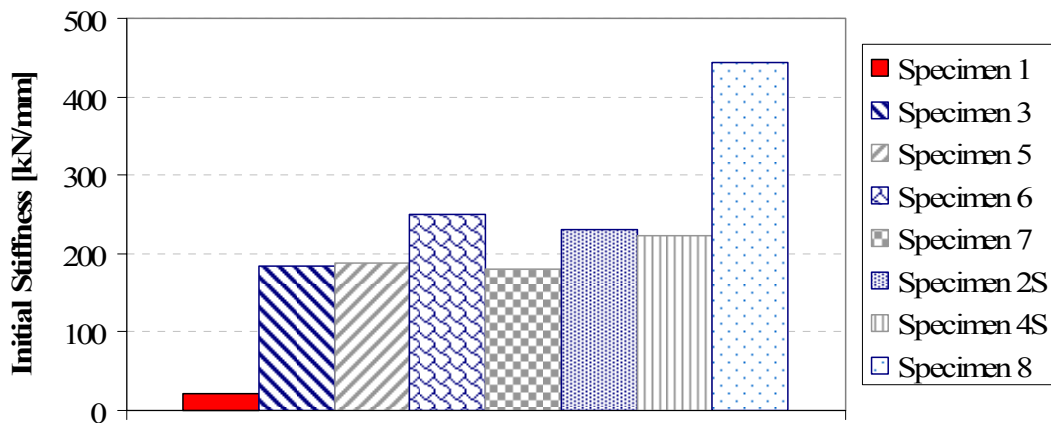


Figure 4.98: Initial stiffnesses of the specimens

4.11.4 Cumulative energy dissipation

As shown in Figure 4.99, the cumulative energy dissipation of the specimens with shotcrete walls that are fully connected to the frame; are 10 and 5 times higher than the bare frame's at 1% and 2% story drift, respectively. For the specimens with gaps; cumulative energy dissipation values are 4, 2.5 and 1.7 times higher than the bare

frame's at 1%, 2% and 3% story drift, respectively. The specimen with the shear wall shows the same amount of energy dissipation with the fully connected shotcrete panel one and could only make 1% story drift.

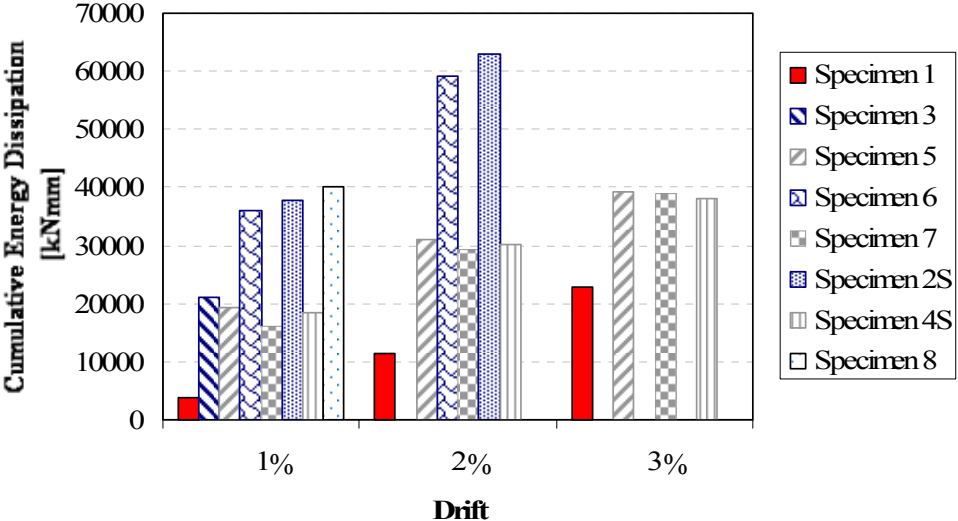


Figure 4.99: Cumulative energy dissipation capacities at various story drifts

The comparison of the cumulative energy dissipation capacities of the two fully connected shotcrete panel specimens to the bare frame's are given in Figure 4.100 and for the two shotcrete specimens, which are connected only to the beams are given in Figure 4.101.

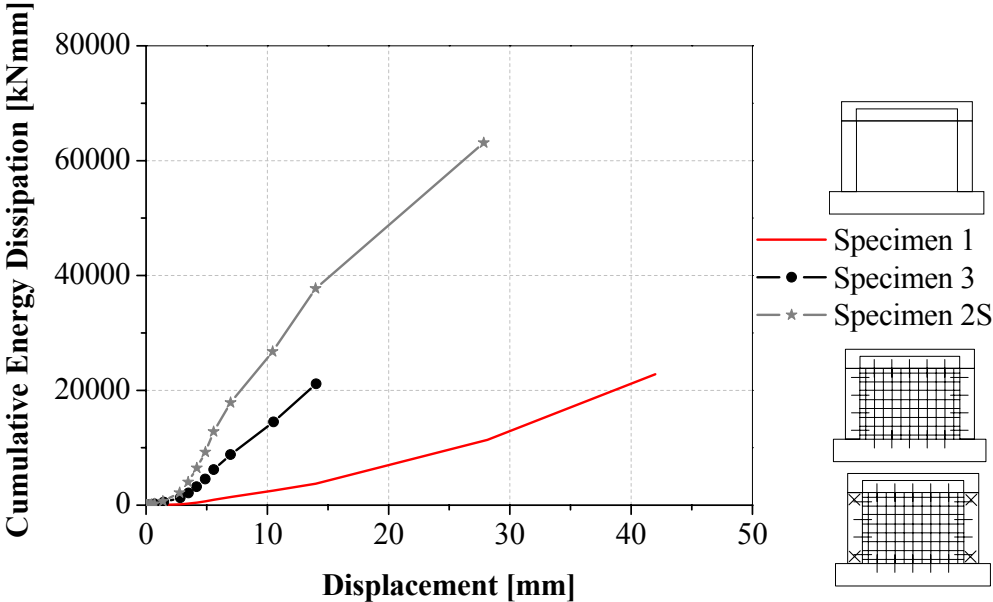


Figure 4.100: The comparison of cumulative energy dissipation capacities of Specimens 1, 2S and 3

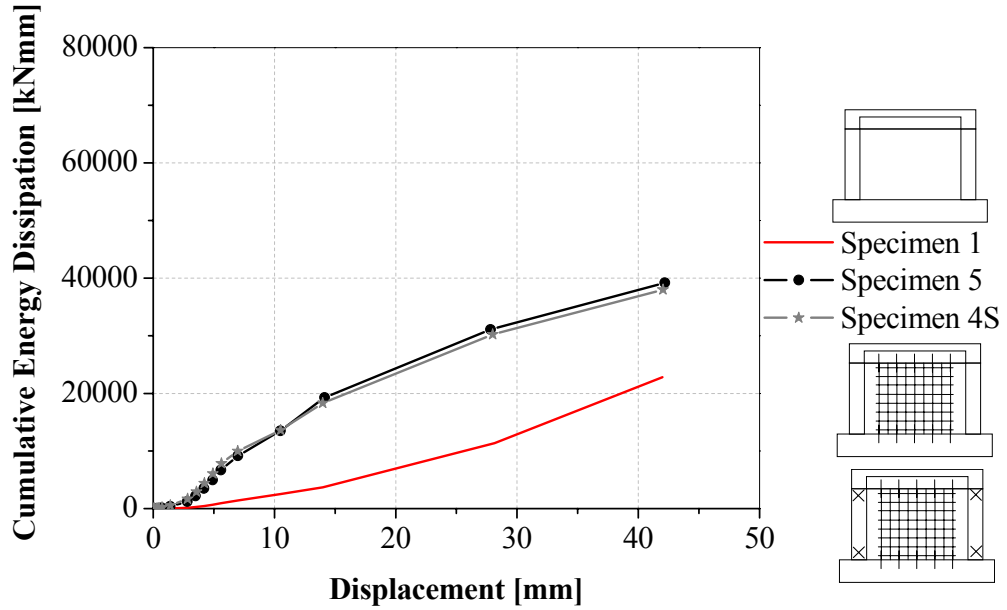


Figure 4.101: The comparison of cumulative energy dissipation capacities of Specimens 1, 4S and 5

The pre-reverse effect on the load carrying capacities can be seen in Figure 4.102 for fully connected shotcrete panel specimens and in Figure 4.103 for shotcrete specimens, which are connected only to the beams, with and without pre-reverse of the beam and in Figure 4.104 only the results of pre-reversed beam specimens are given.

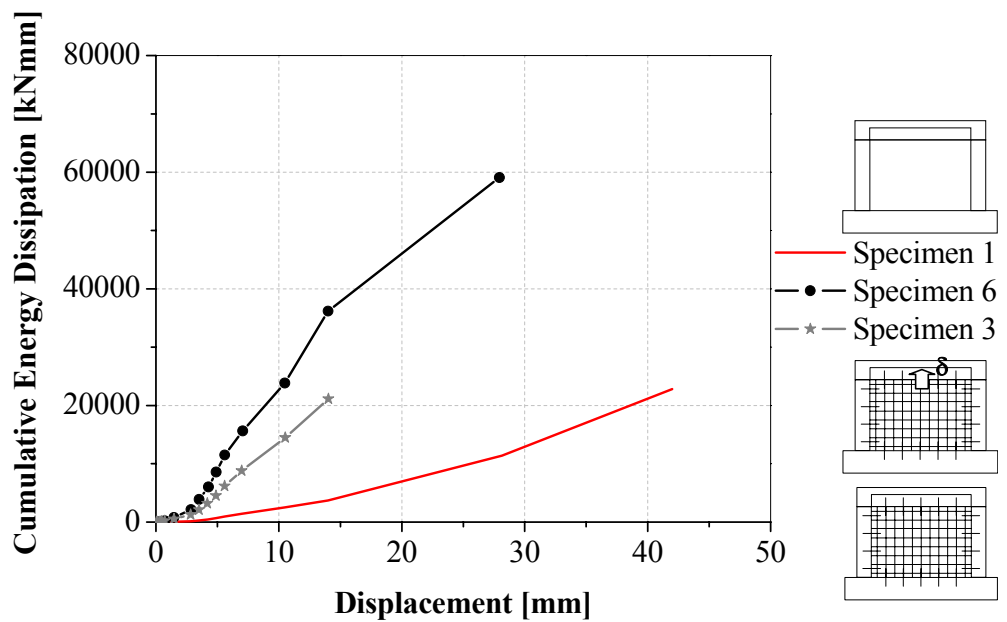


Figure 4.102: The comparison of cumulative energy dissipation capacities of Specimens 1, 3 and 6

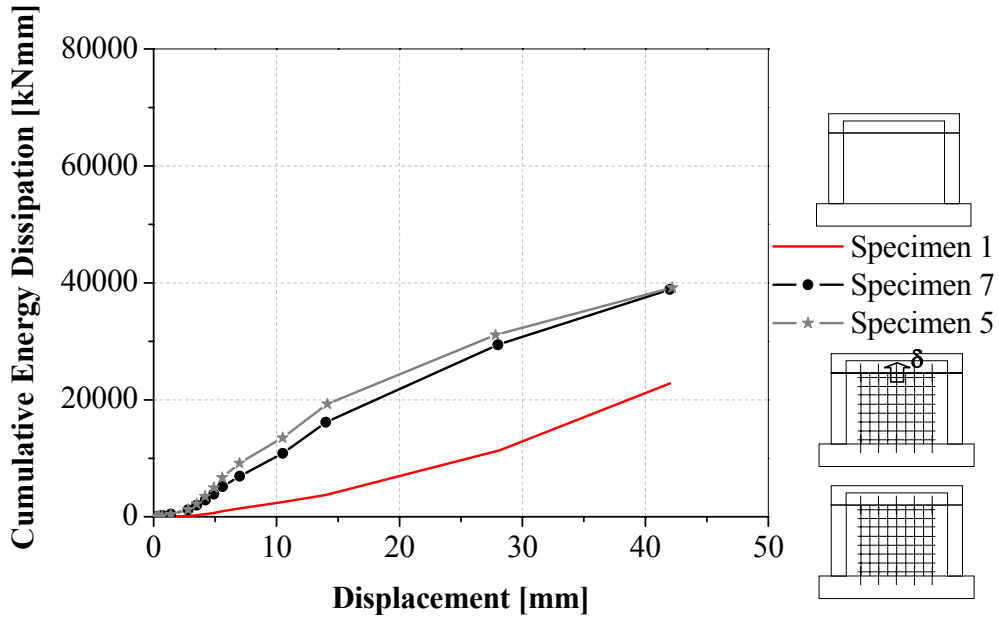


Figure 4.103: The comparison of cumulative energy dissipation capacities of Specimens 1, 5 and 7

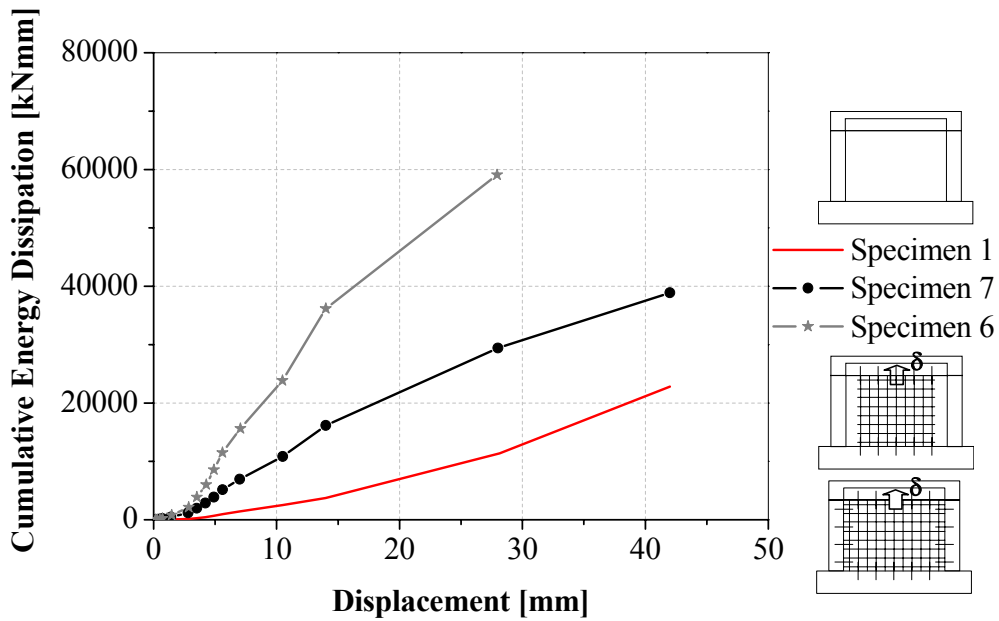


Figure 4.104: The comparison of cumulative energy dissipation capacities of Specimens 1, 6 and 7

The comparison of shotcrete walls with the shear wall is given in Figure 4.105.

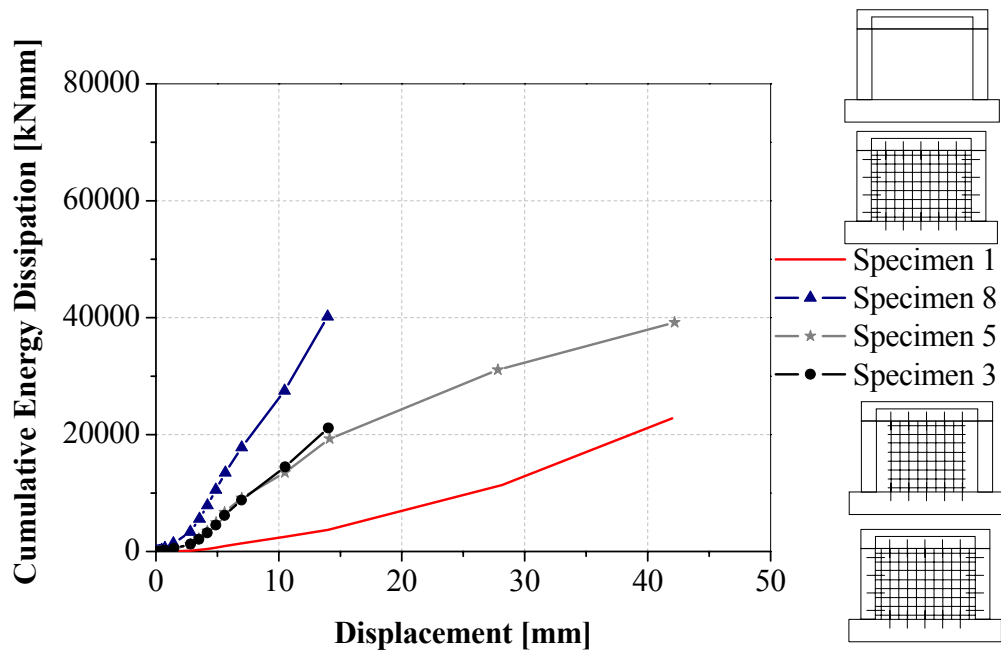


Figure 4.105: The comparison of cumulative energy dissipation capacities of Specimens 1, 3, 5 and 8

4.11.5 Equivalent damping characteristics

Hysteretic damping, $\xi_{hysteretic}$, has been determined for the specimens through the hysteresis lateral load-top displacement curves. Paying attention on the stabilized loops, some average equivalent viscous damping ratios which can be used in the rehabilitation design stage of existing structures were obtained.

The lower and upper limits suggested above have been calculated through the formula which is given in Equation 4.3.

$$\xi_{eq} = 0.05 + \beta \xi_{hysteretic} = 0.05 + \beta \times \left(\frac{W_D}{4\pi W_S} \right) \quad (4.3)$$

where β is a coefficient between 0.33–1.0 in FEMA 273 (1997) and W_D and W_S are indicating the energy dissipated in one cycle of preferably stabilized displacement and the strain energy at the corresponding displacement given in Figure 4.106 as Priestley et al., 2007 suggested.

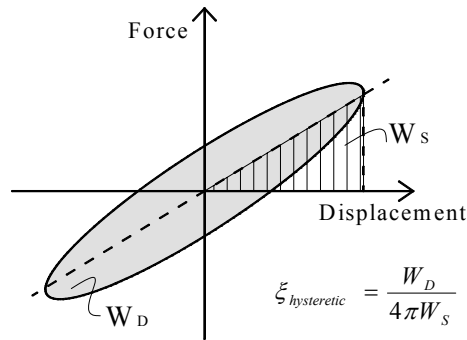


Figure 4.106: Dissipated and strain energy

The constant value of 0.05 in Eq. 4.3 represents the viscous damping of reinforced concrete building inherently exist in the structure and $\xi_{hysteretic}$ can be taken approximately as 10% of critical damping depending on the tests results summarized and the diagrams that are given in Figure 4.107. One can easily find by the corresponding factors for these damping ratios to define the redesign demand curves referring the standard one, which may have some minor differences from source to source, FEMA 273, 1997, NEHRP, 2000.

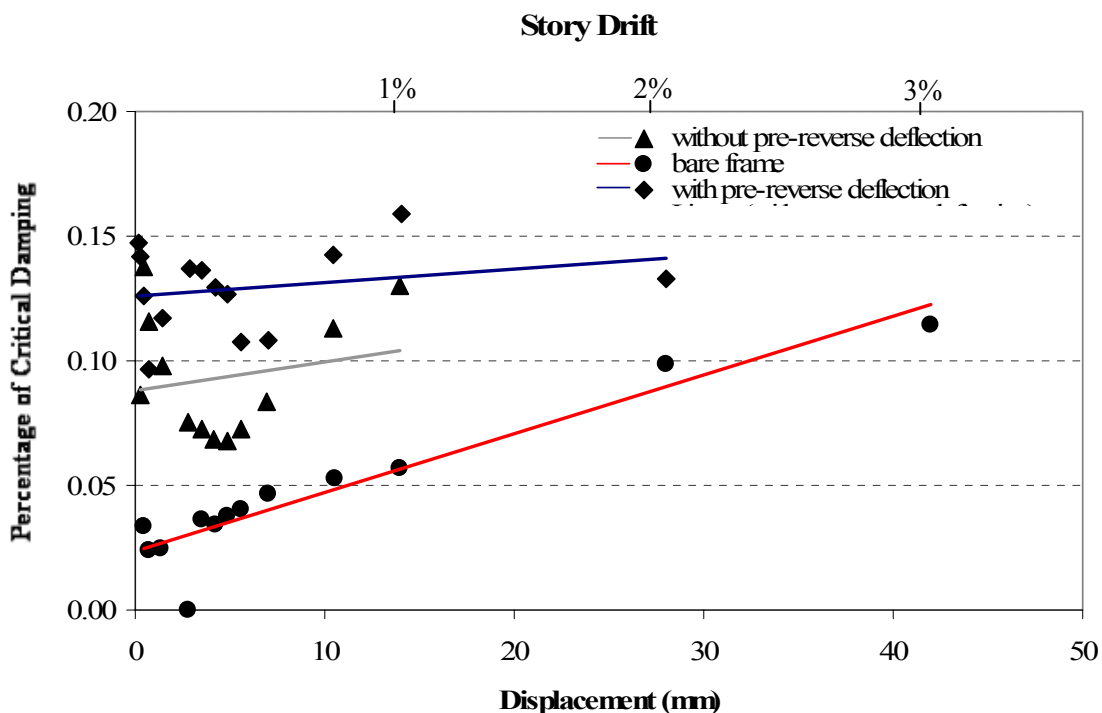


Figure 4.107: Equivalent damping for various tests

It can be concluded that the damping ratio can definitely be taken as higher than 5% of critical damping which is being suggested by current codes, TEC 1997 and 2007. The suggested equivalent viscous damping for rehabilitation design stage is between

8-16% of critical damping depending on the type of modification. At 1% story drift, the observed percentage of critical damping values are 10.5% and 13.5% for without and with pre-reverse deflection on the beam, respectively

4.11.6 Lateral stiffness

The comparison of the lateral stiffness of the two fully connected shotcrete panel specimens to the bare frame's are given in Figure 4.108 and for the two shotcrete specimens, which are connected only to the beams are given in Figure 4.109.

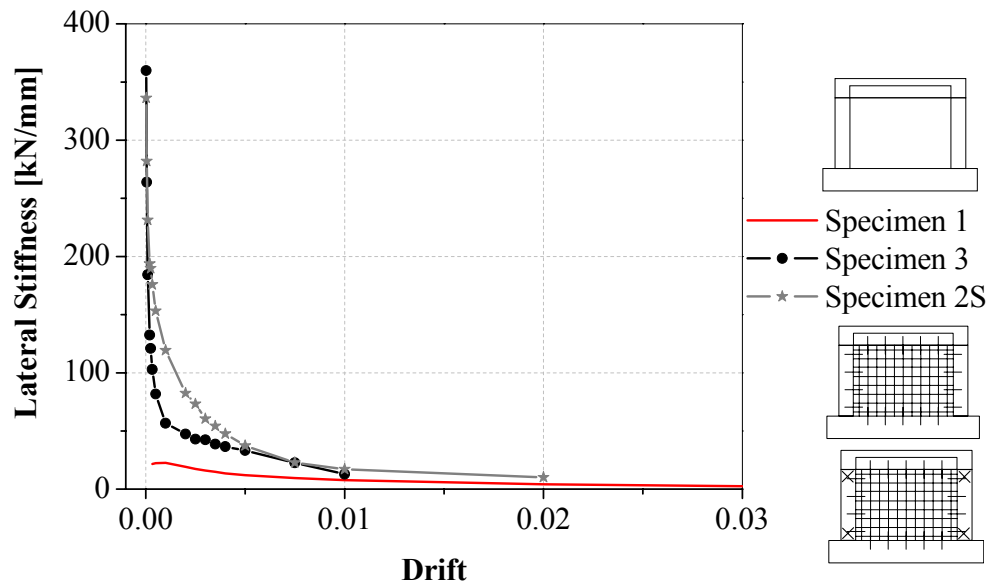


Figure 4.108: The comparison of lateral stiffnesses of Specimens 1, 2S and 3

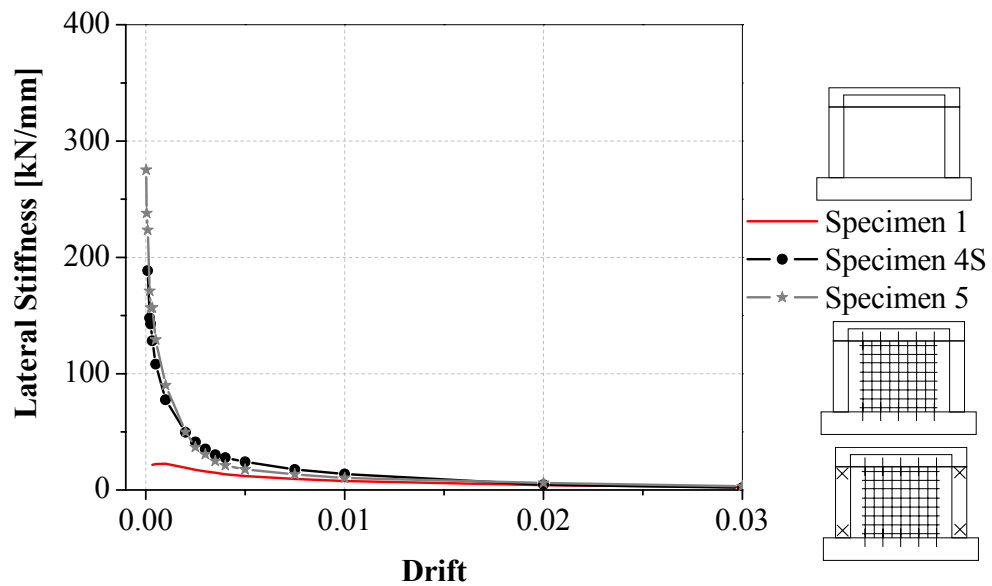


Figure 4.109: The comparison of lateral stiffnesses of Specimens 1, 4S and 5

The pre-reverse effect on stiffness can be seen in Figure 4.110 for fully connected shotcrete panel specimens and in Figure 4.111 for shotcrete specimens, which are connected only to the beams, with and without pre-reverse of the beam and in Figure 4.112 only the results of pre-reversed beam specimens are given.

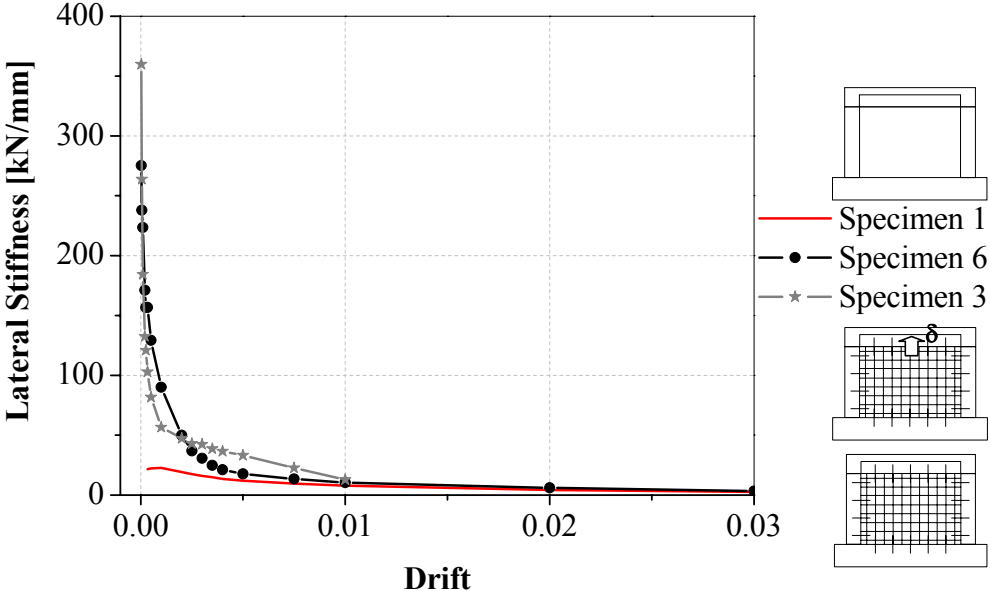


Figure 4.110: The comparison of lateral stiffnesses of Specimens 1, 3 and 6

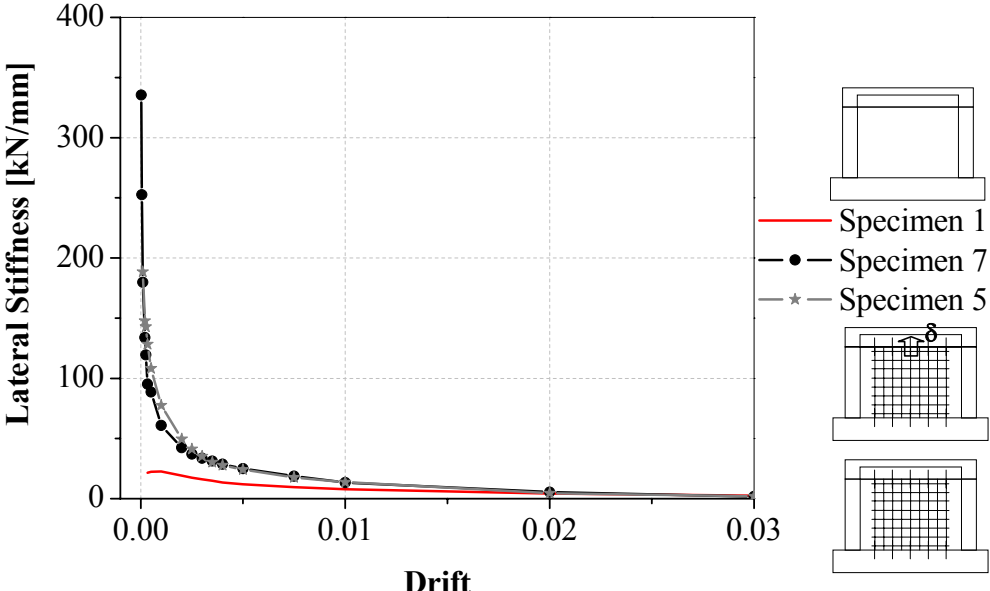


Figure 4.111: The comparison of lateral stiffnesses of Specimens 1, 5 and 7

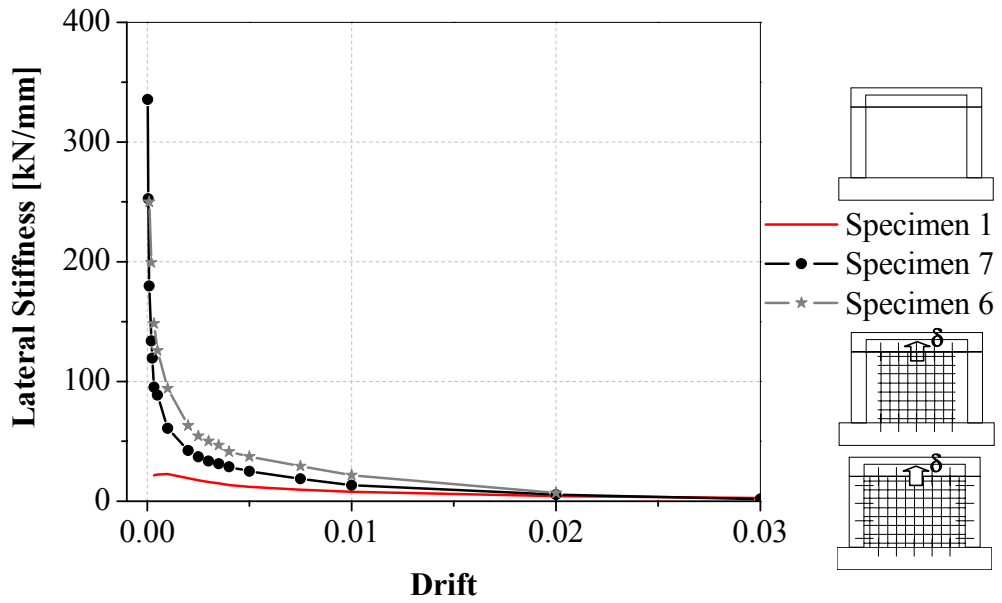


Figure 4.112: The comparison of lateral stiffnesses of Specimens 1, 6 and 7

The comparison of shotcrete walls with the shear wall is given in Figure 4.113.

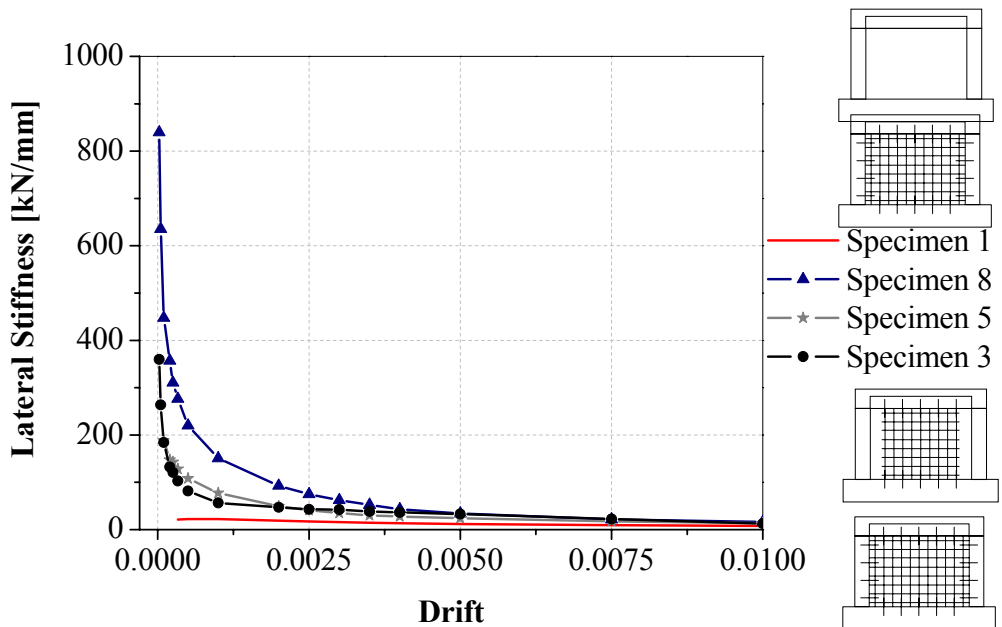


Figure 4.113: The comparison of lateral stiffnesses of Specimens 1, 3, 5 and 8

The lateral stiffness is almost the same for all the test specimens after 1% drift ratio. The pre-reverse is not very effective on the stiffnesses.

4.11.7 Rotation of the panels

The panel base rotations of Specimens were obtained using the measuring system given in Figure 4.114. In the figure; Δ_1 and Δ_2 correspond to the measured shortening and elongation of the related cross section, while x is the distance between them.

The rotation is calculated using Equation 4.4;

$$\theta = (\Delta_1 + \Delta_2) / x \quad (4.4)$$

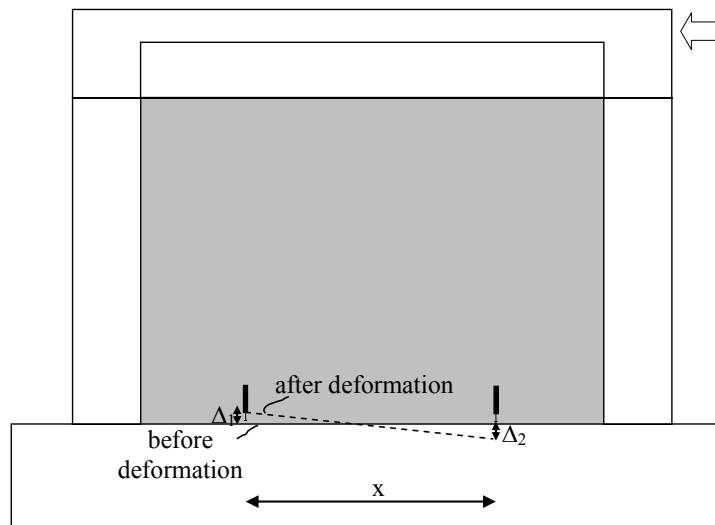


Figure 4.114: Calculation of rotation of the shotcrete panel

Base rotation of the shotcrete panel versus base shear relations are given for Specimens 3, 5 and 8 in Figures 4.115, 4.116 and 4.117, respectively. The graphs are drawn and compared for 1% story drift. From the figures, it can easily be concluded that the response of Specimens 3 and 8 are similar and linear elastic. However in the case of Specimen 5, stable hysteretic loops were observed.

For the 1% story drift level, in Specimens 3 and 8 rotation amplitudes are relatively small, while in Specimen 5 the amplitude of the rotation is relatively higher compared to the others and response shows inelastic excursion.

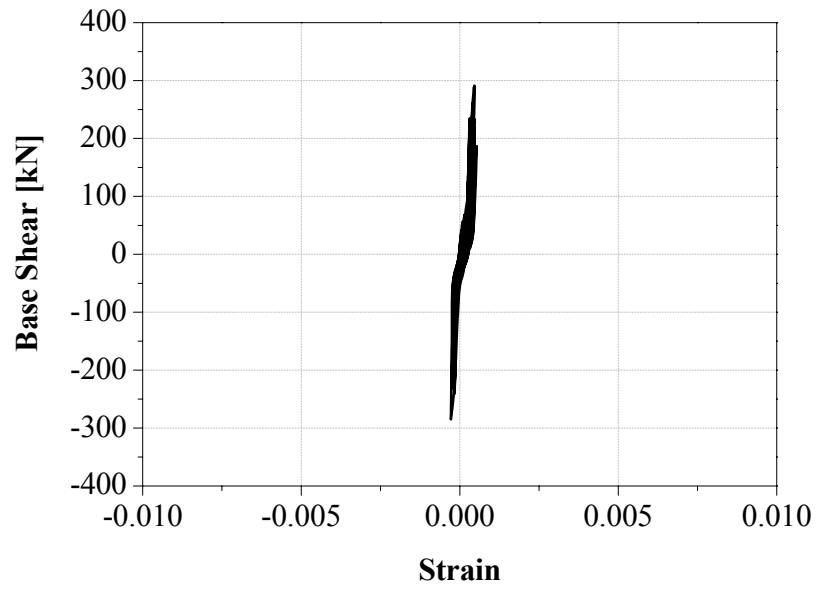


Figure 4.115: The rotation of the panel for Specimen 3

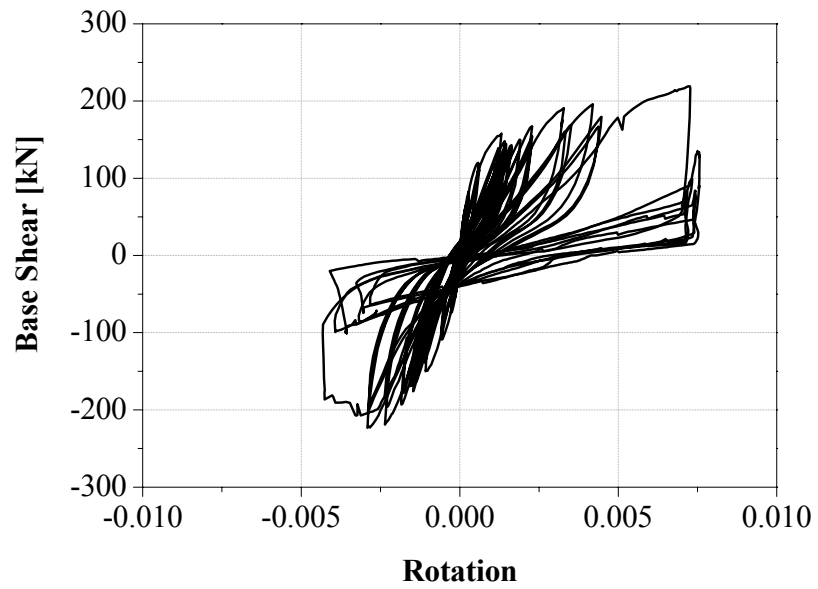


Figure 4.116: The rotation of the panel for Specimen 5

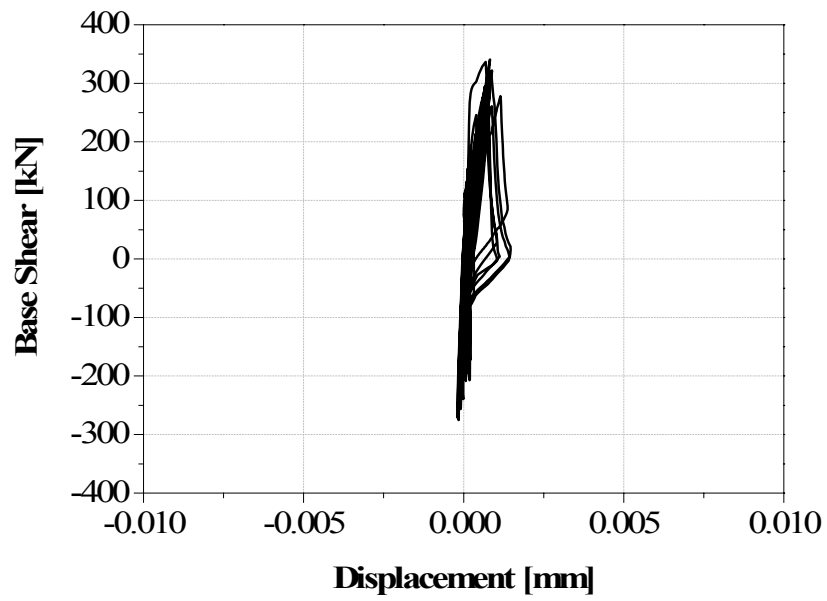


Figure 4.117: The rotation of the panel for Specimen 8

5. ANALYTICAL STUDIES USING THE FINITE ELEMENT METHOD

There are several suggested numerical models to represent the effect of the infill walls on the behaviour of the infilled frames which are adapted in several computer programs. ANSYS, ABAQUS, DIANA, SAP2000, OpenSees, IDARC, SeismoStruct are some of these programs. In this study, the overall effect of the shotcrete wall on the system behavior is investigated. For this reason, SeismoStruct which has a macro approach for the problem considered is preferred. SeismoStruct models the infill wall with some diagonal braces which is a new approach that gives the opportunity to obtain a more acceptable result compared with the experimental studies, (Crisafulli, 1997).

This chapter presents detailed information about the program used to model the experiments tested during the course of this research analytically. The analyses were carried out to predict the load versus drift relations and the failure modes of the specimens. Smyrou et al. (2006), Casarotti and Pinho (2007), Pinho et al. (2007), Cattari and Lagomarsino (2006), Mellal et al. (2003), Kutanis et al. (2007), Crowley and Pinho (2006), Negulescu et al. (2003), Nogueiro et al. (2003), Calvi et al. (2006), Priestley et al. (2007) have studied SeismoStruct and have achieved success in modelling analytically reinforced concrete and steel structure behaviour.

In SeismoStruct, the diagonal braces representing the infill wall and the parameters for defining these braces are designed originally for modelling the brick walls. The model is developed by Crisafulli (1997) and adopted to SeismoStruct by Blandon (2005). In this model, the hysteretic behaviour of masonry in compression is defined by Sargin's (1971) equation which is originally proposed for concrete. The behaviour in tension is assumed to be linear. Since there is not sufficient experimental data related to the cyclic axial behaviour of masonry, Crisafulli used experimental data obtained from concrete specimens to calibrate the model. He also tested concrete specimens under cyclic compression to obtain experimental data and used these results to calibrate the analytical model of inner loops of the hysteretic behaviour in compression.

In this study, the parameters of the diagonal braces which are used to model the shotcrete panel are taken from the material tests which were presented in Chapter 3. While deciding on these parameters, several, necessary discussions have been done with the developer of SeismoStruct, namely Assist.Prof.Dr. Rui Pinho (2006). Since global response is aimed in this study rather than the local effects of the infill wall, by correct calibration of the parameters, the analysis can be valid.

One of the advantages of SeismoStruct is that the interaction between the wall and the surrounding frame can be modelled by defining extra nodes both in the beam and the columns.

5.1 Nonlinear Static Analysis Using SeismoStruct

Inelastic beam-column elements are used in the program. To allow more accurate evaluation of structural damage distribution, material inelasticity is assumed to spread along the member length and across the cross section. This is explicitly represented by implementing a fibre modelling approach as shown in Figure 5.1.

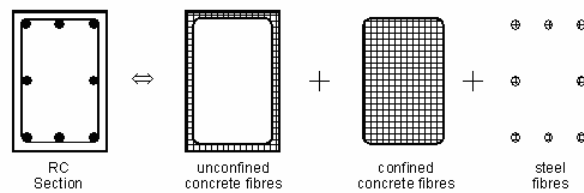


Figure 5.1: Fibre analysis approach

The loading pattern of the experiments is applied in static time-history analysis. In static time-history analysis, the applied loads (displacement, force or a combination of both) can vary independently in the pseudo-time domain, according to a prescribed load pattern. The applied load P_i in a nodal position i is given by $P_i = l_i(t) P_i^0$, i.e. a function of the time-dependent load factor $l_i(t)$ and the nominal load P_i^0 . This type of analysis is typically used to model static testing of structures subjected to various force or displacement patterns.

In the finite element analysis of the tested specimens that are the single story, single bay RC frames infilled with shotcrete panels, strut modelling is used.

5.2 Description of Element Types Used

Inelastic frame elements were used for modelling the RC frame. These are the 3D beam-column elements capable of modelling members of space frames having geometric and material nonlinearities. The sectional stress-strain state of beam-column elements is obtained through the integration of the nonlinear uniaxial material response of the individual fibres in which the section has been subdivided. Local geometric nonlinearity (beam-column effects) is also comprised within the formulation of this element.

If a sufficient number of fibres (200-400 in spatial analysis) are employed, the distribution of material nonlinearity across the section area is accurately modelled, even in the highly inelastic range. Two integration Gauss points as shown in Figure 5.2 per element are then used for the numerical integration of the governing equations of the cubic formulation. If a sufficient number of elements are used such as 5-6 per structural member, the spread of inelasticity along member length can be accurately estimated.

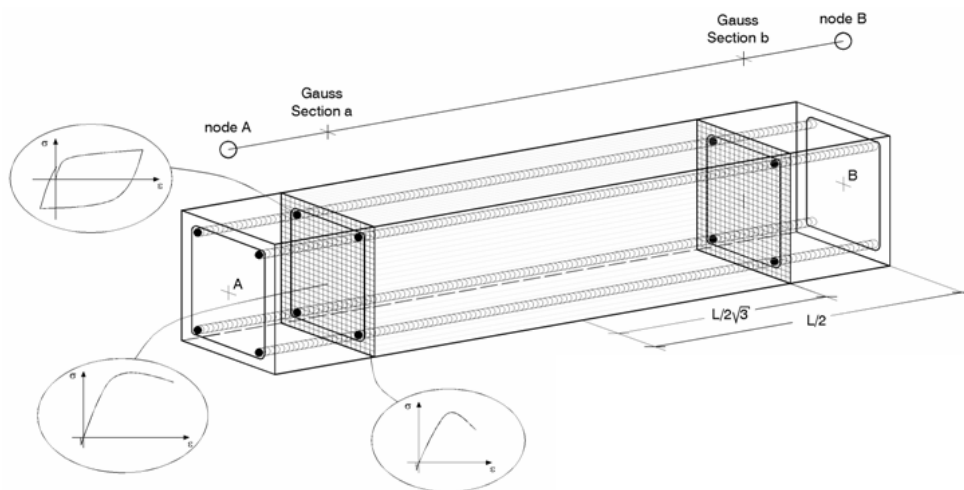


Figure 5.2: Gauss integration points in beam column elements

5.3 Material Models

Some of the defined parameters which are used in the material models are taken from the tests done to get the characteristic values of the materials. The average values of several tests are used both for concrete and reinforcement. For those parameters which cannot be determined from the tests, these values are taken from the interval given in the manual of the program itself.

5.3.1 Material model used for steel reinforcement

Monti-Nutti steel model is used to model the reinforcement in the frame. It is a uniaxial steel model initially programmed by Monti et al. (1996). It uses the Menegotto and Pinto (1973) stress-strain relationship together with the isotropic hardening rules proposed by Filippou et al. (1983). An additional memory rule proposed by Fragiadakis (2001) is also introduced, for higher numerical stability/accuracy under transient seismic loading.

Eleven model-calibrating parameters summarised in Table 5.1 must be defined in order to fully describe the mechanical characteristics of steel reinforcement.

Table 5.1: Input parameters for steel reinforcement

Parameter	Definition
E_s	Modulus of elasticity
f_y	Yield strength
μ	Strain hardening parameter
R_0	Transition curve initial shape parameter
a_1	Transition curve shape calibrating coefficients
a_2	Transition curve shape calibrating coefficients
P	Kinematic/isotropic weighing coefficient
r	Spurious unloading corrective parameter
L	Transverse reinforcement spacing
D	Longitudinal bar diameter
γ	Specific weight

These are:

- 1- *Modulus of elasticity* – E_s : This is the initial elastic stiffness of the material. The value is taken from Table 3.10 which summarises the material test results.
- 2- *Yield strength* – f_y : This is the stress at yield. The value is taken from Table 3.10.
- 3- *Strain hardening parameter* - μ : This is the ratio between the post-yield stiffness (E_{sp}) and the initial elastic stiffness (E_s) of the material. The former is defined as $E_{sp}=(f_{ult} - f_y)/(\epsilon_{ult} - f_y/E_s)$, where f_{ult} and ϵ_{ult} represent the ultimate or maximum stress and strain capacity of the material, respectively. This value is calculated from the reinforcement material test results.
- 4- *Transition curve initial shape parameter* - R_0 : This is the initial (first loading cycle) value of the parameter R , that controls the shape of the transition curve between initial and post-yield stiffness, necessary to accurately represent

Baushinger effects and pinching of the hysteretic loops. The default value is 20. The default value is taken into account during the analysis.

- 5- *Transition curve shape calibrating coefficients - a_1 & a_2* : These are the two coefficients used to calibrate the changes that must be applied to parameter R_0 in order to obtain the updated transition curve shape parameter R_n . Whilst a_1 is usually adopted with an invariable value of 18.5, a_2 might range between 0.05 and 0.15. The default values are 18.5 and 0.15 for coefficients a_1 and a_2 , respectively. The default value is taken into account for a_1 and 0.05 for a_2 during the analysis.
- 6- *Kinematic/isotropic weighing coefficient – P* : This is the weighing coefficient used in this model to define the degree to which kinematic and isotropic hardening are introduced in the stress-strain cyclic response characteristics of the material. A value close to unity implies a kinematic-dominated hardening behaviour, whilst a value close to zero is employed when isotropic hardening controls the response of the material. P is taken as 0.9 during the analysis.
- 7- *Spurious unloading corrective parameter – r* : This is the threshold for small strain reversals, defined as a percentage of the strain measured at the end of a loading cycle, used to prevent the occurrence of spurious strain unloading cycles. Typical values of r vary between 2.5 and 5 percent. r is taken as 2.5% during the analysis.
- 8- *Transverse reinforcement spacing and longitudinal bar diameter - L & D* : These two parameters are required for the definition of the slenderness ratio (L/D) of the longitudinal reinforcement which in turn is used to calibrate the buckling behaviour of this steel model. L is the spacing between the transverse reinforcement and D is the diameter of the longitudinal bars. L is 200 mm and D is 16 mm as shown in Figure 3.4.
- 9- *Specific weight – γ* : This is the specific weight of the material.

E_s , f_y , μ , L and D are taken from the material test results for the reinforcement given in detail in Chapter 3, while R_0 , a_1 , a_2 , P and r are predicted from the test results.

5.3.2 Material model used for concrete

Nonlinear constant confinement concrete model is used to model the concrete surrounded by stirrups. This is a uniaxial nonlinear constant confinement model,

initially programmed by Madas (1993) that follows the constitutive relationship proposed by Mander et al. (1988) and the cyclic rules proposed by Martinez-Rueda and Elnashai (1997). The confinement effects provided by the lateral transverse reinforcement are incorporated through the rules proposed by Mander et al. (1988) whereby constant confining pressure is assumed throughout the entire stress-strain range.

Five model-calibrating parameters summarised in Table 5.2 must be defined in order to fully describe the mechanical characteristics of confined concrete:

Table 5.2: Input parameters for concrete

Parameter	Definition
f_c	Compressive strength
f_t	Tensile strength
ε_c	Strain at peak stress
k_c	Confinement factor
γ	Specific weight

These are:

1- *Compressive strength* – f_c : This is the cylinder compressive strength of the material. The value is taken from Table 3.8 which summarises the material test results for frame concrete.

2- *Tensile strength* – f_t : This is the tensile strength capacity of the material. Usually it can be estimated as $f_t = k_t(f_c)^{1/2}$, where k_t varies from 0.5 (concrete in direct tension) to 0.75 (concrete in flexural tension), as suggested by Priestley et al. (1996). When this value is reached, the concrete is assumed to abruptly lose its tensile resistance, without any sort of tension softening. This values is taken as $0.1*f_c$.

3- *Strain at peak stress* - ε_c : This is the strain corresponding to the point of unconfined peak compressive strength, f_c . This value is taken from the material test result of frame concrete.

4- *Confinement factor* – k_c : This is the constant confinement factor, defined as the ratio between the confined and unconfined compressive stress of the concrete, and used to scale up the stress-strain relationship throughout the entire strain range. Since the unconfined compressive stress of the concrete is known, the confined compressive stress of the concrete is calculated from equation proposed by Mander et al. (1988).

5- *Specific weight* - γ . This is the specific weight of the material.

f_c , f_t and ε_c are taken from the material test results conducted for concrete given in detail in Chapter 3.

5.4 Inelastic Infill Panel Element

The effect of infill materials on the overall structural behavior of infilled frames was investigated previously by many researchers. There are mainly two approaches to model infilled frames. In the first approach the infill panel is modelled by plane stress, shell elements which are interconnected at their nodes using a series of nonlinear springs and struts to represent the shear and normal stresses interaction between the blocks along the mortar head and bed joints. In the second approach, the infill wall is modelled by diagonal struts with equivalent properties determined from experimental tests. Several variations of the diagonal strut modelling have been proposed including the use of multiple struts or truss-shaped struts in lieu of a single strut, nonlinear properties, varying effective areas throughout the loading history and the use of actual load-deflection paths.

Inelastic infill panel element is a four-node masonry panel element developed and initially programmed by Crisafulli (1997) and implemented in SeismoStruct by Blandon (2005), for the modelling of the nonlinear response of infill panels in framed structures. Each panel is represented by six strut members; each diagonal direction features two parallel struts to carry axial loads across two opposite diagonal corners and a third and a fourth one to carry the shear from the top to the bottom of the panel. This latter strut only acts across the diagonal that is on compression; hence its "activation" depends on the deformation of the panel. The axial load struts use the masonry strut hysteretic model, while the shear strut uses a dedicated bilinear hysteretic rule.

Four internal nodes are employed to account for the actual points of contact between the frame and the infill panel (i.e. to account for the width and height of the columns and beams, respectively), whilst four dummy nodes are introduced with the objective of accounting for the contact length between the frame and the infill panel as can be seen in Figure 5.3. These dummy nodes with 2 translational degrees of freedom per node are required to define one end of the strut members, which is not connected to

the corners of the panel. All the internal forces are transformed to the exterior four nodes.

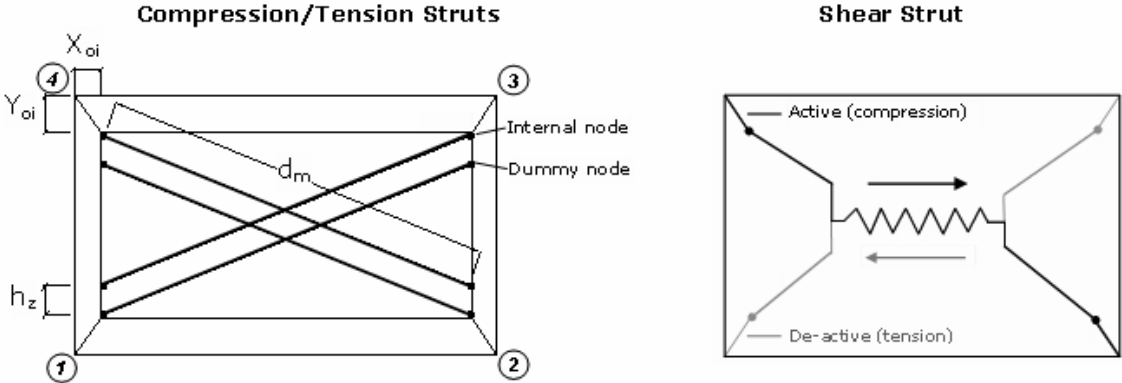


Figure 5.3: Strut model used

In order to fully characterise this type of element, the following parameters need to be defined:

- **Strut Curve Parameters**, employed in the definition of the masonry strut hysteretic model as shown in Figure 5.4, which is modelled with the infill panel strut response curve.

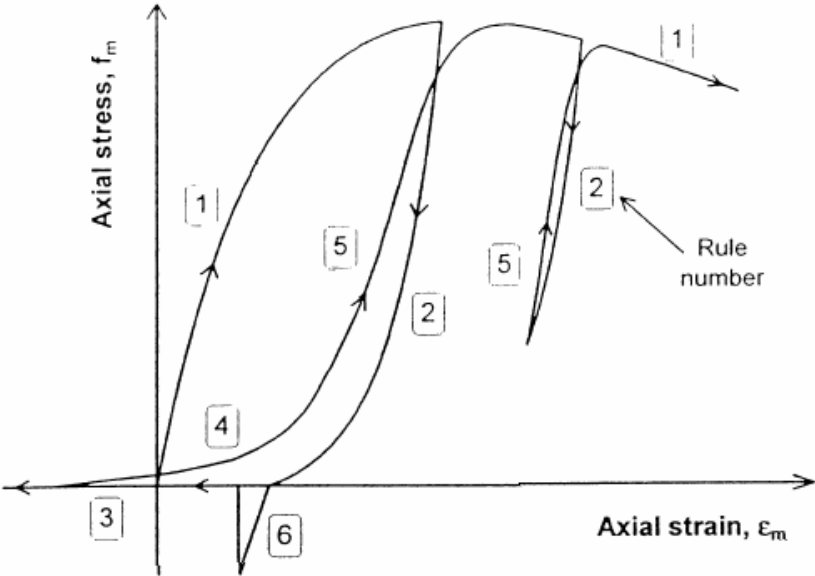


Figure 5.4: General characteristics of the proposed model for cyclic axial behaviour of infill wall, Crisafulli (1997)

The model which defines the cyclic axial behaviour of the wall is composed by five hysteretic rules which are:

- Envelope curve in compression (Rule 1)

- Unloading from the envelope curve (Rule 2)
- No stress (Rule 3)
- Reloading after complete unloading (Rule 4 and 5)
- Unloading and reloading from inside loops (small hysteretic cycle)

These rules are explained in detail in Crisafulli (1997).

Input parameters needed for the infill model are summarized in Table 5.3. Below, these will be explained in detail.

Table 5.3: Input parameters for the infill model

Parameter	Definition
E_m	Initial young's modulus
$f_{m\theta}$	Compressive strength
f_t	Tensile strength
ϵ_m	Strain at maximum stress
ϵ_{ult}	Ultimate strain
ϵ_{cl}	Closing strain
ϵ_1	Strain of initial reduction of area for the strut
ϵ_2	Strain for the residual of strut's area
γ_{un}	Factor to calculate E_{un} (unloading stiffness)
α_{re}	Strain reloading factor
α_{ch}	Factor to calculate u_{ch}
β_a	Factor to calculate u_{pl}
β_{ch}	Factor to calculate f_{ch}
γ_{plu}	Factor to calculate e_{plui} , e_{plu}
γ_{plr}	Factor to calculate e_{plr}
e_{x1}	Exponent to calculate e_{plu}
e_{x2}	Exponent to calculate f_{ch}

Seventeen parameters are needed in order to fully characterise this response curve. These are:

- 1- *Initial Young modulus* – E_m : The elastic modulus represents the initial slope of the stress-strain curve. It is related to the compressive strength of the material ($f_{m\theta}$), and the values can range: $400f_{m\theta} < E_m < 1000f_{m\theta}$, as summarised in Crisafulli (1997). E_m is taken as approximately as $1000f_{m\theta}$ in the analysis. Since the wall is reinforced concrete, the maximum limit value for E_m is taken.
- 2- *Compressive strength* - $f_{m\theta}$: This compressive strength refers to the diagonal capacity of the infill panel, that is, it refers to the capacity of the masonry in the direction of the principal stress f_1 , which, typically, is assumed to coincide with

the diagonal that links two opposite corner. If no diagonal compression test results are available, then the resistance of the masonry in the normal direction f_n , is defined by adapting the failure theory proposed by Mann and Müller (1982), Crisafulli (1997) whom developed the following equation: $f_{m\theta} = f_n / \sin^2 \theta$. The value is taken from Table 3.9 which summarises the material test results for shotcrete concrete.

- 3- *Tensile strength – f_i* : The tensile strength represents the tensile strength of the masonry or the bond-strength of the interface between frame and infill panel. f_i is taken as 0.01 for the analysis.
- 4- *Strain at maximum stress – ε_m* : This parameter represents the strain at maximum stress and influences, via the modification of the secant stiffness, the ascending branch of the stress-strain curve. This value is taken from the material test result of shotcrete concrete.
- 5- *Ultimate strain – ε_{ult}* : This strain is used to control the descending branch of the stress-strain curve, modelled with a parabola so as to obtain better control of the strut's response (Crisafulli, 1997). For relative large values, the decrease of the compressive strength becomes smoother and the analyses more stable. This value is taken from the material test result of shotcrete concrete.
- 6- *Closing strain – ε_{cl}* : This parameter defines the strain after which the cracks partially close allowing compression stresses to develop. Its values may vary between 0 and 0.003, as suggested by Crisafulli (1997). ε_{cl} is taken as 0.003 for Specimen 3, 6, 5 and 7 during the analysis.
- 7- *Strut area reduction strain and Residual strut area strain – ε_1 and ε_2* : These are the two strains associated to the reduction of the strut area. These parameters are difficult to find experimental supporting evidence for considering the empirical nature of the strut area reduction scheme. Reasonable values of ε_1 may be in the range of 0.0003 to 0.0008 whilst for ε_2 values in between 0.0006 and 0.016 may be considered. ε_1 and ε_2 are taken as 0.004 and 0.005 for Specimen 3, 0.01 and 0.02 for Specimen 6, 0.05 and 0.07 for Specimen 5 and 0.01 and 0.02 for Specimen 7 during the analysis, respectively.

8- *Empirical parameters*: The masonry infill strut model requires nine empirical curve-calibrating factors to be defined, as proposed by Crisafulli (1997). Table 5.4 summarizes the suggested and limit values for these parameters.

- *starting unloading stiffness factor* (γ_{un}), is used to define the starting unloading stiffness modulus as a proportion of its loading counterpart. Its value may typically vary between 1.5 and 2.5 (though any value above unity constitutes a valid entry). γ_{un} is taken as 1.7 for Specimen 3 and 6, 1.5 for Specimen 5 and 7 during the analysis.

- *strain reloading factor* (α_{re}), is employed to predict the strain at which the loop reaches the envelope after unloading. Its typical value ranges from 0.2 and 0.4 (though any value above zero constitutes a valid entry). α_{re} is taken as 0.2 for Specimen 3, 6, 5 and 7 during the analysis.

- *strain inflection factor* (α_{ch}), utilised in the computation of the strain at which the reloading curve should feature an inflection point, effectively controlling, in this way, the loops' fatness. Its value may be found within the interval of 0.1 to 0.7. α_{ch} is taken as 0.35 for Specimen 3 and 6, 0.3 for Specimen 5 and 7 during the analysis.

- *complete unloading strain factor* (β_a), used in the definition of the plastic deformation after complete unloading. Its values typically range between 1.5 and 2.0 (though any value above zero constitutes a valid entry). β_a is taken as 2 for Specimen 3, 6, 5 and 7 during the analysis.

- *stress inflection factor* (β_{ch}), employed in the computation of the stress at which the reloading curve should feature an inflection point. Its value may be found within the interval of 0.5 to 0.9. β_{ch} is taken as 0.6 for Specimen 3 and 6, 0.9 for Specimen 5 and 7 during the analysis.

- *zero stress stiffness factor* (γ_{plu}), utilised to define, as a proportion of its initial counterpart (E_m), the stiffness at zero stress, after complete unloading has taken place. Its value may be found within the interval of 0 to 1. γ_{plu} is taken as 1.0 for Specimen 3, 6, 5 and 7 during the analysis.

- *reloading stiffness factor* (γ_{plr}), used to define, as a proportion of its loading counterpart, the reloading stiffness modulus, after complete loading has taken

place. Its value may typically vary between 1.1 and 1.5 (though any value above unity constitutes a valid entry). γ_{plr} is taken as 1.1 for Specimen 3 and 6, 1.5 for Specimen 5 and 7 during the analysis.

- *plastic unloading stiffness factor (e_{x1})*, employed to define, as a proportion of its loading counterpart, the unloading tangent modulus corresponding to the plastic strain. Values ranging from 1.5 and 3.0 have been used (though any value above zero constitutes a valid entry). e_{x1} is taken as 3 for Specimen 3 6, 5 and 7 during the analysis.

- *repeated cycle strain factor (e_{x2})*, utilised in the computation of the strain that the envelope curve should reach after inner cycling. Its value may typically vary between 1.0 and 1.5 (though any value above zero constitutes a valid entry). e_{x2} is taken as 3 for Specimen 3 6, 5 and 7 during the analysis.

$E_m, f_{m\theta}, f_b, \varepsilon_m, \varepsilon_{ult}, \varepsilon_{cb}, \varepsilon_1, \varepsilon_2$ were taken from the material test results for the shotcrete concrete given in detail in Chapter 3. $\alpha_{re}, \alpha_{ch}, \beta_a, \beta_{ch}, \gamma_{plu}, \gamma_{plr}, \gamma_{un}, e_{x1}, e_{x2}$ are also predicted from the values taken from the interval given in the manual depending on the test results.

Table 5.4: Suggested and limit values for empiric parameters

Constant	Suggested Values	Limit Values
α_{re}	0.2-0.4	>0
α_{ch}	0.3-0.6	0.1-0.7
β_a	1.5-2.0	>0
β_{ch}	0.6-0.7	0.5-0.9
γ_{plu}	0.5-0.7	0-1.0
γ_{plr}	1.1-1.5	≥ 1.0
γ_{un}	1.5-2.5	≥ 1.0
e_{x1}	1.5-2.0	≥ 0
e_{x2}	1.0-1.5	≥ 0

- *Shear Curve Parameters*, employed in the definition of the masonry strut hysteretic model, which is modelled with the infill panel shear response curve.

Cyclic shear behaviour of the shear struts are implemented in order to represent the shear behaviour of the infill panel when the failure is given by the loss of bonding along the mortar joints given in Figure 5.5. The model consists of two simple rules and includes the axial load in the masonry as a variable in the shear strength. These rules are

- Elastic response – Rule 1,
- Sliding – Rule 2.

These rules are explained in detail in Crisafulli (1997).

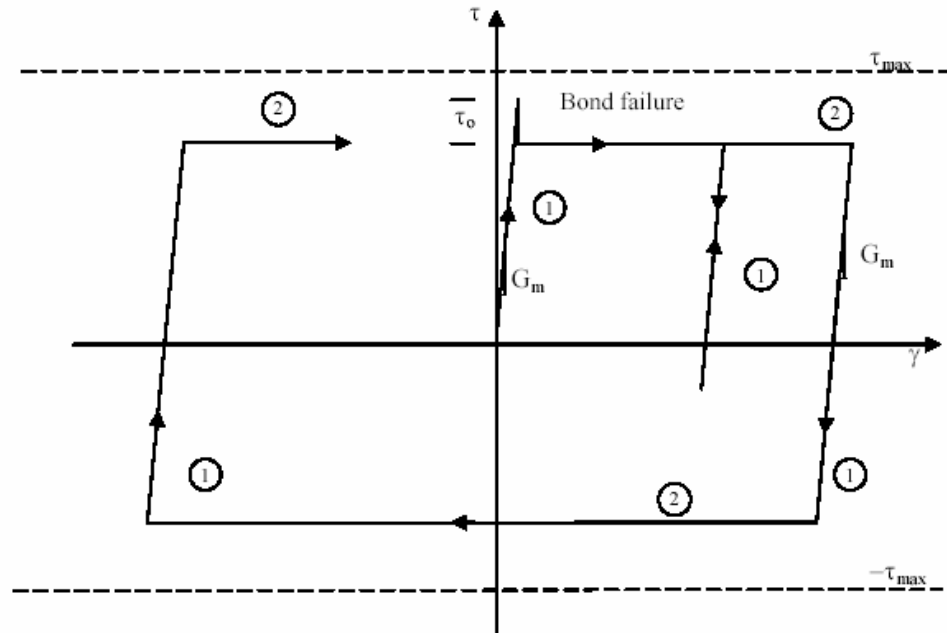


Figure 5.5: Analytical response for cyclic shear response of mortar joints

Table 5.5 gives the input parameters needed for modelling the shear spring.

Table 5.5: Input parameters of the shear spring

Parameter	Definition
τ_0	Shear bond strength
μ	Friction coefficient
τ_{max}	Maximum shear resistance
α_s	Reduction shear factor

Four parameters need to be defined in order to fully characterise this response curve:

- 1- *Shear bond strength* - τ_0 : A range of 0.1 to 1.5 MPa values can be found in the literature from the experimental studies done to find out shear bond strength. From these research initiatives, several empirical expressions have been proposed, dependent on different parameters, but their use must be cautious considering the numerous variables that affect the shear bond strength. μ is taken as 1.0 for Specimen 3 6, 5 and 7 during the analysis.
- 2- *Friction coefficient* - μ : Different researchers presented values of μ that range from 0.1 to 1.2. μ is taken as 0.3 for Specimen 3 6, 5 and 7 during the analysis.

- 3- *Maximum shear strength* - τ_{max} : This is the largest shear stress that may be mobilised by the infill panel and, as stated above, it will depend on the failure mechanism (shear friction failure, diagonal tension failure, compression failure) developed in the latter. In the absence of additional and more precise information, users may assume this value to be equal to the sum of τ_0 and the product of μ by the normal compressive strength of the masonry units. The value is taken from Chapter 3 which summarises the material test results for shotcrete panel.
- 4- *Reduction shear factor* - α_s : This empirical parameter represents the ratio between the maximum shear stress and the average stress in the panel, and may range between 1.4 and 1.65 (Crisafulli, 1997). α_s is taken as 1.4 for Specimen 3, 6, 5 and 7 during the analysis.

τ_{max} is taken from the material test results for the shotcrete concrete given in detail in Chapter 3. τ_0 , μ and α_s are also predicted from the values taken from the interval given in the manual depending on the test results.

- *Infill panel thickness* (t), which may be considered as equal to the width of the panel bricks alone or also include the contribution of the plaster.

- *Out-of-plane failure drift*, introduced in percentage of storey height, and which dictates the de-activation of the element (i.e. once the panel, not the frame, reaches a given out-of-plane drift, the panel no longer contributes to the structure's resistance nor stiffness, since it is assumed that it has failed by means of an out-of-plane failure mechanism). This value is taken as 0.1% for all the specimens.

- *Strut area 1* (A_1), defined as the product of the panel thickness and the equivalent width of the strut (b_w), which normally varies between 10% and 40% of the diagonal of the infill panel (d_m), as concluded by many researchers based on experimental data and analytical results. A_1 is predicted from the behaviour of the wall during the test.

- *Strut area 2* (A_2), introduced as percentage of A_1 , and which aims at accounting for the fact that due to cracking of the infill panel, the contact length between the frame and the infill decreases as the lateral and consequently the axial displacement increases, affecting thus the area of equivalent strut. It is assumed

that the area varies linearly as function of the axial strain as given in Figure 5.6, with the two strains between which this variation takes place being defined as input parameters of the masonry strut hysteretic model.

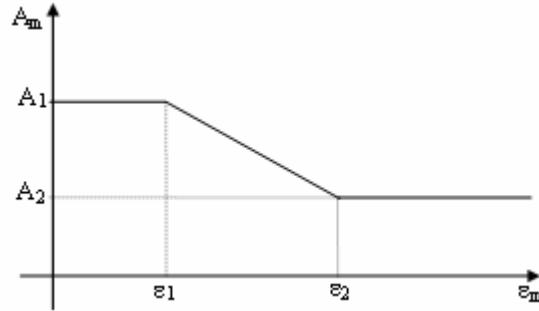


Figure 5.6: Change in the strut area

- *Equivalent contact length (h_z)*, introduced as percentage of the vertical height of the panel, effectively yielding the distance between the internal and dummy nodes, and used so as to somehow take due account of the contact length between the frame and the infill panel. Reasonable results are obtained for values of 1/3 to 1/2 of the actual contact length (z), defined by Stafford-Smith (1966) as equal to $0.5 \cdot \pi \cdot \lambda^{-1}$, where λ is a dimensionless relative stiffness parameter computed by the Eq. 5.1 given below, in which E_m is the Elastic Modulus of the masonry, t_w is the thickness of the panel, θ is the angle of the diagonal strut with respect to the beams, $E_c I_c$ is the bending stiffness of the columns, and h_w is the height of the infill panel.

$$\lambda = \sqrt[4]{\frac{E_m t_w \sin(2\theta)}{4E_c I_c h_w}} \quad (5.1)$$

- *Horizontal and Vertical offsets (x_{oi} and y_{oi})*, introduced as percentage of the horizontal and vertical dimensions of the panel, and which obviously represent the reduction of the latter due to the depth of the frame members. In other words, these parameters provide the distance between the external corner nodes and the internal ones.

- *Proportion of stiffness assigned to shear (γ_s)*, representing the proportion of the panel stiffness (computed internally by the program) that should be assigned to the shear spring. In other words, the strut stiffness (K_A) and the shear stiffness (K_S) are computed in Eq. 5.2 and Eq. 5.3 as follows:

$$K_A = (1 - \gamma_s) \frac{A_{ms} E_m}{2d_m} \quad (5.2)$$

$$K_s = \gamma_s \frac{A_{ms} E_m}{d_m} \cos^2 \theta \quad (5.3)$$

- *Specific weight (γ)*, representing the volumetric weight of the panel.

x_{oi} , y_{oi} , h_z and t_w are taken from the material test results for the shotcrete concrete given in detail in Chapter 3, while A_1 and A_2 is predicted from the behaviour of the wall during the test. γ_s is also predicted from the values taken from the interval given in the manual depending on the test results.

5.5 Comparison of the Results of Analysis with Experimental Results

The analytical model prepared in SeismoStruct is shown in Figure 5.7 and 5.8.

Columns and beam are divided into 8 and 10 pieces, respectively as shown in Figure 5.9. The frame is idealized to have fixed type support. Three degrees of freedom, the translational displacements, u , v and the rotation, θ , are considered at each node of the frame and of the external and internal nodes of the wall.

For modelling the frame with the wall which is not connected to the columns, the x_{oi} and y_{oi} are defined according to geometric properties of the wall. Although these parameters are originally used to define the dimensions of the wall depending on the depth of the frame elements, the obtained results show that it can also be used to model these types of infill walls as well.

The analytical model was subjected to constant vertical point loads on the columns and lateral displacement pattern which is acting at the centre of the loading beam as shown in Figure 5.9.

Analytical studies start with modelling the bare frame first and then move onto the shotcrete panel specimens. In the cross sections of the frame, unconfined and confined concrete properties are taken into account by using existing models in the program. A nonlinear response model existing in the program is assigned to the reinforcements. Longitudinal reinforcement properties such as quantity, diameter and coordinates and diameter and spacing of lateral reinforcement are introduced. The shotcrete panel is modelled by diagonal braces corresponding to the infill wall model

in the program. Although there are several parameters existing in the program to define the response of infill walls, the three parameters namely compressive strength, tensile strength and shear resistance are the most effective ones.

The comparisons of the experimental and analytical results are presented only for retrofitted non-damaged type frame specimens because the program is not capable of modelling pre-damaged type frames.

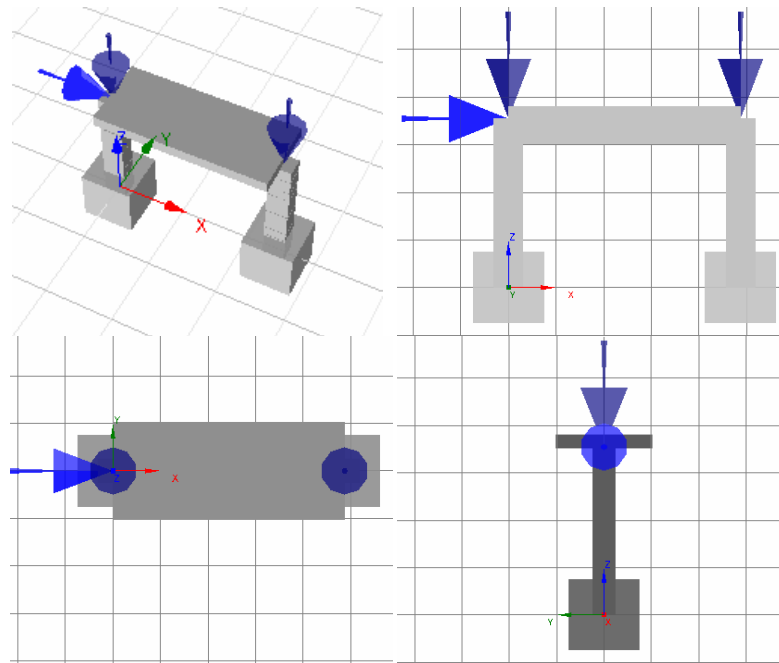


Figure 5.7: Frame model used in SeismoStruct

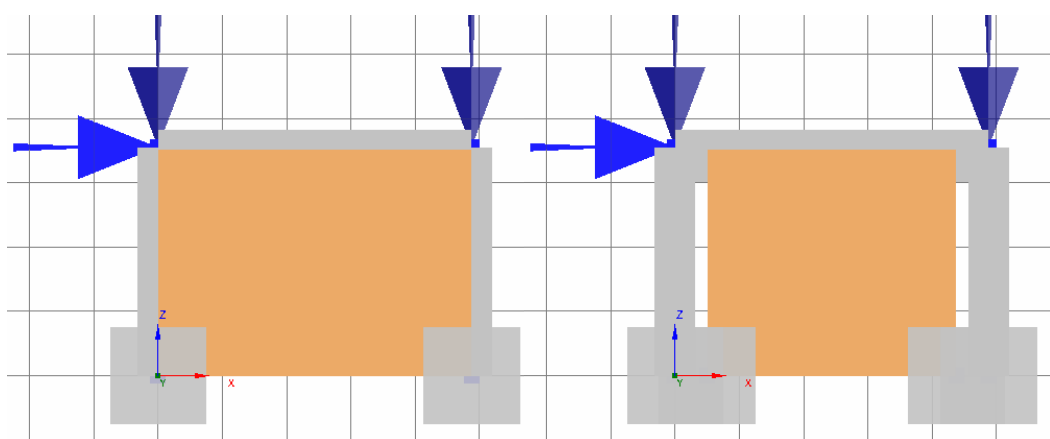


Figure 5.8: Infilled frame models used in SeismoStruct

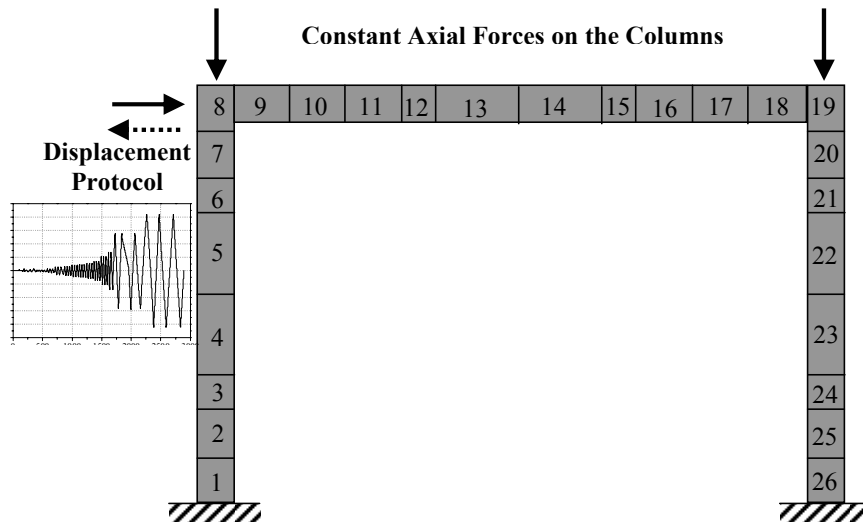


Figure 5.9: Definition of frame element names and the loadings in the mathematical model used in SeismoStruct

Damage states for structural members defined in Turkish Earthquake Code (**TEC, 2007**) are introduced to the program. Strain limits used to define damage states in structural members are given in Table 5.6. At the end of the analysis, the program produces reports about the damage states of the sections, which material inside this section has reached the limit strain and at what stage of loading does the damage occurred.

Table 5.6: Limit strain values to define damage states in structural members according to TEC 2007

Damage States in Structural Members	Strain Limit	Place of Deformation
Minimum Damage Limit (MNc)	<- 0.0035	The outer-most fibre of the concrete of the section
Minimum Damage Limit (MNs)	> 0.01	Longitudinal reinforcement
Safety Limit (GVc)	< -0.0085	The outer fibre of the concrete within the transversal reinforcement
Safety Limit (GVs)	> 0.040	Longitudinal reinforcement
Collapse Limit (GCc)	< -0.011	The outer fibre of the concrete within the transversal reinforcement
Collapse Limit (GCs)	> 0.060	Longitudinal reinforcement

c = concrete, s = steel,

compression (-), tension (+) in strain limits

5.5.1 Specimen 1

The displacement history applied to Specimen 1 (bare frame) in the experimental study is given in Figure 5.10. This loading protocol was applied to the analytical model as well.

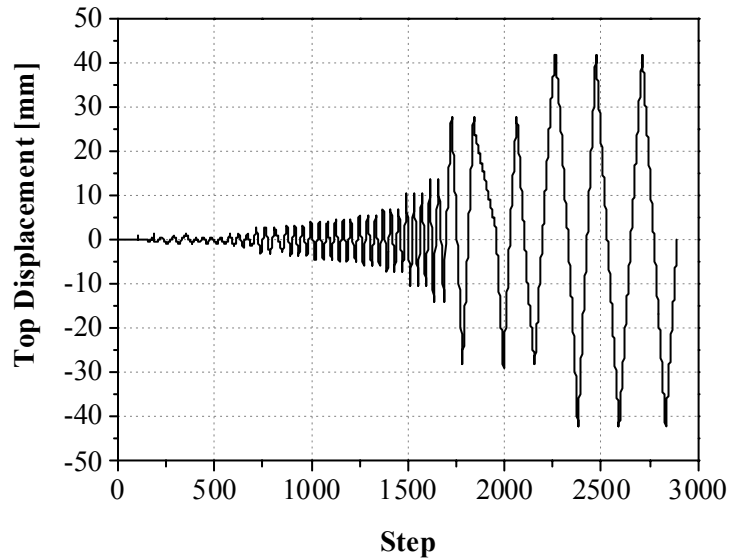


Figure 5.10: The displacement pattern applied to Specimen 1

The comparison of the experimental and analytical results for Specimen 1 is given as hysteretic loops in Figure 5.11 and as envelope curves in Figure 5.12. The envelope curves are obtained by taking the average of load values corresponding to the three cycles of the target displacements.

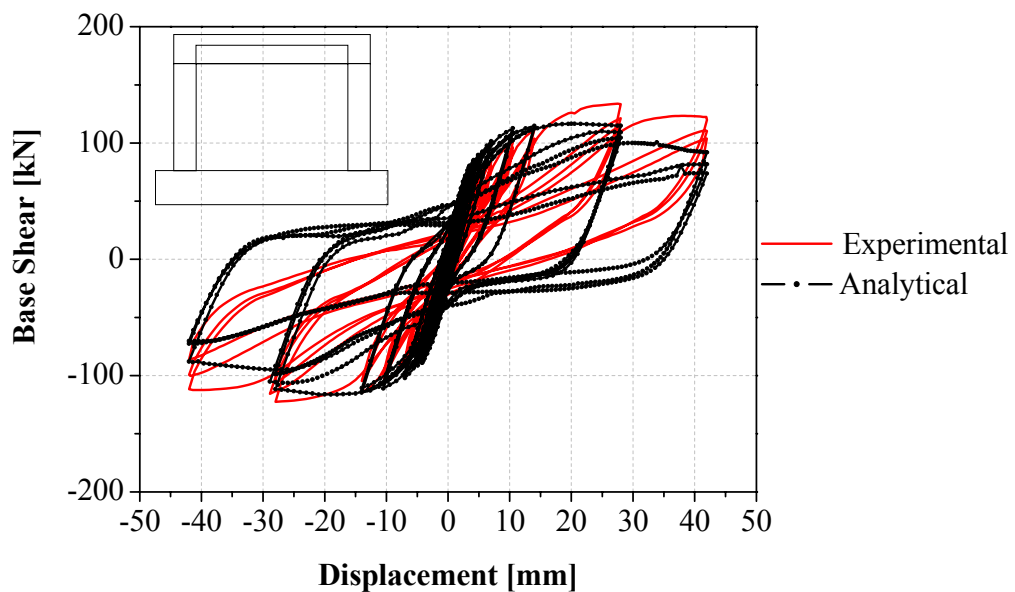


Figure 5.11: Comparison of the hysteretic curves of the experimental and analytical results of Specimen 1

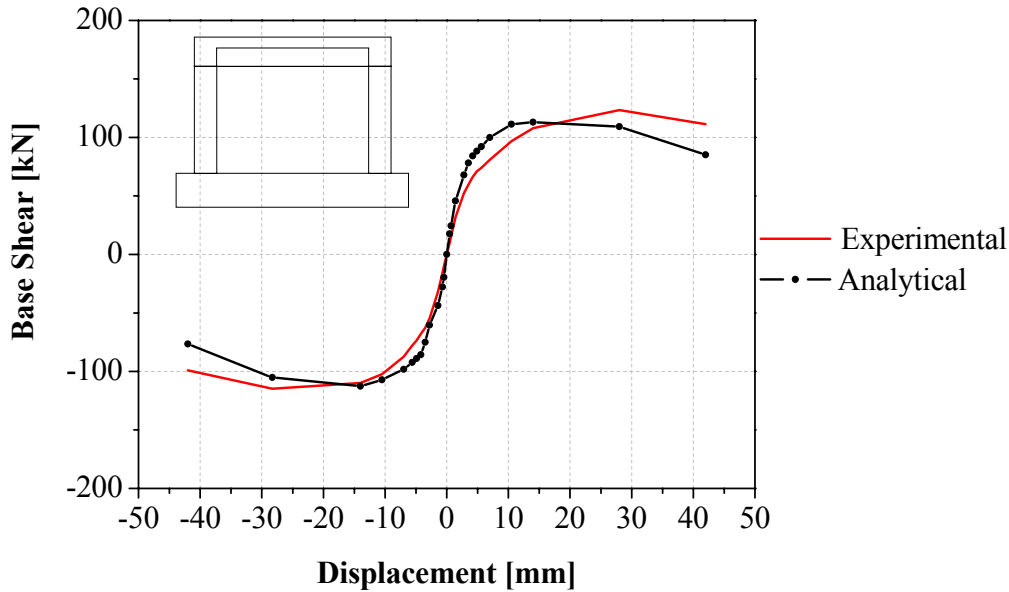


Figure 5.12: Comparison of the envelope curves of the experimental and analytical results of Specimen 1

As seen from Figure 5.11 analytical study overestimates strength values at the initial displacement cycles. The maximum load occurred in the system is captured quite well in the analysis. But the descending branch slope of the analytical results is steeper than the experimental results.

Table 5.7 summarizes the damage states observed in the analytical work. The table summarizes the location of damage and which type of material is damaged. The strain values are also given at the state of the damage. The bold lines in the table match with the experimental result. The analytical results show almost the exact step and position of damage like it has been observed during the experiment.

Figure 5.13 shows the damage states obtained at drift levels. For the pushing cycles, “yield” has occurred first at the bottom and top end of the right column at 0.35% drift levels. Unconfined concrete has reached “minimum damage limit” first at the bottom and top end of the right and the left columns at 0.75% drift level. Reinforcement has reached “minimum damage limit” first at the bottom end of the right column at 1.00% drift levels. Unconfined concrete has reached “safety and collapse limit” first at the bottom end of the left column at 2.00% drift level. For the pulling cycles, at 0.35% drift level, yield occurred at the bottom and top end of the left column. Unconfined concrete has reached “minimum damage limit” first at the bottom end of the right column at 1.00% drift level. Reinforcement has reached “minimum damage limit” at the bottom part and top end of the left column, and also at end of the beam

at 2.00% drift levels. At the same drift level unconfined concrete has reached “safety and collapse limit” at the bottom end of the right column.

Table 5.7: Damage levels for Specimen 1

Target Displacement [mm]	Performance Level	Element name	Place of damage	Damage type	Strain
At the end of 2nd cycle of +4.9	yield	1	Bottom end	Steel	0.002404
At the end of 3rd cycle of +4.9	yield	8	Top end	Steel	0.002373
At the end of 1st cycle of +5.6	yield	1	Top end	Steel	0.002116
At the end of 1st cycle of -5.6	yield	26	Bottom end	Steel	0.002114
At the end of 1st cycle of -5.6	yield	26	Top end	Steel	0.002279
At the end of 2nd cycle of -5.6	yield	18	Right end	Steel	0.002161
At the end of 3rd cycle of -5.6	yield	18	Left end	Steel	0.002270
At the end of 1st cycle of +7.0	yield	8	Bottom end	Steel	0.002203
At the end of 1st cycle of +10.5	MNc	26	Bottom end	Unc Conc	-0.003720
At the end of 1st cycle of +10.5	MNc	1	Top end	Unc Conc	-0.003510
At the end of 1st cycle of +10.5	MNc	8	Top end	Unc Conc	-0.003650
At the end of 1st cycle of -10.5	yield	19	Top end	Steel	0.002301
At the end of 1st cycle of -10.5	yield	19	Bottom end	Steel	0.002406
At the end of 3rd cycle of +10.5	MNc	19	Top end	Unc Conc	-0.003630
At the end of 1st cycle of +14	MNs	1	Bottom end	Steel	0.010224
At the end of 1st cycle of +14	MNc	26	Top end	Unc Conc	-0.003710
At the end of 1st cycle of -14	MNc	1	Top end	Unc Conc	-0.003500
At the end of 1st cycle of +28	MNs	1	Top end	Steel	0.010800
At the end of 1st cycle of +28	MNs	8	Top end	Steel	0.010119
At the end of 1st cycle of +28	MNs	26	Bottom end	Steel	0.010309
At the end of 1st cycle of +28	MNc	8	Top end	Unc Conc	-0.003550
At the end of 1st cycle of +28	MNs	8	Top end	Steel	0.010418
At the end of 1st cycle of +28	MNc	19	Bottom end	Unc Conc	-0.003580
At the end of 1st cycle of +28	GVC	26	Bottom end	Unc Conc	-0.008640
At the end of 1st cycle of +28	MNs	26	Top end	Steel	0.010137
At the end of 1st cycle of +28	MNs	19	Top end	Steel	0.010674
At the end of 1st cycle of +28	GCc	26	Bottom end	Unc Conc	-0.011280
At the end of 1st cycle of -28	GVC	1	Bottom end	Unc Conc	-0.008980
At the end of 1st cycle of -28	GCc	1	Bottom end	Unc Conc	-0.012110
At the end of 1st cycle of -28	MNs	19	Bottom end	Steel	0.010281
At the end of 2nd cycle of +28	MNc	7	Top end	Unc Conc	-0.003520
At the end of 2nd cycle of -28	MNc	25	Bottom end	Unc Conc	-0.003530
At the end of 2nd cycle of -28	MNs	18	Right end	Steel	0.010040
At the end of 3rd cycle of -28	MNs	18	Left end	Steel	0.010046
At the end of 1st cycle of -42	yield	25	Bottom end	Steel	0.002105
At the end of 2nd cycle of +42	MNc	2	Bottom end	Unc Conc	-0.003510
At the end of 2nd cycle of +42	MNc	2	Top end	Unc Conc	-0.003510
At the end of 3rd cycle of -42	MNc	25	Top end	Unc Conc	-0.003520

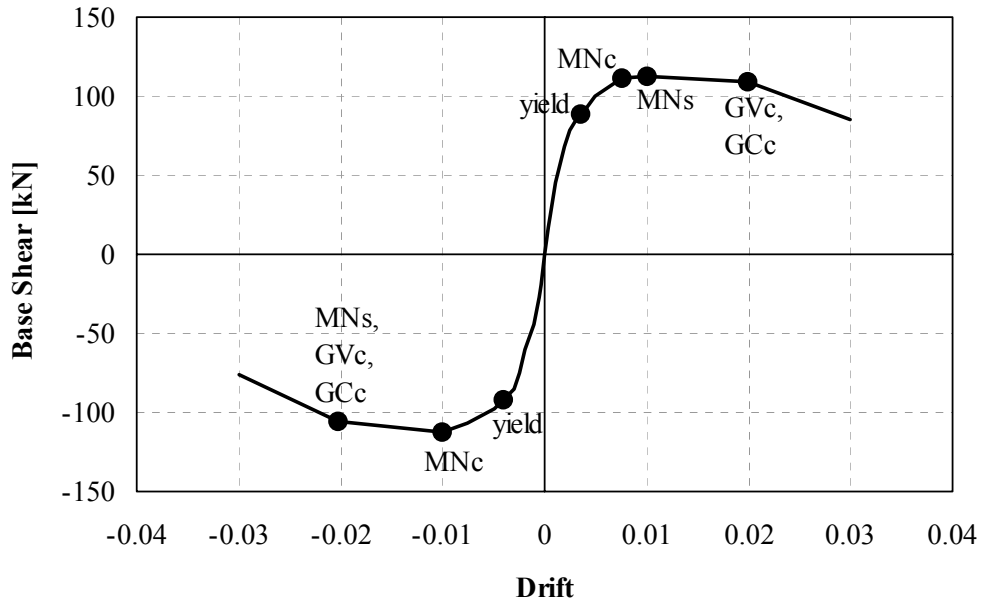


Figure 5.13: Damage states obtained at drift levels at certain drift levels at Specimen 1

Figure 5.14 shows the frame at the end of loading history. The “collapse limit” is attained at the bottom ends of the columns.

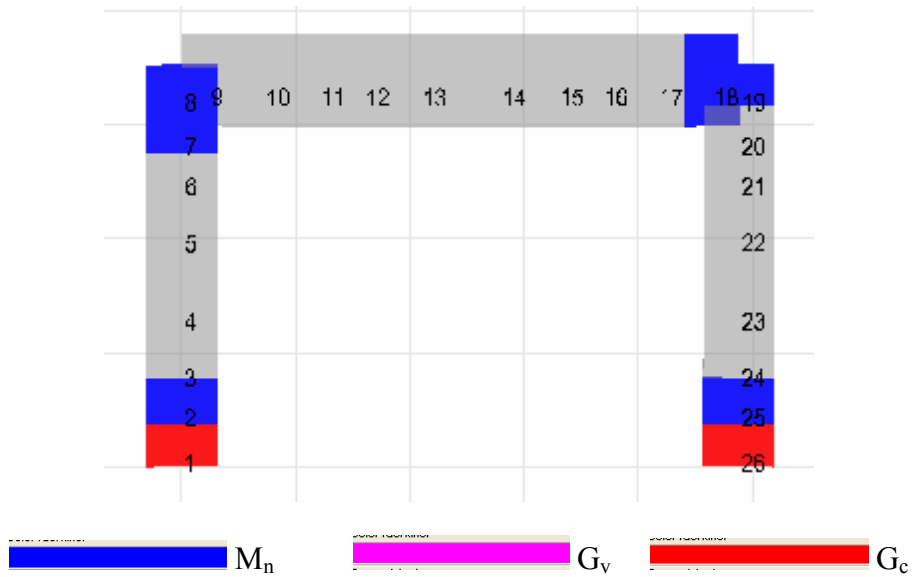


Figure 5.14: Damages occurred at the end of the analysis of Specimen 1

5.5.2 Specimen 3

The displacement history applied to Specimen 3 (fully infilled frame) in the experimental study is given in Figure 5.15. This loading protocol was used for the analytical model as well.

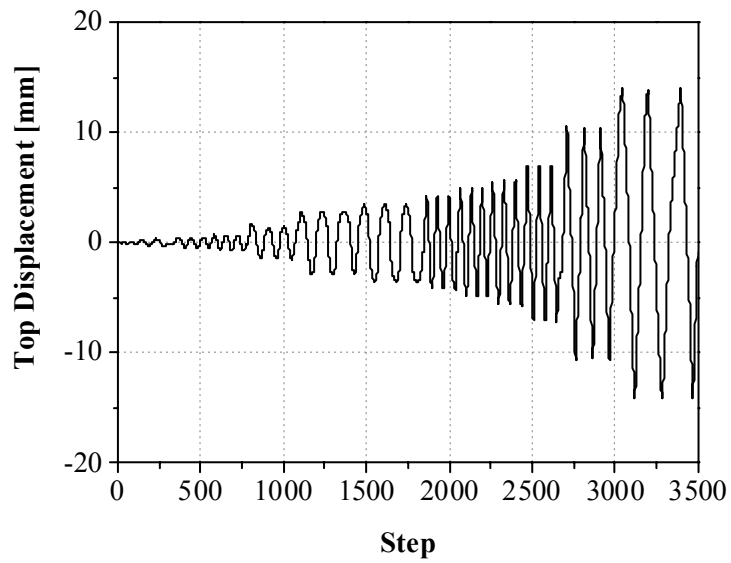


Figure 5.15: The displacement pattern applied to Specimen 3

The comparison of the experimental and analytical results for Specimen 3 is given as hysteretic loops in Figure 5.16 and as envelope curves in Figure 5.17.

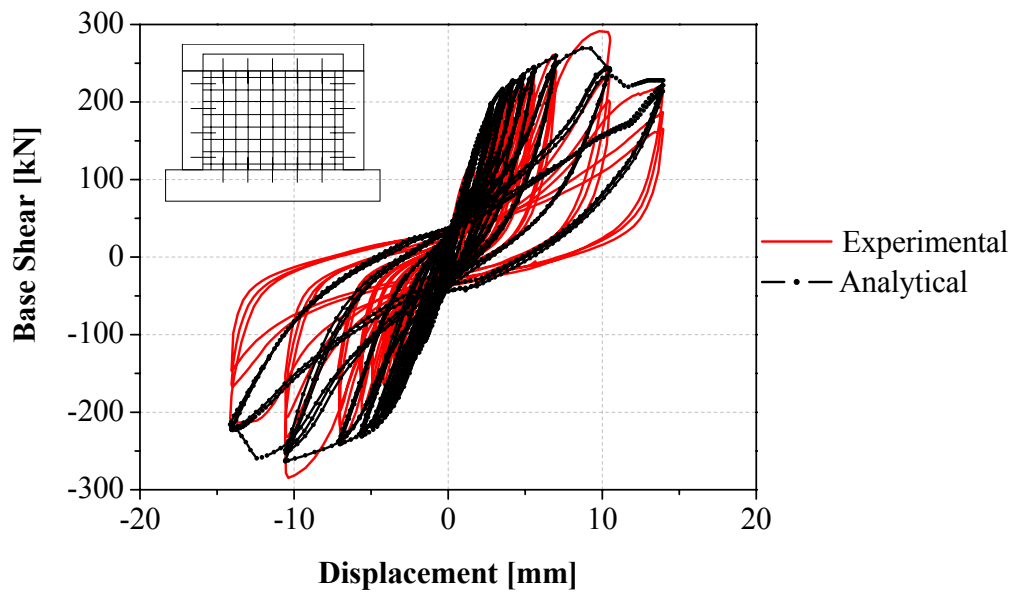


Figure 5.16: Comparison of the hysteretic curves of the experimental and analytical results of Specimen 3

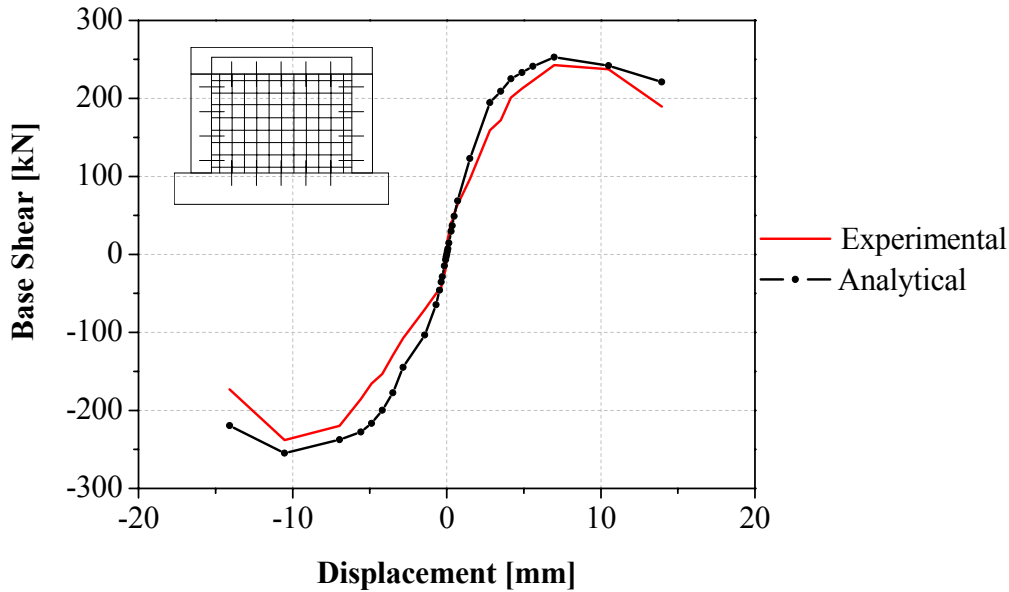


Figure 5.17: Comparison of the envelope curves of the experimental and analytical results of Specimen 3

As seen from Figure 5.16, analytical study predicts strength values at the initial displacement cycles quiet well. The maximum load occurred in the system is underestimated in the analysis. But the ultimate strength values are captured by analytical results agrees well with the experimental results.

Table 5.8 summarizes the damage states observed in the analytical work. The table summarizes the location of damage and which type of material is damaged with strain value at the damage. The bold line in the table, match with the experimental result. The analytical results show almost the exact step and position of damage like it has been observed during the experiment.

Figure 5.18 shows the damage states obtained at drift levels. For the pushing cycles, “yield” has occurred first at the bottom and top end of the right column at 0.25% drift levels. Unconfined concrete has reached “minimum damage limit” first at top ends of the right and the left columns at 0.40% drift level. Reinforcement has reached “minimum damage limit” first at the bottom end of the right column at 1.00% drift levels. For the pulling cycles, at 0.25% drift level, “yield occurred” and unconfined concrete has reached “minimum damage limit” at the top end of the left column. Reinforcement has reached “minimum damage limit” at the bottom end of the left column at 1.00% drift levels. At the same drift level confined concrete has reached “safety limit” at the bottom end of the right column.

Table 5.8: Damage levels for Specimen 3

Target Displacement	Performance Level	Element Name	Place of Damage	Damage type	Strain
At the end of 2nd cycle of +3.5	yield	1	Bottom end	Steel	0.002102
At the end of 2nd cycle of +3.5	yield	8	Top end	Steel	0.002101
At the end of 3rd cycle of +3.5	yield	8	Bottom end	Steel	0.002138
At the end of 3rd cycle of -3.5	MNc	19	Top end	Unc Conc	-0.003531
At the end of 3rd cycle of -3.5	yield	19	Top end	Steel	0.002113
At the end of 1st cycle of +4.9	yield	1	Top end	Steel	0.002202
At the end of 1st cycle of -4.9	yield	19	Bottom end	Steel	0.002305
At the end of 1st cycle of +5.6	MNc	20	Bottom end	Unc Conc	-0.003554
At the end of 1st cycle of +5.6	MNc	8	Top end	Unc Conc	-0.003742
At the end of 1st cycle of -5.6	yield	26	Bottom end	Steel	0.002222
At the end of 1st cycle of -5.6	yield	26	Top end	Steel	0.002107
At the end of 2nd cycle of -5.6	MNc	2	Top end	Unc Conc	-0.003524
At the end of 3rd cycle of -5.6	MNc	2	Bottom end	Unc Conc	-0.003545
At the end of 3rd cycle of -5.6	MNc	19	Bottom end	Unc Conc	-0.003503
At the end of 1st cycle of +7.0	MNc	1	Bottom end	Unc Conc	-0.003639
At the end of 1st cycle of +7.0	MNc	20	Top end	Unc Conc	-0.003733
At the end of 1st cycle of -7.0	MNc	7	Bottom end	Unc Conc	-0.003511
At the end of 1st cycle of +10.5	MNc	8	Bottom end	Unc Conc	-0.003511
At the end of 1st cycle of +10.5	MNc	25	Top end	Unc Conc	-0.003514
At the end of 1st cycle of +10.5	MNc	26	Bottom end	Unc Conc	-0.003697
At the end of 1st cycle of -10.5	MNc	7	Top end	Unc Conc	-0.003530
At the end of 1st cycle of -10.5	yield	20	Top end	Steel	0.002963
At the end of 2nd cycle of -10.5	MNc	25	Bottom end	Unc Conc	-0.003628
At the end of 1st cycle of +14.0	MNc	26	Top end	Unc Conc	-0.003511
At the end of 1st cycle of +14.0	MNc	1	Top end	Unc Conc	-0.003508
At the end of 1st cycle of +14.0	MNs	1	Bottom end	Steel	0.010083
At the end of 1st cycle of -14.0	MNc	3	Bottom end	Unc Conc	-0.003571
At the end of 1st cycle of -14.0	MNs	26	Bottom end	Steel	0.010039
At the end of 2nd cycle of +14.0	MNc	24	Bottom end	Unc Conc	-0.003523
At the end of 3rd cycle of -14.0	Gvc	1	Bottom end	Conf Conc	-0.008617

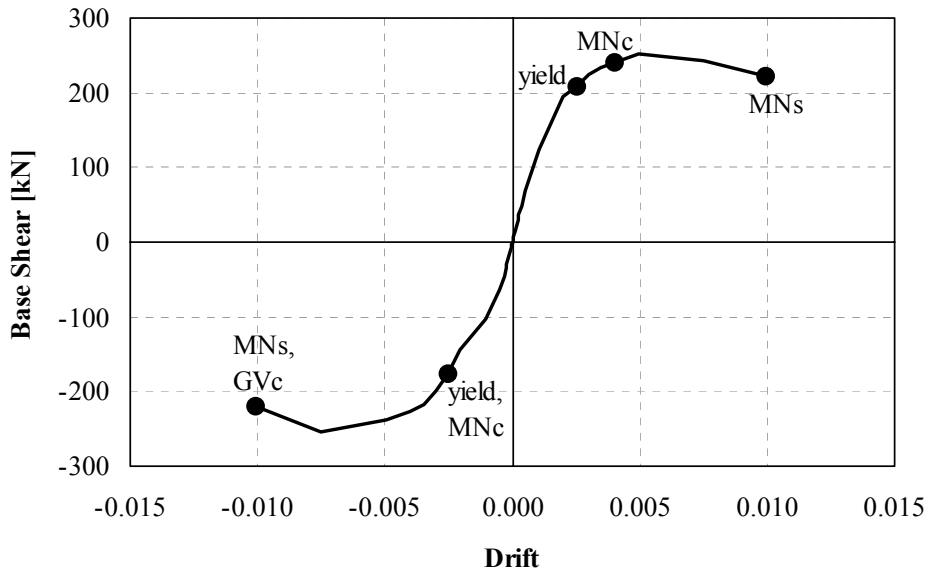


Figure 5.18: Damage states obtained at drift levels at certain drift levels at Specimen 3

Figure 5.19 shows the frame at the end of loading. The “safety limit” is reached at the bottom end parts of the columns.

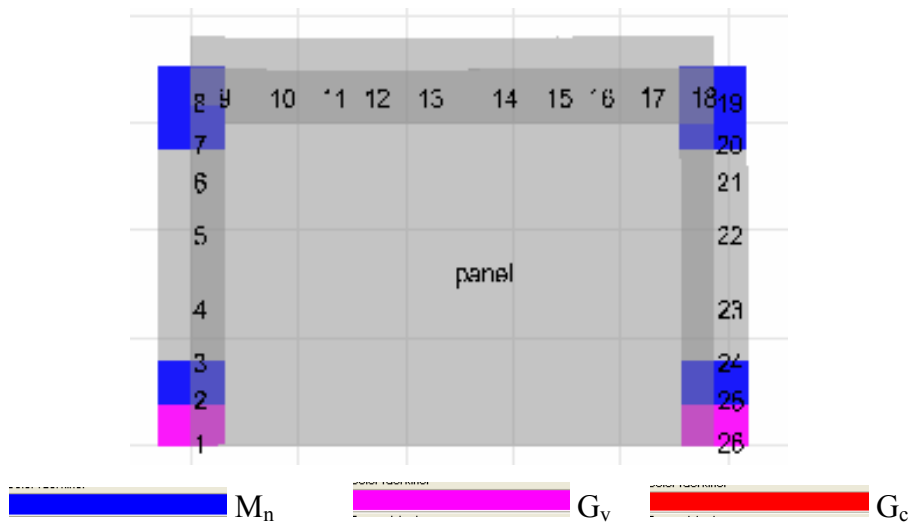


Figure 5.19: Damage occurred at the end of the analysis at Specimen 3

5.5.3 Specimen 5

The displacement history applied to Specimen 5 (partially infilled frame) in the experimental study is given in Figure 5.20. This loading protocol was applied to the analytical model as well.

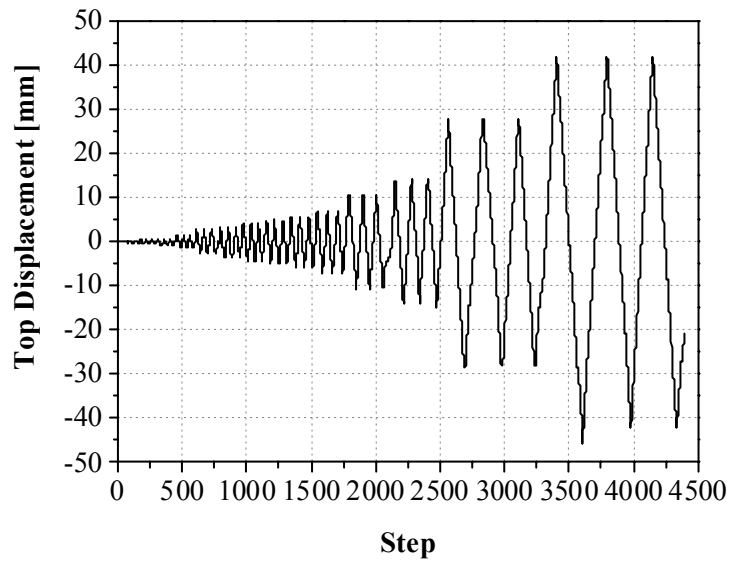


Figure 5.20: The displacement pattern applied to Specimen 5

The comparison of the experimental and analytical results for Specimen 5 is given as hysteretic loops in Figure 5.21 and as envelope curves in Figure 5.22.

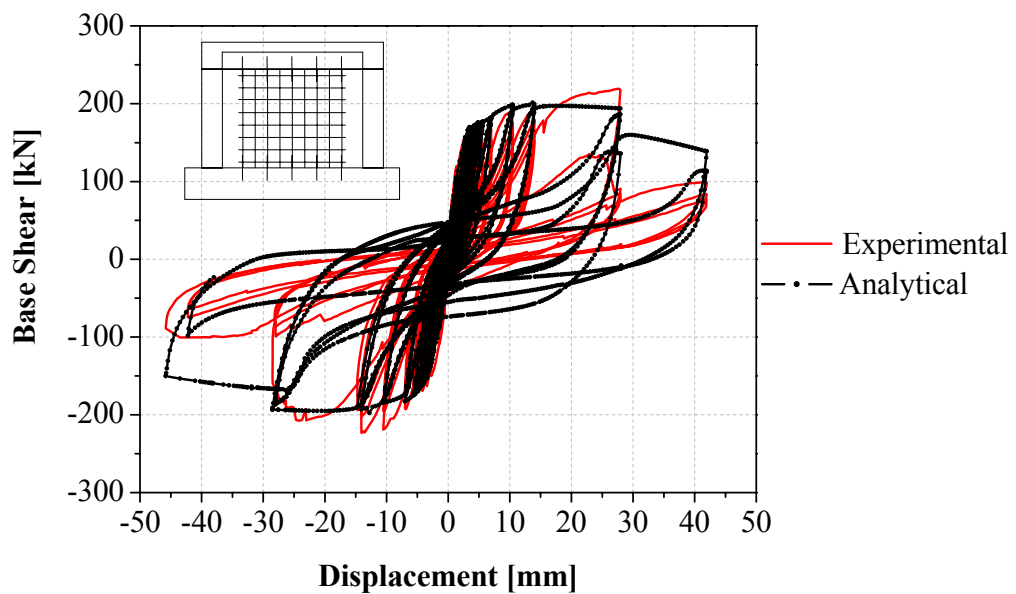


Figure 5.21: Comparison of the hysteretic curves of the experimental and analytical results of Specimen 5

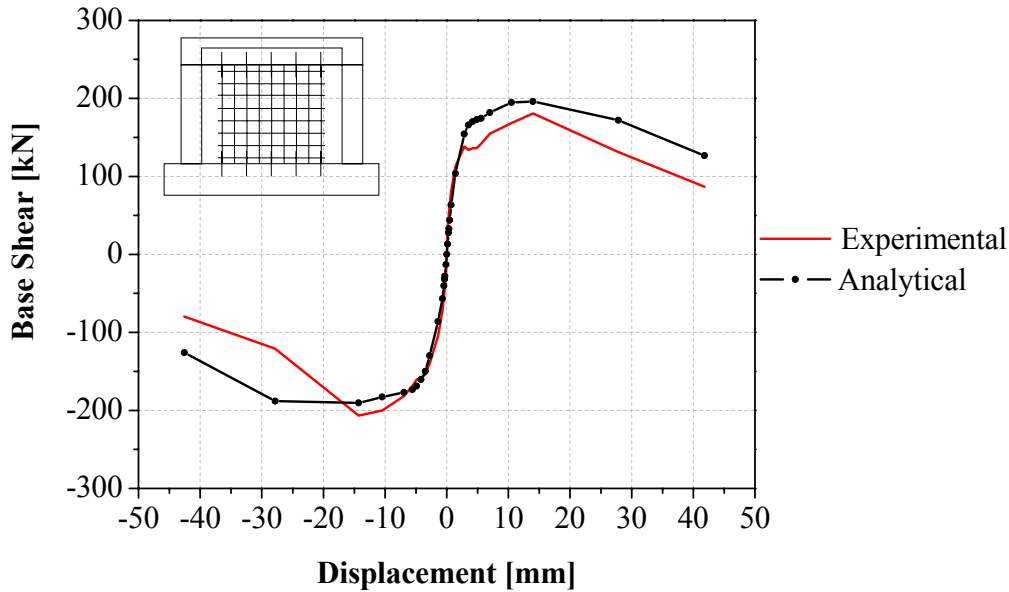


Figure 5.22: Comparison of the envelope curves of the experimental and analytical results of Specimen 5

As seen from Figure 5.21, analytical study predicts strength values at the initial displacement cycles quite well. The maximum load occurred in the system is captured quite good in the analysis as well. But the descending branch slope of the analytical results is steeper than the experimental results.

Table 5.9 summarizes the damage states observed in the analytical work. The table summarizes the location of damage and which type of material is damaged with strain value at the damage. The bold lines in the table match with the experimental result. The analytical results show almost the exact step and position of damage like it has been observed during the experiment.

Figure 5.23 shows the damage states obtained at drift levels. For the pushing cycles, “yield” has occurred first at the bottom end of the right column at 0.25% drift level. Unconfined concrete has reached “minimum damage limit” first at top end of the right and the bottom end of the left column at 0.40% drift level. Reinforcement has reached “minimum damage limit” first at the bottom and top end of the right column at 1.00% drift levels. Confined concrete has reached “safety and collapse limit” at the bottom ends of the right and left column at 2% drift level. Reinforcement has reached “safety limit” at the bottom end of the left column at 3% drift level. For the pulling cycles, at 0.3% drift level “yield” occurred at the end of the beam. Unconfined concrete has reached “minimum damage limit” first at top ends of the right and the left column at 0.50% drift level. Reinforcement has reached “minimum damage

limit” at the bottom end of the left column and at the end of the beam at 1.00% drift level. At the same drift level confined concrete has reached “safety limit” at the bottom end of the right column. Confined concrete has reached “collapse limit” at the bottom end of the left column at 2.00% drift level. Reinforcement has reached “safety limit” at the top end of the left column at 3.00% drift level.

Table 5.9: Damage levels for Specimen 5

Target Displacement [mm]	Performance Level	Element Name	Place of Damage	Damage type	Strain
At the end of 1st cycle of +3.5	yield	1	Bottom end	Steel	-0.002110
At the end of 1st cycle of +4.2	yield	1	Top end	Steel	0.002105
At the end of 1st cycle of -4.2	yield	18	Top end	Steel	0.002182
At the end of 1st cycle of -4.2	yield	18	Bottom end	Steel	0.002335
At the end of 3rd cycle of +4.9	yield	8	Top end	Steel	0.002256
At the end of 3rd cycle of -4.9	yield	26	Bottom end	Steel	0.002114
At the end of 1st cycle of +5.6	yield	8	Bottom end	Steel	0.002186
At the end of 1st cycle of -5.6	yield	26	Top end	Steel	0.002123
At the end of 3rd cycle of +5.6	MNc	8	Top end	Unc Conc	-0.003720
At the end of 3rd cycle of +5.6	MNc	25	Top end	Unc Conc	-0.003566
At the end of 1st cycle of +7.0	MNc	19	Bottom end	Unc Conc	-0.003553
At the end of 3rd cycle of -7.0	MNc	19	Top end	Unc Conc	-0.003561
At the end of 3rd cycle of -7.0	MNc	7	Bottom end	Unc Conc	-0.003514
At the end of 1st cycle of +10.5	MNc	25	Bottom end	Unc Conc	-0.003518
At the end of 1st cycle of +10.5	MNc	26	Bottom end	Unc Conc	-0.003719
At the end of 1st cycle of -10.5	MNc	1	Bottom end	Unc Conc	-0.003705
At the end of 2nd cycle of -10.5	yield	19	Bottom end	Steel	0.002180
At the end of 3rd cycle of +10.5	MNc	8	Bottom end	Unc Conc	-0.003570
At the end of 1st cycle of +14.0	MNc	20	Bottom end	Unc Conc	-0.003606
At the end of 1st cycle of +14.0	MNs	8	Bottom end	Steel	0.010086
At the end of 1st cycle of +14.0	MNs	1	Bottom end	Steel	0.010204
At the end of 1st cycle of -14.0	yield	9	Bottom end	Steel	0.002149
At the end of 1st cycle of -14.0	yield	9	Top end	Steel	0.002245
At the end of 1st cycle of -14.0	yield	19	Bottom end	Steel	0.002198
At the end of 1st cycle of -14.0	MNs	26	Bottom end	Steel	0.010101
At the end of 2nd cycle of -14.0	MNs	18	Bottom end	Steel	0.010428
At the end of 3rd cycle of +14.0	MNc	7	Top end	Unc Conc	-0.003643
At the end of 3rd cycle of -14.0	GVc	1	Bottom end	Conf Conc	-0.008574
At the end of 3rd cycle of -14.0	MNs	18	Top end	Steel	0.010508
At the end of 1st cycle of +28.0	MNc	20	Top end	Unc Conc	-0.003528
At the end of 1st cycle of +28.0	MNs	8	Top end	Steel	0.010191
At the end of 1st cycle of +28.0	MNc	26	Top end	Unc Conc	-0.003513
At the end of 1st cycle of +28.0	MNs	1	Top end	Steel	0.010049
At the end of 1st cycle of +28.0	GVc	26	Bottom end	Conf Conc	-0.008906
At the end of 1st cycle of +28.0	GCc	26	Bottom end	Conf Conc	-0.011526
At the end of 1st cycle of +28.0	yield	20	Top end	Steel	0.002292
At the end of 1st cycle of +28.0	MNc	1	Top end	Unc Conc	-0.003579
At the end of 1st cycle of +28.0	MNs	20	Top end	Steel	0.010176
At the end of 1st cycle of -28.0	GCc	1	Bottom end	Conf Conc	-0.011495
At the end of 1st cycle of -28.0	MNs	26	Top end	Steel	0.010212
At the end of 1st cycle of -28.0	MNc	9	Bottom end	Unc Conc	-0.003527

Table 5.9: Damage levels for Specimen 5 (contd.)

Target Displacement [mm]	Performance Level	Element Name	Place of Damage	Damage type	Strain
At the end of 1st cycle of -28.0	MNs	19	Top end	Steel	0.010350
At the end of 1st cycle of -28.0	MNs	19	Bottom end	Steel	0.010220
At the end of 2 nd cycle of +28.0	MNc	2	Bottom end	Unc Conc	-0.003567
At the end of 2 nd cycle of +28.0	MNc	2	Top end	Unc Conc	-0.003542
At the end of 2 nd cycle of +28.0	yield	2	Bottom end	Steel	0.002189
At the end of 2 nd cycle of -28.0	MNc	9	Top end	Unc Conc	-0.003511
At the end of 2 nd cycle of -28.0	yield	20	Bottom end	Steel	0.002104
At the end of 3rd cycle of +28.0	yield	7	Top end	Steel	0.002105
At the end of 3rd cycle of +28.0	GVc	2	Bottom end	Conf Conc	-0.008507
At the end of 3rd cycle of -28.0	yield	25	Bottom end	Steel	0.002154
At the end of 3rd cycle of -28.0	MNs	9	Bottom end	Steel	0.010117
At the end of 3rd cycle of -28.0	MNs	9	Top end	Steel	0.010173
At the end of 1st cycle of +42.0	yield	7	Bottom end	Steel	0.002100
At the end of 1st cycle of +42.0	MNs	7	Bottom end	Steel	0.010385
At the end of 1st cycle of -42.0	GVs	8	Top end	Steel	0.040009
At the end of 1st cycle of -42.0	GVc	26	Top end	Conf Conc	-0.008519
At the end of 2nd cycle of -42.0	GVs	19	Bottom end	Steel	0.040078
At the end of 2nd cycle of -42.0	GCc	26	Top end	Conf Conc	-0.011038
At the end of 3rd cycle of +42.0	yield	2	Top end	Steel	0.002102
At the end of 3rd cycle of +42.0	GCc	2	Bottom end	Conf Conc	-0.011014
At the end of 3rd cycle of +42.0	GVc	2	Top end	Conf Conc	-0.008707
At the end of 3rd cycle of +42.0	GCc	2	Top end	Conf Conc	-0.011108
At the end of 3rd cycle of +42.0	MNs	2	Top end	Steel	0.010352
At the end of 3rd cycle of +42.0	GVs	26	Bottom end	Steel	0.040103
At the end of 3rd cycle of -42.0	yield	25	Top end	Steel	0.002336
At the end of 3rd cycle of -42.0	GVc	25	Bottom end	Conf Conc	-0.008544
At the end of 3rd cycle of -42.0	MNs	25	Bottom end	Steel	0.010253
At the end of 3rd cycle of -42.0	GVs	1	Bottom end	Steel	0.040083
At the end of 3rd cycle of -42.0	MNs	25	Top end	Steel	0.010413
At the end of 3rd cycle of -42.0	GVc	25	Top end	Conf Conc	-0.008577

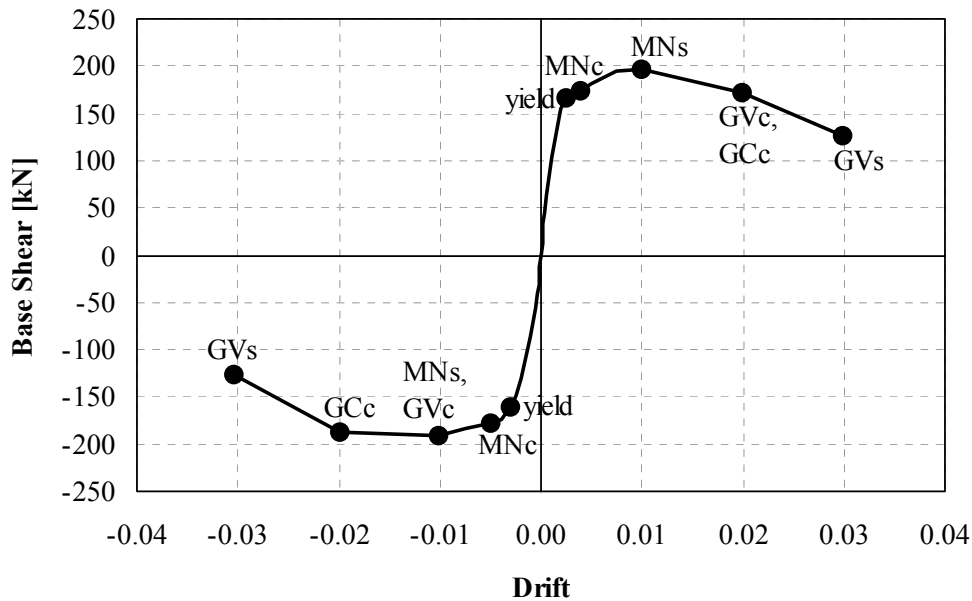


Figure 5.23: Damage states obtained at drift levels at certain drift levels at Specimen 5

Figure 5.24 shows the frame at the end of loading history the “collapse limit” and the “safety limit” are reached at the bottom ends of the columns and at the top ends of the columns, respectively.

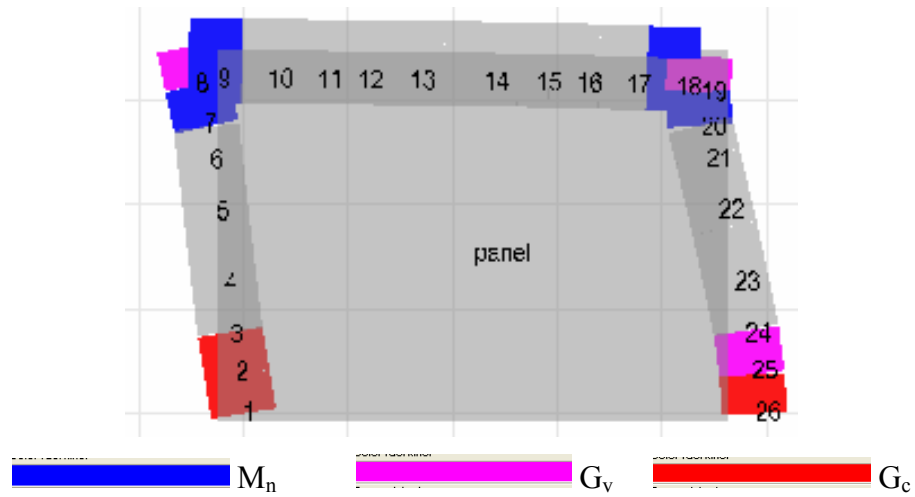


Figure 5.24: Damage occurred at the end of the analysis at Specimen 5

5.5.4 Specimen 6

The displacement history applied to Specimen 6 (fully infilled frame with pre-reverse deflection on the beam) in the experimental study is given in Figure 5.25. This loading protocol was applied to the analytical model as well.

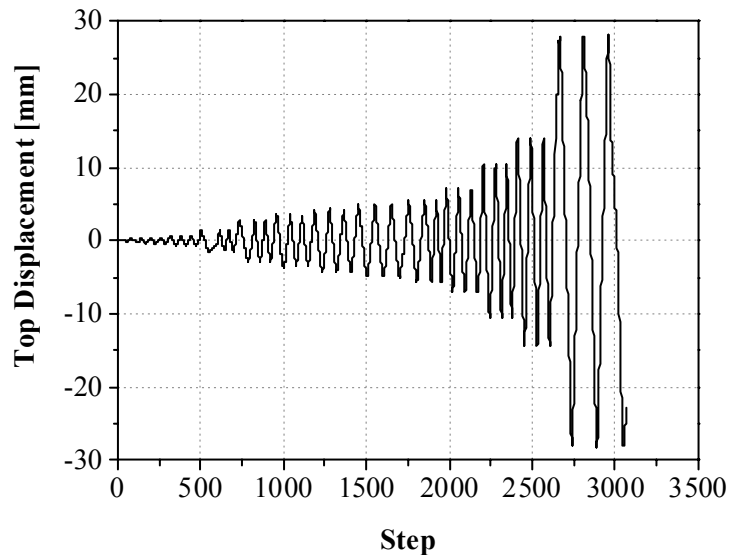


Figure 5.25: The displacement pattern applied to Specimen 6

The comparison of the experimental and analytical results for Specimen 6 is given as hysteretic loops in Figure 5.26 and as envelope curves in Figure 5.27.

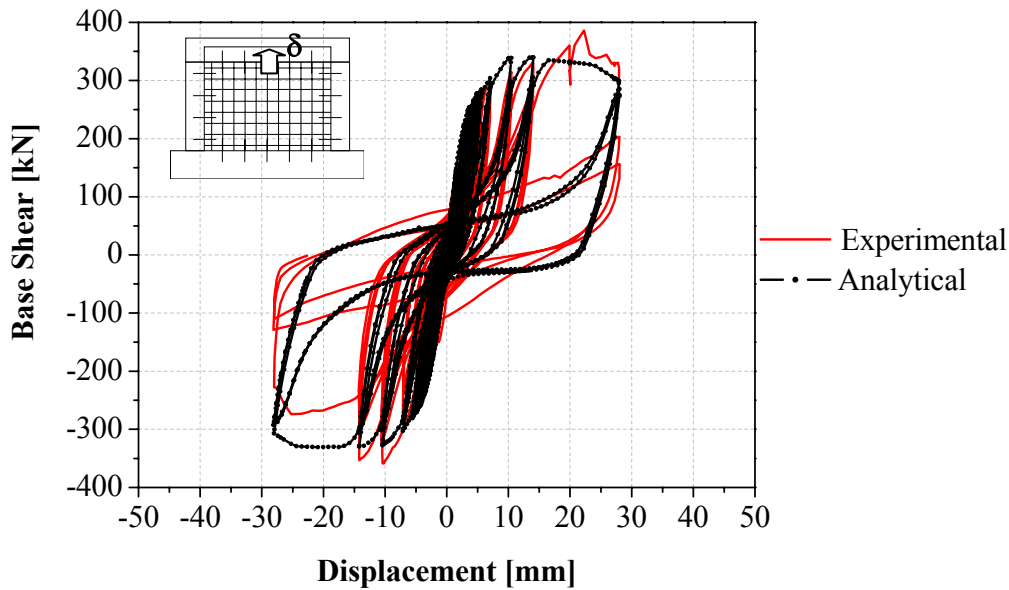


Figure 5.26: Comparison of the hysteretic curves of the experimental and analytical results of Specimen 6

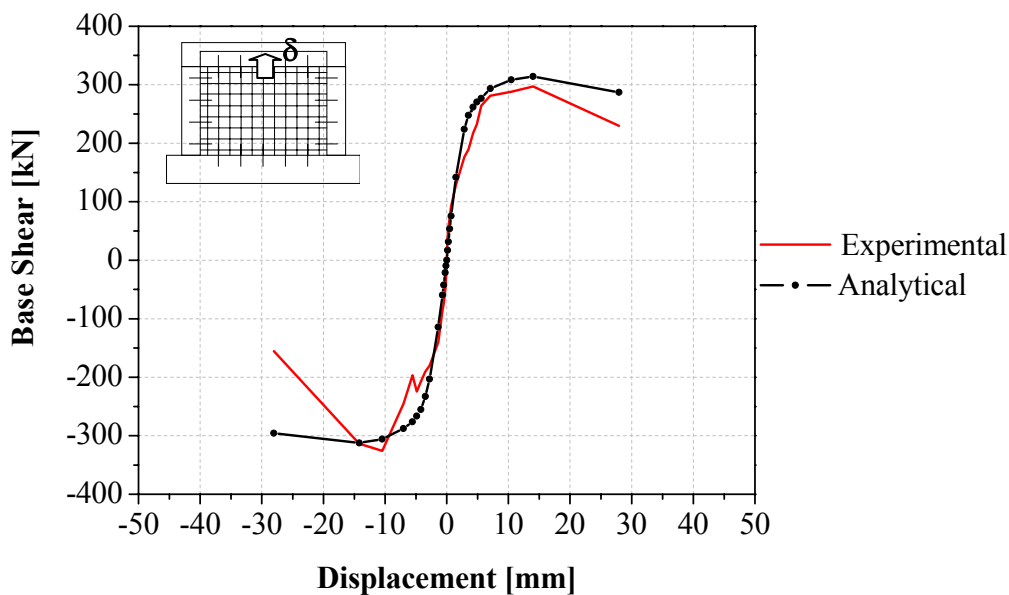


Figure 5.27: Comparison of the envelope curves of the experimental and analytical results of Specimen 6

As seen from Figure 5.26, analytical study captured strength values at the initial displacement cycles, maximum load occurred in the system and the descending branch slope of the analytical results quiet well.

Table 5.10 summarizes the damages states observed in the analytical study. It also gives the location of damage and which type of material is damaged with strain value at the damage. The bold lines in the table match with the experimental result. The

analytical results show almost the exact step and location of damage like it has been observed during the experiment.

Table 5.10: Damage levels for Specimen 6

Target Displacement [mm]	Performance Level	Element name	Place of damage	Damage type	Strain
At the end of 2nd cycle of +1.4	yield	19	Bottom end	Steel	0.002146
At the end of 3rd cycle of -1.4	yield	8	Bottom end	Steel	0.002124
At the end of 3rd cycle of +2.8	MNc	19	Bottom end	Unc Conc	-0.003520
At the end of 2nd cycle of +3.5	yield	26	Bottom end	Steel	0.002137
At the end of 2nd cycle of -3.5	MNc	1	Bottom end	Unc Conc	-0.003550
At the end of 3rd cycle of -3.5	yield	1	Bottom end	Steel	0.002123
At the end of 1st cycle of +4.2	MNs	19	Top end	Steel	0.010015
At the end of 1st cycle of +4.2	yield	26	Top end	Steel	0.002193
At the end of 1st cycle of -4.2	yield	9	Left end	Steel	0.002111
At the end of 1st cycle of -4.2	yield	9	Right end	Steel	0.002174
At the end of 2nd cycle of +4.2	MNc	26	Bottom end	Unc Conc	-0.003530
At the end of 3rd cycle of -4.2	MNs	14	Left end	Steel	0.010047
At the end of 1st cycle of -5.6	MNs	14	Right end	Steel	0.010047
At the end of 2nd cycle of +5.6	MNc	26	Top end	Unc Conc	-0.003600
At the end of 1st cycle of +7.0	yield	1	Top end	Steel	0.002264
At the end of 3rd cycle of -7.0	MNs	9	Left end	Steel	0.010232
At the end of 3rd cycle of -7.0	MNs	9	Right end	Steel	0.010072
At the end of 1st cycle of +10.5	MNc	1	Top end	Unc Conc	-0.003510
At the end of 1st cycle of -10.5	yield	16	Left end	Steel	0.002141
At the end of 1st cycle of -10.5	MNc	2	Bottom end	Unc Conc	-0.003580
At the end of 1st cycle of +14	GVc	26	Bottom end	Conf Conc	-0.008560
At the end of 1st cycle of +14	MNc	8	Bottom end	Unc Conc	-0.003560
At the end of 1st cycle of -14	yield	16	Right end	Steel	0.002286
At the end of 2nd cycle of +14	MNc	20	Top end	Unc Conc	-0.003670
At the end of 2nd cycle of +14	yield	20	Top end	Steel	0.002236
At the end of 3rd cycle of +14	GCc	26	Bottom end	Conf Conc	-0.011080
At the end of 3rd cycle of -14	MNc	9	Left end	Unc Conc	-0.003530
At the end of 3rd cycle of -14	MNc	9	Right end	Unc Conc	-0.003530
At the end of 1st cycle of +28	MNs	26	Bottom end	Steel	0.010484
At the end of 1st cycle of +28	MNs	1	Bottom end	Steel	0.010091
At the end of 1st cycle of +28	MNc	7	Top end	Unc Conc	-0.003510
At the end of 1st cycle of +28	MNs	1	Top end	Steel	0.010088
At the end of 1st cycle of +28	MNs	8	Bottom end	Steel	0.010336
At the end of 1st cycle of +28	MNs	8	Top end	Steel	0.010287
At the end of 1st cycle of +28	GVc	1	Bottom end	Conf Conc	-0.008690
At the end of 1st cycle of +28	MNc	7	Bottom end	Unc Conc	-0.003540
At the end of 1st cycle of -28	MNc	25	Bottom end	Unc Conc	-0.003520
At the end of 1st cycle of -28	yield	25	Bottom end	Steel	0.002188
At the end of 1st cycle of -28	GCc	1	Bottom end	Conf Conc	-0.011070
At the end of 1st cycle of -28	GVc	25	Bottom end	Conf Conc	-0.008950
At the end of 1st cycle of -28	GCc	25	Bottom end	Conf Conc	-0.011850
At the end of 1st cycle of -28	MNs	25	Bottom end	Steel	0.010252
At the end of 2nd cycle of +28	yield	7	Top end	Steel	0.002283
At the end of 2nd cycle of +28	MNs	7	Top end	Steel	0.010898
At the end of 3rd cycle of +28	GVc	1	Top end	Conf Conc	-0.008910
At the end of 3rd cycle of -28	MNc	25	Top end	Unc Conc	-0.003510

Figure 5.28 shows the damage states obtained at drift levels. For the pushing cycles, “yield” has occurred first at the top end of the left column at 0.10% drift levels. Unconfined concrete has reached “minimum damage limit” first at top end of the left columns at 0.20% drift level. Reinforcement has reached “minimum damage limit” first at the bottom end of the left column at 0.30% drift levels. Confined concrete has reached “safety and collapse limit” at the bottom end of the left column at 1.00% drift level. For the pulling cycles, at 0.10% drift level “yield” occurred. Unconfined concrete has reached “minimum damage limit” at the bottom end of the right column at 0.25% drift level. Reinforcement has reached “minimum damage limit” at the middle of the beam at 0.30% drift level. Confined concrete has reached “safety and collapse limit” at the bottom end of the left column and “collapse limit” at the bottom end of the right column at 2% drift level.

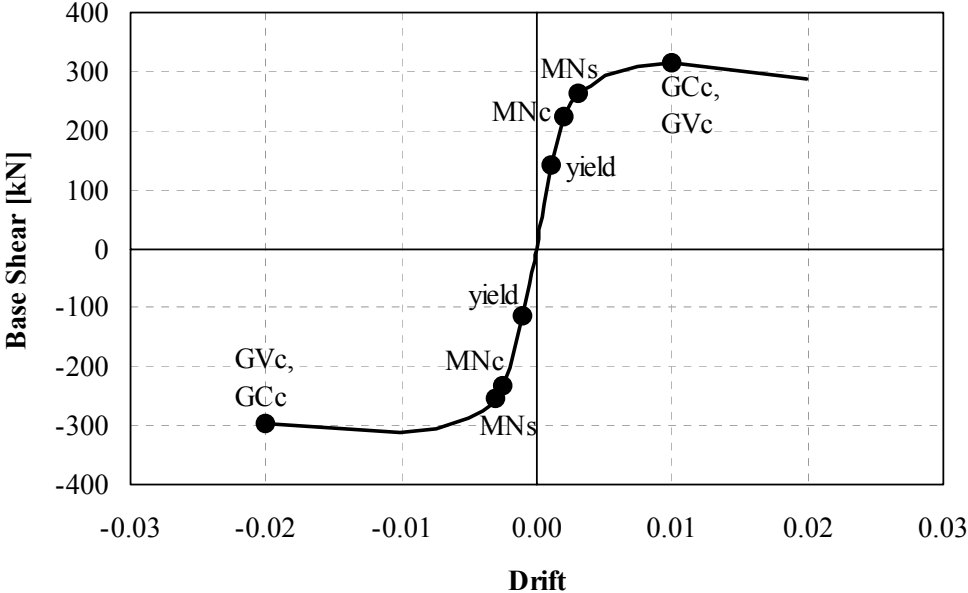


Figure 5.28: Damage states obtained at drift levels at certain drift levels at Specimen 6

Figure 5.29 shows the frame at the end of loading history. The “collapse limit” is reached at the bottom ends of the columns.

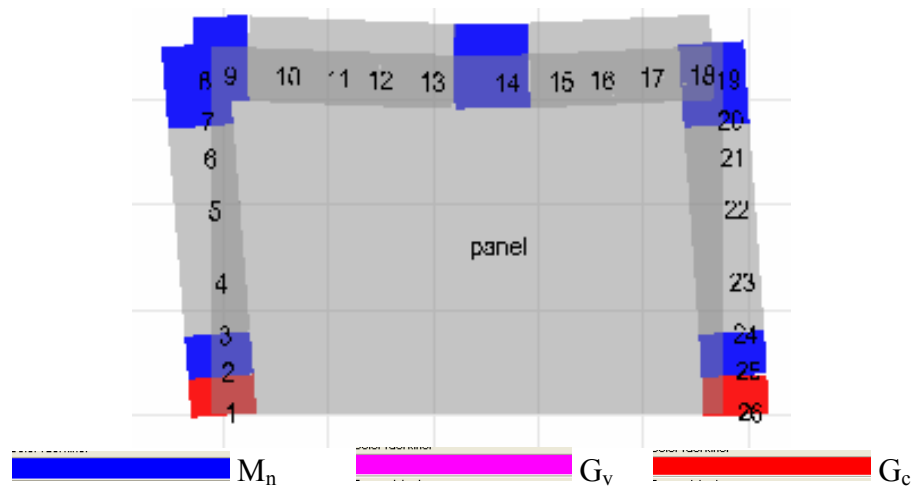


Figure 5.29: Damage occurred at the end of the analysis at Specimen 6

5.5.5 Specimen 7

The displacement history applied to Specimen 7 (partially infilled frame with pre-reverse deflection on the beam) in the experimental study is given in Figure 5.30. This loading protocol was applied to the analytical model as well.

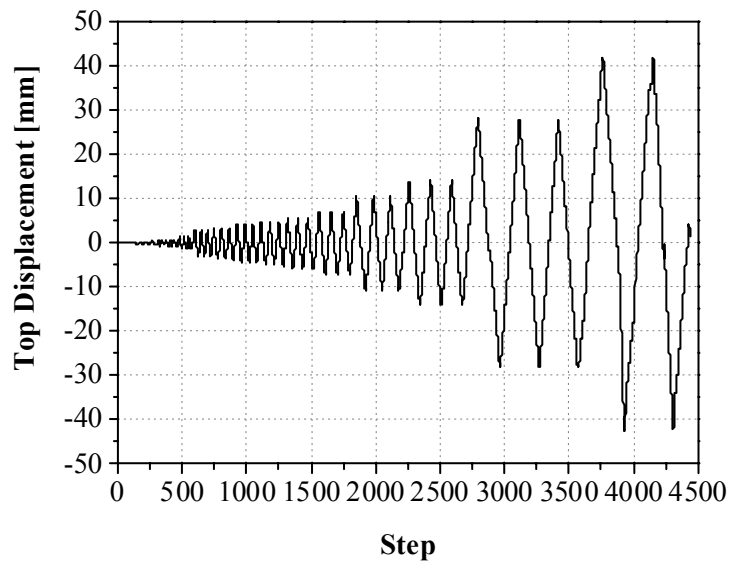


Figure 5.30: The displacement pattern applied to Specimen 7

The comparison of the experimental and analytical results for Specimen 7 is given as hysteretic loops in Figure 5.31 and as envelope curves in Figure 5.32.

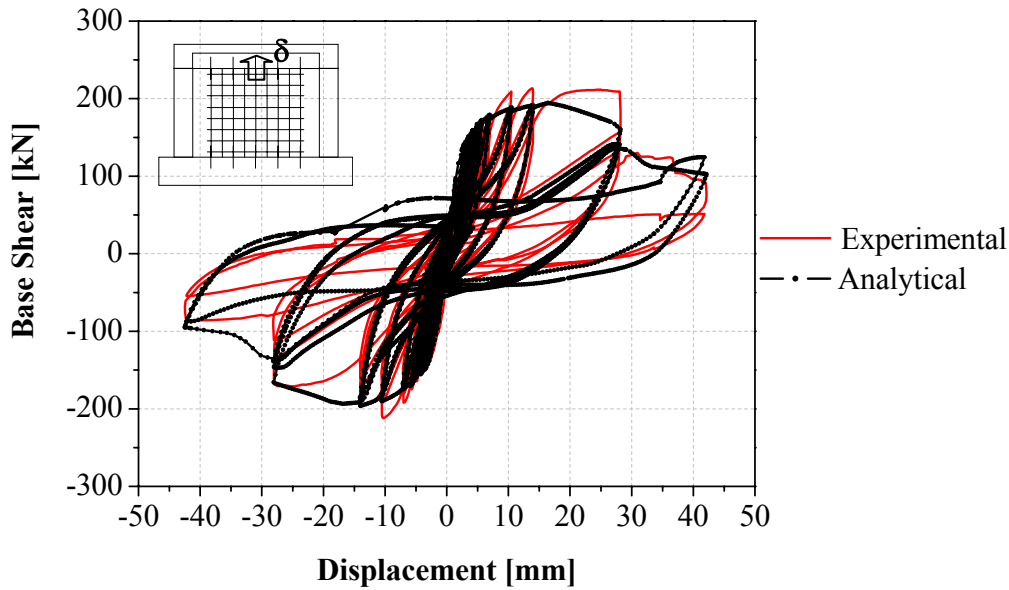


Figure 5.31: Comparison of the hysteretic curves of the experimental and analytical results of Specimen 7

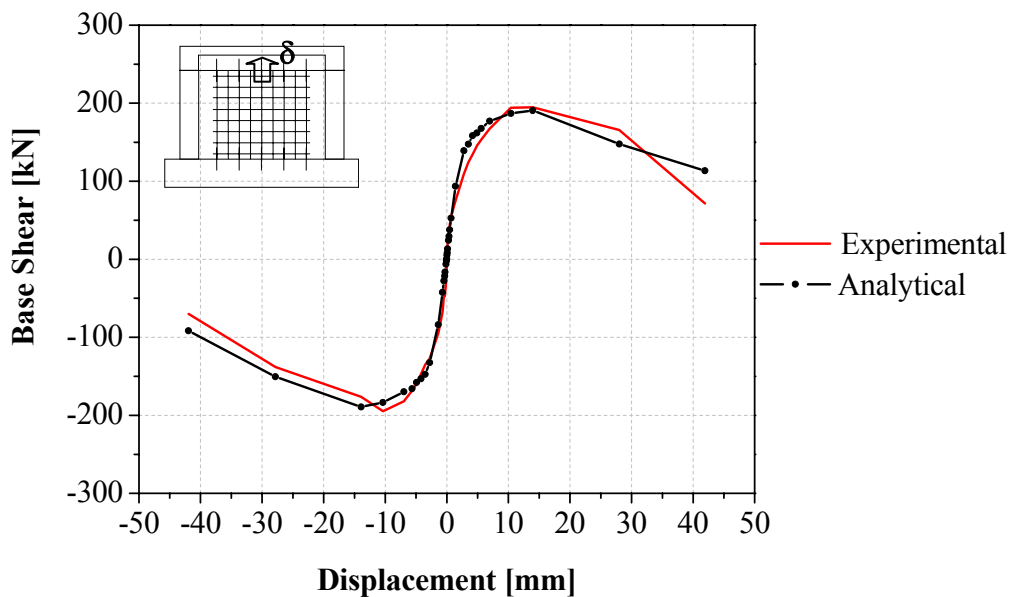


Figure 5.32: Comparison of the envelope curves of the experimental and analytical results of Specimen 7

As seen from Figure 5.31, analytical study captured strength values at the initial displacement cycles, maximum load occurred in the system and the descending branch slope of the analytical results quiet well.

Table 5.16 summarizes the damages states observed in the analytical work. It also gives the location of damage and which type of material is damaged with strain value of the damage. The bold lines in the table match with the experimental result. The analytical results show almost the exact step and position of damage like it has been observed during the experiment.

Table 5.11: Damage levels for Specimen 7

Target Displacement [mm]	Performance Level	Element name	Place of damage	Damage type	Strain
At the end of 1 st cycle of +2.8	yield	19	Bottom end	Steel	0.002136
At the end of 1 st cycle of -2.8	yield	8	Bottom end	Steel	0.002114
At the end of 2 nd cycle of +3.5	yield	26	Bottom end	Steel	0.002113
At the end of 3 rd cycle of -3.5	MNc	1	Bottom end	Unc Conc	-0.003570
At the end of 3 rd cycle of -3.5	yield	1	Bottom end	Steel	0.002359
At the end of 3 rd cycle of -3.5	MNc	8	Bottom end	Unc Conc	-0.003540
At the end of 1 st cycle of +4.2	MNc	26	Bottom end	Unc Conc	-0.003540
At the end of 1 st cycle of +4.2	yield	26	Top end	Steel	0.002115
At the end of 1 st cycle of -4.9	MNc	1	Top end	Unc Conc	-0.003600
At the end of 2 nd cycle of +4.9	MNc	19	Bottom end	Unc Conc	-0.003510
At the end of 1 st cycle of -5.6	yield	16	Right end	Steel	0.002154
At the end of 1 st cycle of -5.6	yield	16	Left end	Steel	0.002165
At the end of 1 st cycle of +7.0	MNs	19	Top end	Steel	0.010120
At the end of 1 st cycle of +7.0	MNc	26	Top end	Unc Conc	-0.003520
At the end of 2 nd cycle of +7.0	MNc	2	Bottom end	Unc Conc	-0.003540
At the end of 2 nd cycle of -7.0	MNc	2	Top end	Unc Conc	-0.003550
At the end of 3 rd cycle of +7.0	yield	1	Top end	Steel	0.002135
At the end of 3 rd cycle of +7.0	yield	11	Left end	Steel	0.002108
At the end of 3 rd cycle of +7.0	yield	11	Right end	Steel	0.002104
At the end of 3 rd cycle of -7.0	MNs	16	Left end	Steel	0.010023
At the end of 3 rd cycle of -7.0	MNs	16	Right end	Steel	0.010015
At the end of 1 st cycle of -10.5	yield	17	Left end	Steel	0.002222
At the end of 1 st cycle of -10.5	yield	17	Right end	Steel	0.002111
At the end of 1 st cycle of -10.5	MNs	8	Top end	Steel	0.010023
At the end of 3 rd cycle of -10.5	GVc	26	Bottom end	Conf Conc	-0.008690
At the end of 1 st cycle of -14.0	yield	18	Right end	Steel	0.002148
At the end of 1 st cycle of -14.0	yield	18	Left end	Steel	0.002188
At the end of 1 st cycle of -14.0	GVc	1	Bottom end	Conf Conc	-0.008800
At the end of 1 st cycle of -14.0	MNc	25	Bottom end	Unc Conc	-0.003530
At the end of 1 st cycle of -14.0	yield	25	Bottom end	Steel	0.002133
At the end of 2nd cycle of +14.0	GCc	26	Bottom end	Conf Conc	-0.011170
At the end of 3 rd cycle of +14.0	MNs	26	Bottom end	Steel	0.010239
At the end of 3rd cycle of -14.0	GCc	1	Bottom end	Conf Conc	-0.011030
At the end of 3 rd cycle of -14.0	yield	25	Bottom end	Steel	0.002105
At the end of 1 st cycle of +28.0	yield	10	Right end	Steel	0.002127
At the end of 1 st cycle of +28.0	yield	10	Left end	Steel	0.002135
At the end of 1 st cycle of +28.0	MNc	20	Top end	Unc Conc	-0.003530
At the end of 1 st cycle of +28.0	yield	2	Bottom end	Steel	0.002114
At the end of 1 st cycle of +28.0	MNs	1	Top end	Steel	0.010109
At the end of 1 st cycle of +28.0	MNs	1	Bottom end	Steel	0.010389
At the end of 1 st cycle of +28.0	yield	7	Top end	Steel	0.002125
At the end of 1 st cycle of +28.0	MNc	7	Top end	Unc Conc	-0.003540
At the end of 1 st cycle of -28.0	MNc	25	Top end	Unc Conc	-0.003520
At the end of 1 st cycle of -28.0	MNs	26	Top end	Steel	0.010168
At the end of 2 nd cycle of -28.0	MNc	3	Bottom end	Unc Conc	-0.003520
At the end of 2 nd cycle of -28.0	MNs	17	Right end	Steel	0.010034
At the end of 2 nd cycle of -28.0	MNs	17	Left end	Steel	0.010000
At the end of 3 rd cycle of +28.0	yield	2	Top end	Steel	0.002135
At the end of 3 rd cycle of +28.0	MNs	7	Top end	Steel	0.010071
At the end of 1 st cycle of +42.0	yield	7	Bottom end	Steel	0.002155
At the end of 1 st cycle of -42.0	GVs	8	Top end	Steel	0.040107

Table 5.11: Damage levels for Specimen 7 (contd.)

Target Displacement [mm]	Performance Level	Element name	Place of damage	Damage type	Strain
At the end of 1st cycle of -42.0	GVC	26	Top end	Conf Conc	-0.008570
At the end of 2nd cycle of +42.0	GVs	26	Bottom end	Steel	0.040135
At the end of 2nd cycle of -42.0	MNs	18	Right end	Steel	0.010168

Figure 5.33 shows the damage states obtained at drift levels. For the pushing cycles, “yield” has occurred first at the top end of the left column at 0.20% drift levels. Unconfined concrete has reached “minimum damage limit” first at bottom end of the left columns at 0.35% drift level. Reinforcement has reached “minimum damage limit” first at the top end of the left column at 0.50% drift levels. Confined concrete has reached “collapse limit” at the bottom end of the left column at 1.00% drift level. Reinforcement has reached “safety limit” at the top end of the right column at 3.00% drift level. For the pulling cycles, at 0.25% drift level “yield” occurred. Unconfined concrete has reached “minimum damage limit” at the bottom end of the right column at 0.30% drift level. Reinforcement has reached “minimum damage limit” at the end of the beam at 0.50% drift level. Confined concrete has reached “safety limit” at the bottom end of the left column at 0.75% drift level. Confined concrete has reached “collapse limit” at the bottom end of the right column at 1.00% drift level. Reinforcement has reached “safety limit” at the top end of the right column at 3.00% drift level.

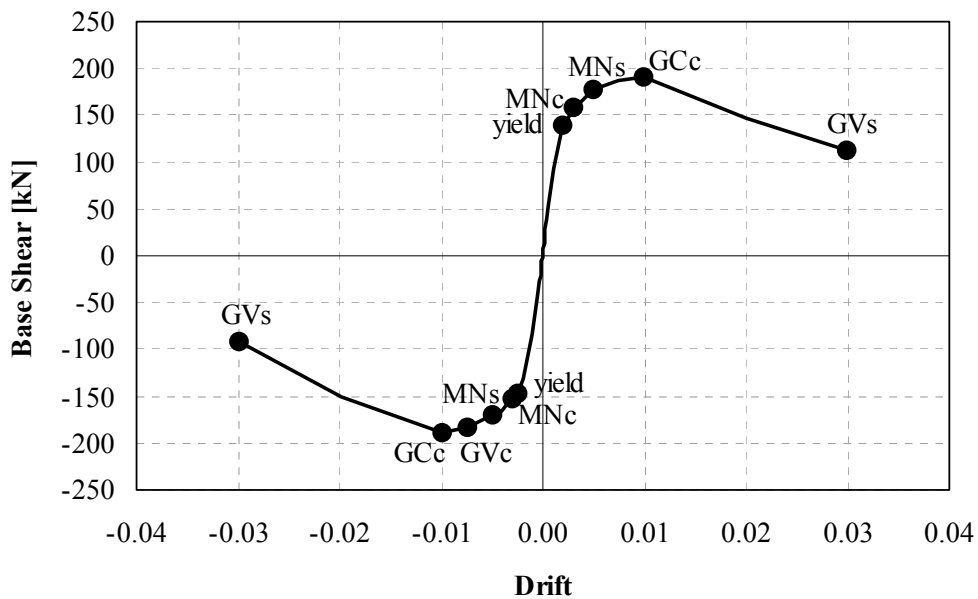
**Figure 5.33:** Damage states obtained at drift levels at certain drift levels at Specimen 7

Figure 5.34 shows the frame at the end of loading history. The “collapse limit” and the “safety limit” are reached at the bottom ends of the columns and the upper end of the column where the lateral load is applied.

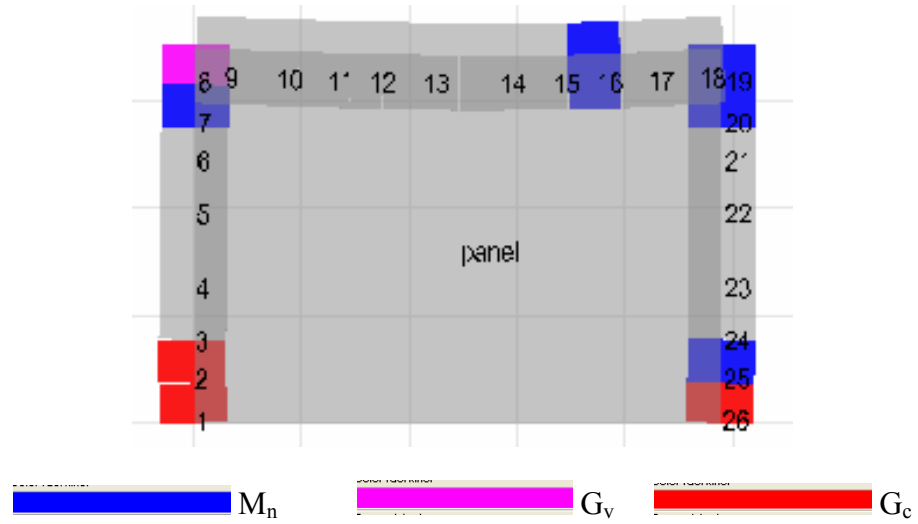


Figure 5.34: Damage occurred at the end of the analysis at Specimen 7

6. PARAMETRIC STUDIES

In this chapter, the model produced for analysing the specimens in experimental study is used to understand the effect of the change in panel thickness, the effect of the concrete compressive strength of the panel and the gap between the panel and the frame on the overall behaviour of the system.

6.1 The Effect of Panel Thickness

The panel thickness is changed proportional to the column width as shown in Table 6.1, the bold line corresponds to the thickness of the specimen in the experimental study. By using the models produced for Specimen 3 (fully infilled frame) and Specimen 5 (partially infilled frame), the effect of change in the panel thickness is studied.

Table 6.1: The change in the thickness of the panel

Case	Column width [cm]	Thickness of the panel [cm]	Thickness proportion
1	20	5	0.25
2	20	10	0.50
3	20	15	0.75
4	20	20	1.00

Figure 6.1 shows the change in the lateral load carrying capacity of Specimen 3 according to the thickness change in the panel. The envelope curves of base shear versus displacement relations are only given for the pushing cycles in Figure 6.2. The points on the envelope curves are calculated as the average of the three cycles at each target displacement levels.

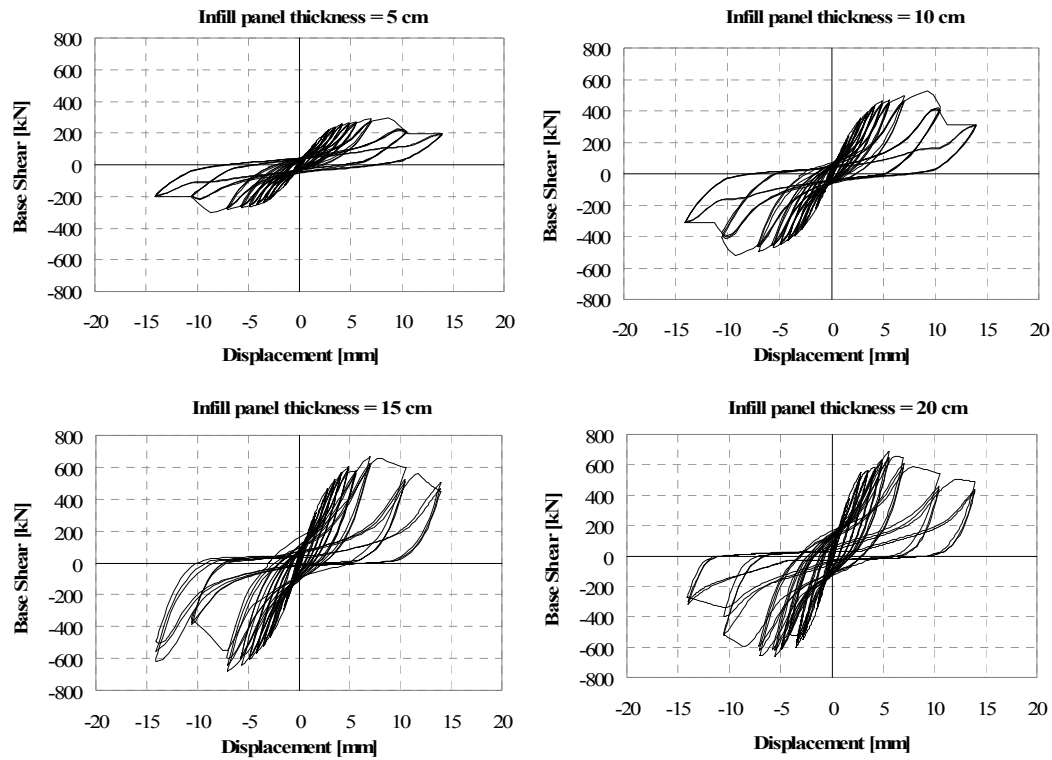


Figure 6.1: Base shear-top displacement curves for the infill panel thickness changes in Specimen 3

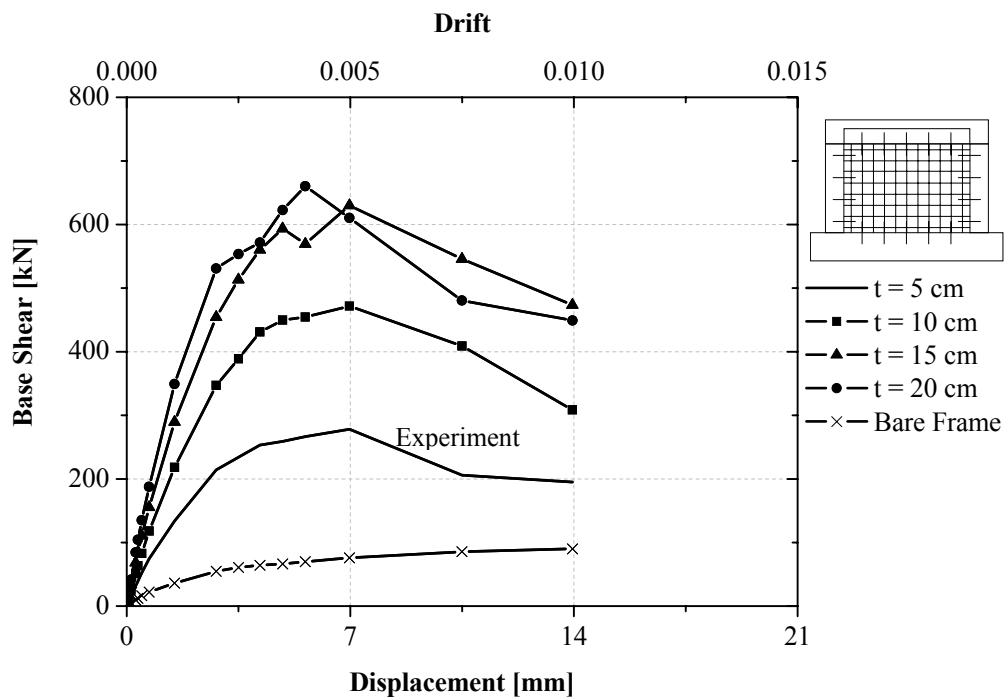


Figure 6.2: Envelope curves for the thickness changes in Specimen 3

The lateral load carrying capacity of the frame increases as the thickness of the shotcrete panel increases. This behaviour is valid until the thickness is 15 cm. The

frames having 15 cm and 20 cm (which is the width of the column) thick panels seem to have almost the same lateral load resistance.

The lateral load carrying capacity of the frames;

- When $t=10$ cm, it is 4.8 times more at 7 mm (0.5% story drift), it is 3.4 times more at 14 mm (1% story drift),
- When $t=15$ cm, it is 6.4 times more at 7 mm (0.5% story drift), it is 5.3 times more at 14 mm (1% story drift),
- When $t=20$ cm, it is 5.6 times more at 7 mm (0.5% story drift), it is 5.0 times more at 14 mm (1% story drift)

compared with the bare frame's.

Initial stiffness changes depending on the thickness change is given in Figure 6.3.

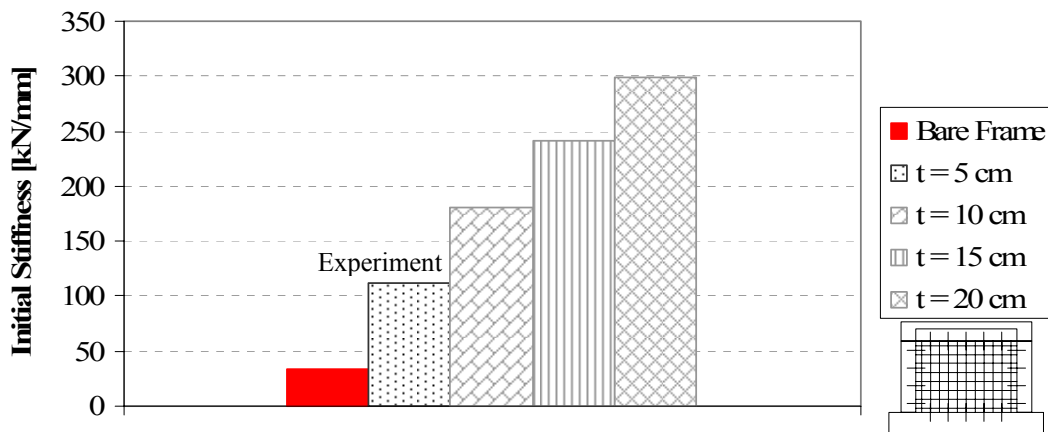


Figure 6.3: Initial stiffness of Specimen 3 for the change in panel thickness

Energy dissipation capacities depending on the thickness change in panel are given in Figure 6.4.

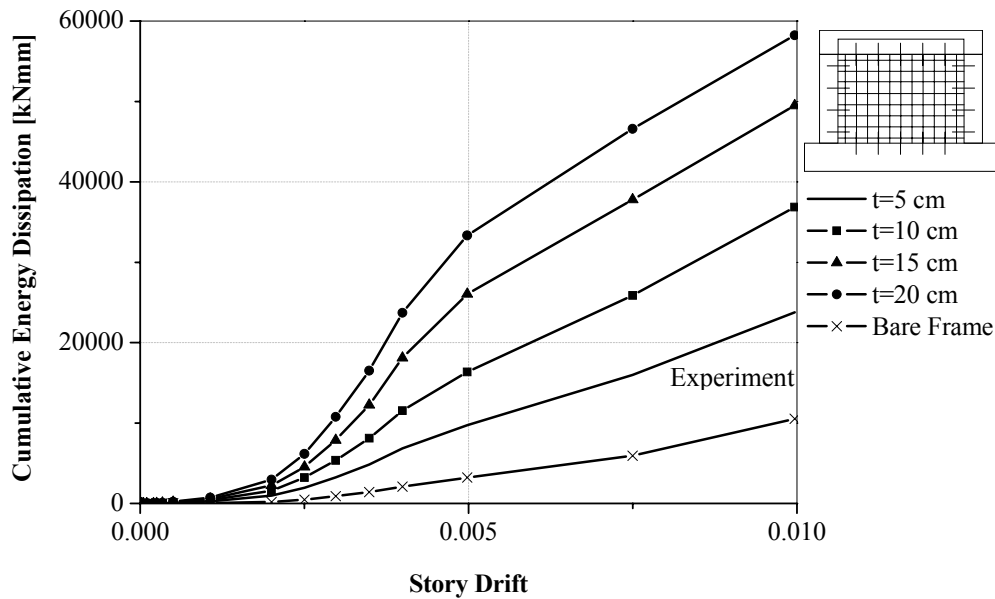


Figure 6.4: The comparison of cumulative energy dissipation capacities of Specimen 3 for the change in panel thickness

The dissipated energy of the specimens;

- When $t=10$ cm, it is 5.0 times more at 7 mm (0.5% story drift), it is 3.5 times more at 14 mm (1% story drift),
- When $t=15$ cm, it is 8.0 times more at 7 mm (0.5% story drift), it is 4.7 times more at 14 mm (1% story drift),
- When $t=20$ cm, it is 10.4 times more at 7 mm (0.5% story drift), it is 5.5 times more at 14 mm (1% story drift),

compared with the bare frame's.

As can be seen in Figure 6.1, the system behaviour of the frames with 15 and 20 cm thick panels are almost the same. It is predicted that this behaviour is due to the high difference between the concrete compressive strengths of the frame and the shotcrete panel. For investigating the correctness of this prediction, Specimen 3 is studied analytically for the case where the concrete compressive strengths of both frame and panel are identical. The concrete compressive strengths are taken as 25 MPa and the hysteretic and envelope curves of base shear versus top displacement obtained for this case are shown in Figure 6.5 and 6.6, respectively. As can be seen in these figures, the general response obtained is different for 15 and 20 cm thick panel cases which prove the prediction.

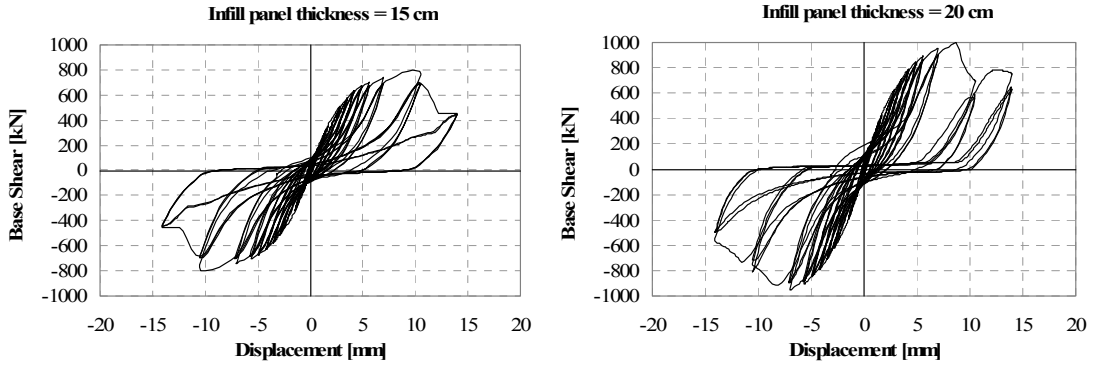


Figure 6.5: Base shear-top displacement curves for the infill panel thickness changes in Specimen 3

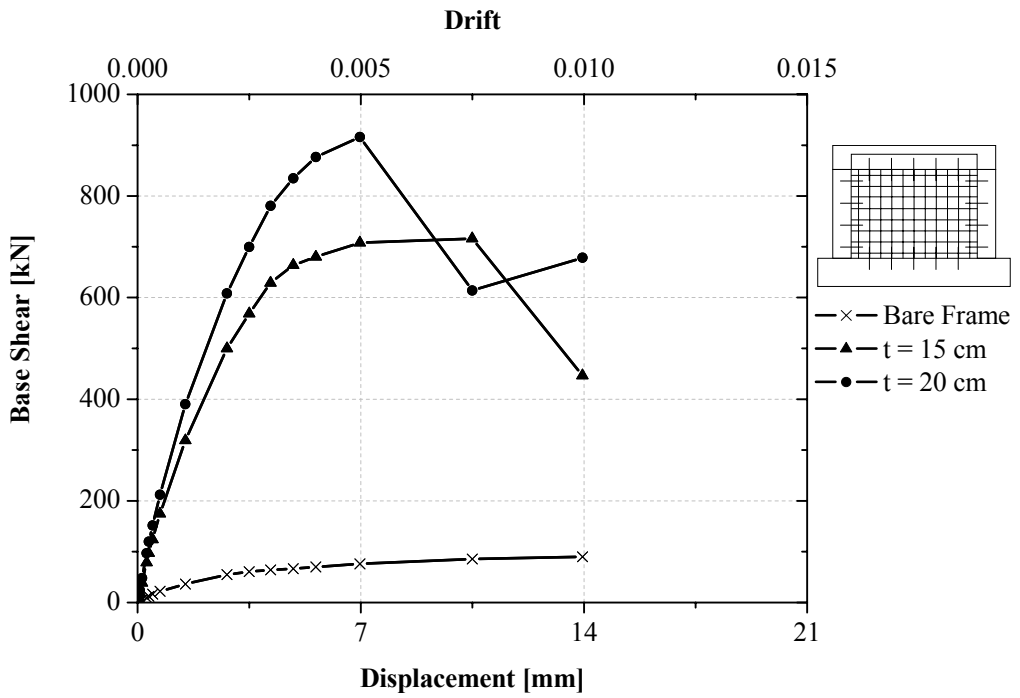


Figure 6.6: Envelope curves for the thickness changes in Specimen 3

Figure 6.7 shows the change in the lateral load carrying capacity of Specimen 5 according to the thickness change in the panel. The envelope curves are given in Figure 6.8 for the pushing cycles.

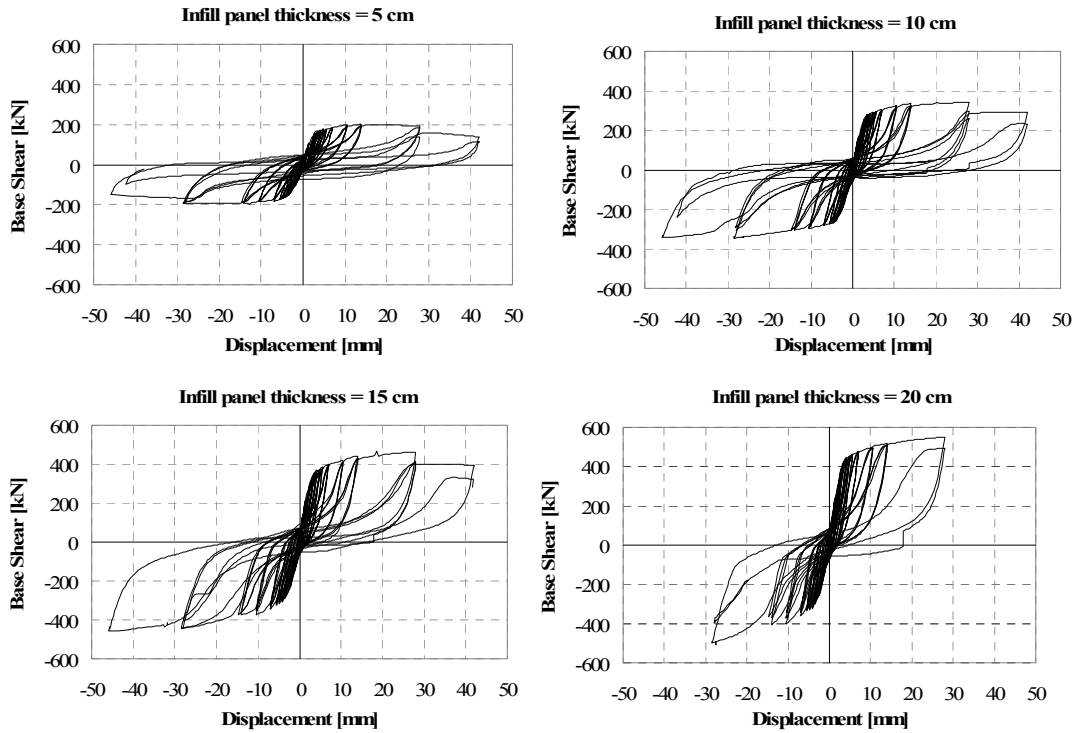


Figure 6.7: Base shear-top displacement curves for the infill panel thickness changes in Specimen 5

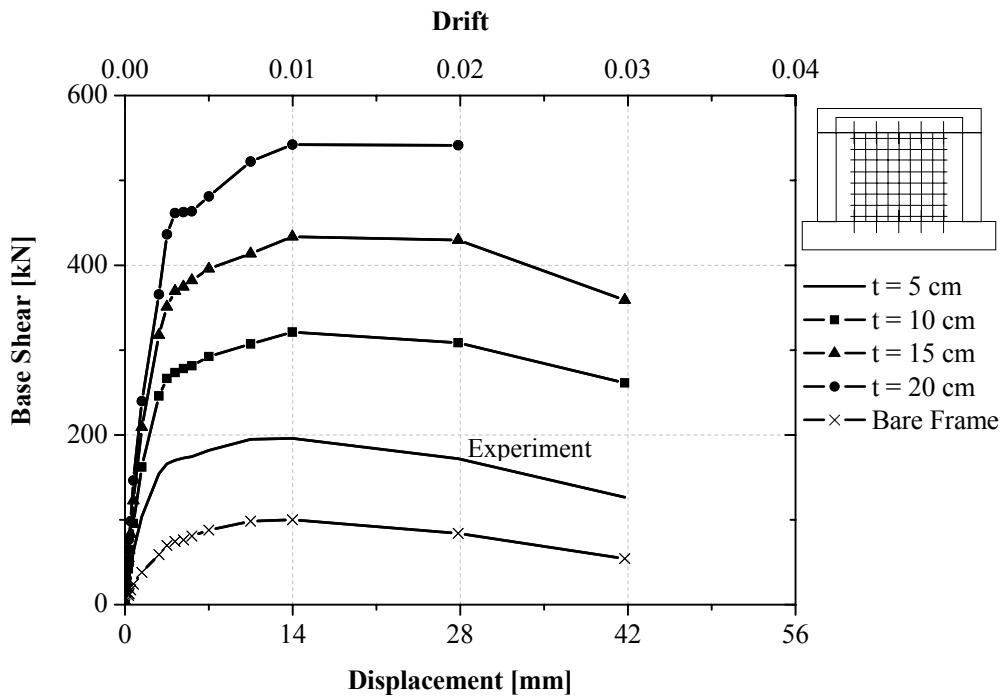


Figure 6.8: Envelope curves for the thickness changes in Specimen 5

The lateral load carrying capacity increased by 1.6 times more for 10 cm-thick panel, 2.2 times more for 15 cm-thick panel and 2.8 times more for 20 cm-thick panel at 14 mm (0.01 story drift); 1.8 times more for 10 cm-thick panel, 2.5 times for 15 cm-

thick panel and 3.2 times more for 20 cm-thick panel at 28 mm (0.02 story drift); 2.0 times for 10 cm-thick panel and 2.8 times for 15 cm-thick panel at 42 mm (0.03 story drift) compared to the specimen in the experiment with 5 cm-thick panel..

The lateral load carrying capacity of the frames;

- When $t=10$ cm, it is 3.3 times more at 7 mm (0.5% story drift), it is 3.2 times more at 14 mm (1% story drift), it is 3.7 times more at 28 mm (2% story drift), it is 4.8 times more at 42 mm (3% story drift),
- When $t=15$ cm, it is 4.5 times more at 7 mm (0.5% story drift), it is 4.3 times more at 14 mm (1% story drift), it is 5.1 times more at 28 mm (2% story drift), it is 6.6 times more at 42 mm (3% story drift),
- When $t=20$ cm, it is 5.5 times more at 7 mm (0.5% story drift), it is 5.4 times more at 14 mm (1% story drift), it is 6.4 times more at 28 mm (2% story drift),

compared with the bare frame's.

Initial stiffness changes depending on the thickness change are given in Figure 6.9.

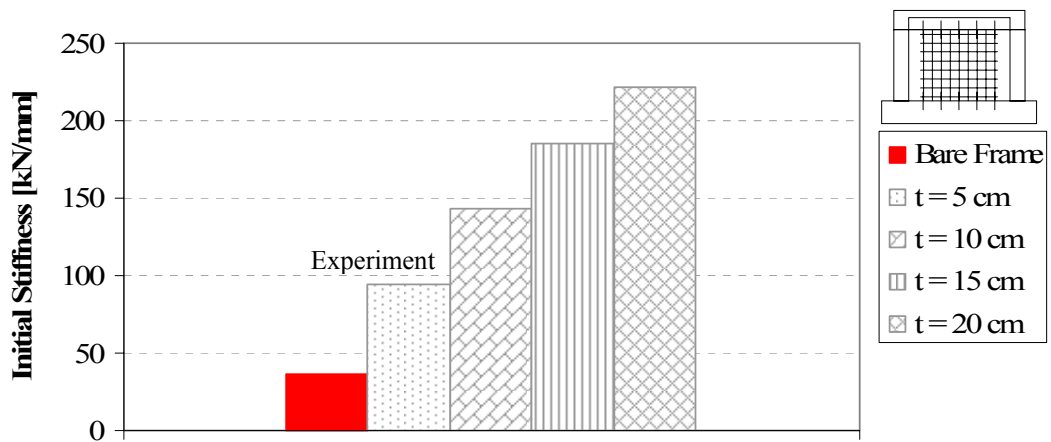


Figure 6.9: Initial stiffness of Specimen 5 for the change in panel thickness

The initial lateral stiffness of the frames;

- increased by 3.9 times for $t=10$ cm,
- increased by 5.0 times for $t=15$ cm,
- increased by 6.0 times for $t=20$ cm,

compared with the bare frame's.

Energy dissipation capacities depending on the thickness change in panel are given in Figure 6.10.

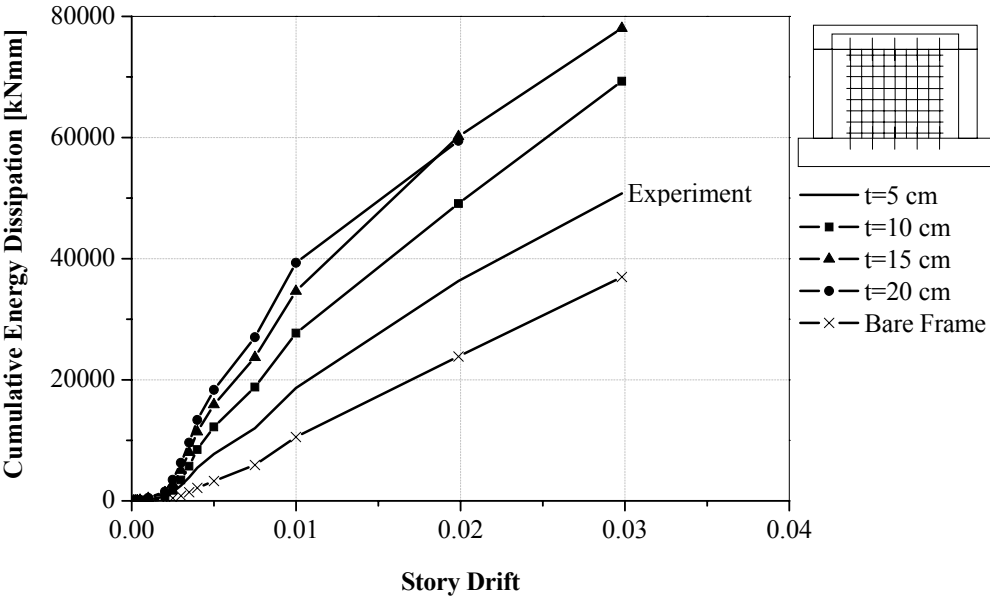


Figure 6.10: The comparison of cumulative energy dissipation capacities of Specimen 5 for the change in panel thickness

The energy dissipation of the specimens with 10 cm-thick panel and 15 cm-thick panel compared to the test specimen (5cm-thick panel) are 1.6 and 2.0 times more at 0.005 story drift, 1.5 and 1.9 times more at 0.01 story drift, 1.4 and 1.7 times more at 0.02 story drift, 1.4 and 1.5 times more at 0.03 story drift respectively as shown in Figure 6.8. The 15 cm-thick and 20 cm-thick panels have almost the same energy dissipation capacity. Since the analysis for 20 cm-thick panel did not converge until the end of the load pattern; it seems that they have the same energy dissipation capacity at 0.02 story drift. But 20 cm-thick panel has only done two cycles of 28 mm target displacement. So actually the 15 cm-thick and 20 cm-thick panels don't have the same energy dissipation at 0.01 story drift.

The energy dissipation of the specimens;

- When t=10 cm, it is 3.7 times more at 7 mm (0.5% story drift), it is 2.6 times more at 14 mm (1% story drift), it is 2.0 times more at 28 mm (2% story drift), it is 1.9 times more at 42 mm (3% story drift),
- When t=15 cm, it is 4.8 times more at 7 mm (0.5% story drift), it is 3.3 times more at 14 mm (1% story drift), it is 2.5 times more at 28 mm (2% story drift), it is 2.0 times more at 42 mm (3% story drift),

- When $t=20$ cm, it is 5.6 times more at 7 mm (0.5% story drift), it is 3.7 times more at 14 mm (1% story drift), it is 2.5 times more at 28 mm (2% story drift),

compared with the bare frame's.

6.2 The Effect of the Distance between the Panel and the Frame

The gap, a , is changed proportional to the distance between the inside face of the columns, L , as shown in Figure 6.11. The calculated gap size according to the proportional ratio, a/L , and panel widths are given in Table 6.2 to be used in the models produced for Specimen 5. The bold line in the table shows the thickness of the specimen used in the experimental study.

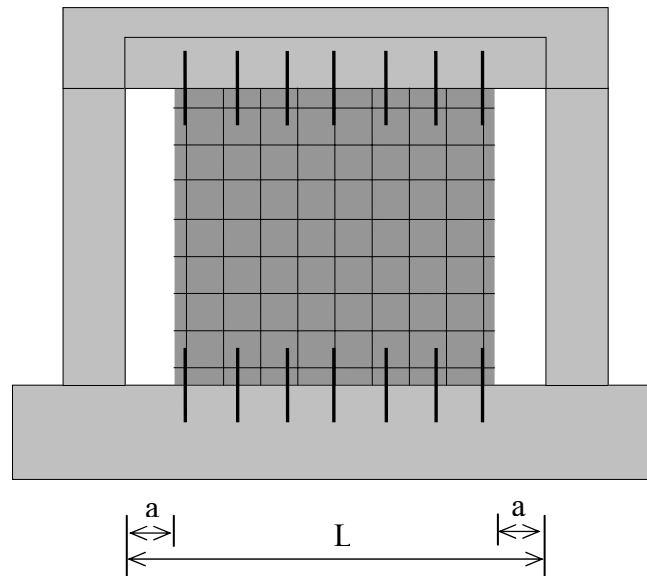


Figure 6.11: The gap, a , and the distance between the inside face of the columns, L , in the model used

Table 6.2: The change in the distance between the column and the panel

Case	L, Frame width [cm]	a; Gap between panel and column [cm]	a/L	Panel width
1	170	1.7	0.01	166.6
2	170	8.5	0.05	153.0
3	170	17.0	0.10	136.0
4	170	20.0	0.12	130.0
5	170	25.5	0.15	119.0
6	170	34.0	0.20	102.0

Figure 6.12 shows the change in the lateral load carrying capacity of Specimen 5 according to the distance change between the column and the panel. The envelope curves are given in Figure 6.13 for the pushing cycles.

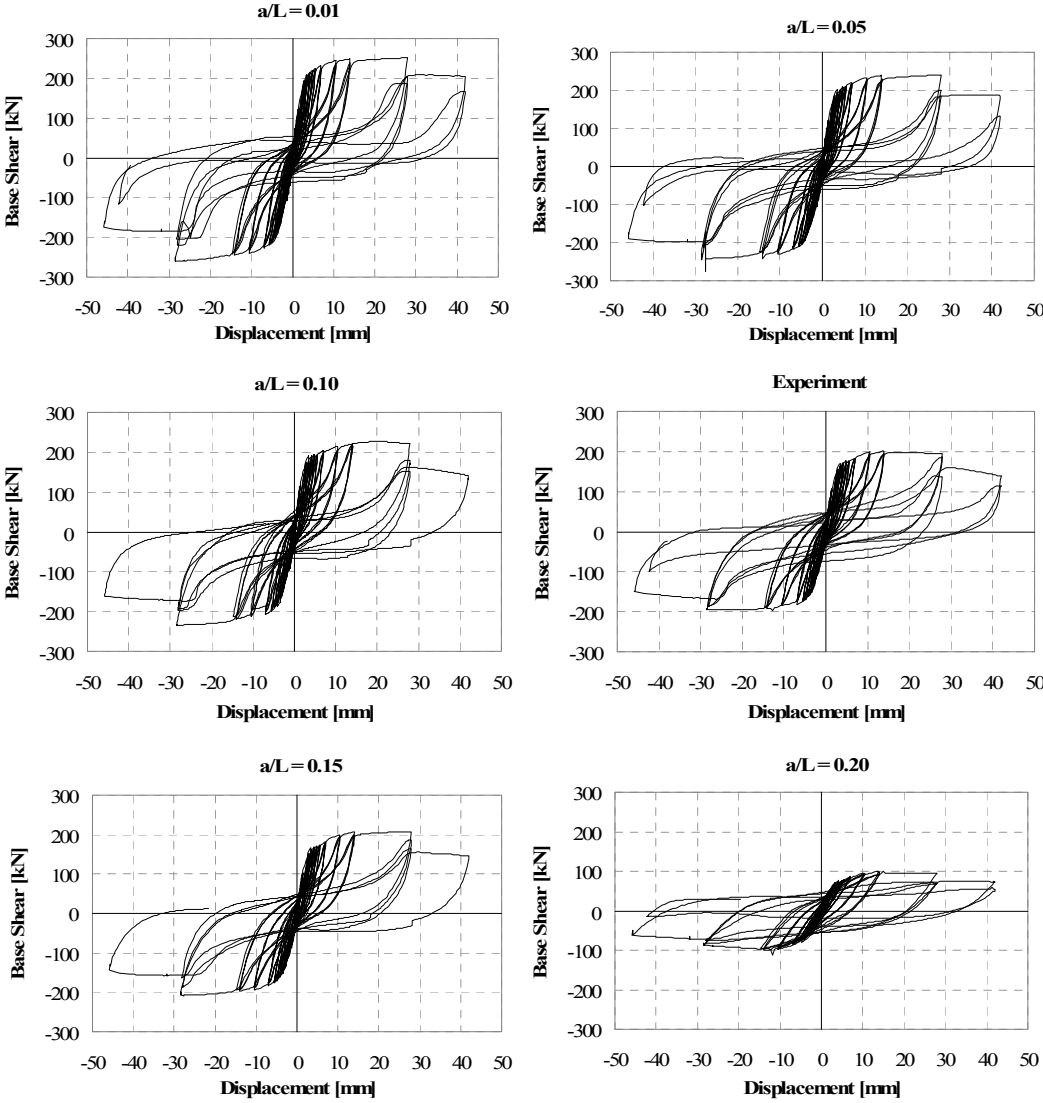


Figure 6.12: Base shear-top displacement curves for the gap size changes in Specimen 5

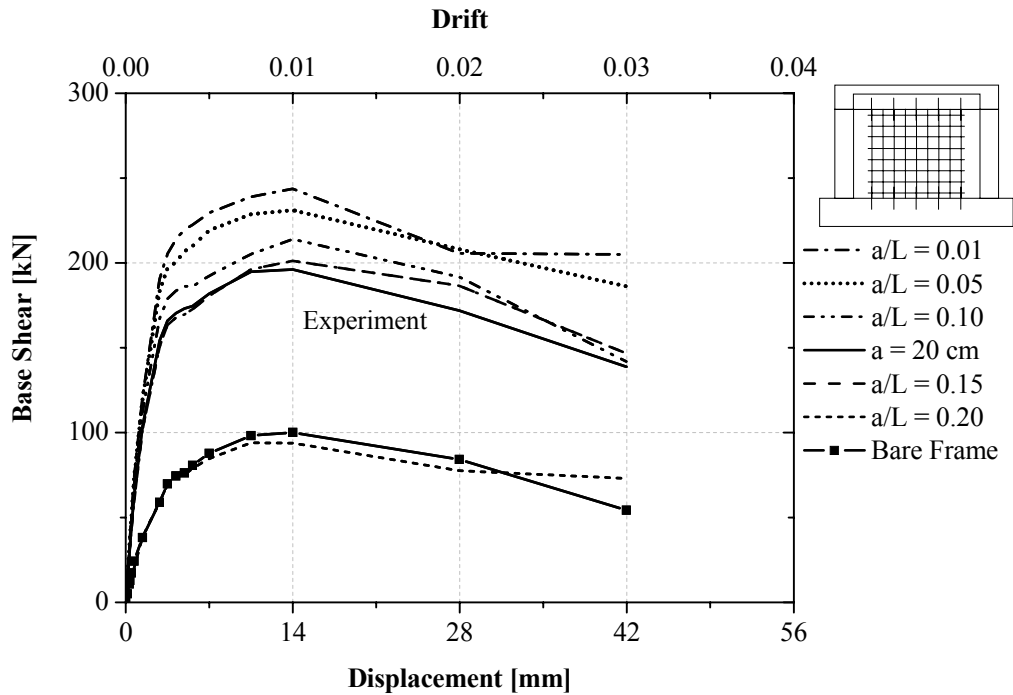


Figure 6.13: Envelope curves for the gap size changes in Specimen 5

The analytical study shows that when a/L ratio changes from 1% to 15%, the lateral load carrying capacity of the system is almost the same. While a/L ratio is 20% or more, the panel does not have any effect on the lateral load carrying capacity and the frame acts like a bare frame.

The lateral load carrying capacity of the system;

- When $a/L=0.01$, it is 2.6 times more at 7 mm (0.5% story drift), it is 2.4 times more at 14 mm (1% story drift), it is 2.4 times more at 28 mm (2% story drift), it is 3.8 times more at 42 mm (3% story drift),
- When $a/L=0.05$, it is 2.5 times more at 7 mm (0.5% story drift), it is 2.3 times more at 14 mm (1% story drift), it is 2.5 times more at 28 mm (2% story drift), it is 3.4 times more at 42 mm (3% story drift),
- When $a/L=0.10$, it is 2.2 times more at 7 mm (0.5% story drift), it is 2.0 times more at 14 mm (1% story drift), it is 2.3 times more at 28 mm (2% story drift), it is 2.6 times more at 42 mm (3% story drift),
- When $a/L=0.15$, it is 2.0 times more at 7 mm (0.5% story drift), it is 2.0 times more at 14 mm (1% story drift), it is 2.2 times more at 28 mm (2% story drift), it is 2.7 times more at 42 mm (3% story drift),

- When $a/L=0.20$, it is 0.96 times less at 7 mm (0.5% story drift), it is 0.94 times less at 14 mm (1% story drift), it is 0.92 times less at 28 mm (2% story drift), it is 1.3 times more at 42 mm (3% story drift),

compared with the bare frame's.

The initial lateral stiffness of the frames;

- increased by 2.9 times for $a=1.7$ cm,
- increased by 2.9 times for $a=8.5$ cm,
- increased by 2.8 times for $a=17$ cm,
- increased by 2.5 times for $a=25.5$ cm
- no increase for $a=34$ cm

compared with the bare frame's.

Energy dissipation capacities depending on the distance change between the panel and the frame are given in Figure 6.12.

When a/L ratio varies between 1% to 15%, the energy dissipation of the specimen is almost the same at all story drift levels. When a/L is 20%, the energy dissipation capacity is 33%, 33%, 43% times less than the energy dissipation capacity of the test specimen at 0.01, 0.02 and 0.03 story drift levels, respectively as shown in Figure 6.14.

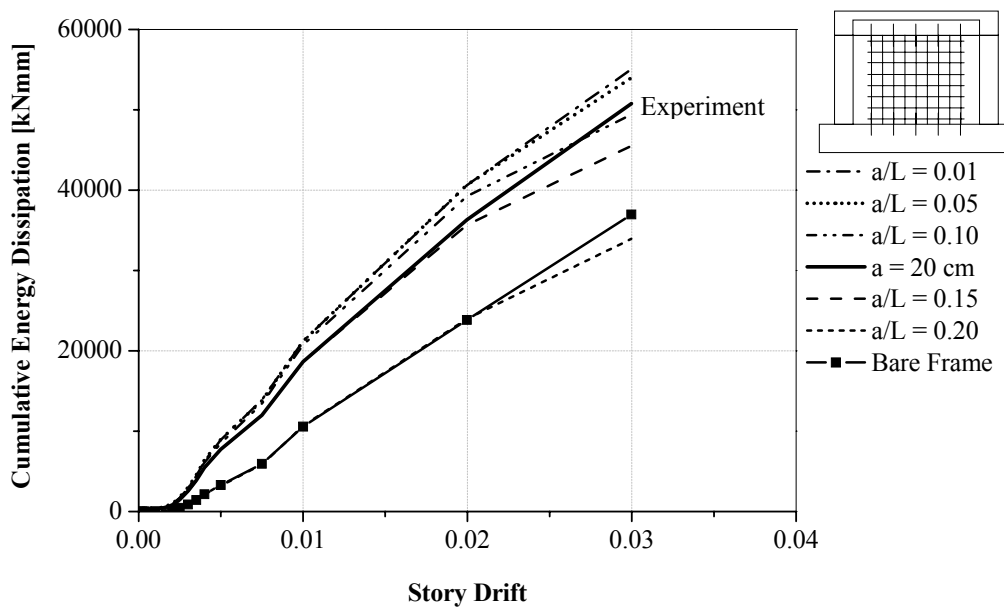


Figure 6.14: The comparison of cumulative energy dissipation capacities of Specimen 5 for the gap size changes

The energy dissipation of the specimens;

- When $a/L=0.01$, it is 2.7 times more at 7 mm (0.5% story drift), it is 2.0 times more at 14 mm (1% story drift), it is 1.7 times more at 28 mm (2% story drift), it is 1.5 times more at 42 mm (3% story drift),
- When $a/L=0.05$, it is 2.7 times more at 7 mm (0.5% story drift), it is 2.0 times more at 14 mm (1% story drift), it is 1.7 times more at 28 mm (2% story drift), it is 1.5 times more at 42 mm (3% story drift),
- When $a/L=0.10$, it is 2.6 times more at 7 mm (0.5% story drift), it is 2.0 times more at 14 mm (1% story drift), it is 1.6 times more at 28 mm (2% story drift), it is 1.3 times more at 42 mm (3% story drift),
- When $a/L=0.15$, it is 2.3 times more at 7 mm (0.5% story drift), it is 1.8 times more at 14 mm (1% story drift), it is 1.5 times more at 28 mm (2% story drift), it is 1.2 times more at 42 mm (3% story drift),
- When $a/L=0.20$, it is 0.98 times less at 7 mm (0.5% story drift), it is 1.0 times less at 14 mm (1% story drift), it is 1.0 times less at 28 mm (2% story drift), it is 0.92 times less at 42 mm (3% story drift),

compared with the bare frame's.

6.3 Panel Concrete Compressive Strengths

To investigate how the panel concrete compressive strength effects the general response of the system, an analytical study was carried on Specimen 3. The concrete compressive strength of the panel was 22 MPa for the experiment. In the analytical work, it is taken as 30 MPa and 40 MPa and the results are compared as hysteretic loops, envelope curves and initial stiffness.

Figure 6.15 shows the change in the lateral load carrying capacity of Specimen 3 according to the concrete compressive strengths change in the panel. The envelope curves are given in Figure 6.16 for the pushing cycles.

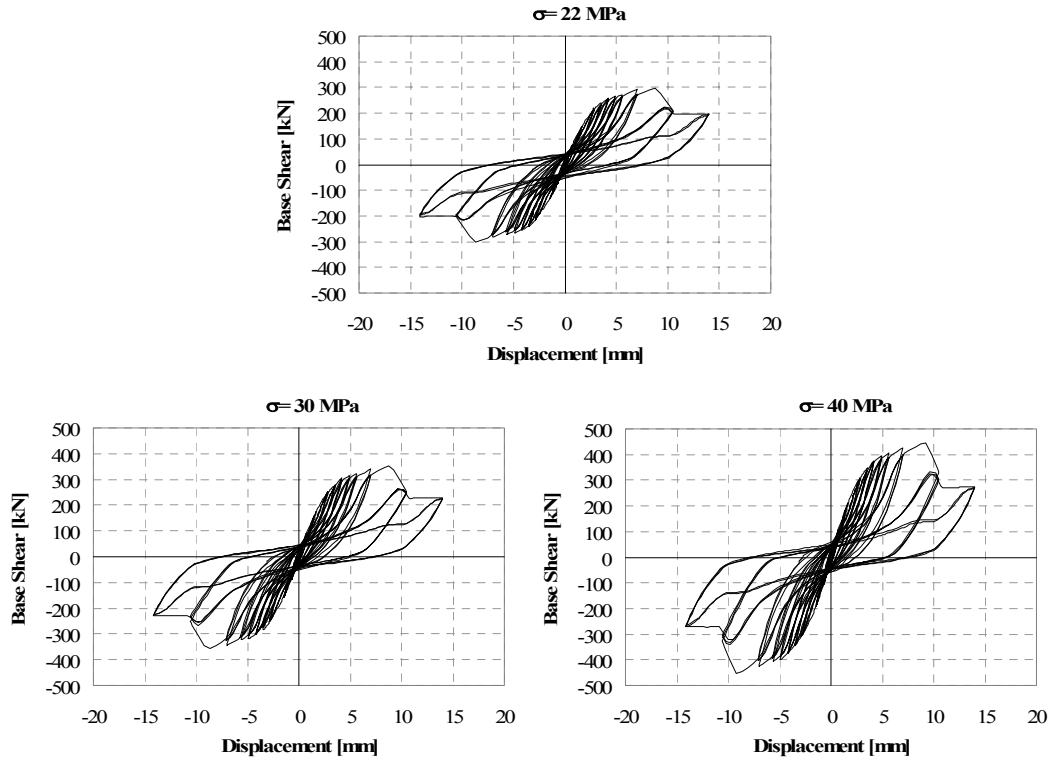


Figure 6.15: Base shear-top displacement curves for the infill panel concrete compressive changes in Specimen 3

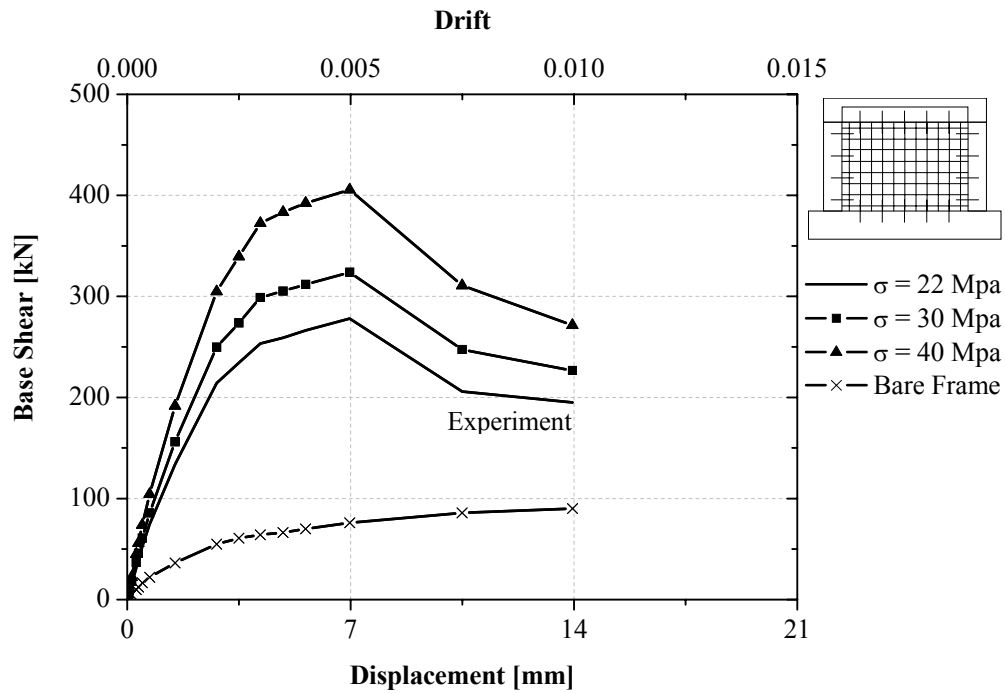


Figure 6.16: Envelope curves for the infill panel concrete compressive changes in Specimen 3

The lateral load carrying capacity of the frames;

- When $\sigma=30$ MPa, it is 4.3 times more at 7 mm (0.5% story drift), it is 2.5 times more at 14 mm (1% story drift),
- When $\sigma=40$ MPa, it is 5.3 times more at 7 mm (0.5% story drift), it is 3.0 times more at 14 mm (1% story drift),

compared with the bare frame's.

Initial stiffness changes depending on the infill panel concrete compressive changes are given in Figure 6.17.

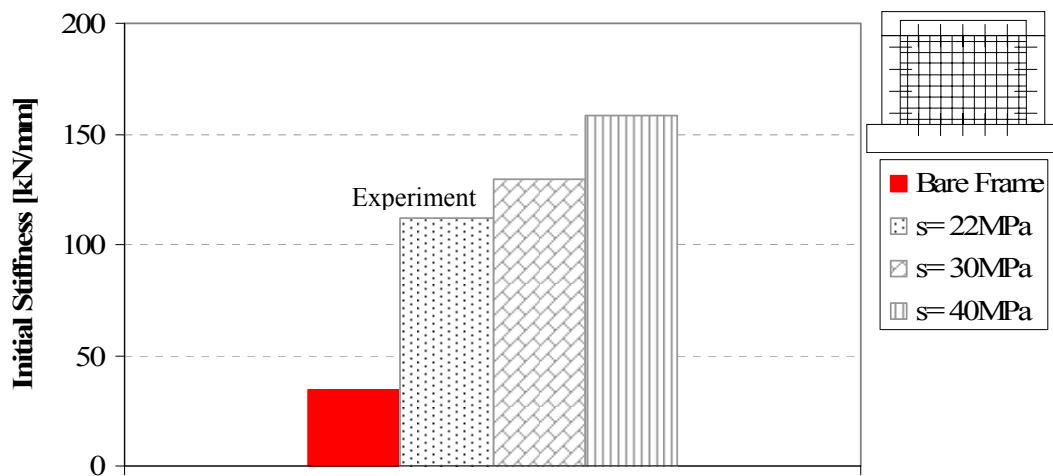


Figure 6.17: Initial stiffness of Specimen 3 for the infill panel concrete compressive changes

The initial lateral stiffness of the frames;

- increased by 3.8 times for $\sigma=30$ MPa,
- increased by 4.6 times for $\sigma=40$ MPa,

compared with the bare frame's.

Energy dissipation capacities depending on the concrete compressive changes in panel are given in Figure 6.18.

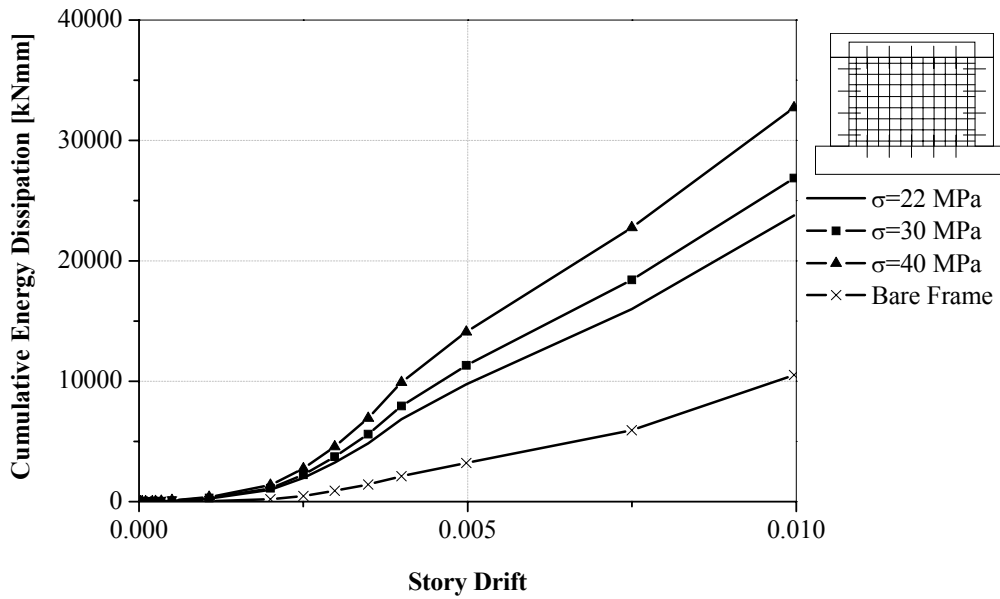


Figure 6.18: The comparison of cumulative energy dissipation capacities of Specimen 3 for the infill panel concrete compressive changes

The energy dissipation of the specimens;

- When $\sigma=30$ MPa, it is 3.5 times more at 7 mm (0.5% story drift), it is 2.6 times more at 14 mm (1% story drift),
- When $\sigma=40$ MPa, it is 4.4 times more at 7 mm (0.5% story drift), it is 3.1 times more at 14 mm (1% story drift),

compared with the bare frame's.

6.4 Application of the Retrofitting Technique to a Representative Frame

In this section, the proposed retrofitting technique is applied on a 2D frame of a building representing the typical RC frame type structures in Turkey, (Girgin 1986, Yıldız 2008). The elevation of the frame can be seen in Figure 6.19. The frame has six storeys with a total height of 21 m. Storey heights are identical and equal to 3.5 m and span lengths are 5 m. The slabs have a thickness of 15 cm.

Two outer spans of the frame, namely AB and DE, are filled with 15 cm thick shotcrete panels as can be seen in Figure 6.20 for retrofitting purpose. Since the geometry of the representative frame is almost 3 times bigger than the tested specimens, the panel thickness is chosen as 15 cm.

Steel quality is S420a and concrete quality for frame and shotcrete panel are C16 and C20, respectively. The dimensions and longitudinal reinforcement data of columns are presented in Figure 6.21 and Table 6.3. The dimensions and longitudinal reinforcement data of beams are presented in Figure 6.22 and Table 6.4. All the beams are 300 mm in width and 600 mm in depth. The concrete cover of beams and columns are selected as 40 mm. The lateral reinforcement of columns and beams are $\phi 10/200$.

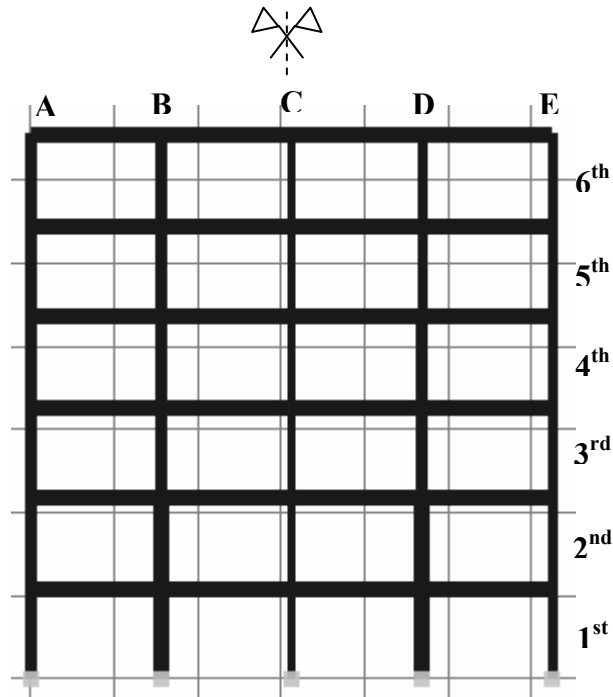


Figure 6.19: The representative frame

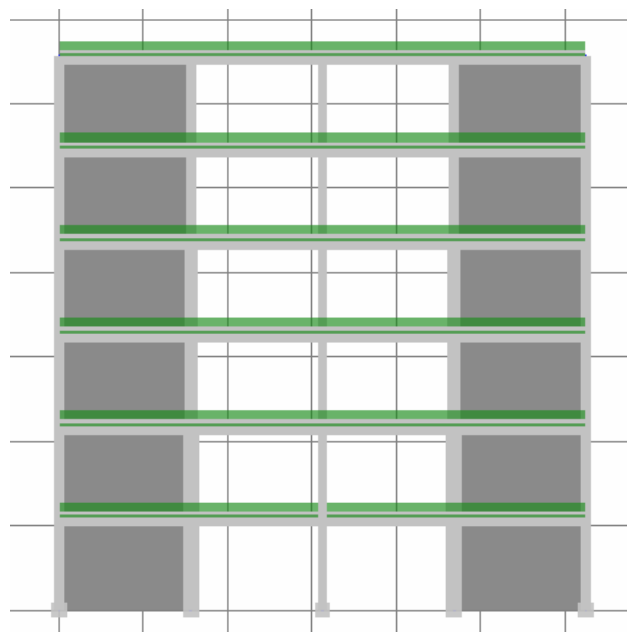


Figure 6.20: Retrofitting of the frame by shotcreted walls

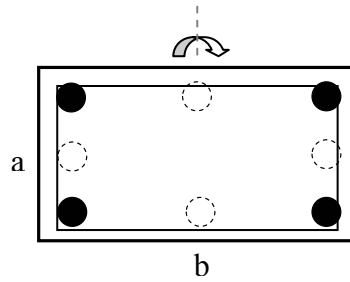


Figure 6.21: Cross section of the column

Table 6.3: The dimensions and reinforcement of the columns

Story	Axes		
	A	B	C
5 - 6	a/b=300/400 mm 4 Φ 18 + 4 Φ 16	a/b=300/400 mm 4 Φ 16 + 4 Φ 16	b/a=400/300 mm 4 Φ 16 + 4 Φ 14
3 - 4	300/400 mm 4 Φ 18 + 4 Φ 16	300/500 mm 4 Φ 20 + 4 Φ 20	500/300 mm 4 Φ 20 + 4 Φ 20
1 - 2	300/400 mm 4 Φ 18 + 4 Φ 16	300/600 mm 4 Φ 22 + 4 Φ 20	600/300 mm 4 Φ 20 + 4 Φ 20

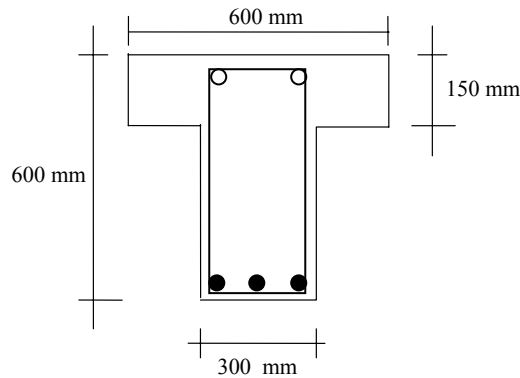


Figure 6.22: Cross section of the typical beam

Table 6.4: The reinforcement of the beams

Story	Place of reinforcement	A - B Beam			B - C Beam		
		Left support	Span	Right support	Left support	Span	Right support
6 - 5	Top	2 ϕ 12+2 ϕ 18	2 ϕ 12	2 ϕ 12+2 ϕ 18	2 ϕ 12+2 ϕ 18	2 ϕ 12	2 ϕ 12+2 ϕ 14
	Bottom	3 ϕ 16	3 ϕ 16	3 ϕ 16	3 ϕ 16	3 ϕ 16	3 ϕ 16
4 - 3	Top	2 ϕ 14+3 ϕ 20	2 ϕ 14	2 ϕ 14+3 ϕ 20	2 ϕ 14+3 ϕ 20	2 ϕ 14	2 ϕ 14+2 ϕ 20
	Bottom	4 ϕ 16	4 ϕ 16	4 ϕ 16	4 ϕ 16	4 ϕ 16	4 ϕ 16
2 - 1	Top	3 ϕ 14+2 ϕ 22	3 ϕ 14	3 ϕ 14+3 ϕ 22	3 ϕ 14+3 ϕ 22	3 ϕ 14	3 ϕ 14+1 ϕ 22
	Bottom	4 ϕ 16	4 ϕ 16	4 ϕ 16	4 ϕ 16	4 ϕ 16	4 ϕ 16

Analytical study is conducted by using SeismoStruct to evaluate the effect of the retrofitting technique on the response of the frame. The response parameters defined for shotcrete panel in Chapter 5 are adapted here. Since the shotcrete panel used in

this demonstrative example is aimed to be fully connected to outer frames, the parameters obtained for Specimen 3 is used.

Two types of analysis have been carried out; pushover and nonlinear dynamic time history analysis (NDTHA). The frame is idealized to have fixed type support in the analysis.

Bilinear steel model is used to model the reinforcement given in Figure 6.23a. This is a uniaxial bilinear stress-strain model with kinematic strain hardening, whereby the elastic range remains constant throughout the various loading stages, and the kinematic hardening rule for the yield surface is assumed as a linear function of the increment of plastic strain.

Uniaxial nonlinear constant confinement concrete model is used for confined concrete seen in Figure 6.23b.

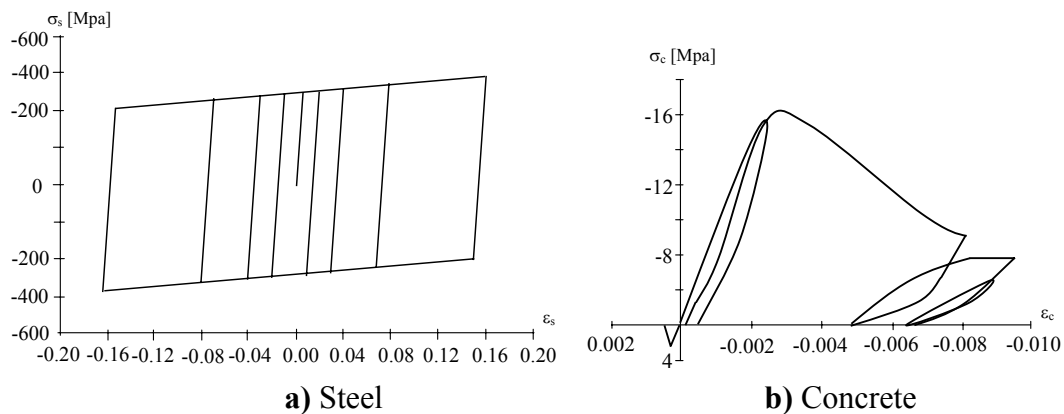


Figure 6.23: Constitutive models used in analytical study

Sum of the dead loads and 30% of the live loads are taken into account in the calculation of seismic weight. The mass values used in the analysis are given in Table 6.5 for two cases.

Table 6.5: Concentrated mass values at each floor levels

Storey	Storey mass [kNsec ² /m]	
	Bare frame	Shotcreted frame
6	49.0	55.6
5	78.7	92.0
4	79.7	93.0
3	80.3	93.6
2	81.2	94.6
1	80.9	94.2

The building is assumed to be constructed on firm soil (Z2 type) at seismic zone 1 defined in TEC, 2007.

The first natural vibrational periods for the bare frame and the shotcreted frame are $T_1 = 0.992$ sec and $T_1 = 0.430$ sec, respectively. First mode shapes of both cases can be seen in Figure 6.24.

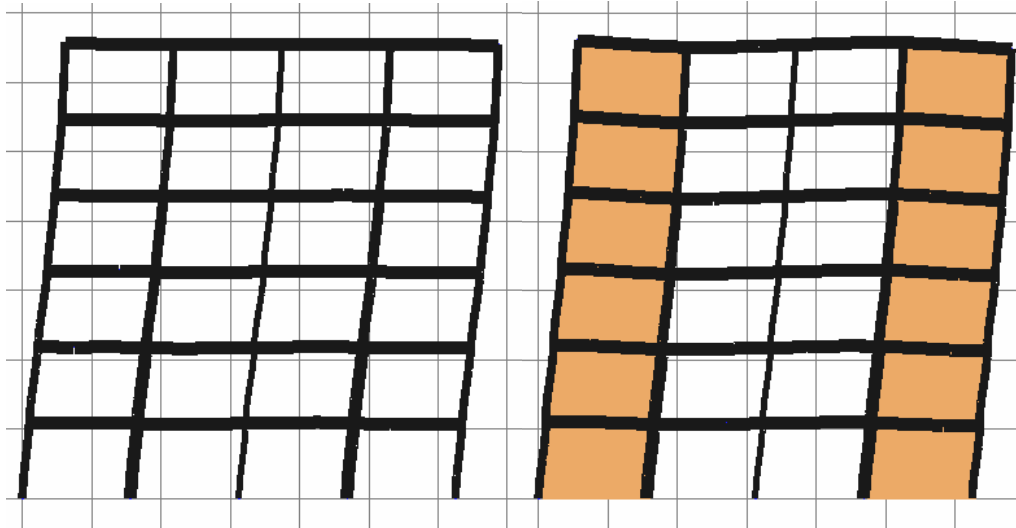


Figure 6.24: First mode shapes of bare and retrofitted frame

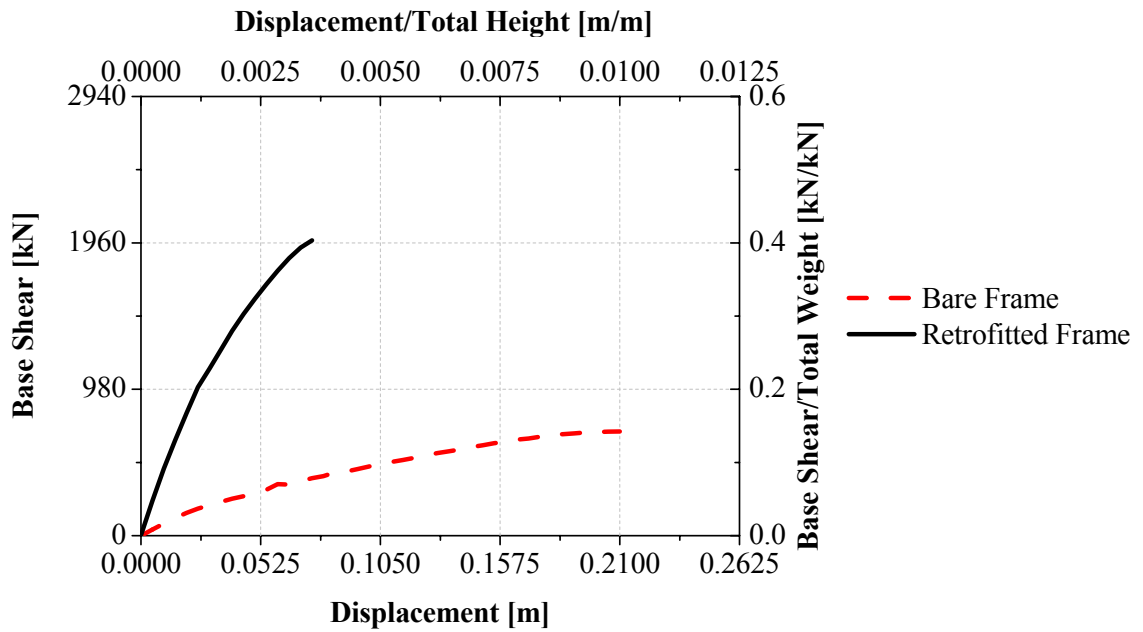
In Table 6.6, the lateral load ratios to be used in the push-over analysis are calculated. They are obtained from the static moments of the storey seismic weights to the ground. The obtained lateral load distribution is close to 1st vibration mode of the frames. The base shear-top displacement relation determined by the analysis is presented in Figure 6.25. The stiffness and the maximum strength of the retrofitted frame are expectedly much larger. In the case of the bare frame and the retrofitted frame, maximum strength is about $0.16W$ and $0.39W$, respectively. The displacement capacity of the retrofitted frame decreased by 2.8 times compared to the bare frame.

Table 6.6: Forces applied during pushover analysis

a) Bare frame				
Storey	W_i (kN)	H_i (m)	$W_i * H_i$	$(W_i * H_i) / \sum(W_i * H_i)$
6	480.87	21.0	10098.27	0.197
5	772.25	17.5	13514.38	0.264
4	782.01	14.0	10948.14	0.214
3	787.73	10.5	8271.16	0.162
2	796.60	7.0	5576.20	0.109
1	793.38	3.5	2776.83	0.054
Σ	4412.84		5217.63	1.000

Table 6.6: Forces applied during pushover analysis (contd.)

b) Retrofitted frame				
Storey	W (kN)	H _i (m)	W _i *H _i	(W _i *H _i)/∑(W _i *H _i)
6	546.50	21.0	11476.48	0.193
5	903.50	17.5	15811.25	0.266
4	913.26	14.0	12785.65	0.215
3	918.98	10.5	9649.25	0.162
2	927.85	7.0	6494.96	0.109
1	924.63	3.5	3236.20	0.054
∑	5134.72		6060.53	1.000

**Figure 6.25:** Base shear-top displacement and base shear/total weight-top displacement/total height diagram

Nonlinear dynamic time history analysis (NDTHA) is also performed. Three earthquake records were taken from PEER (2007) data bank to generate artificial accelerograms. The detailed information about the earthquakes is given in Table 6.7. The original earthquake acceleration records are drawn in Figure 6.26, 6.27 and 6.28.

Table 6.7: Earthquake records

Earthquake	Date	Station / Direction	M	PGA (g)
Erzincan	13.03.1992	Erzincan / EW	6.9	0.496
İzmit	17.08.1999	İzmit / 090	7.4	0.220
Düzce	12.11.1999	Bolu / 090	7.1	0.822

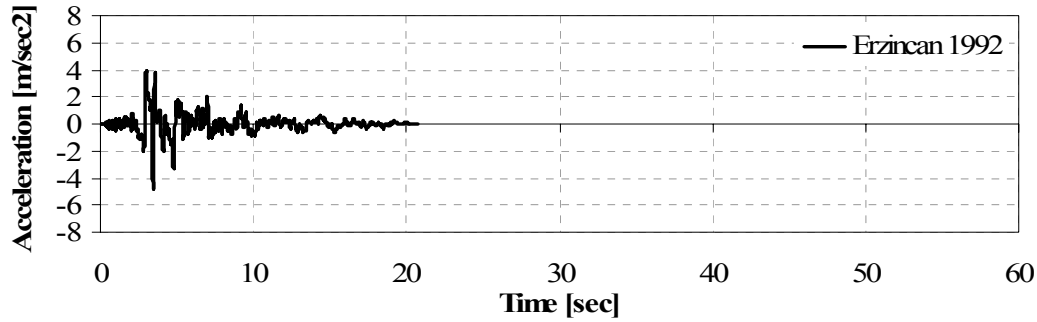


Figure 6.26: The acceleration record of Erzincan Earthquake

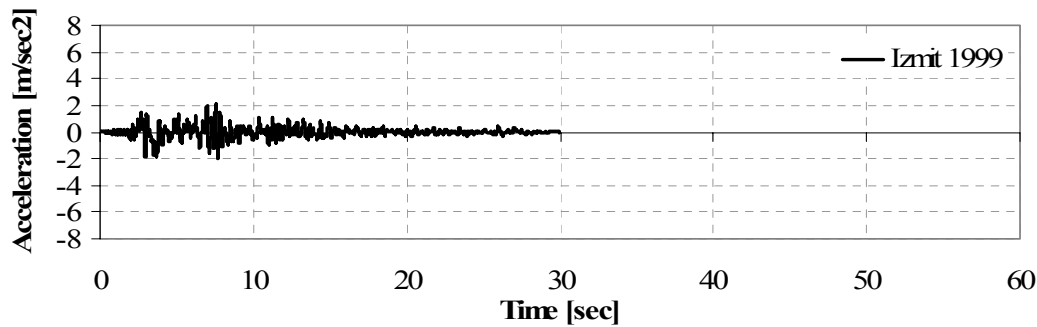


Figure 6.27: The acceleration record of İzmit Earthquake

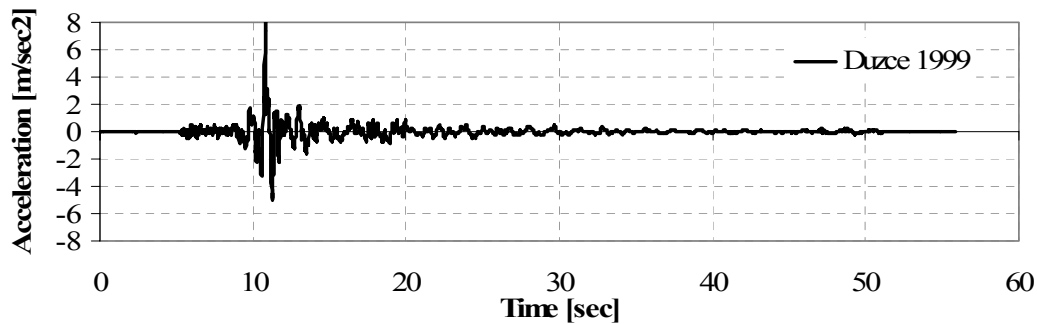


Figure 6.28: The acceleration record of Düzce Earthquake

The original acceleration records of the three earthquakes given above are modified respect to the acceleration spectra defined for Z2 type soil given in TEC, 2007. Two versions of the earthquakes are produced named as “service” and “design” earthquakes, (Yıldız, 2008).

The modified earthquake records obtained are given in Figure 6.29 as “service” and in Figure 6.30 as “design” earthquakes.

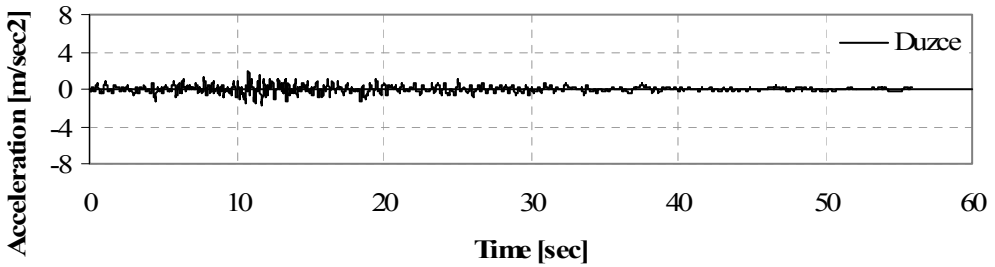
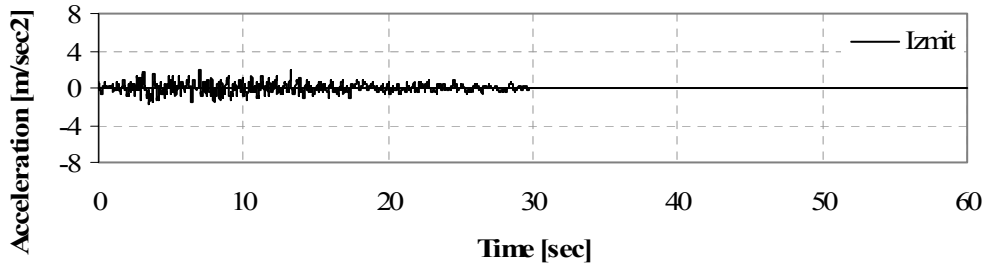
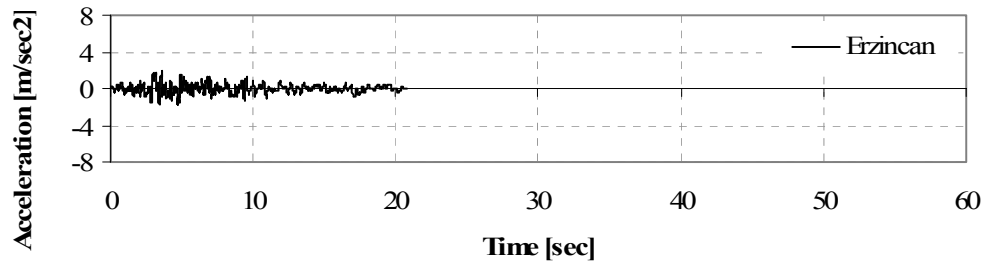


Figure 6.29: “Service” type acceleration records

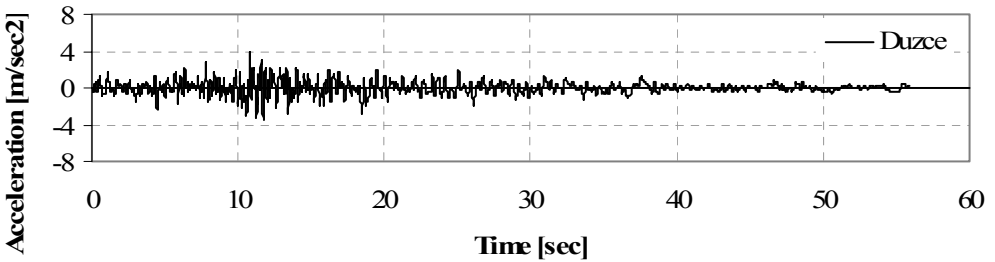
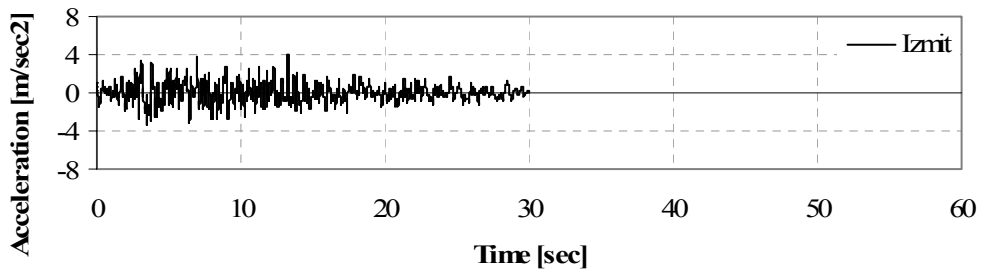
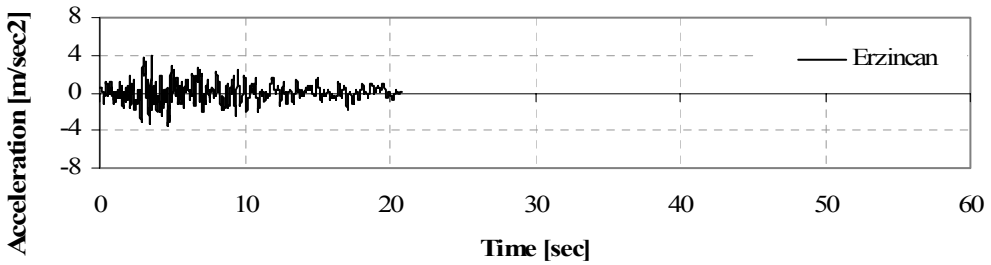


Figure 6.30: “Design” type acceleration records

The mean spectrum of the modified design earthquakes is drawn with the design spectrum for Z2 type soil in Figure 6.31.

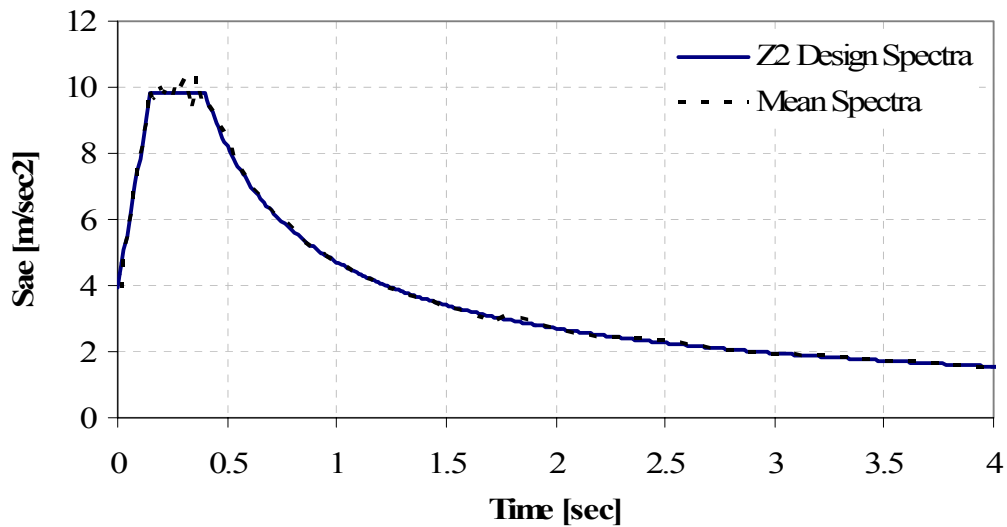


Figure 6.31: Design spectrum defined in TEC, 2007

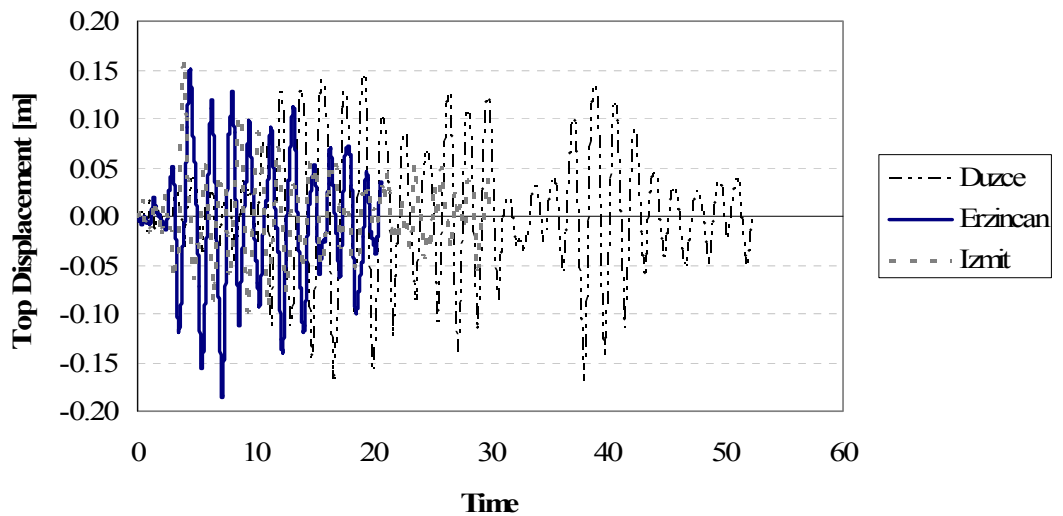
In NDTHA, the direct integration of the equations of motion is accomplished using the numerically dissipative α -integration algorithm Hilber et al. (1977) with automatic time-step adjustment for optimum accuracy and efficiency.

For each increment, several iterations are carried out until convergence is achieved. If convergence is not reached within the specified maximum number of iterations, the load increment (or time-step) is reduced and the analysis is restarted from the last point of equilibrium (end of previous increment or time-step). This step reduction, however, is not constant but rather adapted to the level of non-convergence verified. At the end of a solution step or increment; a convergence ratio indicator, defined as the maximum of ratios between the achieved and the required displacement/force convergence factors is computed. Then, depending on how far away the analysis was from reaching convergence, a small, average or large step reduction factor is adopted and employed in the calculation of the new step factor. The product between the latter and the initial time-step or load increment, defined by the user at the start of the analysis, yields the reduced analysis step to be used in the subsequent increment, (SeismoStruct, 2007).

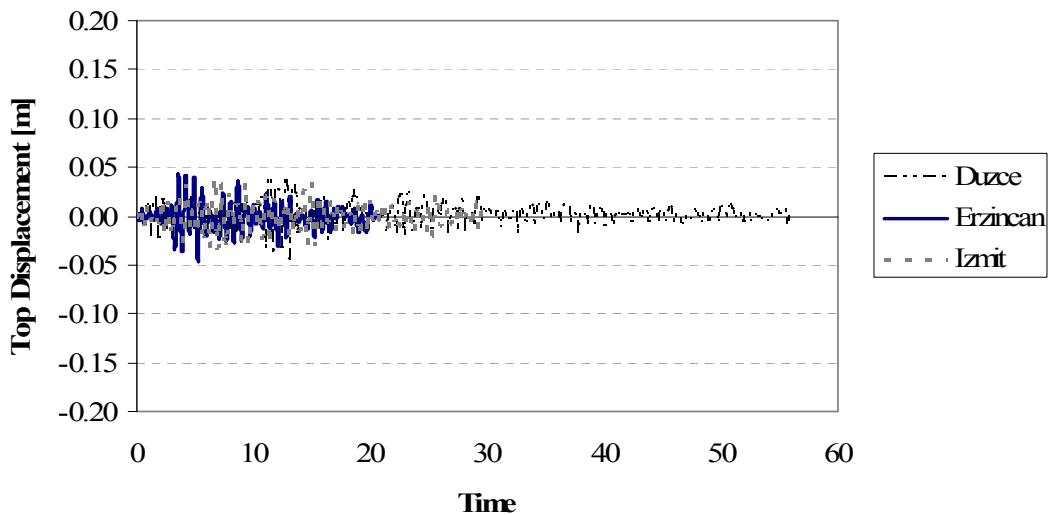
Top displacement-time graphs for the bare and retrofitted frame under service and design earthquakes are given in Figure 6.32 and 6.34, respectively. The displacement demand for bare frame is 0.18 m under service earthquake. After retrofitting, the displacement demand decrease to 0.04 m. Under design earthquakes the

displacement of the bare frame increases to 0.32 m. After infilling of two spans with shotcrete panels, this demand decreases to 0.09 m.

Base shear-time graphs for the bare and retrofitted frame under service and design earthquakes are given in Figure 6.33 and 6.35, respectively. The shear force demand for bare frame is 592 kN under service earthquake. After retrofitting, the displacement demand becomes 1562 kN. Under design earthquakes the shear force demand of the bare frame increases to 715 kN. After infilling of two spans with shotcrete panels, this demand becomes 1963 kN.

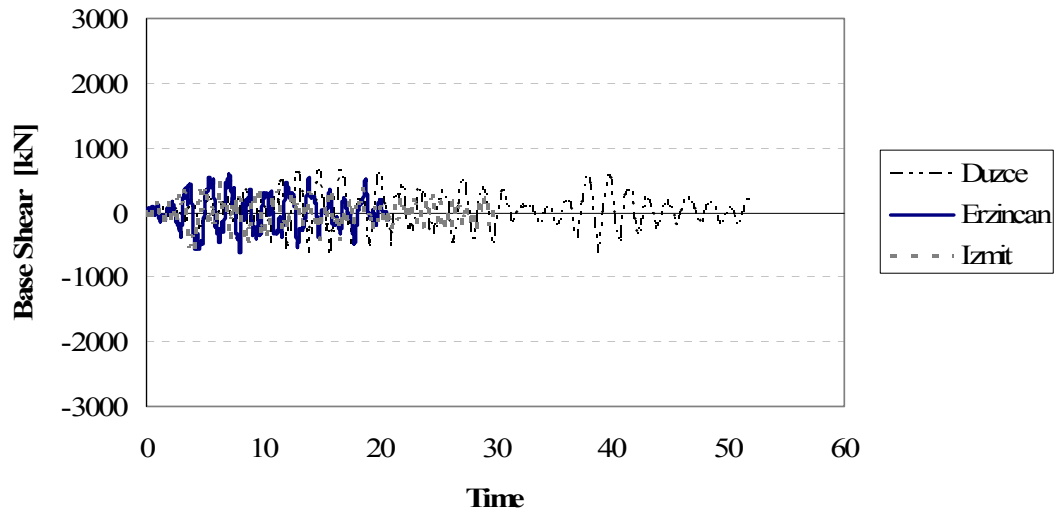


a) Bare frame

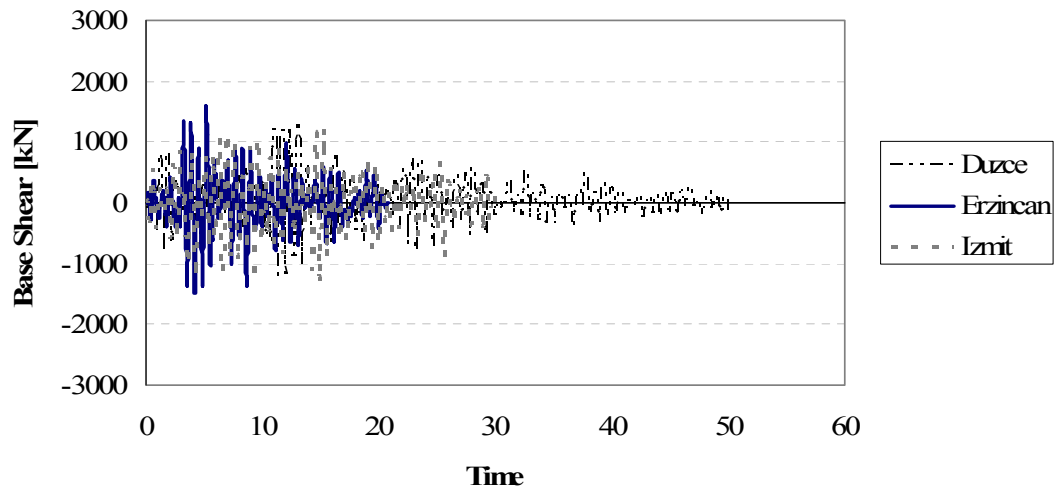


b) Retrofitted frame

Figure 6.32: Time versus top displacement graphs for bare and retrofitted frame under service earthquakes



a) Bare frame

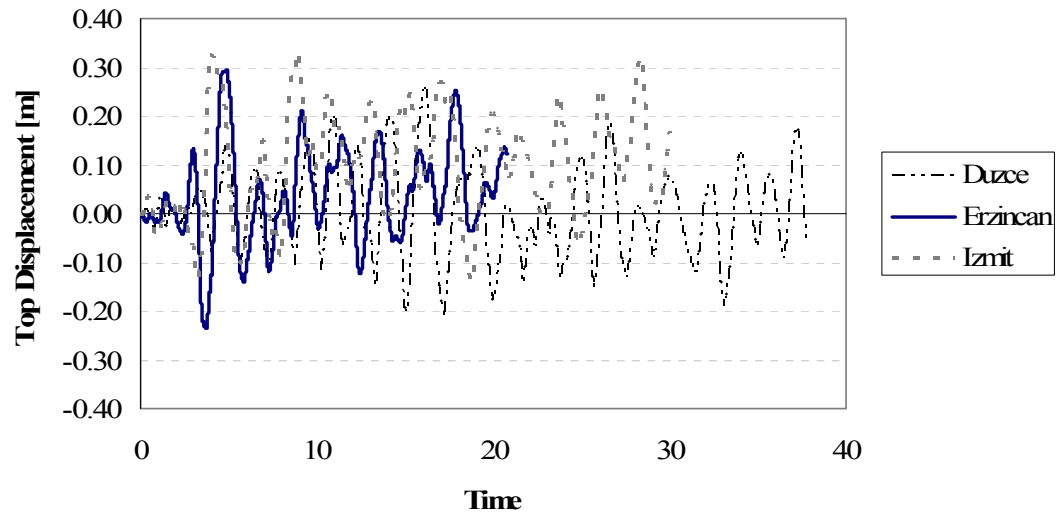


b) Retrofitted frame

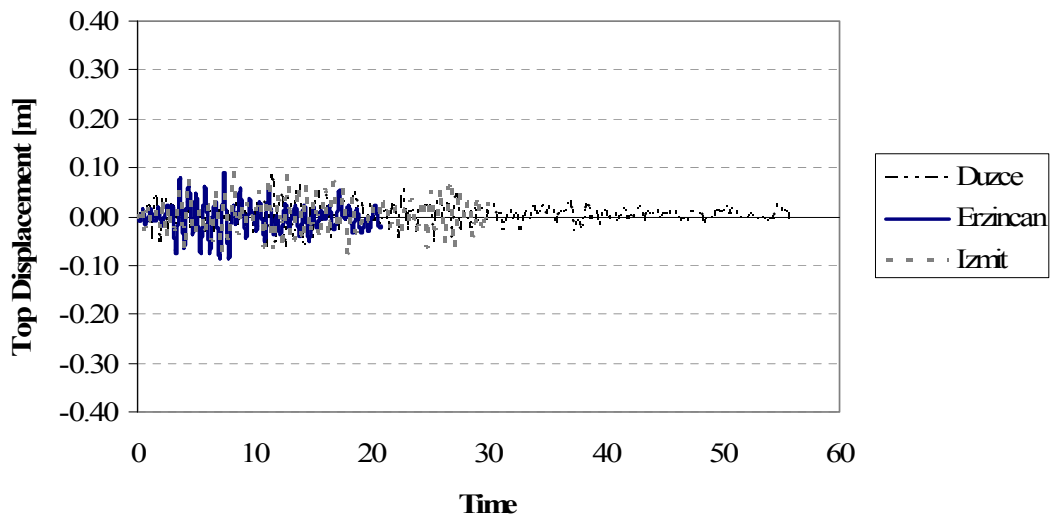
Figure 6.33: Time versus base shear force graphs for bare and retrofitted frame under service earthquakes

From NDTHA displacement, interstorey drift ratio and shear force demands of shotcreted frames are compared with the bare frames'. In Figure 6.36, 6.37 and 6.38, the comparisons of the results obtained for service and design earthquake are given. The results given in the figures are the average of results of the three earthquakes.

The displacement demands of the bare frame under service and design earthquakes are 0.17 m and 0.29 m, respectively. After placing shotcrete panels in the two spans, these values decrease to 0.04 m and 0.12 m. The interstorey drift ratio is below 1% under service and design earthquakes. Under design earthquakes, it is slightly higher than 1% only at the 1st.



a) Bare frame



b) Retrofitted frame

Figure 6.34: Time versus top displacement graphs for bare and retrofitted frame under design earthquakes

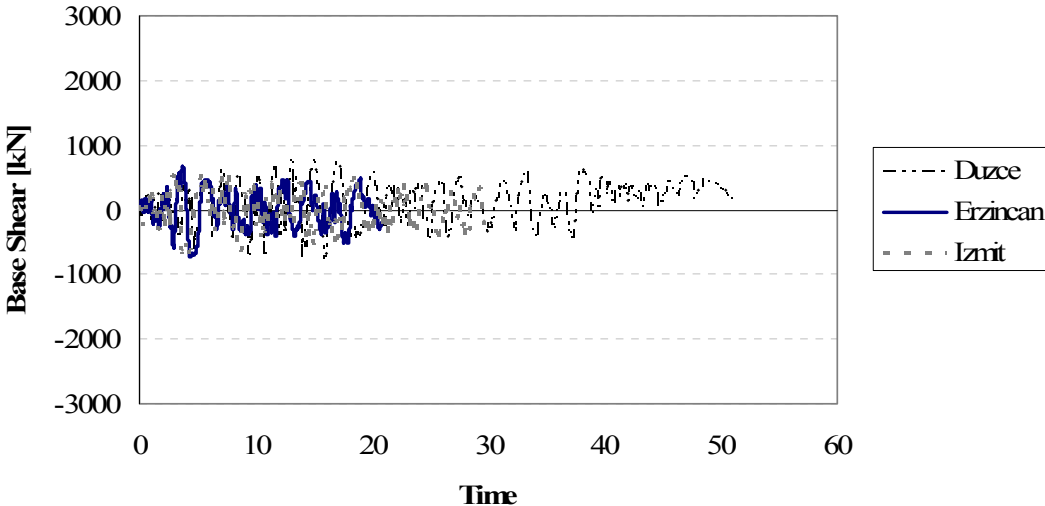
The nominal shear stress obtained for the design earthquake is 1026 kN/m^2 at the 1st floor, which is lower than the nominal shear stress, 2130 kN/m^2 , obtained in the experimental study.

The behaviour of the shotcrete panel predicted from the experimental study in Chapter 4 and adapted to the numerical study in Chapter 5, applied to on a 2D frame of a building representing the typical RC frame type structures in Turkey.

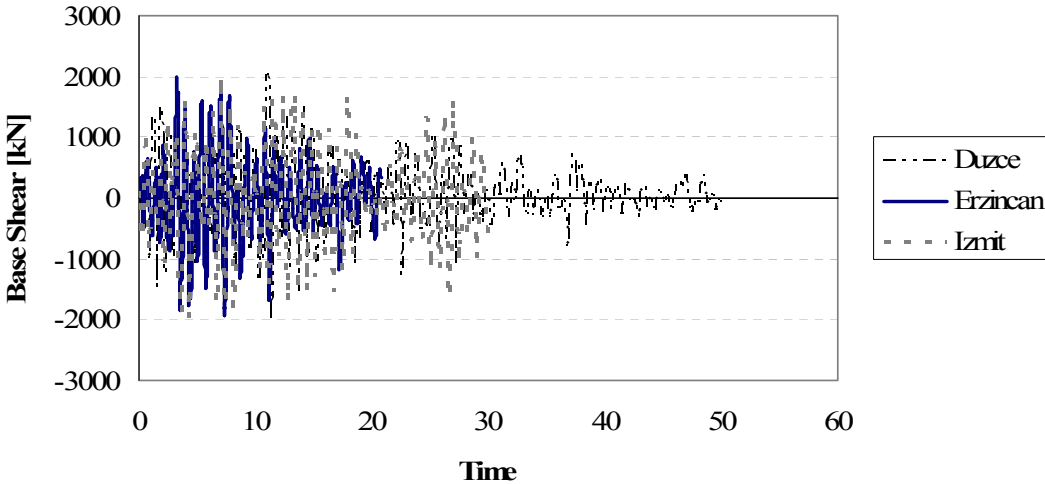
Two outer spans of the bare frame are retrofitted with shotcrete panels. Pushover and NDTHA analysis are performed using SeismoStruct. The frame's resistance and rigidity has increased significantly after retrofitting with shotcrete panels given in

Figure 6.25. The effect of retrofitting is also studied with NDTHA and the results are compared according to displacement, interstorey drift and interstorey shear force demand in Figure 6.36, 6.37 and 6.38.

Under these results it can be concluded that; after the retrofitting of the typical RC frame with shotcrete panels, this frame can carry the design loads defined in TEC 2007.



a) Bare frame



b) Retrofitted frame

Figure 6.35: Time versus base shear force graphs for bare and retrofitted frame under design earthquakes

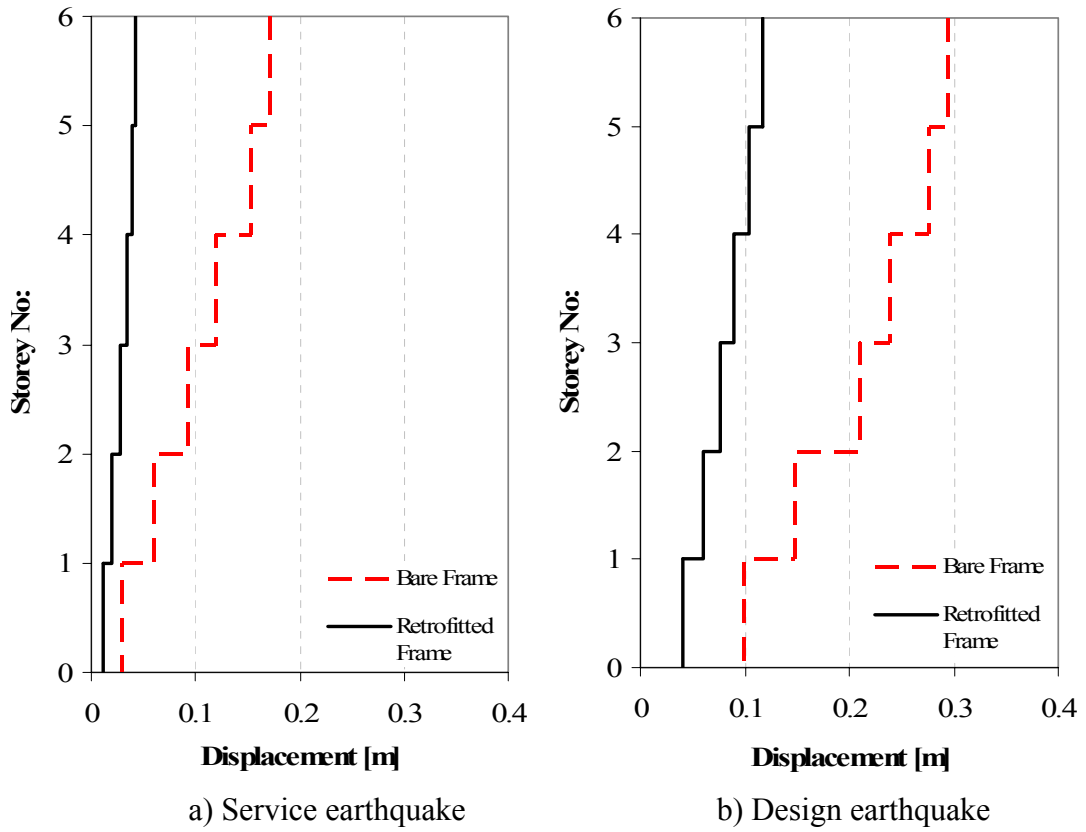


Figure 6.36: Comparison of the maximum story displacements of the frame with and without shotcrete panel for service and design earthquakes

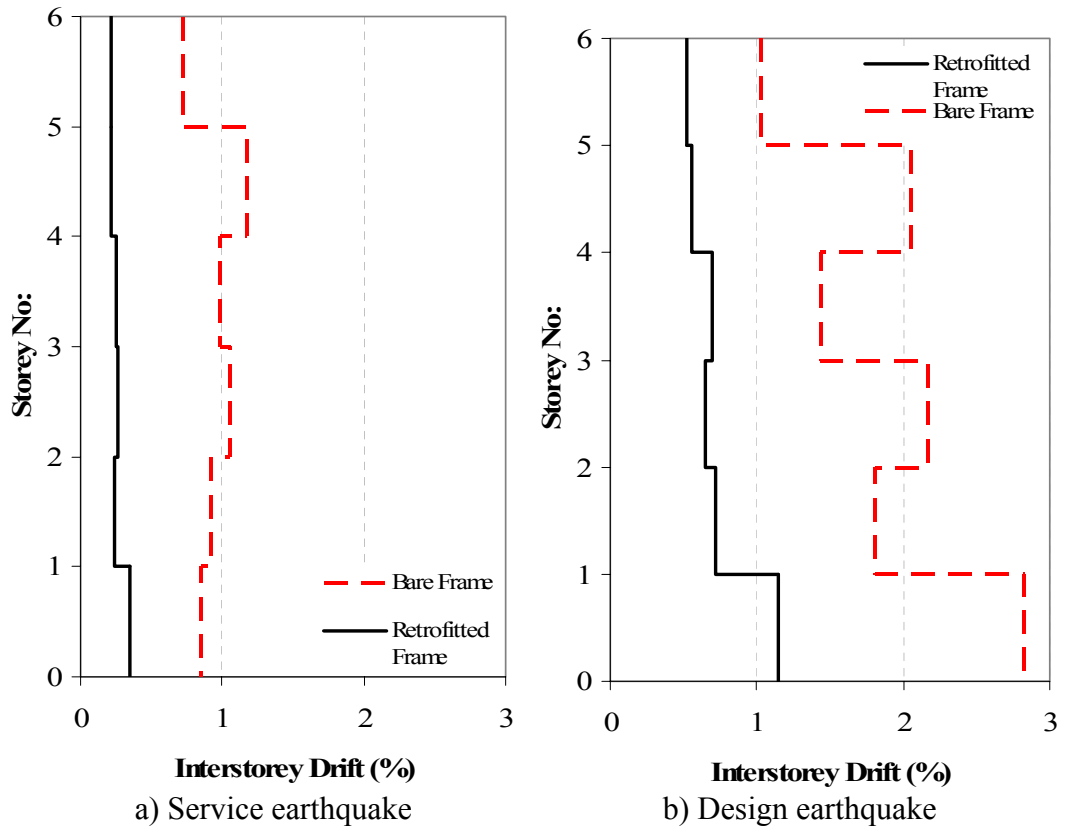


Figure 6.37: Comparison of the maximum interstorey drift of the frame with and without shotcrete panel for service and design earthquakes

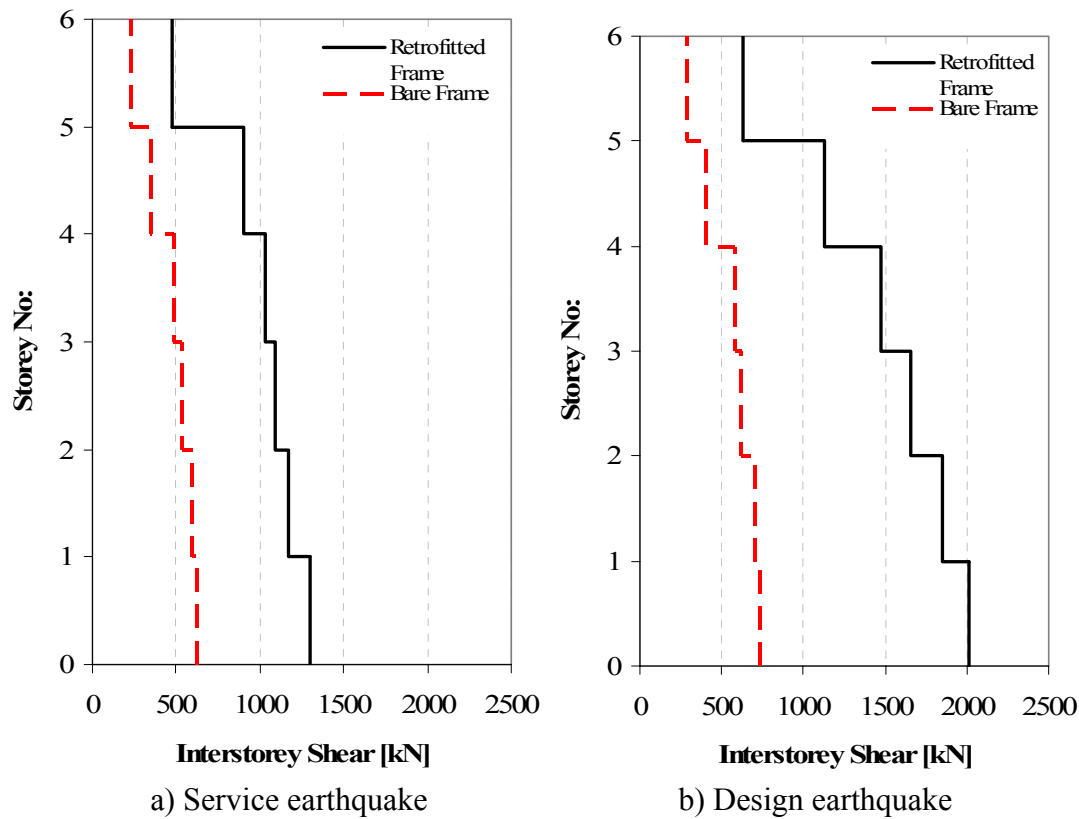
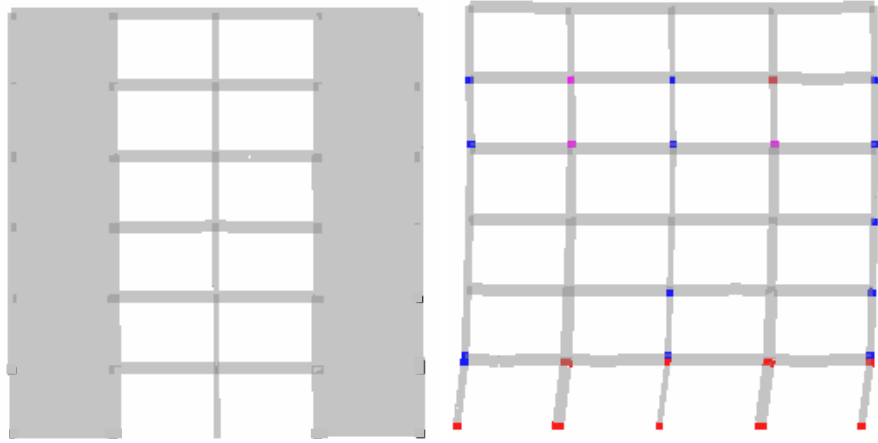


Figure 6.38: Comparison of the maximum interstorey shear force of the frame with and without shotcrete panel for service and design earthquakes

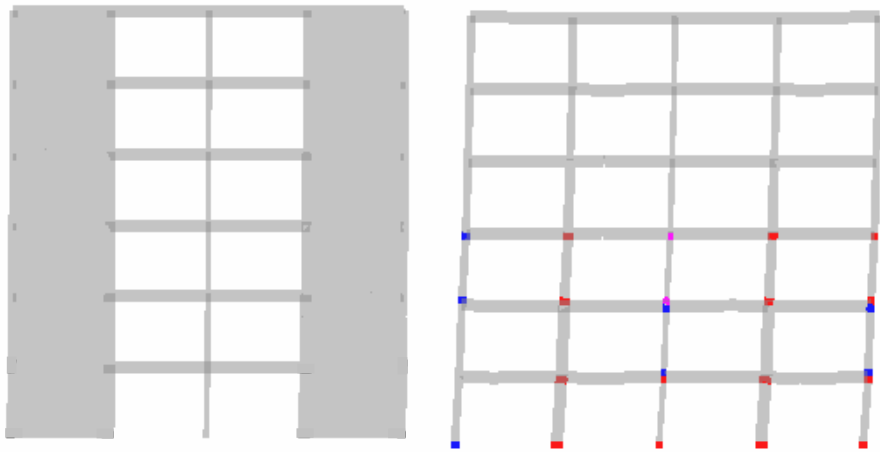
The observed sectional performances of the bare and retrofitted systems in the case of the design earthquakes are illustrated in Figure 6.39. Various colours used in this figure correspond to performance levels defined in Table 5.6. It can be concluded that in the case of the bare frame, vulnerability of the ground floor is relatively higher than the upper floors. The story mechanism for the ground floor is the common damage pattern observed for the used earthquake records.

After introducing the shotcrete panels to the outer spans; even though yielding of reinforcement for some critical section has been observed, both beams and columns stayed in performance level named as *Minimum Damage State*.

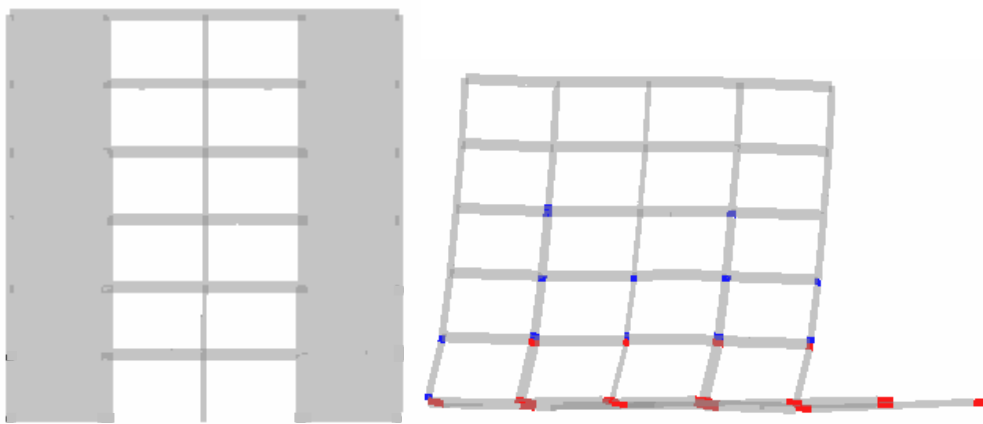
For the bare and retrofitted cases, the strain history of the main reinforcement and the confined concrete at the bottom section of the column, which is located in Axis C at 1st floor, is given for design earthquakes in Figures 6.40 and 6.41, respectively.



b) Design Erzincan



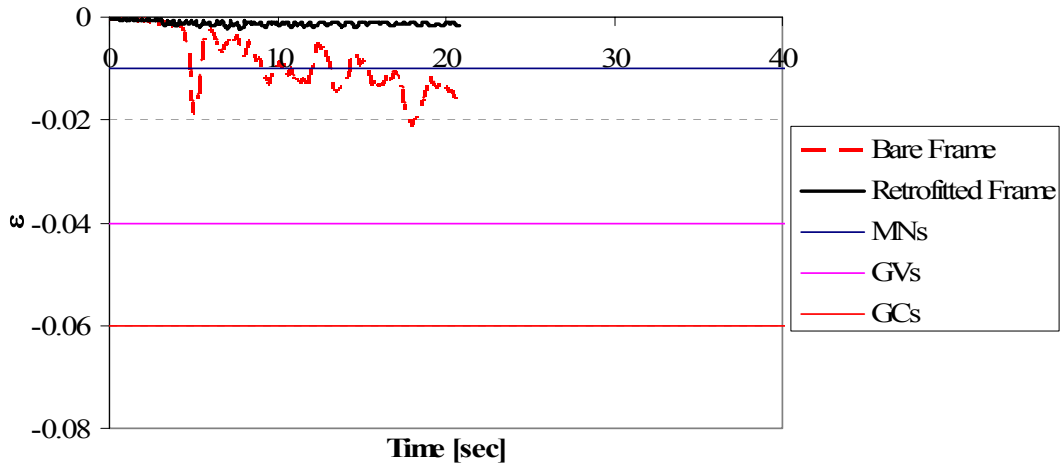
c) Design Izmit



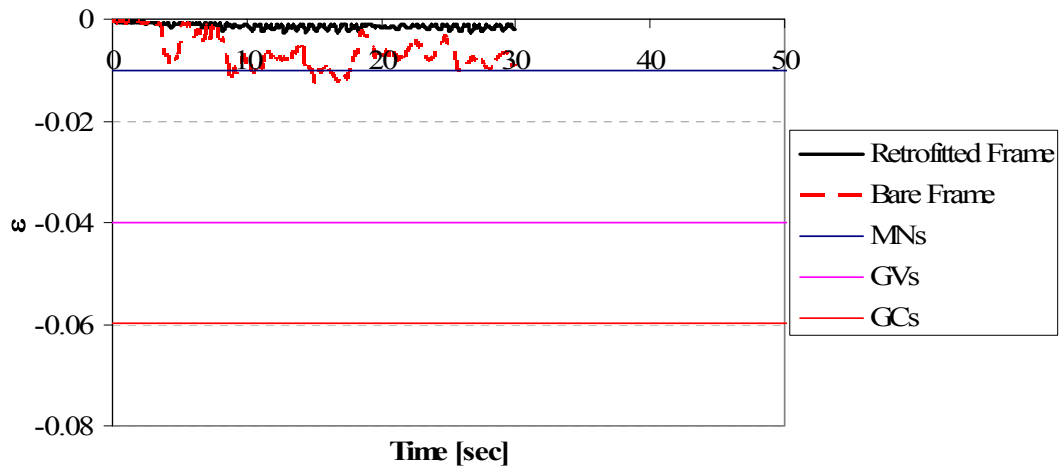
a) Design Duzce



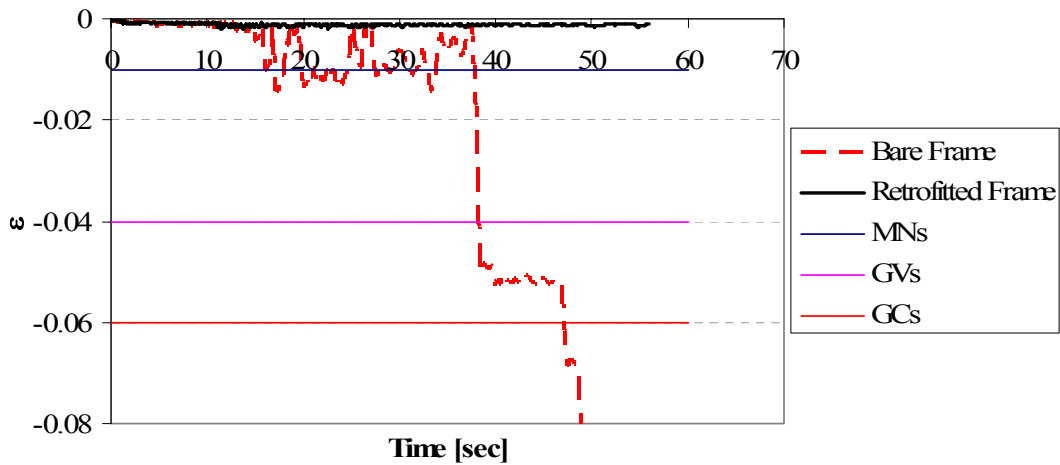
Figure 6.39: Performance of the bare and retrofitted systems under design earthquakes



a) Erzincan earthquake



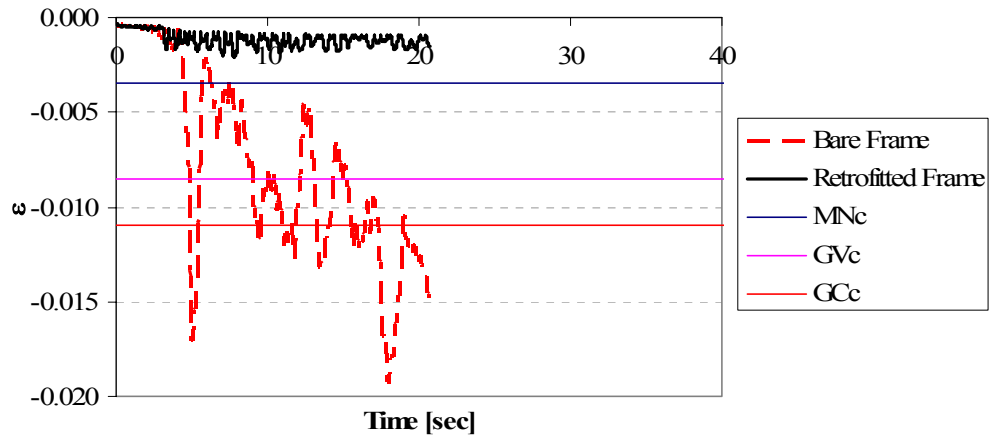
b) Izmit earthquake



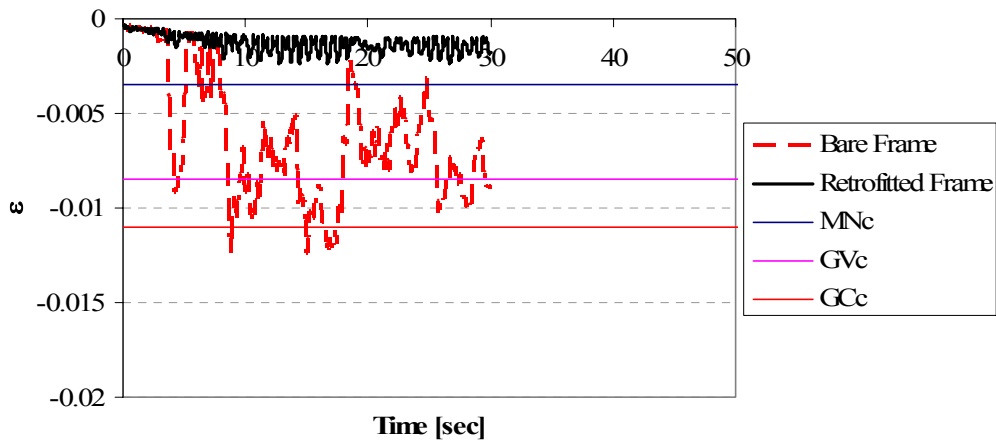
c) Düzce earthquake

Figure 6.40: Comparison of the reinforcement strains with and without shotcrete panel for design earthquakes

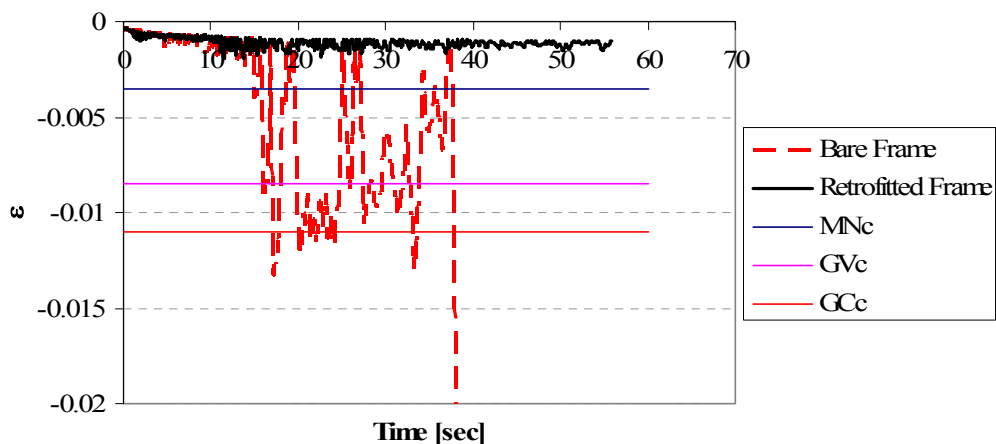
In the case of bare frame, the performance level of the reinforcement is attained to the *Collapse State* for Düzce Earthquake. However for Erzincan and Izmit Earthquakes the performance levels correspond to *Safety State*. After introducing the shotcrete panels to the system, the reinforcement performs in the *Minimum Damage State* for all design earthquakes.



a) Erzincan earthquake



b) Izmit earthquake



c) Düzce earthquake

Figure 6.41: Comparison of the confined concrete strains with and without shotcrete panel for design earthquakes

In the case of bare frame, the performance level of the confined concrete is attained to the *Collapse State* for all design earthquakes. After introducing the shotcrete panels to the system, the confined concrete performs in the *Minimum Damage State* for all design earthquakes.

7. CONCLUSIONS

Application of shotcrete directly on the partition walls or creating conventional shear walls in the vulnerable masonry and reinforced concrete structures are commonly used retrofitting techniques in Turkey. Usage of shotcrete is fast, easy and cost effective compared with the other retrofitting techniques. Construction of shotcrete infill panels in reinforced concrete frames is studied here in experimental and analytical manner.

The experimental test program to evaluate the performance of a structural system consisting of shotcrete panel in existing vulnerable frames was described in Chapter 3 in detail.

The test specimens were chosen to represent the vulnerable low-rise low-cost reinforced concrete structures in Turkey especially constructed before the validation of the last two earthquake codes. All test specimens are single story, single bay frames. The shotcrete panels made from wet-mixed shotcrete in lieu of a traditional masonry wall are used as an infill within the frames. The study is composed of testing four undamaged and two damaged frames with shotcrete panels. A bare frame and a conventional shear wall type frame were also tested in the study to be used as reference frames.

The main aim of this study is to adapt the shotcrete panel systems to reinforced concrete structures to find a fast, cheap and effective retrofitting technique. To understand the effectiveness of this retrofitting technique, experimental and analytical researches were carried out. The results obtained are emphasized in the following section.

7.1 Conclusions

The comparison of the experimental results of the six test specimens with shotcrete panel and one shear wall specimen to the bare frame specimen are explained briefly here and were described in Section 4.11 in detail. Failure modes, lateral load carrying

capacities, initial stiffness, energy dissipation capacities, stiffness degradations and equivalent damping characteristics are discussed.

Failure mode: The bare frames had bending and shear type cracks at column ends, while the retrofitted frames had shear cracks at column ends. No matter how strong wet-mixed sprayed concrete panels were, the ultimate failure mode of the systems were controlled by the existing shear capacity of the main frames. All of the strengthened frame experiments were ended due to severe shear cracks occurring at the end of the columns. During the experiments of specimens with partially infilled shotcrete panel, shear cracks are observed on the webs of the short beam that are on the left and right side of the panel. These cracks width are 0.4 mm at the end of the tests. These types of cracks were not observed during the experiments of specimens with fully infilled shotcrete panel.

Lateral load carrying capacity: As summarized in Table 4.32, the lateral load carrying capacity increased between 2.2 to 3.2 times for the specimens with shotcrete panel fully connected to the frame (Specimens 2S and 3) and between 1.6 to 1.8 times for the specimens with shotcrete panel with a gap between the panel and the columns (Specimens 4S and 5) compared with the bare frame's (Specimen 1). The specimen with the shear wall (Specimen 8) shows the same amount of increase with the fully connected shotcrete panel ones given in Figure 4.96. Pre-reverse deflection seems to make a 30% increase in the lateral load carrying capacity of the specimen for the specimens with shotcrete panel fully connected to the frame (Specimen 6) given in Figure 4.92, but it does not make an increase for the specimens with shotcrete panel with a gap between the panel and the columns (Specimen 7) given in Figure 4.94.

Initial stiffness: The lateral stiffness of the frames, right before the first cracks occurred in the system, increased by 10 times for the damaged frames Specimens 2S and 4S and 8.5 times for undamaged frames Specimens 3 and 5 compared with the bare frame's. The pre-reversed shotcrete panel specimens also showed almost the same amount of increase in stiffness while the shear wall (Specimen 8) increased the stiffness 20 times as can be seen in Table 4.33.

Cumulative energy dissipation capacity: At 1% story drift level, the cumulative energy dissipation capacities of Specimen 2S and Specimen 3 are 10 times, while

Specimen 4S and Specimen 5 are 4 times greater than Specimen 1. At 2% story drift level, the ratios become 5 and 2.5 times, respectively. At 3% drift ratio, only Specimen 4S and Specimen 5 are increased by 1.7 times compared to Specimen 1, as shown in Figure 4.98. Specimen 8 shows the same amount of energy dissipation with Specimen 3 and could only get to drift level of 1%.

Equivalent damping characteristics: The achieved equivalent viscous damping ratios for retrofitted specimens vary between 8-16% of critical damping at increasing drift levels. Particularly at 1% story drift, 10.5% and 13.5% of critical damping observed for without and with pre-reverse deflection on the beam, respectively. It can be concluded that the observed damping ratios are definitely higher than 5% of critical damping which is commonly used in the design process of reinforced concrete structures.

The analytical works which were conducted by using the finite element program of *SeismoStruct*, initiated with the calibration of some parameters in the response models with the tested specimens. The analytical results agree well and give quiet close results with the experimental ones and are able to catch not only the maximum forces, which had occurred at the target displacements, but also the similar damage propagation that is observed during the test given in Figures 5.14, 5.19, 5.24, 5.29 and 5.34.

The calibrated models have been used in the parametric study which includes understanding the effect of the panel thickness, the concrete compressive strength of the panel and the gap size between the panel and the frame. Various illustrations have been presented to evaluate the effect of the defined parameters. The analytical studies showed that the lateral load carrying capacity of the frame increases as the thickness of the shotcrete panel increases; and when the ratio between the gap and distance between the inside face of the columns (a/L) changes from 1% to 15%, the lateral load carrying capacity of the system is almost the same. While a/L ratio is 20% or more, the panel does not have any effect on the lateral load carrying capacity and the frame acts like a bare frame.

The investigated retrofitting technique has been applied on a planar frame of a building representing the typical RC frame type structures in Turkey presented. Two outer spans of this frame are retrofitted with shotcrete panels through the height of

the frame continuously. The models, which represent the inelastic behaviour of shotcrete panel used in this study, are adapted from the calibrated models that were developed for the test specimens. Pushover and nonlinear dynamic time history analysis have been performed on the bare and the retrofitted frames. Depending on the capacity curves attained in the pushover analyses, maximum base shear capacity of the frame is increased from 16% to 39% of the seismic weights at bare and retrofitted cases. On the other hand, the displacement capacity of the retrofitted frame decreased by 2.8 times compared to the bare frame.

The nonlinear time history analyses performed for the selected earthquake records yield out in terms of strains of confined concrete and longitudinal reinforcement, that several cross sections of the bare frame have attained the *collapse state* defined in TEC 2007, however the retrofitted frame performs within the *minimum damage state*. The interstory drift ratios obtained for the retrofitted specimens are around 1% which is the value observed from experimental study that corresponds to minor damages on the system. The nominal shear stress calculated by using the maximum base shear resulted from the design earthquakes are around 1026 kN/m^2 which is lower than the nominal shear stress, 2130 kN/m^2 , obtained in the experimental study.

Results of the experimental and analytical works prove that the retrofitting technique improves the earthquake response of reinforced concrete frames having insufficient safety.

7.2 Research Needs

Depending on the experiences obtained from this study, the following research topics are suggested to be investigated experimentally: Performing full scale tests, testing of the various shotcrete panel thicknesses, testing of various pre-reversing amount, the variation of gap size between shotcrete panel and columns and its effect on the short beam behavior, testing of specimens in which shear behavior of the columns and beam-column joints are improved before construction of shotcrete panel.

REFERENCES

- Abrams, D. P. And Lynch, J. M.**, 2001. Flexural behavior of retrofitted masonry piers, *KEERC-MAE Joint Seminar on Risk Mitigation for Regions of Moderate Seismicity*, Illinois, USA.
- Al-Chaar, G., Sweeney, S. and Brady, P.**, 1996. Pushover Laboratory Testing of Unreinforced Masonry Infills, *Wind and Seismic Effects*, NIST SP904, 257-269.
- Altın, S, Ersoy U. and Tankut T.**, 1992. Hysteretic Response of Reinforced Concrete Infilled Frames, *Journal of Structural Engineering*, Vol.118, no.8, pp.2133-2150.
- Aydoğan M. and Öztürk T.**, 2002. Betonarme Yapılarda Güçlendirme Uygulamaları, Prof.Dr. Kemal Özden'i Anma Semineri Yapıların Onarım ve Güçlendirilmesi Alanında Gelişmeler, 39-69, İstanbul
- Badoux M. and Jirsa J.O.**, 1990. Steel Bracing of RC Frame for Seismic Retrofitting, *Journal of Structural Engineering*, Vol.116, no.1, pp.55-74.
- Ballou M. and Niermann M.**, 2002. Soil and rock slope stabilization using fiber-reinforced shotcrete in north america, *Shotcrete Magazine*.
- Blandon, C.A.**, 2005. *Implementation of an Infill Masonry Model for Seismic Assessment of Existing Buildings*, Individual Study, European School for Advanced Studies in Reduction of Seismic Risk (ROSE School), Pavia, Italy.
- Bousias, S. N., Fardis M.N., Spathis A. and Biskinis D.**, 2005. Concrete or FRP Jacketing of Concrete Columns for Seismic Retrofitting.
- Bush T.D, Wyllie L.A. and Jirsa J.O.**, 1991. Observations on two seismic strengthening schemes for concrete frames, *Earthquake Spectra*, Vol.7, No. 4, pp.511-527.
- Calvi G. and Magenes G.**, 1994. Experimental results on unreinforced masonry shear walls damaged and repaired, 10th IB2MaC, Calgary, Canada, 509-518.
- Calvi G.M., Pinho R. and Crowley H.**, 2006. State-of-the-knowledge on the period elongation of RC buildings during strong ground shaking, *First European Conference on Earthquake Engineering and Seismology* (a joint event of the 13th ECEE & 30th General Assembly of the ESC), Geneva, Switzerland, 3-8 September 2006, Paper Number: 1535.
- Casarotti C. and Pinho R.**, 2007. An adaptive capacity spectrum method for assessment of bridges subjected to earthquake action, *Bull Earthquake Engineering*.

- Cattari S. and Lagomarsio S.**, 2006. Non linear Analysis of mixed masonry and reinforced concrete buildings, *First European Conference on Earthquake Engineering and Seismology* (a joint event of the 13th ECEE & 30th General Assembly of the ESC), Geneva, Switzerland, 3-8 September 2006, Paper Number: 927
- Celep Z.**, 1998. Post-earthquake rehabilitation of moderately damaged masonry structures, *Second Japan-Turkey Workshop on Earthquake Engineering*, V.1, 73-90, İstanbul
- Clements M.**, 2003. Shotcreting in Australian underground mines: a decade of rapid movement, *Shotcrete Magazine*.
- Crisafulli F.J.**, 1997. Seismic Behaviour of Reinforced Concrete Structures with Masonry Infills, *PhD Thesis, University of Canterbury*, New Zealand.
- Crowley H. and Pinho R.**, 2006. Simplified equations for estimating the period of vibration of existing buildings, *First European Conference on Earthquake Engineering and Seismology* (a joint event of the 13th ECEE & 30th General Assembly of the ESC), Geneva, Switzerland, 3-8 September 2006, Paper Number: 1122
- Daniel N. A., Lechner M.K. and Lamb I.**, 2001. M5 East Tunnels: A Flat Roofed, Bolt, and Shotcrete-Lined Highway, *RETC Proceedings*.
- Del Valle, E.**, 1980. Some lessons from the March 14 earthquake in Mexico City. *Proc, 7th World Conf. on Earthquake Engrg.*, İstanbul, Turkey.
- ElGawady M., Hegner J., Lestuzzi P. and Badoux M.**, 2004a. Static Cyclic Tests on URM Wall Before and After Retrofitting with Composites, *13th International Brick and Block Masonry Conference*.
- ElGawady M., Lestuzzi P. and Badoux M.**, 2004b. A Review of Conventional Seismic Retrofitting Techniques for URM, *13th International Brick and Block Masonry Conference*.
- Erol G., Karadoğan H.F. and Çılı F.**, 2008. Seismic Strengthening of Infilled RC Frames by CFRP, *14th World Conference on Earthquake Engineering*, October 12-17, 2008, Beijing, China
- Erol G., Demir C., İlki A., Yüksel E. and Karadoğan H.F.**, 2006. Effective Strengthening of RC Frames With and Without Lap Splice Problems, *8th National Conference on Earthquake Engineering*, 19-21 April, San Francisco, California, USA.
- Erol G., Taşkın K., Yüksel E. and Karadoğan H.F.**, 2005. Strengthening of Infilled RC Frames by CFRP, *5th International Conference on Earthquake Resistant Engineering Structures*, 30 May-1 June, Skiathos, Greece.
- Erol G., Yüksel E., Saruhan H., Sağbaş G., Teymür Tuğa P. and Karadoğan F.**, 2004. A Complementary Experimental Work on Brittle Partitioning Walls and Strengthening by Carbon Fibers, *13th World Conference On Earthquake Engineering*, August 1-6, Vancouver, B.C., Canada
- FEMA 273**, 1997. NEHRP guidelines for the seismic rehabilitation of buildings. Federal Emergency Management Agency, Washington D.C.

- Fernandez-Luco L., Río O., Schreyer J. and Rivas J.L.**, 2006. D.2.4.1.1: State of the Art. Report highlighting needs on standards and in technological research and operational innovations
- Filippou F.C., Popov E.P. and Bertero V.V.**, 1983. "Modelling of R/C joints under cyclic excitations," *Journal of Structural Engineering*, Vol. 109, No. 11, pp. 2666-2684.
- Foti D. and Monaco P.**, 2000. Post-tensioned masonry: state of the art, *Prog. Struc. Eng. Mat.*, 2, 311-318.
- Fragiadakis M.**, 2001. *Nonlinear Material Modelling of Reinforcement Steel Bars under Transient Loading*, MSc Dissertation, Dept. of Civil Engineering, Imperial College, London, UK.
- Fragiadakis M., Pinho R. and Antoniou S.**, 2004. "Modelling of reinforcing steel bars under transient loading and subjected to buckling
- Frosch R.J., Li W., Jirsa J. and Kreger M.E.**, 1996. Retrofit of Non-ductile Moment-resisting Frames Using Precast Infill Wall Panels, *Earthquake Spectra*, Vol.12, No. 4, pp.741-760.
- Fu Y.**, 1996. "Frame Retrofit by Using Viscous and Viscoelastic Dampers," *Proc., 11th World Conference on Earthquake Engineering*, Acapulco, Mexico
- Gates W.E., Hart G.C. and Crouse, C.B.**, 1990. "Vibration Studies of an Existing Building for Base Isolation Retrofit," *Proc., 4th U.S. National Conference on Earthquake Engineering*, Palm Springs, CA, 3, 559-568.
- Girgin K.**, 1996. A method of load increments for determining the second-order limit load and collapse safety of RC framed structures, Ph.D. Thesis, ITU, (in Turkish).
- Goel S.C. and Masri A.C.**, 1996. "Seismic Strengthening of an RC Slab-Column Frames with Ductile Steel Bracing," *Proc., 11th World Conference on Earthquake Engineering*, Acapulco, Mexico
- Govindan, P., Lakshmipathy, M. and Santhakumar, A.R.**, 1986. Ductility of Infilled Frames, *ACI Structural Journal*, 567-576.
- Grimstad E.**, 1999. Experineces from Excavation Under High Rock Stress in the 24.5km Long Laerdal Tunnel, International Conf. On Rock Engineering Techniques for site Characterisation. Bangalore India.pp 135-146.
- Hamid A.A., Drysdale R.G. and Heidebrecht A.C.**, 1979. Shear Strength of Concrete Masonry Joints, *Journal of Structural Division*, Vol.105, no.7, pp. 1127-1240.
- Hamid A., El-Sayed T. and Salama, A.**, 1999. Seismic retrofit of historic multiwythe stone masonry walls, 8th NAMC, Austin, Texas, USA.
- Hamid A., Mahmoud A. and Abo El Maged, S.**, 1994. Strengthening and repair of unreinforced masonry structures: state-of-the-art, 10th IB2MaC, Calgary, Canada, 485-497.

- Higashi Y., Endo T., Ohkubo M. and Shimizu Y.,** 1980. Experimental Study on Strengthening RC Structures by adding Shear Walls, Proceedings of the 7th World Conference on Earthquake Engineering, V.7, pp.173-180.
- Hilber H.M., Hughes T.J.R. and Taylor R.L.,** 1977. "Improved numerical dissipation for time integration algorithms in structural dynamics," *Earthquake Engineering and Structural Dynamics*, Vol. 5, No. 3, pp. 283-292.
- Hutchison D., Yong P. and McKenzie G.,** 1984. Laboratory testing of a variety of strengthening solutions for brick masonry wall panels, 8th WCEE, San Francisco, USA, 575-582.
- Inukai M. and Kaminoson T.,** 2000. Seismic Performance of and Existing RC Frame Retrofitted by Precast Prestressed Concrete Shear Walls, *12th World Conference On Earthquake Engineering*
- Kahn L.,** 1984. Shotcrete retrofit for unreinforced brick masonry, 8th WCEE, USA, 583-590.
- Karantoni F.V. and Fardis M.N.,** 1992. Effectiveness of Seismic Strengthening Techniques for Masonry Buildings, *Journal of Structural Engineering*, Vol.118, no.7, pp. 1884-1902.
- Kawamura S., Sugisaki R., Ogura K., Maezawa S., Tanaka S. and Yajima A.,** 2000. Seismic Isolation Retrofit in Japan, Proc. 12th World Conference on Earthquake Engineering, Auckland, New Zealand.
- Klingner, R.E. and Bertero, V.V.,** 1978. Earthquake Resistance of Infilled Frames, *Journal of Structural Division*, 104 (ST6), 973-989.
- Kunisue A., Koshika N., Kurokawa Y., Sakamoto M., Suzuki N. and Tagami J.,** 2000. Retrofitting Method of Existing Reinforced Concrete Buildings Using Elasto-Plastic Steel Dampers, Proc. 12th World Conference on Earthquake Engineering, Auckland, New Zealand.
- Kutunis M., Orak E. and Özcan Z.,** 2007. Betonarme Binaların Performans Düzeylerinin Deprem Geçirmiş Binalarla İlişkilendirilerek Belirlenmesi, *Altıncı Ulusal Deprem Mühendisliği Konferansı*, 16-20 Ekim 2007, İstanbul
- Laursen P., Davidson B. and Ingham J.,** 2002. Seismic analysis of prestressed concrete masonry shear walls, 12th ECEE, London, England, Paper reference 247.
- Lee, H. and Woo, S.,** 2002. Effect of Masonry Infills on Seismic Performance of a 3-Storey R/C Frame with Non-Seismic Detailing, *Earthquake Engineering and Structural Dynamics*, 31, 353-378.
- Lissel S. and Shrive, N.,** 2003 Construction of diaphragm walls post-tensioned with carbon fiber reinforced polymer tendons, 9th NAMC, Clemson, South Carolina, USA, 192-203.
- Lombard J., Humar J.L. and Cheung M.S.,** 2000. Seismic Strengthening and Repair of Reinforced Concrete Shear Walls, Proc. 12th World Conference on Earthquake Engineering, Auckland, New Zealand.

- Madas P.**, 1993. *Advanced Modelling of Composite Frames Subjected to Earthquake Loading*, PhD Thesis, Imperial College, University of London, London, UK.
- Mann W. and Müller H.**, 1982. Failure of Shear-Stresses Masonry - An Enlarged Theory, Tests and Application to Shear Walls, *Proceedings of the British Ceramic Society*, 30,139-149.
- Mander J.B., Priestley M.J.N. and Park R.**, 1988. Theoretical stress-strain model for confined concrete, *Journal of Structural Engineering*, Vol. **114**, no. 8, pp. 1804-1826.
- Marshall O. and Sweeney S.**, 2004. FRP Strengthening of Unreinforced and Lightly Reinforced Masonry Walls, *Composites 2004*.
- Martinez-Rueda J.E. and Elnashai A.S.**, 1997. Confined concrete model under cyclic load, *Materials and Structures*, Vol. **30**, no. 197, pp. 139-147.
- Mellal A., Commend S. and Geiser F.**, 2003. 3D finite element seismic analyses of bridges and dams, *Numerical Models in Geomechanics – NUMOG X*, – Pande & Pietruszczak (eds)
- Menegotto M. and Pinto P.E.**, 1973. Method of analysis for cyclically loaded R.C. plane frames including changes in geometry and non-elastic behaviour of elements under combined normal force and bending, *Symposium on the Resistance and Ultimate Deformability of Structures Acted on by Well Defined Repeated Loads*, International Association for Bridge and Structural Engineering, Zurich, Switzerland, pp. 15-22.
- Miranda E. and Bertero V.V.**, 1990. “Post-tensioning Techniques for Seismic Upgrading of Existing Low-Rise Buildings,” *Proc., 4th U.S. National Conference on Earthquake Engineering*, Palm Springs, CA, 3, 393-402.
- Monti G. and Nuti C.**, 1992. Nonlinear cyclic behaviour of reinforcing bars including buckling, *Journal of Structural Engineering*, Vol. **118**, no. 12, pp. 3268-3284
- Monti, G., Nuti, C. and Santini, S.**, 1996. *CYRUS - Cyclic Response of Upgraded Sections*, Report No. 96-2, University of Chieti, Italy
- Mourtaja, W., Yüksel, E., İlki, A. and Karadoğan, H.F.**, 1998. “Strengthening and/or upgrading the RC frames by means of special shotcreted diaphragms”, *Second Japan-Turkey Workshop on Earthquake Engineering*, **1**, 318-326, İstanbul
- Munshi J.A.**, 1998. “Energy Dissipation of Viscoelastically Damped Reinforced Concrete Systems,” *Proc., 6th U.S. National Conference on Earthquake Engineering*, Seattle, WA
- Negulescu C., Foerster E. and Rohmer J.**, 2003. Settlement vulnerability assessment of RC frame, Sub-Project 4, *Landslide Risk Scenarios and Loss Modelling-Lessloss Final Workshop*, Risk Mitigation for Earthquakes and Landslides Integrated Project
- National Earthquake Hazard Reduction Program**, 2000. NEHRP recommended provisions for seismic regulations for new buildings and other structures. Federal Emergency Management Agency Washington D.C.

- Nogueiro P., Simões da Silva L., Bento R. and Simões R.**, 2003. Numerical implementation and calibration of a hysteretic model with pinching for the cyclic response of steel and composite joints
- Parker H., Godlewski P. and Guardia R.**, 2002. Shotcrete Magazine, The art of tunnel rehabilitation with shotcrete
- PEER**, Pacific Earthquake Engineering Research Center, 2007.
- Pekcan G. Mander J.B. and Chen S.S.**, 1995. The Seismic Response of a 1:3 Scale Model R.C. Structure with Elastomeric Spring Dampers, *Earthquake Spectra*, Vol.11, no. 2, pp.249-267.
- Plecnik J., Cousins T., O'connor E.**, 1986. Strengthening of unreinforced masonry buildings, *J. Of Struc. Eng.*, ASCE, 112, 1070-1087.
- Pincheira J.A. and Jirsa J.O.**, 1995. Seismic response of RC frames retrofitted with steel braces or walls, *Journal of Structural Engineering*, Vol.121, no.8, pp. 1225-1235.
- Pinho R., Casarotti C. and Antoniou S.**, 2007. A comparison of single-run pushover analysis techniques for seismic assessment of bridges, *Earthquake Engineering and Structural Dynamics*
- Rodriguez M. and Park R.**, 1991. Repair and strengthening of reinforced concrete buildings for seismic resistance. *Earthquake Spectra (EERI)*,7 (3), 439–459.
- Porter S.J., McRae M.T. and Wright R.**, 1997. Design and Construction of the new Tunnel at Genting Sempah, Malaysia, T-RETC Proceedings.
- Priestley M.J.N., Calvi G.M. and Kowalsky M.J.**, 2007. *Displacement-based Seismic Design of Structures*, Structural Analysis CD, IUSS Press
- Priestley M.J.N., Seible F. and Calvi G.M.**, 1996. *Seismic Design and Retrofit of Bridges*, John Wiley & Sons Inc., New York.
- Rai D. and Goel S.**, 1996. Seismic strengthening of unreinforced masonry piers with steel elements, *Earth. Spec.*, 12, 845-862.
- Rispin M., Knight B. and Dimmock R.**, 2003. Early Re-Entry into Working Faces in Mines through Modern Shotcrete Technology – Part II, CIM-MOC Saskatoon 2003
- Robbins H.L.**, 2004. Shotcrete foundation walls at the Smithsonian Portrait Gallery in Washington, DC, Shotcrete magazine Schultz, A., Bean, J., Stolarski, H., 2003, Resistance of slender post-tensioned masonry walls with unbonded tendons to transversal loading, 9th NAMC, South Carolina, USA, 463-473
- Rosenboom O.A. and Kowalsky M.J.**, 2004. Reversed In-Plane Cyclic Behavior of Posttensioned Clay Brick Masonry Walls, *Journal of Structural Engineering*, Vol.130, no.5, pp. 787-798.
- Sargin, M., Ghosh, S.K. and Handa, V.K.**, 1971. Effects of lateral reinforcement upon the strength and deformation properties of concrete. *Magazine of Concrete Research*, V. 23, No: 75-76, pp.99-110.

- Schuller, M., Atkinson, R. and Borgsmiller, J.,** 1994. Injection grouting for repair and retrofit of unreinforced masonry. 10th IB2MaC, Calgary, Canada, 549-558B
- Schultz, A., Bean, J. and Stolarski, H.,** 2003. Resistance of slender post-tensioned masonry walls with unbonded tendons to transversal loading, 9th NAMC, South Carolina, USA, 463-473
- SeismoSoft** 2006. SeismoStruct – A Computer Program for Static and Dynamic Nonlinear Analysis **Mourtaja, W., Yuksel, E., Ilki, A. and Karadogan, H.F.** 1998, Strengthening and/or Upgrading the RC frames by Means of Special Shotcreted Diaphragms, *Second Japan-Turkey Workshop on Earthquake Engineering*, 1, 318-326. of Framed Structures, (online), available from URL: <<http://www.seismosoft.com>>.
- Sheppard P. and Tercelj S.,** 1980. The effect of repair and strengthening methods for masonry walls, 7thWCEE, Istanbul, vol. 6, 255-262.
- Smyrou E., Blandon-Uribes C., Antoniou S., Pinho R. and Crowley H.,** 2006. Implementation and verification of a masonry panel model for nonlinear pseudo-dynamic analysis of infilled RC frames, *First European Conference on Earthquake Engineering and Seismology* (a joint event of the 13th ECEE & 30th General Assembly of the ESC), Geneva, Switzerland, 3-8 September 2006, Paper Number: 355
- Stafford-Smith B.,** 1966. Behavior of square infilled frames, *Journal of Structural Division*, Vol.92, no.1, pp. 381-403.
- Sugano, S. and Fujimura, M.,** 1980. Aseismic Strengthening of Existing Reinforced Concrete Buildings, *Proceedings of the 7th World Conference on Earthquake Engineering*, 4, 449-456.
- Taghdi M., Bruneau M. and Saatcioglu M.,** 2000a. Analysis and Design of Low-Rise Masonry and Concrete Walls Retrofitted using Steel Strips, *Journal of Structural Engineering*, Vol.126, no.9, pp. 1026-1032.
- Taghdi M., Bruneau M. and Saatcioglu M.,** 2000b. Seismic Retrofitting of Low-Rise Masonry and Concrete Walls using Steel Strips, *Journal of Structural Engineering*, Vol.126, no.9, pp. 1017-1025.
- Taşkın K., Yardımcı N. and Karadoğan F.,** 2007. Betonarme Çerçevelerin Çelik Çaprazlı Sistemlerle Güçlendirilmesi, 2.Ulusal Çelik Yapılar Sempozyumu, Mayıs 2007, Eskişehir
- Tena-Colunga A., Gomez-Soberon C. and Munoz-Loustaunau A.,** 1997. Seismic Isolation of Buildings Subjected to Typical Subduction Earthquake Motions for the Mexican Pacific Coast, *Earthquake Spectra*, Vol.13, no.3, pp.505-532.
- Teran-Gilmore A., Bertero V.V. and Youssef N.,** 1995. "Seismic Rehabilitation of Framed Buildings Infilled with Unreinforced Masonry Walls Using Post-tensioned Steel Braces," *UCB/EERC-95/06*, Berkeley, Earthquake Engineering Research Center (EERC), University of California, Berkeley

- Thermou G E. and Elnashai A.S.**, 2006. Seismic retrofit schemes for RC structures and local–global consequences, *Earthquake Engineering and Structural Dynamics*, 8, pp.1–15.
- Tomazevic M.**, 2000. Some aspects of experimental testing of seismic behavior of masonry walls and models of masonry buildings, *ISET Journal of Earthquake Technology*, Vol.37, no.4, pp. 101-117.
- Turkish code for earthquake resistant design**, 1997. Ministry of Public Works and Settlement Ankara.
- Turkish code for earthquake resistant design**, 2007. Ministry of Public Works and Settlement Ankara.
- Vandewalle M.**, 2003. The use of steel fiber-reinforced shotcrete for the support of mine openings, *Shotcrete magazine*
- Von der Hofen M.H.**, 2008. Forming and constructing structural shotcrete walls, *Shotcrete magazine*
- Wasti S.T., Erberik M.A., Kaur C. and Sucuoğlu H.**, 1997. Dinar depreminde hasar görmüş yığma yapıların onarım ve güçlendirme çalışması, Dördüncü Ulusal Deprem Mühendisliği Konferansı, 230-241, Ankara.
- Yıldız D.H.**, 2008. Comparison of the evaluation methods to determine of seismic performance of buildings, M.Sc. Thesis, ITU, (in Turkish).
- Yorgun C., Yardımcı N., Karadoğan H.F., Yüksel E. And Taşkın K.**, 2008. Depreme Karşı Güçlendirmede Dış Merkez Çaprazlar, 106M045 numaralı TÜBİTAK proje sonuç raporu
- Yüksel, E., Ilki, A. and Karadogan, H.F.**, 1998a. Brick Masonry Infill Walls Integrated to the Peripheral RC Element and Strengthening, *Second Japan-Turkey Workshop on Earthquake Engineering*, 1, 309-317.
- Yüksel, E., Ilki, A. and Karadogan, H.F.**, 1998b. Strengthening of Reinforced Brittle Masonry, *11th European Conference on Earthquake Engineering*, Paris
- Yüzügüllü Ö.**, 1980. Multiple precast reinforced concrete panels for aseismic strengthening of RC frames, *Proceedings of the 7th World Conference on Earthquake Engineering*, V.6, pp.263-270.
- Zarnic, R. and Tomazevic, M.**, 1984. The Behavior of Masonry Infilled Reinforced Concrete Frames Subjected to Cyclic Lateral Loading, *Proceedings of the 8th World Conference on Earthquake Engineering*, 6, 863-870.
- Zarnic, R. and Tomazevic, M.**, 1988. An Experimentally Obtained Method for Evaluation of the Behavior of Masonry Infilled RC Frames, *Proceedings of the 9th World Conference on Earthquake Engineering*, 6, 163-168.
- Zynda C.**, 2007. A pictorial description of a shotcrete and precast parking garage construction, *Shotcrete magazine*



CURRICULUM VITA

Candidate's full name: Pınar TEYMÜR

Place and date of birth: Istanbul 1974

Permanent Address: Kozyatağı-Istanbul

Universities and Colleges attended: Istanbul Technical University

Publications:

- **Teymür, P.**,1999 Yapı Sistemlerinin Birinci Doğal Titreşim Periyotlarının Hesabı için Ampirik Periyot İfadeleri. Yüksek Lisans Tezi, Fen Bilimleri Enstitüsü, İTÜ.
- Pala, S., Karadoğan, F. ve **Teymür, P.**, 1999 Code Recommended versus Theoretically and Experimentally Found Dynamic Characteristics of Building Type Structures. Fourth International Conference on Vibrational Problems, Hindistan.
- Pala, S., Özmen G., Atabey M. and **Teymür, P.**, 2000. Planda Düzensiz Yapılarda Kat Döşemelerinin Deprem Etkileri Altındaki Davranışı. Advances in Civil Engineering, 4th International Congress, pp 523-532. Kasım 1-3, Gazimagusa, KKTC.
- Yüksel, E., **Teymür, P.**, 2001 Bölme Duvarlarına Yönelik Çalışmalar, Yapı Mekanikliği Laboratuvarları Toplantısı, Tübitak.
- Yüksel, E., Karadoğan, F., Yıldırım, H., Pala, S., Saruhan, H., **Teymür, P.**, Sağbaş, G., 2001 Tarihi Eser Niteliği Taşıyan Bir Yapının Deprem Güvenliğinin İrdelenmesi ve Güçlendirme Önerisi, Türkiye İnşaat Mühendisleri Odası 16. Teknik Kongre Sergisi.
- Karadoğan, F.,Yüksel, E., **Teymür, P.**, Sağbaş, G.,Saruhan, H., 2001: Report on Seismic Evaluation of Five Representative RC Buildings, İTÜ Geliştirme Vakfı yönetmelikleri çerçevesinde hazırlanmış araştırma projesi.
- Yüksel, E., Karadoğan, F., Yıldırım, H., Pala, S., Saruhan, H., **Teymür, P.**, Sağbaş, G., 2002 “Experiments Carried Out on a Historical Masonry Building for Retrofitting Purposes”, 12th European Conference on Earthquake Engineering, 9-13 Eylül 2002, Londra, İngiltere, paper reference 317
- Gülay, F.G., Şen, B., **Teymür, P.**, 2002: An Investigation on Behavior of Slabs with Large Openings under Earthquake Loading, 3rd European Workshop on the Seismic Behavior of Irregular and Complex Structures”, 17-18 Eylül 2002, Floransa, İtalya

- Yüksel, E., Erol, G., **Teymür, P.**, Sağbaş, G., Saruhan, H., Karadoğan, F.,2003: Yüksek Dayanımlı Bölme Duvarlarının Yapısal Özelliklerini Belirlemeye Yönelik Bir Deneysel Çalışma, II. Yapı Mekaniği Laboratuvarları Toplantısı, 19-20 Haziran 2003, Konya
- Erol, G., Yüksel, E., Saruhan, H., Sagbas, G., **Teymur, P.**, Karadogan, F.,2004: “A Complimentary Experimental Work on Brittle Partitioning Walls and Strengthening by Carbon Fibers”, 2004, 13th World Conference on Earthquake Engineering, Vancouver, Canada.
- Karadoğan, F., Bingöl, Y., Erol, G., Yüce, S., Yüksel, E., **Teymur, P.**,2004: Savunma Yapılarının Deprem Güvenliği ve Deprem Güvenliğinin Saptanmasında Ordu Desteği, SAVTEK 2004, Savunma Teknolojileri Kongresi, Ankara.
- **Teymür, P.**, Yüksel, E., Pala, S., Taşkın, K., Karadoğan, F.,2006: “Wet-Mixed Shotcrete Usage in Low-Ductile Reinforced Concrete Frames, First European Conference on Earthquake Engineering and Seismology, Cenevre, İsviçre, 3-8 Eylül 2006, Bildiri Numarası: 892.
- Yüksel, E., Yıldız, D., **Teymür, P.**, Nur, C., 2008: Seismic Performance Assessment of RC Buildings According to the 2007 Turkish Earthquake Code, 8th International Congress on Advances in Civil Engineering, 15-17 September 2008 Eastern Mediterranean University, Famagusta, North Cyprus.
- **Teymur, P.**, Yüksel, E., Pala, S.,2008: “Wet-Mixed Shotcrete Walls to Retrofit Low Ductile RC Frames”, The 14th World Conference on Earthquake Engineering, October 12-17, 2008, Beijing, China
- Kabdaşlı, N. I., Tünay, O. and **Teymür, P.**, 1996: Lead Treatment by Chemical Precipitation. Journal of Turkish Water Pollution Control, 6, 1, 41-47 (in Turkish with an English abstract).
- Karadogan, F., Yüksel, E., **Teymur, P.**, Sagbas, G., Saruhan, H., “Final Report on Seismic Evaluation of Five Representative RC Buildings”, ITU, 2001
- Karadogan, F., Yüksel, E., Bozdog, E., **Teymur, P.**, Sagbas, G., Bozdog, E., Saruhan, H.,2002: Technical report on seismic evaluation of a private factory, ITU, January 2002 (in Turkish)
- Karadogan, F., Lav, A., Yüksel, E., **Teymur, P.**, Sagbas, G., Bozdog, E., Sunbuloglu, 2002: “Research on the effects of yayılan vibrations on the surrounding residences during dynamic compaction at Derince port”, ITU, November 2002 (in Turkish)